ASPECTS OF THE ELECTROCHEMISTRY OF THE CHEMELEC CELL®

by

Simon A. Cotgreave

Supervisor: Professor N.A. Hampson

Industrial Supervisor: Dr. A. Tyson

A doctoral thesis submitted in partial fulfilment of the requirements for the award of Doctor of Philosophy of the Loughborough University of Technology, February 1983.

I kept my answers small and kept them near;
Big questions bruised my mind but still I let
Small answers be a bulwark to my fear.

The huge abstractions I kept from the light;
Small things I handled and caressed and loved.
I let the stars assume the whole of night.

But the big answers clamoured to be moved
Into my life. Their great audacity
Shouted to be acknowledged and believed.

Even when all small answers build up to
Protection of my spirit, still I hear
Big answers striving for their overthrow.

And all the great conclusions coming near.

(Answers,
Elizabeth Jennings, 1926-)

The work described in this thesis has not been submitted in full, or in part, to this or any other institution for a higher degree.

ACKNOWLEDGEMENTS

My sincere thanks are due to Professor Noel Hampson for supervision, advice, guidance and encouragement without which this thesis would not have been possible.

I should like to acknowledge the generous financial support of the Electricity Council. I am grateful to Dr. Alan Tyson of the Electricity Council Research Centre, Capenhurst, for his supervision, interest and readiness to help in any way possible. My thanks are also due to Alison Bettley, also of E.C.R.C., for fruitful discussions and help.

Professor Bentley is kindly thanked for the provision of research facilities and the administrative and secretarial staff for their many efforts on my behalf.

The almost miraculous enterprises of A. Bower (electrical), A. Stevens (mechanical) and M. Coupe (glassblowing) are gratefully noted.

Dr. Julian Tyson is thanked for the provision of atomic adsorption facilities.

The help of Claire Lazarides and Ray Barton in photographic and other matters is appreciated.

I am grateful to Dr. D.R. Gabe (Materials Engineering and Design) for his help with the literature.

I am indeed indebted to my fellow research workers for their great friendship, willing help and many useful and other discussions. Especially to Dr. S.A.G.R. Karunathilaka for help with impedance data.

Finally, my deepest gratitude is afforded to Katy Garfield for the patient and careful typing of this thesis, a task which she has performed with her usual good nature and competence.

DEDICATION

To my Mother and Father whose encouragement, help and love have been a continued source of inspiration, in gratitude for my education.

SYNOPSIS

The Chemelec Cell® is an electrochemical reactor which achieves the recovery of metals from electroplating effluent by electrodeposition at concentrations too low to be considered for conventional electrolysis. The combination of a mesh-type configuration of electrodes together with the use of a non-conducting (inert) fluidised bed electrolyte engenders a sufficiently high rate of mass transport in the cell for efficient deposition to be carried out at metal ion concentrations below 1.0 gl^{-1}.

Two approaches have been made to the investigation of the system. First, experiments have been conducted using a laboratory scale Chemelec Cell® in which the electrodeposition of nickel from Watts electrolytes has been carried out under a wide range of conditions of electrode potential, pH and metal ion concentration. Relatively long-term experiments have been attempted in which the cell is operated under conditions of constant electrode potential, temperature, pH and fluidisation and the fall of nickel ion concentration plotted as a function of time. Measurement of the charge passed (also as a function of time) has allowed access to the cathode current efficiency. Polarisation data, comprising two regions of electrode potential in which the current density varies semi-logarithmically with a large apparent Tafel slope (~ 570 mV/dec.) separated by a region of some 300-500 mV in which the current density is almost independent of potential, have been obtained under these different conditions. An interpretation of these somewhat unusual characteristics has been sought.

Secondly, more fundamental studies concerning the electrode kinetics of cadmium in various electrolytes have been carried out.

The techniques of faradaic impedance, linear sweep voltammetry and the rotating disc have been applied and the results of these experiments interpreted. The presence of a hydroxide film on the electrode has been demonstrated and this obscures the true kinetics.

Finally, the observed electrode kinetics and the experimental results obtained from the operation of the Chemelec Cell® are compared and critically discussed.

SYMBOLS

a	Tafel intercept	-
A	Electrode area	m^2
b	Tafel slope	V
c	Electrolyte concentration	mol m^{-3}
c_c	Specific capacitance (compact layer)	F m^{-2}
c_d	Specific capacitance (diffuse layer)	F m^{-2}
c_j^b	Bulk concentration (species j)	mol m^{-3}
c_j^s	Surface concentration (species j)	mol m^{-3}
c_L	Specific double layer capacitance	F m^{-2}
C_L	Double layer capacitance	F
d	Thickness of the Helmholtz layer	m
D_i	Differential coefficient of Z_{cal} with respect to P_i at $P_i = \Delta P_i$	-
D_j	Diffusion coefficient (species j)	m^2 s^{-1}
e	The electron	-
e	Electronic charge (1.604×10^{-19})	C
e_i	Cathode current efficiency	%
E	Electrode potential	V
E_i	Initial electrode potential	V
E_p	Peak potential	V
E_r	Reversible potential	V
E_z	Potential of zero charge	V
$E^\ominus$	Standard electrode potential	V
$\underline{f}$	Volume force	N m^{-3}
F	The Faraday (96487)	C mol^{-1}
i	Net (reduction) current density	A m^{-2}
i_o	Exchange current density	A m^{-2}
i_p	Peak current density	A m^{-2}

i_L	Limiting current density	A m^{-2}
i_{Ni}	Partial current density for nickel electrodeposition	A m^{-2}
$\vec{i}$, $\overleftarrow{i}$	Cathodic, anodic partial current density	A m^{-2}
i_∞	Current density at infinite rotation speed	A m^{-2}
I	a.c. current	A
I_m	Amplitude of I	A
J_j	Flux (species j)	mol m^{-2} s^{-1}
$\vec{k}$, $\overleftarrow{k}$	Cathodic, anodic rate constant	m s^{-1}
$\vec{k}_o$, $\overleftarrow{k}_o$	Cathodic, anodic standard rate constant	m s^{-1}
k^o	Standard rate constant	m s^{-1}
m_1	Intercept to log{c} versus t plot	-
m_2	Slope of log{c} versus t plot	s^{-1}
n	Number of parameters for the equivalent circuit	-
$n_\pm$	Anion, cation surface ionic excess	m^{-2}
N	Number of frequencies	-
O	Oxidised species	-
p	Pressure gradient	Pa
P_i	Parameter i of the equivalent circuit	-
Pr_j	Prandtl number (species j)	-
q	Charge	C
R	Reduced species	-
R	The Gas constant (8.314)	J K^{-1} mol^{-1}
R_Ω	Solution resistance	Ω
t	Time	s
T	Absolute temperature	K
U_o	Fluid velocity	m s^{-1}

$\underline{v}$	Velocity profile	$m\ s^{-1}$
V	Electrolyte volume	m^3
V	a.c. voltage	V
V_m	Amplitude of V	V
x	Distance	m
<x>	Mean distance of the net distributed charge	m
$<x_\pm>$	Mean distance of $n_\pm$ from the electrode	m
z	Charge transfer valence	-
z	Ionic valence	-
z_j	Ionic valence (species j)	-
z_α	Number of electrons transferred up to and including the rate determining step	-
Z	Experimental value of Z' or Z''	Ω
$\underline{Z}$	Impedance	Ω
Z_{cal}	Calculated value of the impedance	Ω
$\underline{Z}_W$	Warburg impedance	Ω
Z'	Real part of $\underline{Z}$	Ω
Z''	Imaginary part of $\underline{Z}$	Ω
α	Charge transfer coefficient (cathodic)	-
δ	Diffusion layer thickness	m
δ_j	Diffusion layer thickness (species j)	m
δ_O	Prandtl boundary layer thickness	m
γ	Roughness factor	-
ε	Residual error	-
ε	Relative permittivity	-
ε_o	Permittivity of free space (8.854×10^{-12})	$F\ m^{-1}$
η_D	Charge transfer overpotential	V
θ	Charge transfer resistance	Ω

μ	Viscosity	Pa s
ν	Kinematic viscosity	$m^2\ s^{-1}$
ν	Sweep rate	$V\ s^{-1}$
ρ	Density	$kg\ m^{-3}$
σ	Warburg coefficient	$\Omega s^{-\frac{1}{2}}$
σ_R, σ_C	Resistive, capacitive Warburg coefficient	$\Omega s^{-\frac{1}{2}}$
$\sigma_{\pm}$	Anion, cation excess distribution	m^{-2}
τ	Transition time	s
ϕ	Phase angle	rad
ϕ	Galvani potential	V
ϕ_0	Galvani potential (x = 0)	V
ϕ_1	Galvani potential (IHP)	V
ϕ_2	Galvani potential (OHP)	V
ω	Angular frequency	$rad\ s^{-1}$

CONTENTS

CHAPTER ONE

INTRODUCTION

1.1 A selective account of the history of nickel and cadmium electrodeposition

Electroplating has been, and indeed still is, a particularly practical subject. Thus it was known, according to the Greek historian Zosimus, to the ancients who coated iron swords with copper by immersion in waters rich in copper salts.[1]

It was not until after the pioneering work of Galvani[2] (1791) and Volta[3] (1800) that some hint of the rôle of electricity in such processes was first given. The deposition of metals from solutions of their salts by the passage of electrical current was first reported by Cruickshank[1] as early as 1803, still some twenty four years in advance of the exposition of Faraday's Laws.[4]

This is remarkable in view of the fact that the voltaic pile was replaced with the first battery in 1800 and that the first magneto-electric machines were developed by Faraday in 1831. As cheaper and more easily managed sources of electricity became available, so research and development in the field of electrodeposition advanced apace.

The electrodeposition of nickel from sulphate or chloride solutions was first reported by Bird[5] in 1837 and the first patent for commercial nickel plating granted to Shore[6] in 1840. Experiments by de Ruolz[7] of France were said to be less than satisfactory in terms of the adhesion of the deposit. Smee[8] also published results concerning the electrodeposition of nickel, but again his attempts to

produce a satisfactory deposit were less than entirely satisfactory. More acceptable deposits were obtained in Germany by Böttger[7], using an acid ammonium sulphate bath. A variety of different electrolytes were subsequently proposed and some granted patents. The solution of Böttger[7] was to remain in commercial use for a number of years. A process involving neutral nickel ammonium sulphate was suggested by Gore[9] in 1855 and later by Becquerel[10] in 1862. The process is often attributed, however, to Adams.[11] Whilst Adams was not the first to propose this bath, he was the first to patent it[12,13] and this, latter, patent aided him to establish a virtual monopoly over commercial nickel plating for some years. A third patent[14] was granted to him for a plating bath based on nickel sulphate. 1878 saw the addition of boric acid to improve the quality of the deposit by Weston.[15] The additives citric and benzoic acids were patented by Powell[16] in the following year. A further year saw a second patent to Powell[17] claiming the pyrophosphate bath. In Germany the work of Langbein and Pfanhauser was continued by Springer who first revealed[18] the essential nature of the chloride ion to satisfactory anode corrosion, this being later stressed by Bancroft.[19] It was the work of Foerster[20], however, that did much to elucidate the basis of nickel plating and, in particular, the importance of temperature to the plating process. The effect of acidity on the production of thick deposits had already been described in a patent, claiming any and all salts and acids from which nickel plating appeared possible, to Vandermersch.[21] Research on plating solutions, however, was still far from exhausted. The year 1909 saw the introduction of the nickel fluoroborate bath by Kern[22], a bath which is still in use today. The most important breakthrough was, however, that of Watts[23] who described a plating bath for rapid nickel plating at current densities an order of magnitude higher than those previously achieved. The composition of the Watts Bath, as it has

become known, was given as:

$NiSO_4.7H_2O$	240 gl^{-1}
$NiCl_2.6H_2O$	20 gl^{-1}
H_3BO_3	20 gl^{-1}

This bath is, with minor modifications, the bath used by the majority of nickel platers even today. The Watts Bath was to be maintained acid and worked hot. Other plating baths, which are still in commercial use, include the sulphamate solution of Cambi and Piontelli[24] and the all-chloride electrolyte of Wesley and Carey.[25]

By this time the emphasis on research was shifting towards the elucidation of methods for the production of 'bright' nickel. As early as 1910, small amounts of cadmium had been added to nickel plating baths, though with limited success. From the 1930's onwards, and especially under the influence of the world wars, bright nickel plating baths were much improved. The first real results in bright nickel plating are attributed to Schlötter[26] for the addition of aromatic sulphonic acids; his work led to commercial bright nickel plating being employed in a variety of situations. A rival process, due to Weisberg[27], involving the deposition of a nickel-cobalt alloy in the presence of formate, was found to be too expensive. Research into different additives for brightening, levelling and the generation of specific physical properties still continues and many such compounds have been proposed.

Owing to the high cost and relative scarcity of cadmium, it has received markedly less attention than has nickel. The history of its development is of less interest. The metal was first deposited by

Smee[8], from ammoniacal solutions of cadmium sulphate, and noted the difficulties of obtaining good deposits from either cadmium chloride or cadmium sulphate. A solution of cadmium bromide, slightly acidified with sulphuric acid, was used successfully by Bertrand.[1] The solution of Russell and Woolrich[28], a basic solution of cadmium cyanide, forms the basis of all cadmium plating today. The method of preparation of the solution has varied somewhat and again a range of different additives have been proposed, but the essential components of cadmium plating solutions remain largely unaltered.

The tremendous advances which had been made concerning plating solutions were only to set the scene for other developments which were to transform the face of industrial electroplating. A patent to Remington[29] claiming the use of electrolytic nickel anodes contained in insoluble (platinum) baskets was perhaps, in some sense, a starting point for this change. Slowly, the small-scale manual plant, in which work was moved from tank to tank by hand, gave way to the fixed sequence plants in which jigs moved automatically from one tank to the next, residing in and above each for a fixed period of time. Such plant was capable of much greater throughput than was the manual plant. Eventually the fixed sequence plant itself gave way to the variable programme plant. This, fully automatic, design enabled the jigs to be lowered into a pre-programmed selection of the available process tanks for predetermined lengths of time. This has undoubtedly improved, facilitated and helped to optimise the plating process. Other advances included the introduction of air agitation (which proved popular with British platers as early as the 1920's) as well as the development of the barrel plating process. This latter allowed the economical plating of vast numbers of small items in an economic manner for the first time, and was of especial importance in nickel

electroplating.

The frequent need for a process tank to be followed by a static or 'drag-out' tank and one or more running rinse tanks demands the use of a very large volume of water, whose cost requires that it is efficiently used and re-used. So while the industrial process of electroplating (often despite the absence of a knowledge of the electrochemical kinetics concerned) is now well established for a range of metals, further effort is clearly desirable in attendant areas of plating practice, not least in waste water treatment. There is clearly an incentive for research into novel effluent treatment methods.

1.2 Effluent treatment in the electroplating industry

Under the terms of the Water Act of 1973, Regional Water Authorities were set up to administer the watercourses and sewers of Great Britain. These Authorities have the power to impose discharge consents, monitor discharges and to levy charges for the discharge of effluent. Electroplating processes produce effluents containing metal ions, a variety of anions which may or may not be toxic (e.g. cyanides) and a range of organic compounds used for their brightening or levelling properties. As a consequence of the charges levied by Water Authorities it is clearly important to subject such effluents to an efficient treatment programme prior to discharge. Effluent treatment is thus of importance to the economics of the plating process as well as to the environment. It is to be expected that as the technology available for effluent treatment becomes more advanced, so the legislation controlling discharges will become more stringent.

1.2.1 Conventional Effluent Treatment

It is only recently in the history of electroplating that supplementary techniques have been available. In the past, if effluent treatment were to be attempted at all, then the following type of process would have been used in isolation.

In general, individual effluent streams are not kept separate unless recovery is envisaged or such streams contain hexavalent chromium or cyanides. In the latter cases cyanides are treated with gaseous chlorine or sodium hypochlorite and hexavalent chromium reduced with gaseous sulphur dioxide or sodium bisulphite. Except where recovery is to be attempted, such streams may now be combined and the pH adjusted to cause precipitation of the metals present. The resulting precipitate is allowed to settle in large tanks and various methods have been employed to aid this process. Once settling is complete the supernatant liquor may be discharged and the sludge removed either as a slurry or, after de-watering, as a cake. The costs of disposal of such sludges are considerable and the possibility of metal recovery remote.

Where this method is the only form of effluent treatment, there is a considerable waste of resources and obvious disadvantages (including the environmental ones) are apparent. It was estimated that, in the United Kingdom, in 1976 approximately 700 tonnes of nickel were lost to drag-out, at a value of £2,800/tonne.[30] This represents a significant incentive for the development of the novel methods for metal recovery which are currently enjoying success in the electroplating industry. Some of these methods are described below.

1.2.2 Evaporative Recovery

The drag-out tank contains, by definition, much of the material required in order to maintain the plating bath at its operating concentration. The salts are present in the correct proportions, although the dilution involved prevents their immediate return to the bath. If the salts contained in the drag-out tank are to be re-cycled, some form of concentration must first be effected. Evaporative recovery is one technique currently used in industry for this purpose. There are four types of evaporator which are commercially available.

1.2.2.1 Climbing Film Evaporator

The drag-out solution is made to rise up the inside of externally heated tubes. A film of solution climbs the walls of the tubes and evaporates at an enhanced rate under the slightly reduced pressure at which the system operates. The water vapour is condensed for re-use and the concentrated drag-out returned to the plating tank, making good the evaporative losses.

1.2.2.2 Flash Evaporator

The drag-out solution is pre-heated at atmospheric pressure and then fed into a reduced pressure system at fairly high vacuum. The water boils and the vapour is condensed at the top of the system. Concentrated drag-out solution collects at the bottom and return to the process is again possible.

1.2.2.3 Submerged Tube Evaporator

Submerged steam coils are used to heat the solution under fairly high vacuum.

1.2.2.4 Forced Draught Atmospheric Evaporator

The solution is heated prior to descending a column against an ascending air flow. The air carries steam into the atmosphere and a more concentrated drag-out solution collects at the bottom of the apparatus.

1.2.3 Ion Exchange

Columns of ion exchange resins have been successfully used for the concentration of effluent streams and for the production of de-ionised water. The recovery of specific metal ions may be envisaged although the direct return of plating constituents to the plating bath is not possible due to the nature and composition of the regenerating solutions. This method has found its widest application in the recovery of gold and silver, where the metal is recovered by burning the resins rather than regenerating them. In situations where the resins are regenerated the resulting solutions may be further treated, for example, by electrolysis. This approach, however, has found a more limited market.

1.2.4 Reverse Osmosis

In this technique the application of an external pressure

opposing the osmotic pressure causes a transfer of solvent from the stronger to the weaker solution. The solution to be concentrated is separated from the solvent by a semi-permeable membrane. The concentrated solution is often capable of being directly recycled. Small ions may, however, pass through the membrane with the solvent. The method has most successfully been used in connection with Watts Bath drag-out, although its industrial occurrence is rare.

1.2.5 Electrochemical Recovery

The electrochemical recovery of metals from dilute solutions of their ions is a topic of increasing interest. The conventional electrolysis of such solutions, with metal ion concentrations typically below 1.0 gl^{-1}, is not economically viable. The mass transport régime of these cells is such that a large value for the diffusion layer thickness results and a small limiting current density pertains to the metal deposition reaction. Acceptable cathode current efficiencies are achieved only where the cells are operated at very low currents, when the rate of metal deposition is exceedingly slow. Conventional electrolysis has been employed, however, following an initial concentration of the electrolyte by evaporative recovery or reverse osmosis.

The desire to carry the electrolysis of dilute solutions both quickly and efficiently has, over the past decade, led to the development of a considerable number of novel electrochemical reactors. Two approaches to the problem have been considered. First, the use of electrodes of high surface area allows the passage of high currents, i.e. a high rate of metal deposition at a moderate current density. Secondly, and perhaps more fundamentally, the mass transport limitation

has been alleviated by means of some sort of solution and/or electrode movement. In some cases a combination of these two approaches has been beneficial.

The field was reviewed by Kuhn[31] and presented to a symposium on "Novel electrode systems for dilute metal bearing liquors" in 1978. The review discussed the commercial need for such devices as well as some of the reactors themselves. A more recent review is that of Kreysa[32], but the most recent and exhaustive work is that of Walsh and Gabe.[33]

In introducing the Chemelec Cell® it is instructive to view the cell against other designs, and a number of these are described below. The classification of Goodridge[34], though sometimes misleading, has been borne in mind according to which §1.2.5.1-3 deal with stationary two-dimensional electrodes, §1.2.5.4-5 with dynamic two-dimensional electrodes, §1.2.5.6-7 with stationary three-dimensional electrodes and §1.2.5.8 with dynamic three-dimensional electrodes. It should be realised that whilst the majority of cells have been discussed, it has not been practicable to give details of all of them. Among those which have been omitted from the following are the Rotating Multipolar Electrode[35-41], the CJB Cell[42], the Inclined, Moving Particulate Electrode[43], the Moving Bed Electrode[44] and the Rotating Packed Bed Cell[45] which, with the exception of the first, dynamic two-dimensional electrode, are all examples of dynamic three-dimensional electrodes.

1.2.5.1 Bipolar Trickle Tower Reactor

The reactor, developed at Newcastle and Southampton Universities[46], is shown in Fig. 1.2.1 and consists of a cylindrical column containing layers of conductive material separated by thin sheets of insulating mesh. A potential difference is applied to a pair of feeder electrodes circumjacent to the conductive layers, inducing bipolarity in these layers. The electrolyte is fed into the top of the tower through which it percolates under the influence of gravity. The metal is recovered as a plate or powder depending on the form of conducting material used. This is usually carbon in the form of hollow cylinders, perforated plates, felts, cloths, fibres or particles. The particulate tower is actually a three-dimensional electrode. The electrode is of high surface area and the device can reduce metal ion concentration to p.p.m. levels, although the current efficiency is not high. Operation is in the batch recycle mode. A prototype commercial trickle tower is being evaluated for gold recovery using a disposable electrode/separator cartridge.

1.2.5.2 Swiss-Roll Cell

The Swiss-Roll Cell[47-50], developed in Switzerland by Robertson and Ibl, is shown in Fig. 1.2.2. The favourable ratio of surface area to volume has been achieved by constructing a sandwich of electrodes and separators, rolled round a common axis and enclosed in a cylinder. The electrolyte flows axially through the cell. The electrodes may be sheets or nets and the separators cloths, ion exchange membranes or porous, non-woven materials. The metal is recovered as an

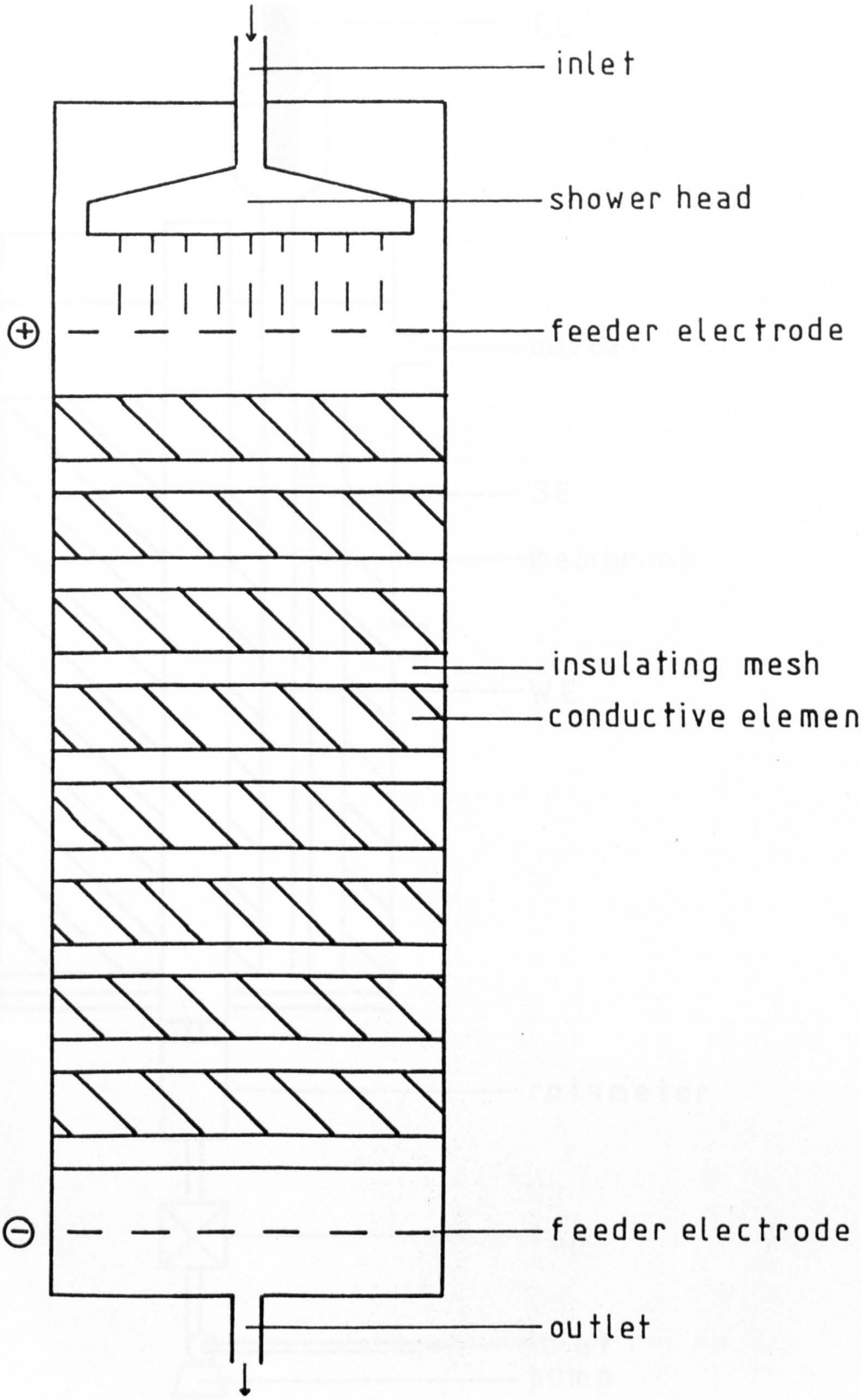

Fig. 1.2.1 Bipolar Trickle Tower Reactor

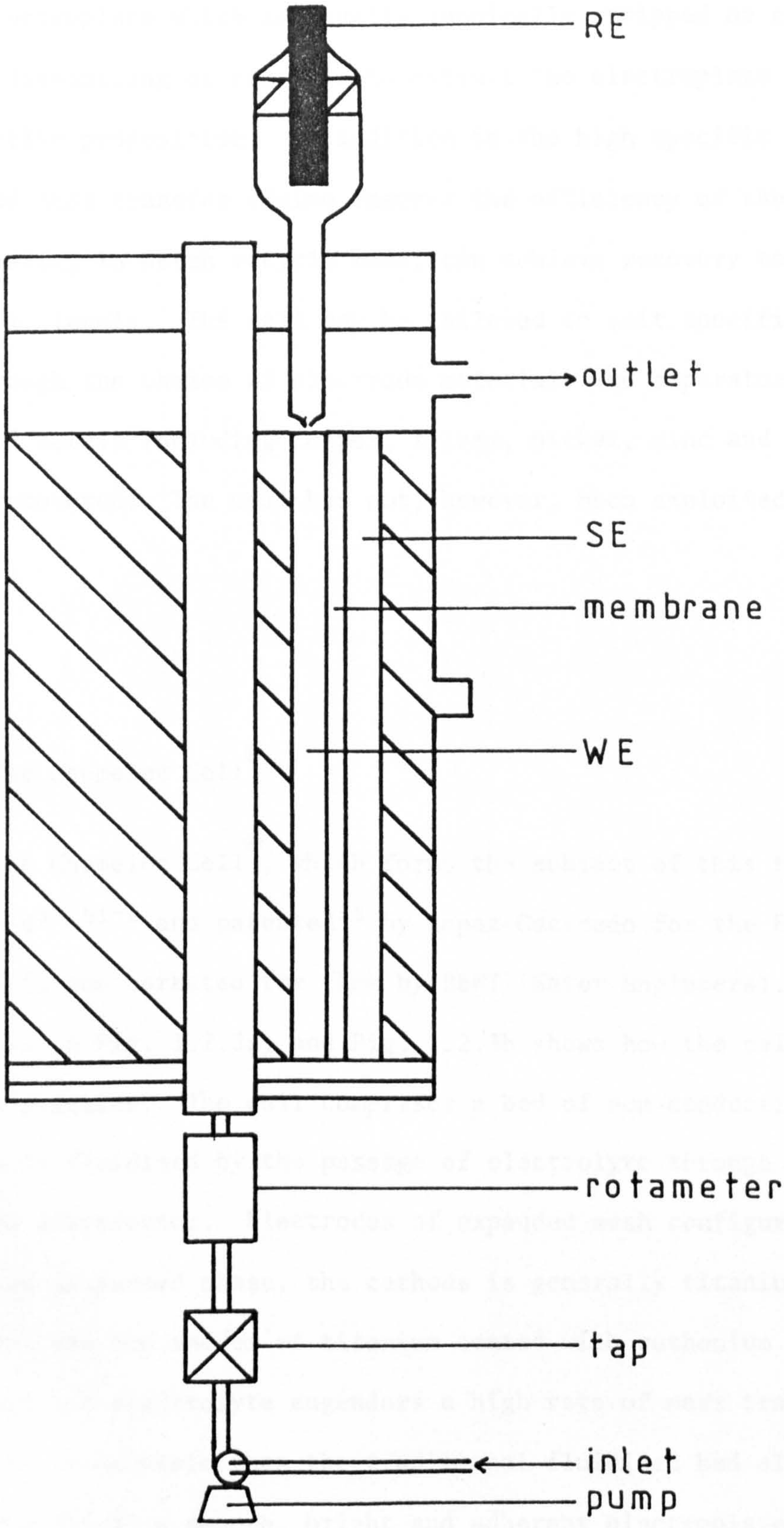

Fig. 1.2.2 Swiss-Roll Cell

adherent electroplate which is usually anodically stripped or chemically dissolved; dismantling of the cell to extract the electroplate being an unattractive proposition. In addition to the high specific surface area, a good mass transfer régime ensures the efficiency of the cell which, operating in batch recycle mode, can achieve recovery to p.p.m. or sub-p.p.m. levels. The cell may be tailored to suit specific applications through the choice of electrode materials and separators, and a variety of metals including copper, silver, nickel, zinc and gold have been recovered. The cell has not, however, been exploited commercially.

1.2.5.3 The Chemelec Cell®

The Chemelec Cell®, which forms the subject of this thesis, was developed[30,51-2] and patented[53] by Lopez-Cacicedo for the Electricity Council and is now marketed for them by BEWT (Water Engineers). The cell is shown in Fig. 1.2.3a, and Fig. 1.2.3b shows how the cell operates in practice. The cell comprises a bed of non-conducting glass beads which is fluidised by the passage of electrolyte through the slotted flow distributor. Electrodes of expanded mesh configuration reside in the dispersed phase, the cathode is generally titanium or mild steel and the anodes of titanium coated with ruthenium dioxide. The fluidised bed electrolyte engenders a high rate of mass transfer, but is easier to maintain than the traditional fluidised bed electrode. Metal recovery is as a smooth, bright and adherent electroplate which may subsequently be used as a process plating anode. Operation of the cell is in the batch recycle mode. Recovery of copper, nickel, zinc,

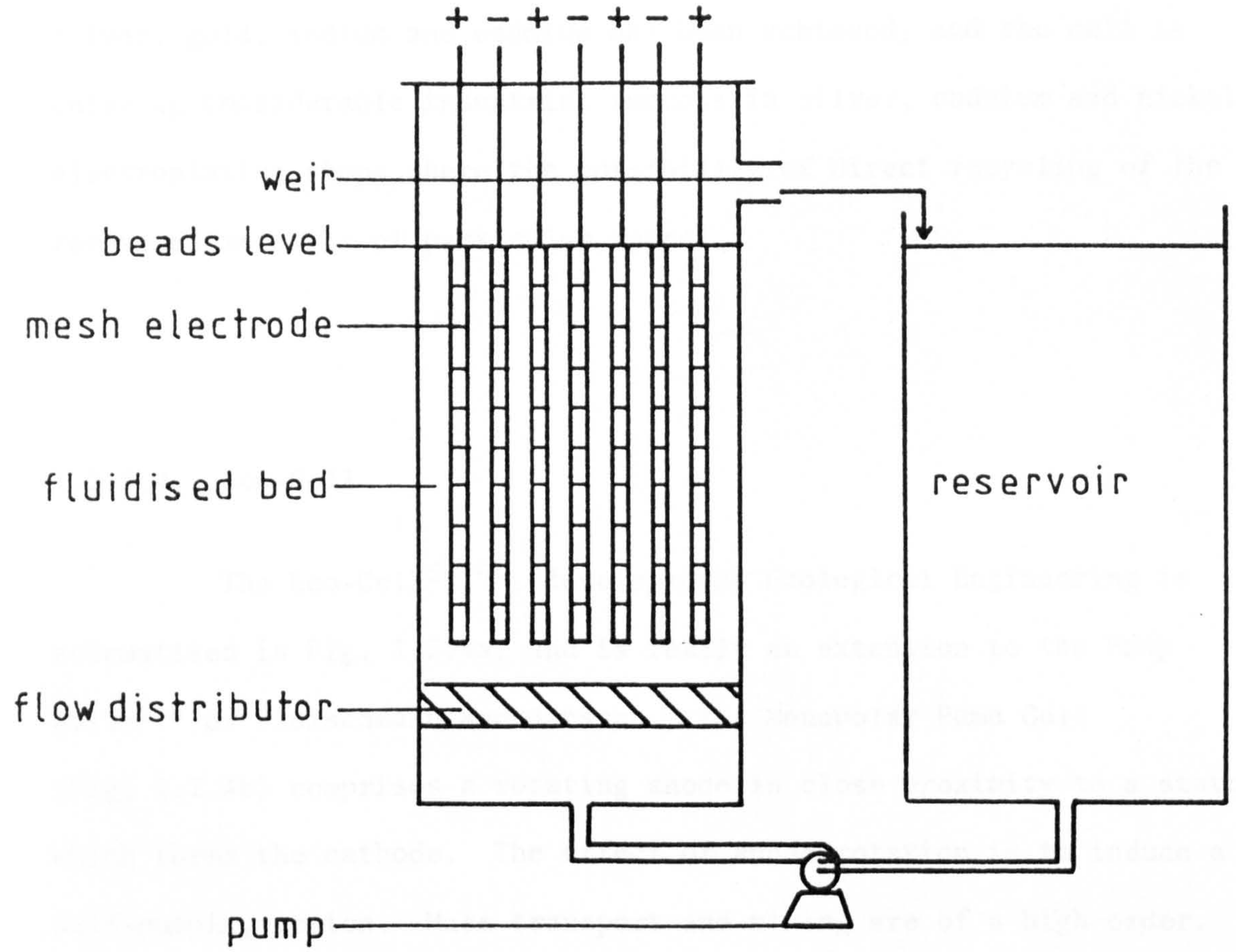

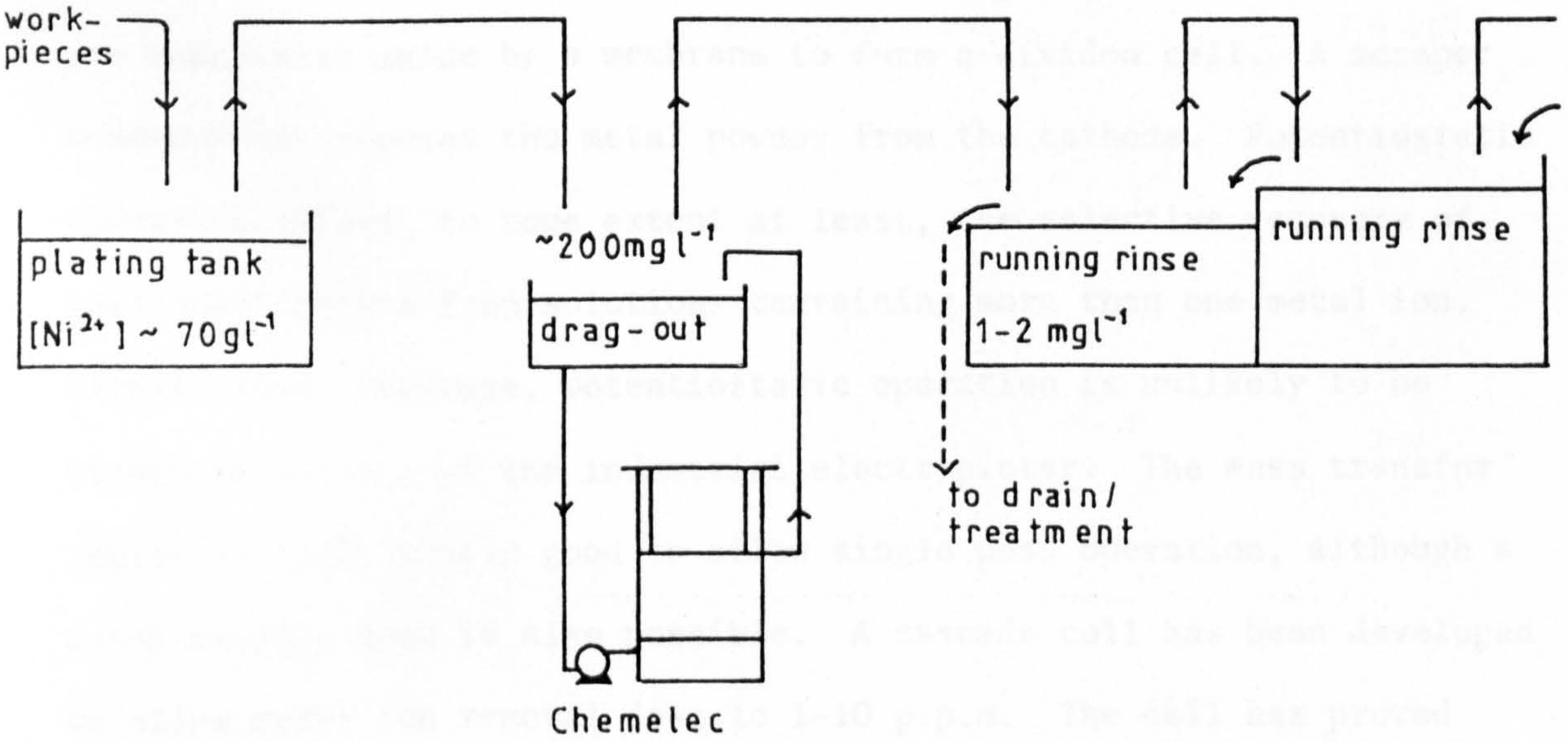

Fig. 1.2.3 (a) Components of the Chemelec Cell®

(b) Operation of the Cell

silver, gold, indium and cadmium has been achieved, and the cell is enjoying considerable industrial success in silver, cadmium and nickel electroplating shops where the possibility of direct recycling of the recovered metal is of particular appeal.

1.2.5.4 Eco-Cell

The Eco-Cell[54-60], developed by Ecological Engineering is schematised in Fig. 1.2.4a, and is really an extension to the Pump Cell[61-6] of Fleischmann and Jansson. The Monopolar Pump Cell (Fig. 1.2.4b) comprises a rotating anode in close proximity to a stator which forms the cathode. The effect of anode rotation is to induce a self-pumping action. Mass transport and mixing are of a high order. A metal powder is formed which detaches itself from the electrode under the influence of tangential shear forces. Unlike the Eco-Cell, however, the Pump Cell remains commercially unexploited.

The Eco-Cell differs from the Pump Cell in that the rotating disc is replaced by a rotating cylinder cathode which is separated from its concentric anode by a membrane to form a divided cell. A scraper continuously removes the metal powder from the cathode. Potentiostatic operation allows, to some extent at least, the selective recovery of particular metals from solutions containing more than one metal ion. Despite this advantage, potentiostatic operation is unlikely to be viewed favourably by the industrial electroplater. The mass transfer régime is sufficiently good to allow single pass operation, although a batch recycle mode is also possible. A cascade cell has been developed to allow metal ion removal down to 1-10 p.p.m. The cell has proved commercially viable and remains the main rival to the Chemelec Cell®.

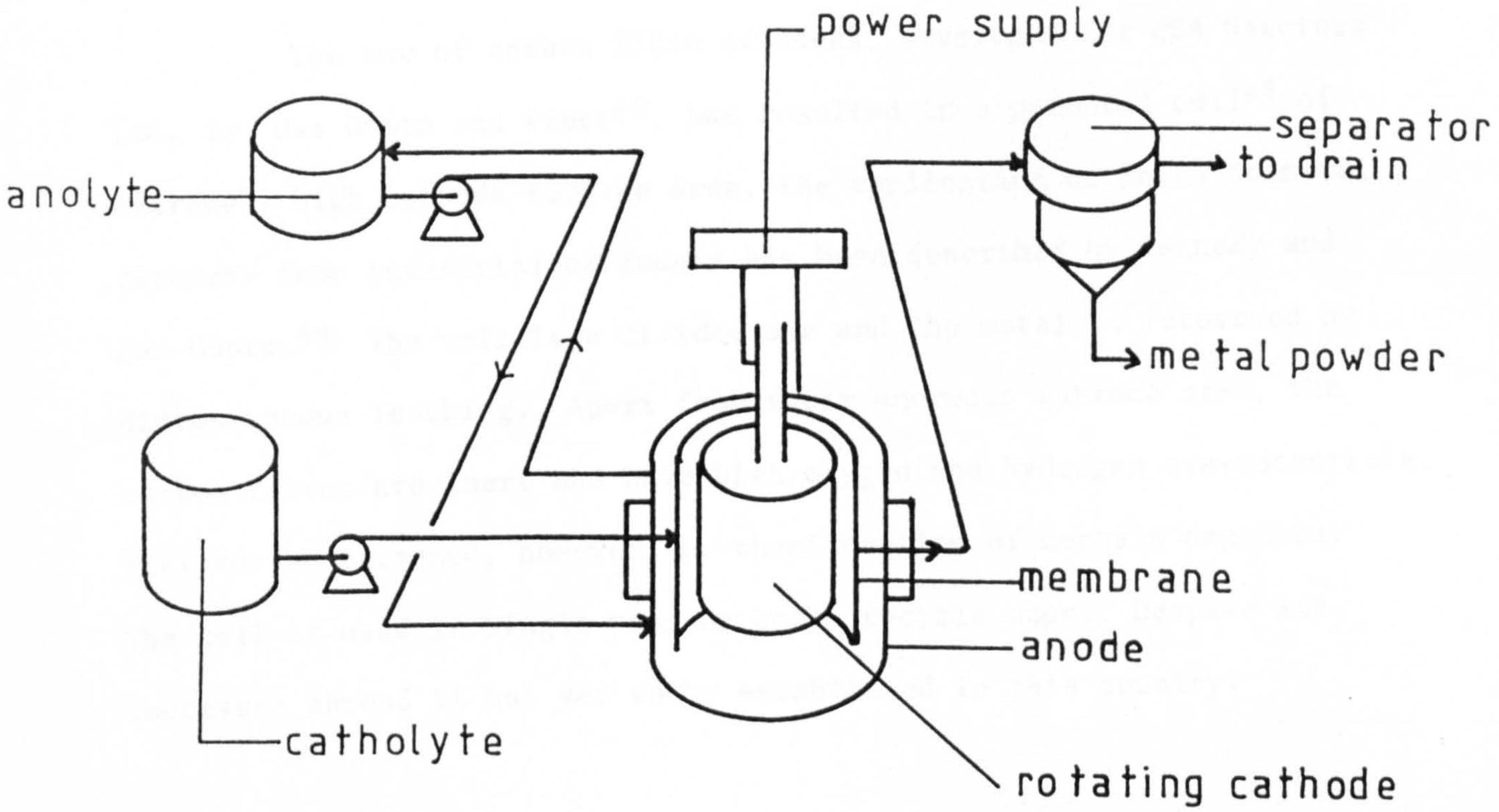

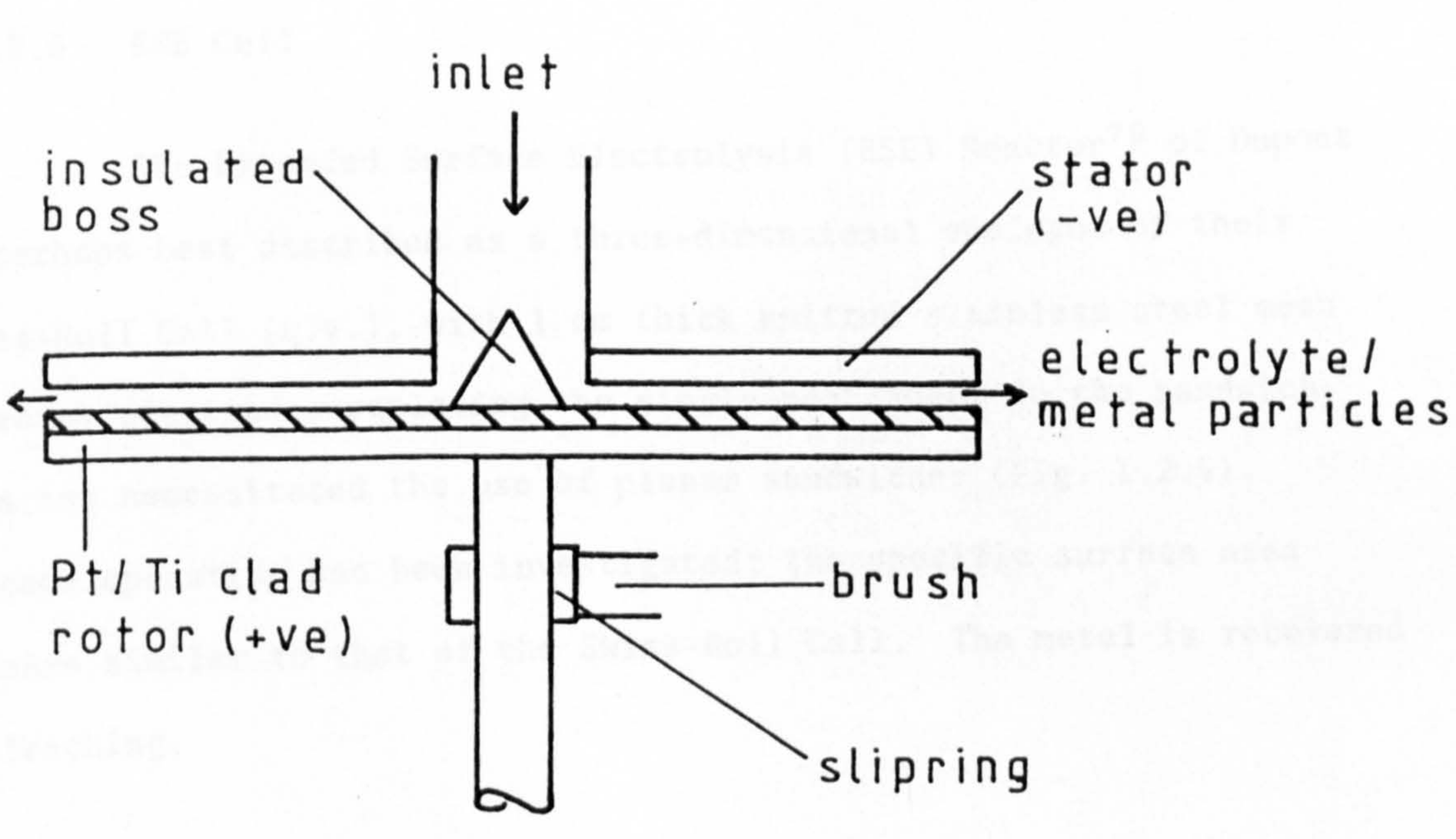

Fig. 1.2.4 (a) Eco-Cell

(b) Monopolar Pump Cell

1.2.5.5 HSA Reactor

The use of carbon fibre cathodes, developed for HSA Reactors Ltd. by Das Gupta and Fleet[67], has resulted in a patented cell[68] of extremely high cathode surface area, the application of which to metal recovery from industrial effluents has been described by Kennedy and Das Gupta.[69] The cell is a divided one and the metal is recovered by discontinuous leaching. Apart from their enormous surface area, the carbon fibres are inert and have high oxygen and hydrogen overpotentials. They may be poisoned, however, by chemisorption of certain organics. The cell is used in single pass or batch recycle mode. Despite its successes abroad it has yet to be established in this country.

1.2.5.6 ESE Cell

The Extended Surface Electrolysis (ESE) Reactor[70] of Dupont is perhaps best described as a three-dimensional analogue of their Swiss-Roll Cell (q.v.), with 1 cm thick knitted stainless steel mesh (porous) electrodes replacing the single mesh/sheet in the sandwich. This has necessitated the use of planar sandwiches (Fig. 1.2.5). Cascade operation has been investigated; the specific surface area appears similar to that of the Swiss-Roll Cell. The metal is recovered by leaching.

1.2.5.7 Parallelepiped Packed Bed Cell

The Parallelepiped Cell of Kreysa[71-2] is a particularly interesting example of a packed bed cell. It is shown diagramatically

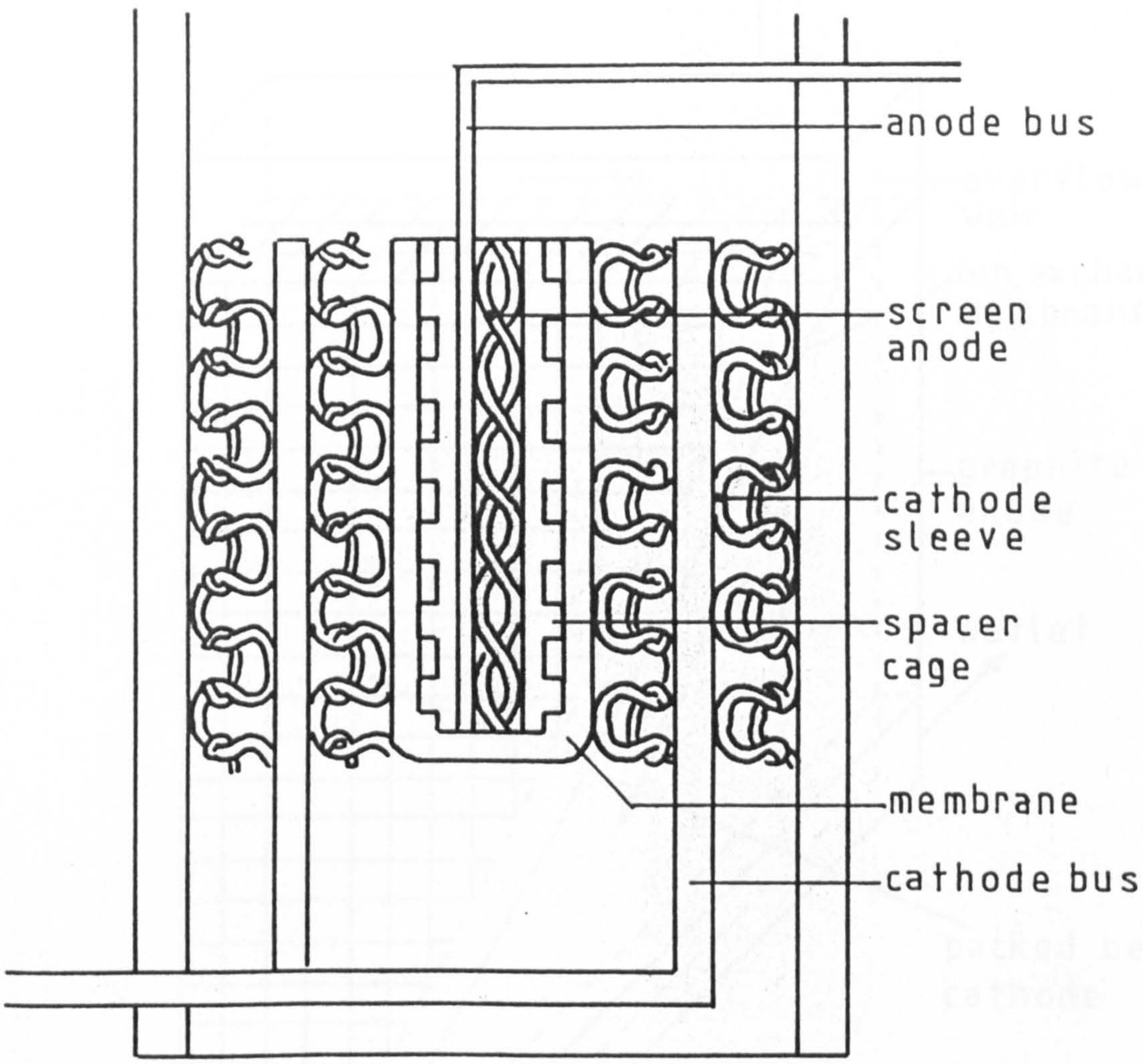

Fig. 1.2.5 E.S.E. Cell

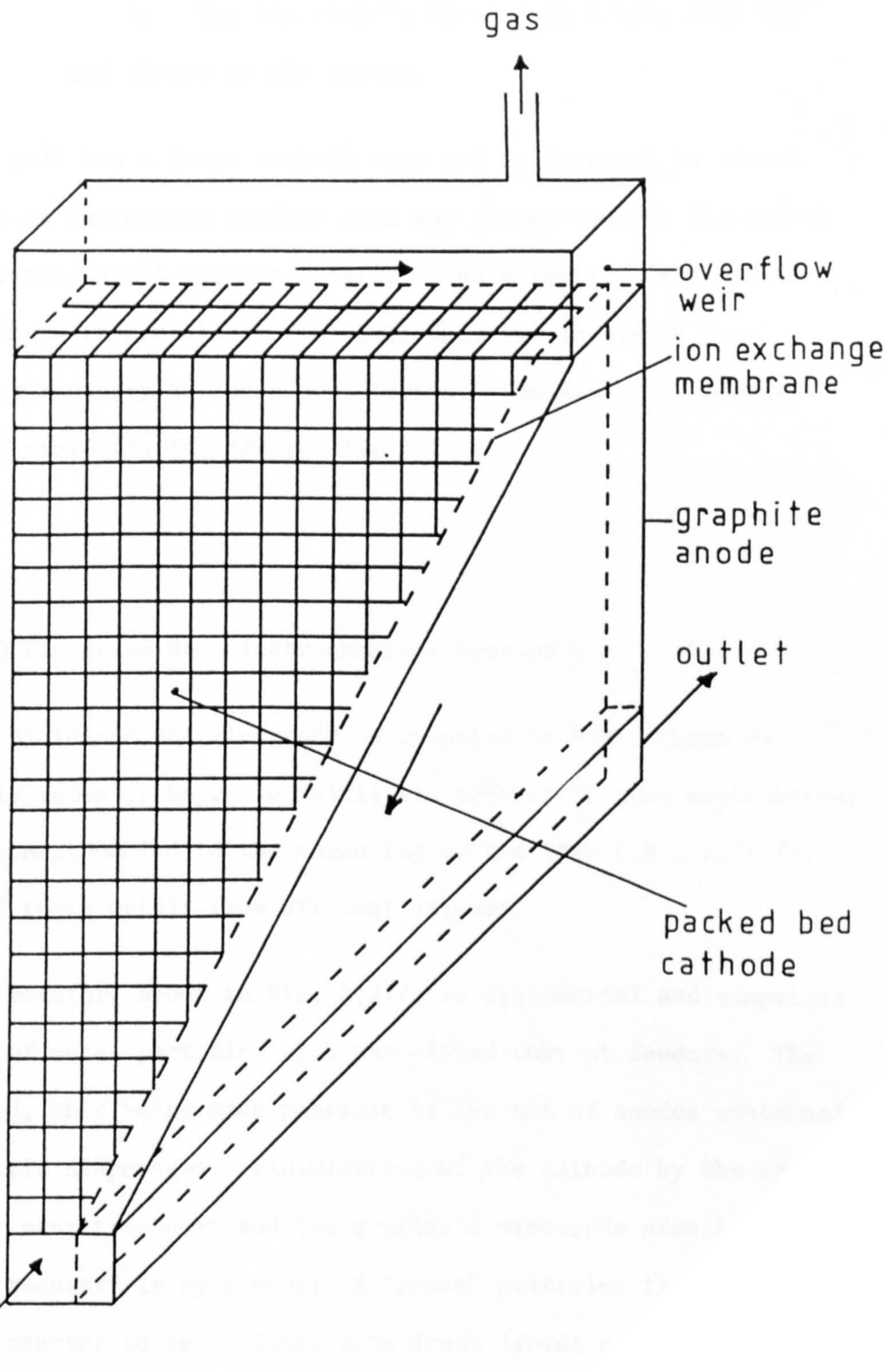

Fig. 1.2.6 Parallelepiped Cell

in Fig. 1.2.6. The electrolyte is pumped through the inlet and percolates upwards through a packed bed of carbon granules. The bed is separated from the anode compartment by an ion exchange membrane; the anode is planar graphite. The electrolyte flows over a weir into the anode compartment and thence to the outlet.

The cell has a large cathode area and is designed in such a was as to have an increasing surface area and volume towards the outlet causing a decrease in the current density. The potential drop across the reactor length is minimised. The cell operates in single pass mode, achieving recovery to sub-p.p.m. levels. The design is recent and has yet to prove itself commercially.

1.2.5.8 AKZO Fluidised Bed Electrochemical Reactor.

The Fluidised Bed Electrode as invented by Fleischmann et al[73-4] has only fairly recently begun to fulfil its promise in such applications. One such development has led to the marketing of the AKZO F.B.E.R.[75] for the removal of toxic metals from effluent streams.

The reactor, shown in Fig. 1.2.7, is cylindrical and comprises a cathode bed of metal particles with associated current feeders. The cell is divided, this being made possible by the use of anodes contained within concentric diaphragms. Fluidisation of the cathode by the catholyte enhances mass transport and the available electrode area is very large. Metal recovery is by removal of 'grown' particles from the bottom of the reactor to be replaced with fresh 'seed' particles added at the top. The design of the reactor is such that many of the traditional problems associated with fluidised bed electrodes have been overcome. The cell operates in single pass mode.

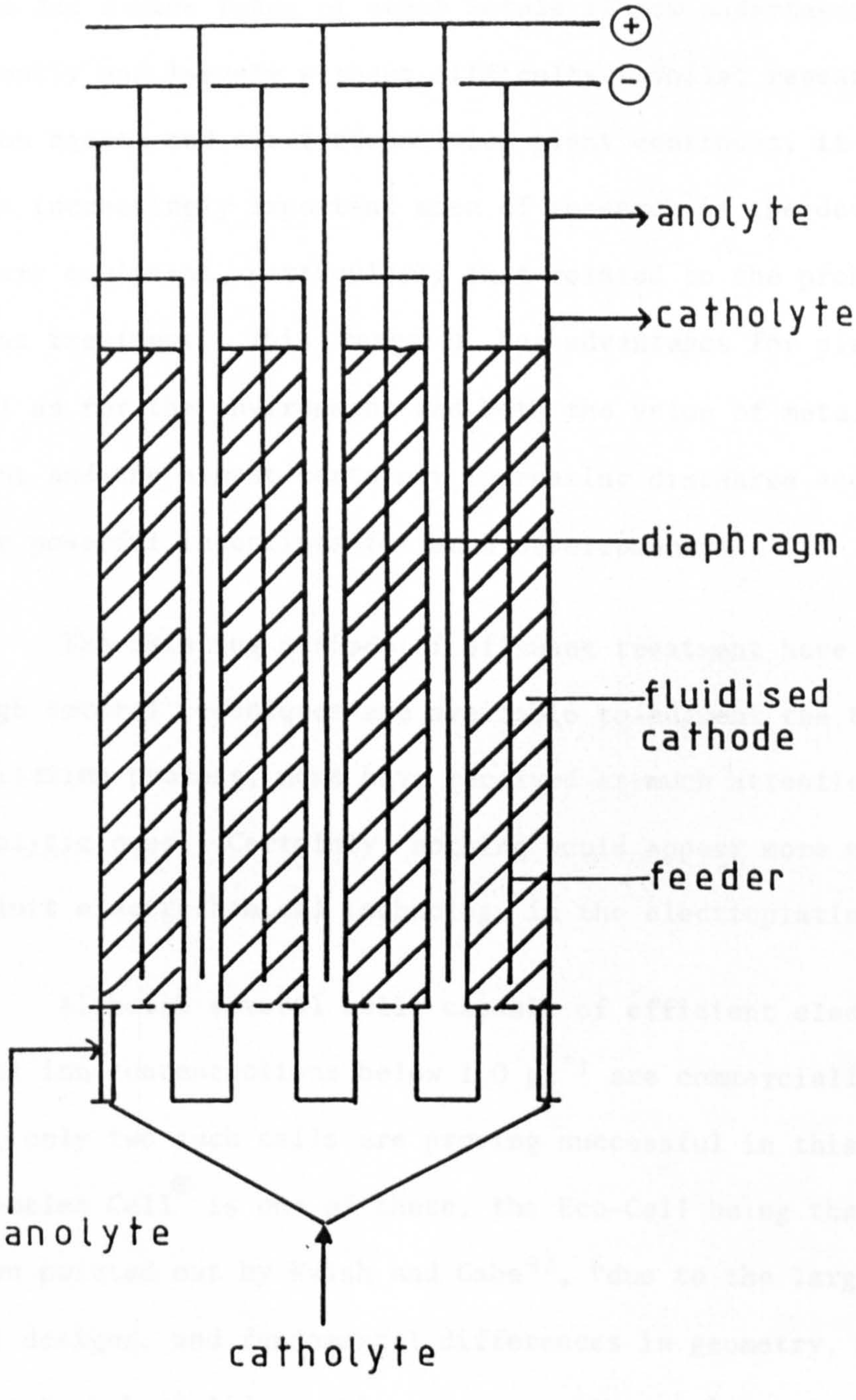

Fig. 1.2.7 AKZO Fluidised Bed Electrochemical Reactor

1.3 The Chemelec Cell® in Context

It has been argued that the electrodepositon of nickel, cadmium and a wide range of other metals is now undertaken routinely, efficiently and largely without difficulty. Whilst research into addition agents and electrodeposition plant continues, it is apparent that an increasingly important area of research is the development of ancillary equipment, particularly that related to the problem of effluent treatment. This research has advantages for plant economy as well as for the environment and both the value of metal lost to effluent and the almost certainly increasing discharge and water costs provide powerful incentives for such developments.

The existing methods of effluent treatment have been described. Although several techniques are available to augment the traditional precipitation process, none have received as much attention as have the electrolytic ones. Certainly, nothing would appear more natural than to exploit electrochemical technology in the electroplating industry!

Although several cells capable of efficient electrodeposition at metal ion concentrations below 1.0 gl^{-1} are commercially available abroad, only two such cells are proving successful in this country. The Chemelec Cell® is one of these, the Eco-Cell being the other. As has been pointed out by Walsh and Gabe[33], "due to the large spectrum of cell designs, and fundamental differences in geometry, it is not possible to make valid quantitative comparisons without referring to several indices of performance".

PROPERTY	CHEMELEC CELL®	ECO-CELL
Cell Geometry	Planar	Cylindrical
Classification[34]	Stationary 2-D*	Dynamic 2-D
Form of metal	Electroplate	Powder
Normally divided?	No	Yes
Control	Galvanostatic	Potentiostatic
Operating mode	Batch recycle	Single pass/ Batch recycle

TABLE 1.1. Comparisons of Chemelec Cell® & Eco-Cell Designs

The fundamental design differences between the Chemelec Cell® and the Eco-Cell are apparent from Table 1.1. A valid quantitative comparison of the two cells cannot be made, but some critical evaluation is possible. In particular it should be noted that the Eco-Cell is capable of efficient metal removal down to 1-10 p.p.m., whilst the normal operating concentration of the Chemelec Cell® is some 200 p.p.m. For the needs of the industrial electroplater, however, the simpler design and operation of the Chemelec Cell®, together with the more suitable form of its product, make it a more attractive propostion. In terms of effluent treatment, a Chemelec Cell® could be followed by an Eco-Cell.[76] The Chemelec Cell® would reclaim the majority of the metal from the drag-out (maintaining it at ∿ 200 p.p.m.) and the over-flow passed on to the Eco-Cell which would render it suitable for discharge. Unfortunately, the capital cost of such an arrangement is prohibitively high.

---

* the term 'stationary' refers to the electrode and not the electrolyte.

It follows that careful optimisation of the Chemelec Cell® and an understanding of the mechanisms by which electrodepostion occurs will benefit the commercial viability of the cell and this thesis represents a first attempt in this direction.

CHAPTER TWO

THEORETICAL PRINCIPLES

2.1 The electrode/electrolyte interphase

The region between a solid electrode and the bulk of an electrolyte solution is known as the electrode/electrolyte interphase or, more commonly, the electrical double layer. It is, as the term suggests, a region whose physical properties are intermediate between those of the two phases. As charge transfer (the passage of electrons from one phase to the other) must take place across this interphase, it is clearly important to possess a model of this region if one is to gain an understanding of charge transfer processes. However, since this thesis does not dwell on the study of the electrical double layer per se, it will suffice to limit discussion to a general account of the various models which have been proposed, without recourse to detailed quantitative arguments.

The historical origins of a model for the electrical double layer may be found in the works of Helmholtz[77] and Quincke[78], who perceived the interphase as consisting of two fixed layers of equal and opposite charge (Fig. 2.1.1a), one residing on the electrode itself and the other at a fixed distance from the electrode on the solution side of the interphase. This distribution of charge is analogous to that in a parallel plate condenser and is responsible for the use of the term 'double layer' for the electrode/electrolyte interphase. The variation of the Galvani potential, ϕ, with distance from the electrode, x, is given in Fig. 2.1.1b. By analogy with electrical theory, the charge density, σ, may be given by:

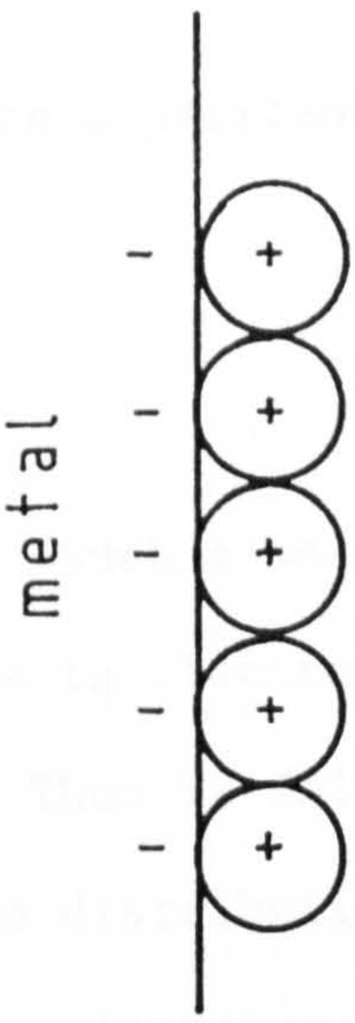

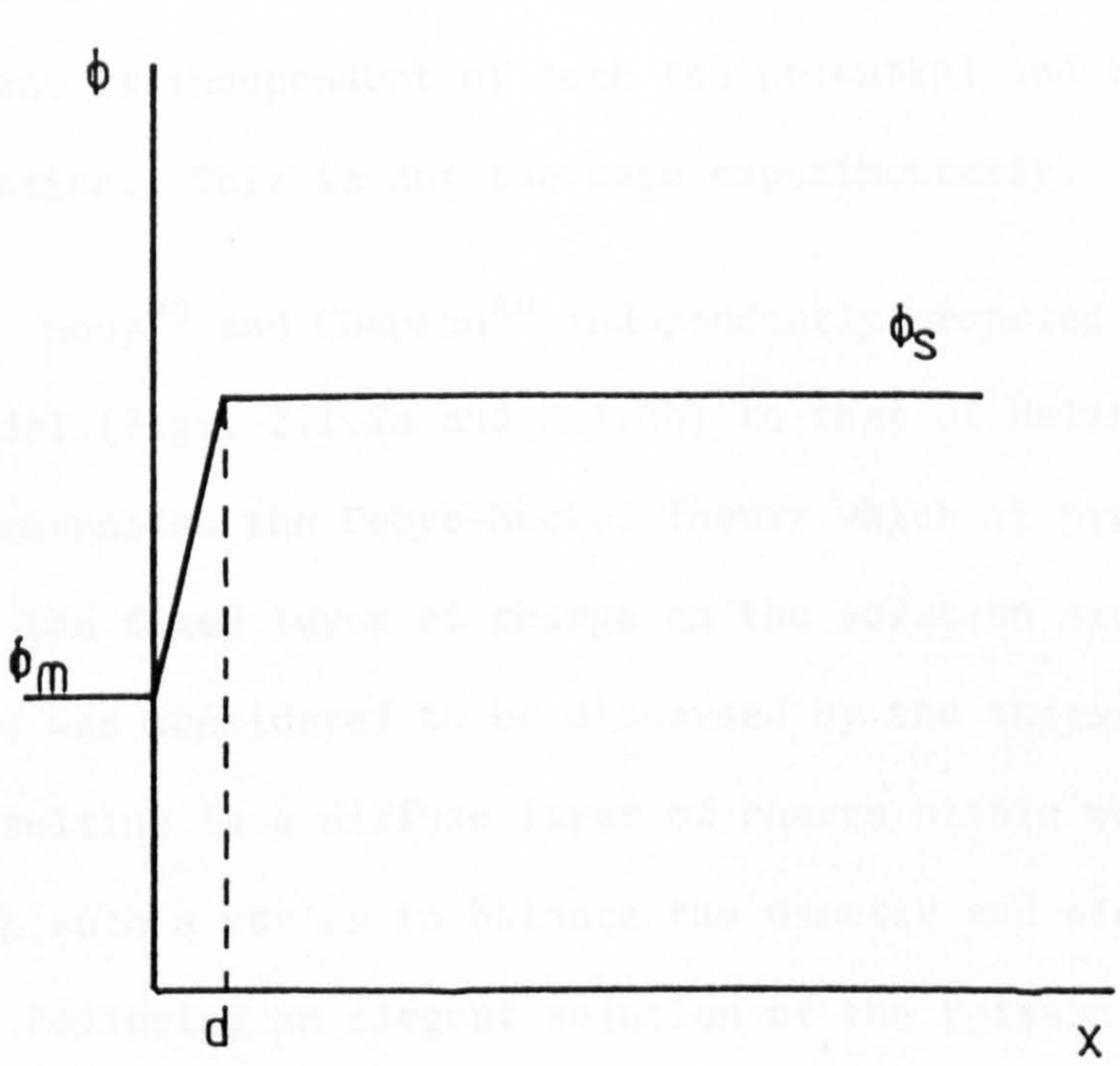

Fig. 2.1.1 (a) Helmholtz Model of the Double Layer

(b) Potential Distribution corresponding to (a)

$$\sigma = \frac{\varepsilon\varepsilon_o}{d} \cdot \Delta\phi \qquad (2.1.1)$$

whence the capacitance is:

$$c_c = \frac{\partial\sigma}{\partial\Delta\phi} = \frac{\varepsilon\varepsilon_o}{d} \qquad (2.1.2)$$

Such a model, and indeed others, assumes that the separated charge is in electrostatic equilibrium and that no charge transfer occurs. Thus it follows that changes in the electrode potential merely alter the distribution of charge and that the double layer is entirely capacitive in nature. This is an unjustified assumption, as in most cases where a net charge resides on an electrode there will be at least a small current due to some faradaic process. Electrodes for which the assumption holds are termed 'ideally polarisable'. The Helmholtz model also predicts (equation 2.1.2) that the double layer capacitance is independent of both the potential and the electrolyte concentration. This is not the case experimentally.

Gouy[79] and Chapman[80] independently proposed a more sophisticated model (Figs. 2.1.2a and 2.1.2b) to that of Helmholtz. The model closely resembles the Debye-Hückel Theory which it preceded by a decade. The fixed layer of charge on the solution side of the electrode was considered to be dispersed by the thermal motion of the ions, resulting in a diffuse layer of charge within which rearrangement occurs in such a way as to balance the osmotic and electrostatic forces. Following an elegant solution of the Poisson-Boltzmann Equation in one dimension

$$\frac{d^2\phi}{dx^2} = \frac{F}{\varepsilon\varepsilon_o} \cdot \Sigma\, z_j c_j \cdot \exp(-\frac{z_j F\phi}{RT}) \qquad (2.1.3)$$

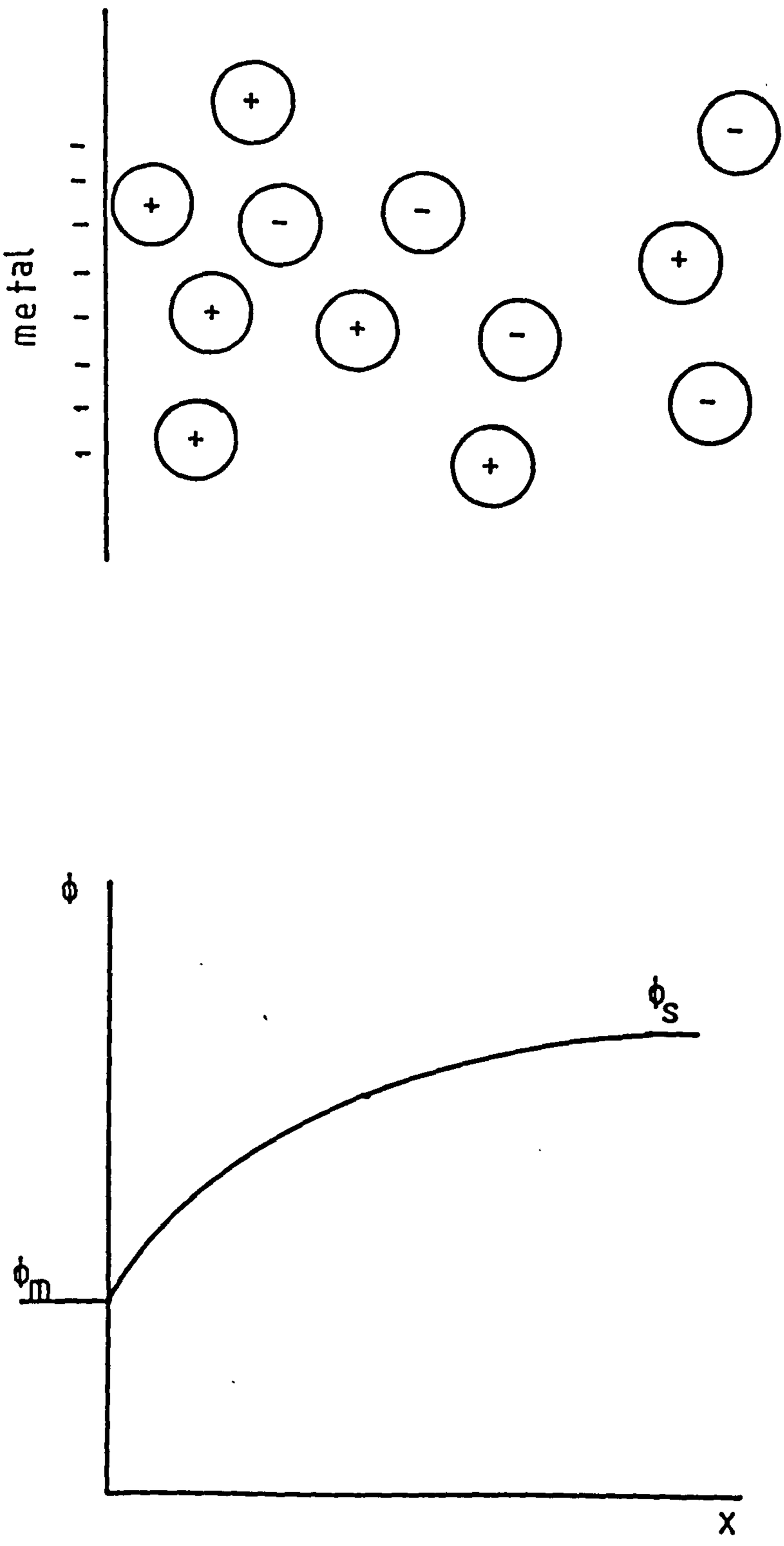

Fig. 2.1.2 (a) Gouy-Chapman Model of the Double Layer

(b) Potential Distribution corresponding to (a)

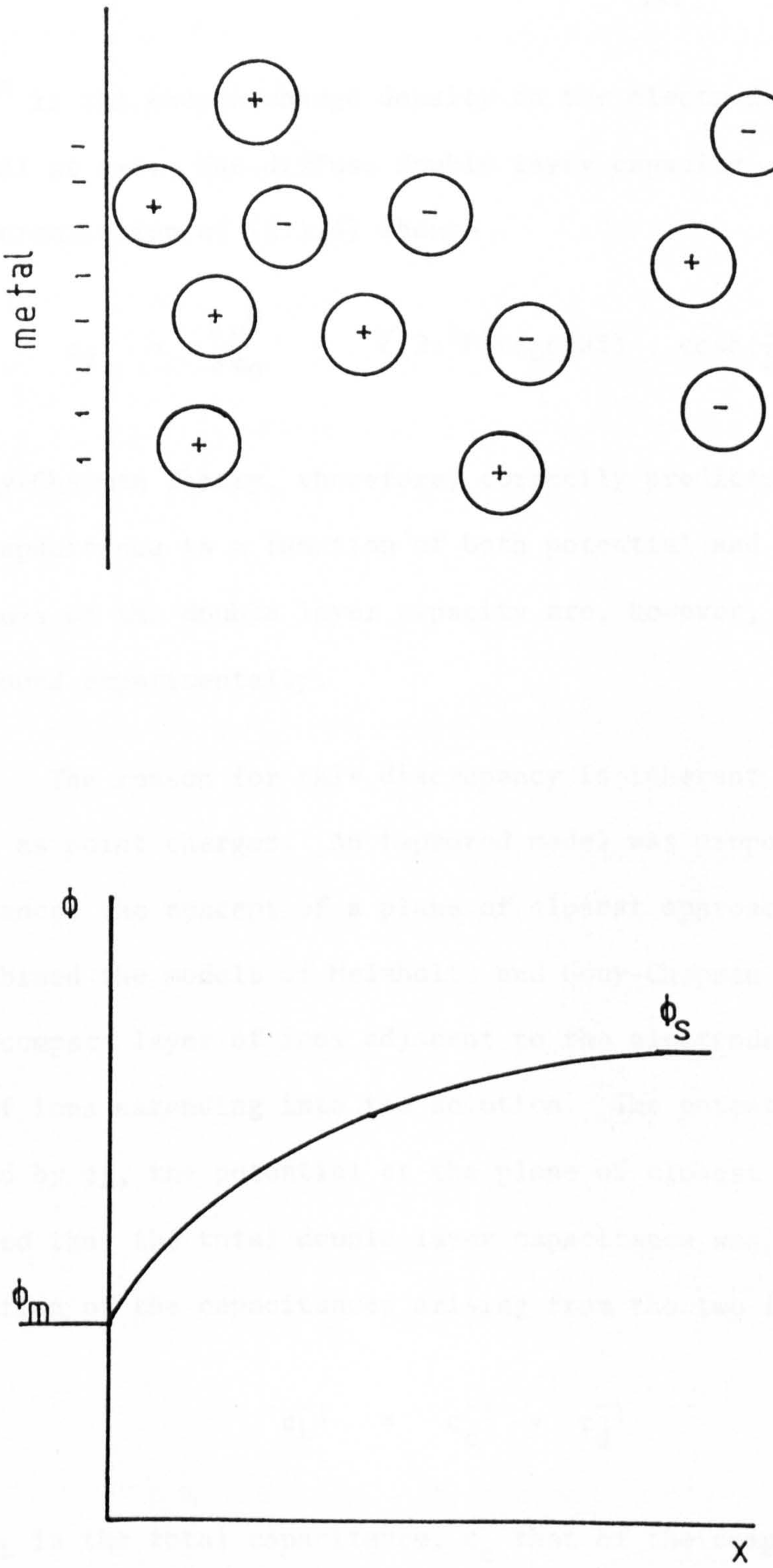

Fig. 2.1.2 (a) Gouy-Chapman Model of the Double Layer

(b) Potential Distribution corresponding to (a)

they obtain, for a symmetrical electrolyte,

$$\sigma^m = \surd(8RT\varepsilon\varepsilon_o c) \cdot \sinh(\frac{zF\phi_o}{2RT}) \qquad (2.1.4)$$

where σ^m is the excess charge density on the electrode and ϕ_o is the potential at x=o. The diffuse double layer capacity, c_d, is obtained on differentiation of (2.1.4) whence

$$c_d = \frac{\partial \sigma^m}{\partial \phi_o} = \surd(2z^2F^2\varepsilon\varepsilon_o c/RT) \cdot \cosh(\frac{zF\phi_o}{2RT}) \qquad (2.1.5)$$

The Gouy-Chapman Theory, therefore, correctly predicts that the double layer capacitance is a function of both potential and concentration. The values of the double layer capacity are, however, in excess of those found experimentally.

The reason for this discrepancy is inherent in the treatment of ions as point charges. An improved model was proposed by Stern[81] who advanced the concept of a plane of closest approach to the electrode and combined the models of Helmholtz and Gouy-Chapman by postulating both a compact layer of ions adjacent to the electrode and a diffuse layer of ions extending into the solution. The potential ϕ_o is now replaced by ϕ_2, the potential at the plane of closest approach. He suggested that the total double layer capacitance was due to the series combination of the capacitances arising from the two layers, viz.,

$$c_L^{-1} = c_c^{-1} + c_d^{-1} \qquad (2.1.6)$$

where c_L is the total capacitance, c_c that of the compact and c_d of the diffuse layer. It follows that in dilute solution and at potentials close to the point of zero charge the double layer capacitance is

essentially that of the diffuse layer (and thus potential and concentration dependent) whilst in more concentrated solutions and at higher polarisations the double layer capacitance is essentially that of the compact layer and therefore independent of these quantities. Whilst this model is a considerable improvement over the Gouy-Chapman approach, and the theoretical values of the double layer capacitance are in better agreement with experiment, discrepancies still exist. Not least among these is the fact that the capacitance of the compact layer is not entirely independent of potential. The model of Stern is shown in Fig. 2.1.3a and the associated potential distribution in Fig. 2.1.3b. It was Stern, also, who distinguished between ions at their closest distance of approach and specifically adsorbed anions.

A further refinement, admitted by Stern[81], was developed by Grahame[82] who recognised two planes of closest approach. The inner Helmholtz plane was defined as the plane passing through the centres of adsorbed anions whilst the outer Helmholtz plane was that passing through the centres of hydrated cations at their closest distance of approach. Fig. 2.1.4a illustrates this concept, and the corresponding potential distribution is given in Fig. 2.1.4b. The compact layer is bounded by the outer Helmholtz plane. This model forms the basis of our understanding of the double layer. However, it is inadequate in many respects and further, more sophisticated models have been proposed.

According to Bockris, Devanathan and Müller[83] many of the remaining discrepancies between theory and experiment can be overcome by the adoption of a model such as that shown in Fig. 2.1.5. The rôle of the solvent is considered in detail. According to the authors, the

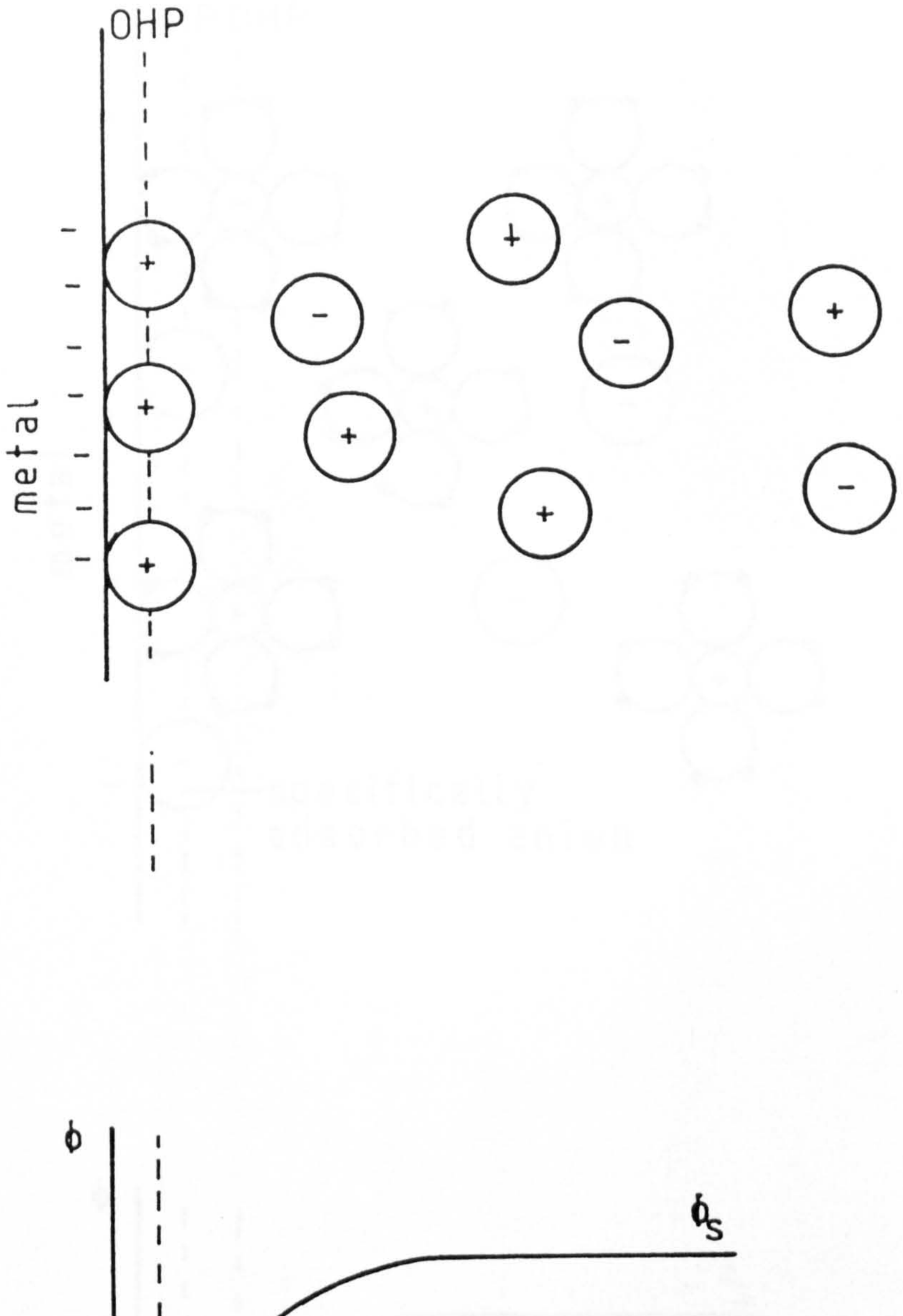

Fig. 2.1.3 (a) Stern Model of the Double Layer

(b) Potential Distribution corresponding to (a)

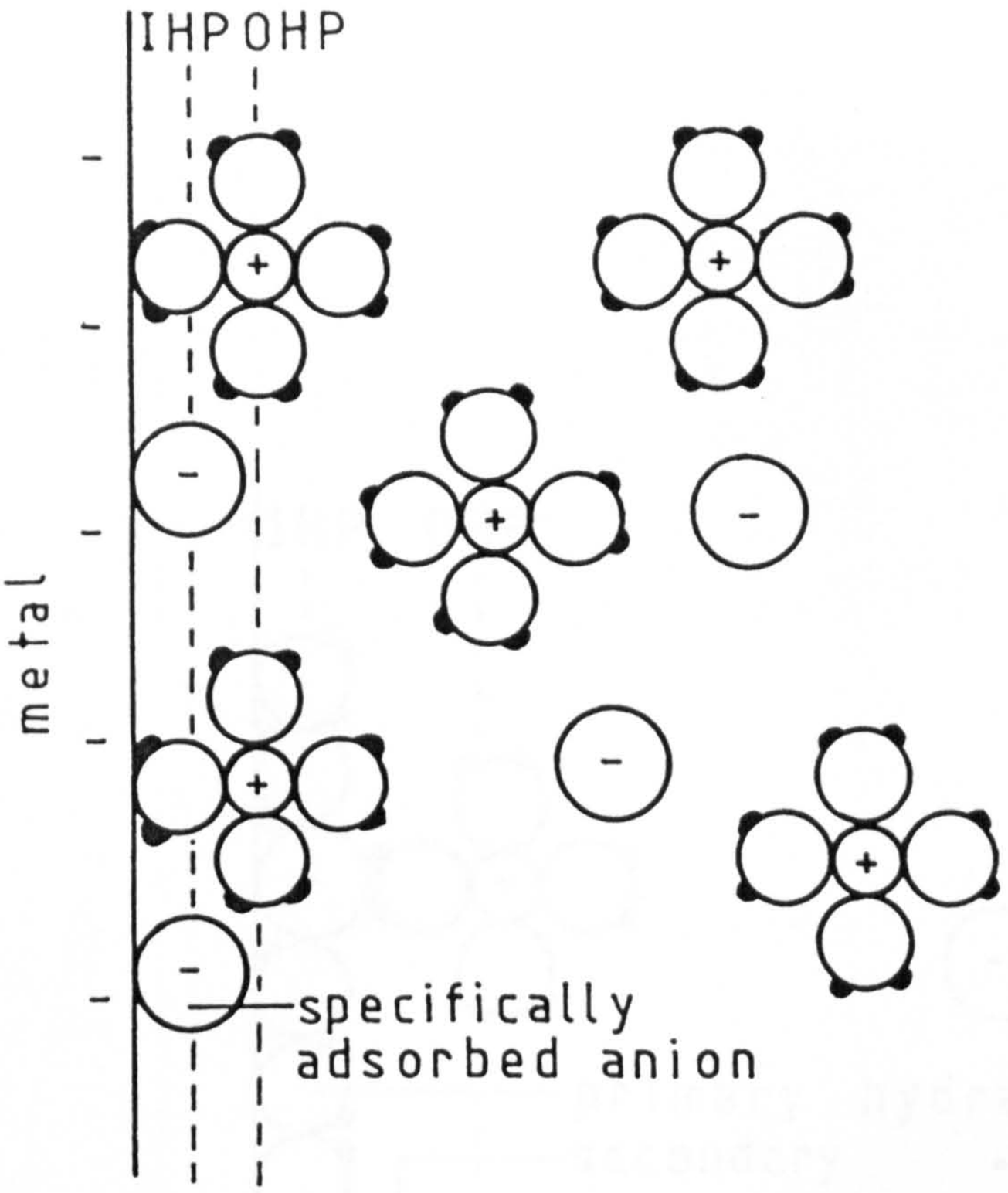

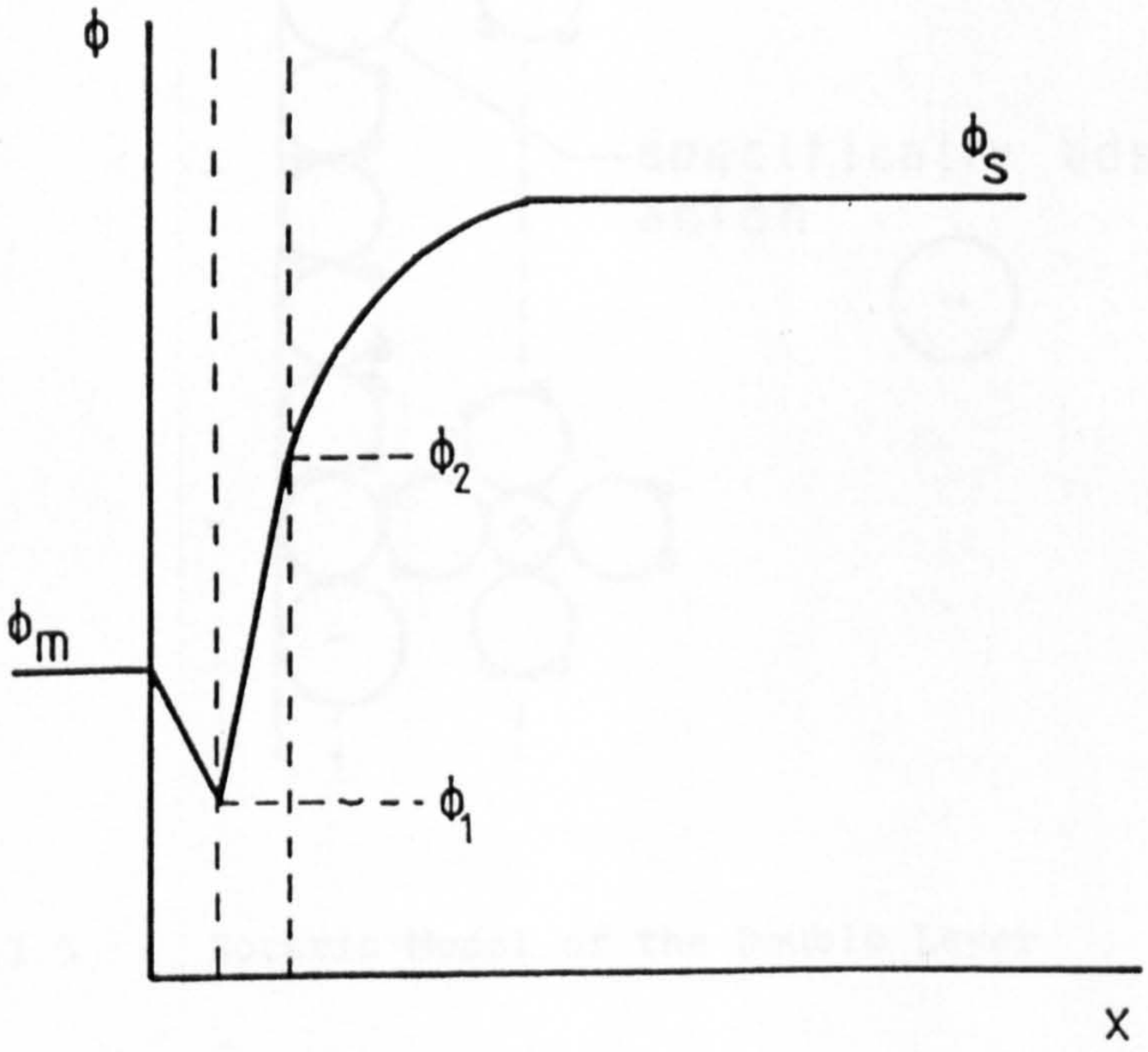

Fig. 2.1.4 (a) Grahame Model of the Double Layer

(b) Potential Distribution corresponding to (a)

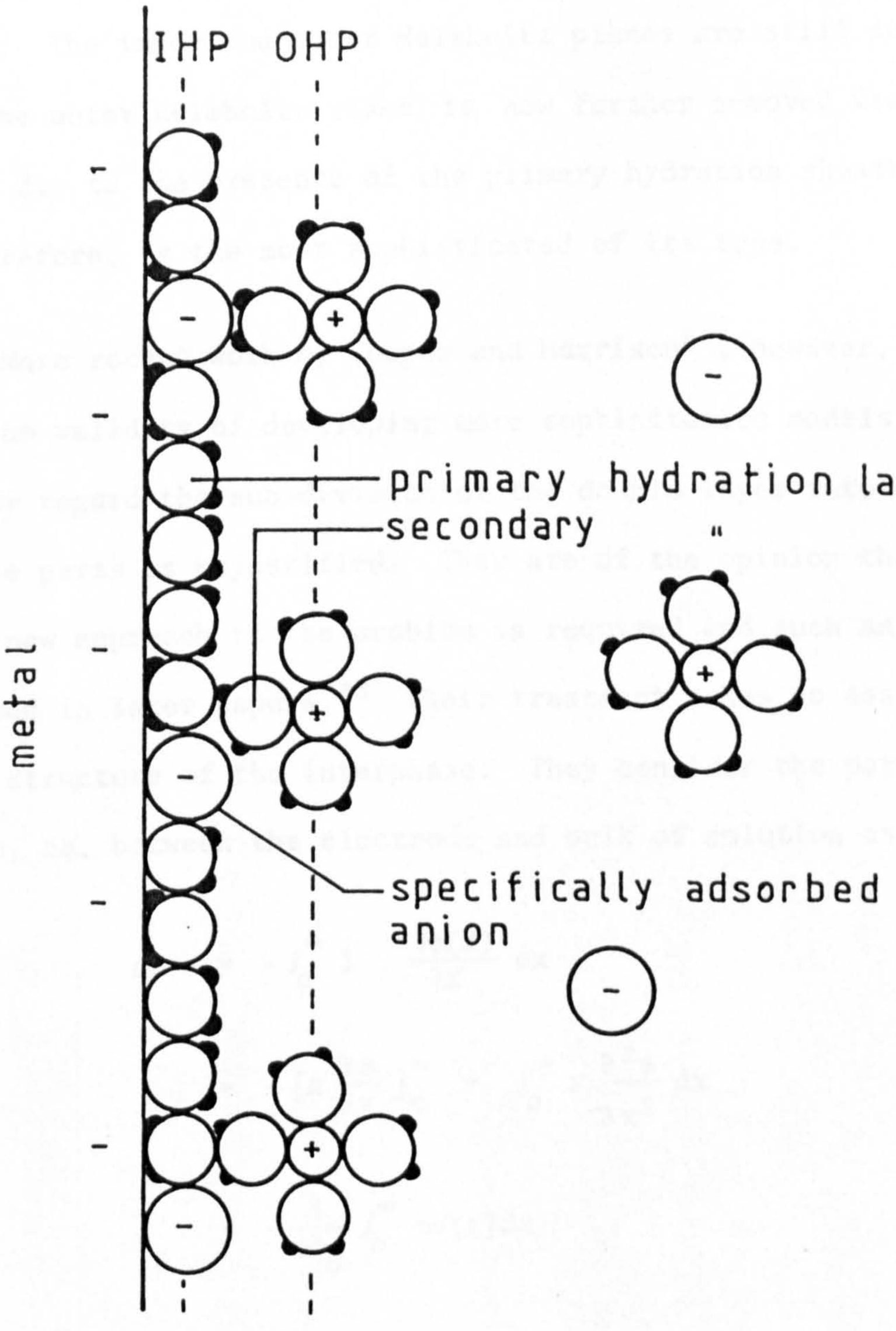

Fig. 2.1.5 Bockris Model of the Double Layer

electrode is bounded by a primary hydration layer of oriented dipoles. This layer is field independent and of low dielectric constant and may be penetrated by specifically adsorbed anions. Such anions would possess little or no hydration energy. Outside this layer is a second, comprising the water of hydration of solvated cations at their closest distance of approach. The secondary hydration layer is of intermediate dielectric. The inner and outer Helmholtz planes are still defined, although the outer Helmholtz plane is now further removed from the electrode, due to the presence of the primary hydration sheath. This model, therefore, is the most sophisticated of its type.

More recent work by Cooper and Harrison[84], however, has cast doubt on the validity of developing more sophisticated models of this type. They regard the sub-division of the double layer into compact and diffuse parts as unjustified. They are of the opinion that a radically new approach to the problem is required and such an approach is developed in later papers.[85] Their treatment makes no assumptions about the structure of the interphase. They consider the potential difference, $\Delta\phi$, between the electrode and bulk of solution as:

$$\Delta\phi = -\int_o^\infty 1 \cdot \frac{\partial\phi(x)}{\partial x}\,dx$$

$$= -\left[x\,\frac{\partial\phi}{\partial x}\right]_o^\infty + \int_o^\infty x\,\frac{\partial^2\phi}{\partial x^2}\,dx$$

$$= -\frac{1}{\varepsilon\varepsilon_o}\int_o^\infty x\sigma(x)dx \qquad (2.1.7)$$

where the symbols have their usual meanings. The charge density is simply related to the excess distributions $\sigma_{\pm}(x)$ of anions and cations at the interface with respect to bulk, whence,

$$\Delta\phi \quad = \quad \frac{e}{\varepsilon\varepsilon_o}\left[\int_o^\infty x\sigma_-(x)dx - \int_o^\infty x\sigma_+(x)dx\right]. \qquad (2.1.8)$$

They define the surface ionic excesses, $n_\pm$, and their mean distances, $\langle x_\pm \rangle$, from the electrode by:

$$n_\pm \quad = \quad \int_o^\infty \sigma_\pm(x)dx \qquad (2.1.9)$$

$$\langle x_\pm \rangle \quad = \quad \frac{1}{n_\pm}\int_o^\infty x\sigma_\pm(x)dx \qquad (2.1.10)$$

whence,

$$\Delta\phi \quad = \quad \frac{e}{\varepsilon\varepsilon_o}\left[n_-\langle x_-\rangle - n_+\langle x_+\rangle\right] \qquad (2.1.11)$$

They further define the mean distance, $\langle x \rangle$, of the net distributed charge as:

$$\langle x \rangle \quad = \quad \frac{\int_o^\infty x\sigma(x)dx}{\int_o^\infty \sigma(x)dx}$$

$$\equiv \quad \frac{en_+\langle x_+\rangle - en_-\langle x_-\rangle}{(en_+ - en_-)} \qquad (2.1.12)$$

So that,

$$\Delta\phi \quad = \quad \frac{(en_- - en_+)\langle x\rangle}{\varepsilon\varepsilon_o} = \frac{\sigma^m\langle x\rangle}{\varepsilon\varepsilon_o} \qquad (2.1.13)$$

The specific differential capacitance is then,

$$C_L \quad = \quad \frac{\partial\sigma^m}{\partial\phi}$$

$$= \quad \frac{\varepsilon\varepsilon_o}{\langle x\rangle + \sigma^m(d\langle x\rangle/d\sigma^m) - \sigma^m(\langle x\rangle/\varepsilon\varepsilon_o)(d\varepsilon\varepsilon_o/d\sigma^m)} \qquad (2.1.14)$$

This equation may be simplified depending on the circumstances, but in its present form is independent of any specific molecular model for the excess distributions $\sigma_{\pm}(x)$. Notice that the excess distributions, $\sigma_{\pm}(x)$, are required in order to obtain $n_{\pm}$, $\langle x_{\pm} \rangle$ and hence $\langle x \rangle$ from (2.1.9), (2.1.10) and (2.1.12). The quantity $\langle x \rangle$ therefore requires a knowledge of σ_{+} based, preferably, on sound and detailed statistical theories.

In conclusion, whilst the model of Cooper and Harrison is both simple and theoretically elegant and allows more accurate predictions of double layer properties, the need for detailed statistical theories and the absence of a physical model lessen its usefulness to the average electrochemist, for whom the model of Grahame suffices.

2.2 Charge Transfer

A general charge transfer reaction may be represented by the equation:

$$O + ze \underset{\overleftarrow{k}}{\overset{\overrightarrow{k}}{\rightleftharpoons}} R \qquad (2.2.1)$$

where O is an oxidised and R a reduced species; $\overrightarrow{k}$ the cathodic and $\overleftarrow{k}$ the anodic rate constant; z the number of electrons, e, transferred across the interphase in each charge transfer step. The transfer of charge in this way inevitably leads to the generation of electrical currents. We write

$$\overrightarrow{i} = zF\overrightarrow{k}c_O^s \qquad (2.2.2)$$

$$\overleftarrow{i} = zF\overleftarrow{k}c_R^s \qquad (2.2.3)$$

where $\overrightarrow{i}$, $\overleftarrow{i}$ are the cathodic and anodic partial current densities respectively and c_j^s the surface concentration of species j. It is clear that the net current density in an external circuit is given by the difference between the two partial current densities, viz.,

$$i = \overrightarrow{i} - \overleftarrow{i} = zF(\overrightarrow{k}c_O^s - \overleftarrow{k}c_R^s) \qquad (2.2.4)$$

At electrochemical equilibrium there is no net flow of current, hence the partial current densities must be equal. Under these conditions,

$$\overrightarrow{k}c_O^s = \overleftarrow{k}c_R^s \qquad (2.2.5)$$

The electrochemical rate constants $\vec{k}$, $\overleftarrow{k}$ may be seen to depend on the electrode potential, E, as follows. We apply the Nernst Equation[86] at the electrode surface with the assumption of unit activity coefficients, hence,

$$E_r = E^{\ominus} + \frac{RT}{zF} \ln \{c_O^S / c_R^S\} \qquad (2.2.6)$$

Here, E_r is the reversible potential and $E^{\ominus}$ the standard electrode potential. Substituting from (2.2.5) we obtain, for (2.2.6),

$$E_r = E^{\ominus} + \frac{RT}{zF} \ln \{\overleftarrow{k}/\vec{k}\} \qquad (2.2.7)$$

whence, upon differentiation,

$$\partial E_r = \frac{RT}{zF} \partial \ln \{\overleftarrow{k}/\vec{k}\} \qquad (2.2.8)$$

$$\Rightarrow \quad \frac{RT}{zF} \left[\frac{\partial \ln \{\overleftarrow{k}\}}{\partial E_r} - \frac{\partial \ln \{\vec{k}\}}{\partial E_r}\right] = 1 \qquad (2.2.9)$$

If we set,

$$\frac{RT}{zF} \cdot \frac{\partial \ln \{\overleftarrow{k}\}}{\partial E_r} = 1-\alpha \qquad (2.2.10)$$

then,

$$\frac{RT}{zF} \cdot \frac{\partial \ln \{\vec{k}\}}{\partial E_R} = -\alpha \qquad (2.2.11)$$

Integrating (2.2.10) and (2.2.11) with respect to E_r from $E^{\ominus}$ to E we obtain, on rearrangement,

$$\overleftarrow{k} = \overleftarrow{k}_o \cdot \exp \{ zF(1-\alpha)(E-E^{\ominus})/RT\} \qquad (2.2.12)$$

$$\vec{k} = \vec{k}_o \cdot \exp \{ -zF\alpha(E-E^{\ominus})/RT\} \qquad (2.2.13)$$

where $\vec{k}_o$, $\overleftarrow{k}_o$ are constants which may be defined as the values of $\vec{k}$,$\overleftarrow{k}$ at $E=E^{\ominus}$. From (2.2.7), however, we see that at the standard electrode potential these constants must be equal. We may therefore replace these two constants by the single quantity k^o, known as the standard rate constant. Thus we write (2.2.12) and (2.2.13),

$$\overleftarrow{k} = k^o \cdot \exp\{zF(1-\alpha)(E-E^{\ominus})/RT\} \qquad (2.2.14)$$

$$\vec{k} = k^o \cdot \exp\{-zF\alpha(E-E^{\ominus})/RT\} \qquad (2.2.15)$$

Hence, the potential dependence of $\vec{k}$,$\overleftarrow{k}$ is apparent. Substituting into (2.2.4)

$$i = zFk^o[c_O^s \cdot \exp\{-zF\alpha(E-E^{\ominus})/RT\} - c_R^s \cdot \exp\{zF(1-\alpha)(E-E^{\ominus})/RT\}] \qquad (2.2.16)$$

At electrochemical equilibrium, however, we have seen that $\vec{i}$ and $\overleftarrow{i}$ are equal and we define the exchange current density, i_o, from (2.2.2) and (2.2.15) and from (2.2.3) and (2.2.14) whence,

$$i_o = zFk^o c_O^s \cdot \exp\{-zF\alpha(E_r-E^{\ominus})/RT\}$$

$$= zFk^o c_R^s \cdot \exp\{zF(1-\alpha)(E_r-E^{\ominus})/RT\} \qquad (2.2.17)$$

We may now write (2.2.16) in terms of the exchange current density, viz:

$$i = i_o[\exp\{-zF\alpha\eta_D/RT\} - \exp\{zF(1-\alpha)\eta_D/RT\}] \qquad (2.2.18)$$

where the charge transfer overpotential, η_D, is given by:

$$\eta_D = E - E_r \qquad (2.2.19)$$

Equation (2.2.18) is the well-known Erdey-Gruz and Volmer Equation[87], upon which the study of electrode kinetics is largely based.

The Erdey-Gruz and Volmer Equation is generally simplified in one of two ways. First, where the overpotential is small ($|\eta_D| << RT/F$) the exponentials may be expanded and terms of second and higher order may be neglected to give:

$$i = - i_o \cdot \frac{zF\eta_D}{RT} \qquad (2.2.20)$$

A plot if i versus η_D is, therefore, linear and passes through the origin. The slope of the curve determines the charge transfer resistance, θ, as:

$$\theta A = -1/(\partial i/\partial \eta_D)_{\eta_D = 0}$$

$$= \frac{RT}{zFi_o} \qquad (2.2.21)$$

Secondly, where the overpotential is large, the Erdey-Gruz and Volmer Equation reduces to the Tafel Equation.[88] This is achieved by neglecting one of the terms of (2.2.18), whence:

$$i = i_o \cdot \exp\{-zF\alpha\eta_D/RT\} \ , \ \eta_D << 0 \qquad (2.2.22)$$

$$i = -i_o \cdot \exp\{zF(1-\alpha)\eta_D/RT\} \ , \ \eta_D >> 0 \qquad (2.2.23)$$

These equations may be rearranged to give the Tafel Equation

$$\eta_D = a + b \log\{i\} \qquad (2.2.24)$$

where the constants a and b, related to α and i_o, are dependent on

whether an anodic or a cathodic reaction is under consideration.

Consideration of (2.2.6) and (2.2.18) yields the concentration dependence of i_o, viz:

$$i_o = zFk^o(C_O^s)^{1-\alpha}(C_R^s)^{\alpha} \qquad (2.2.25)$$

Where the process is reversible, the surface concentration may be replaced by the more easily accessible bulk concentration. Consideration of equations (2.2.21) and (2.2.25) leads to the relation:

$$\theta A = \frac{RT}{z^2F^2k^o} \cdot (c_O^b)^{\alpha-1}(c_R^b)^{-\alpha} \qquad (2.2.26)$$

whence a plot of $\ln\{\theta A\}$ versus $\ln\{c_O^b\}$ is expected to be linear, and:

$$\left(\frac{\partial \ln\{\theta A\}}{\partial \ln\{C_O^b\}}\right)_{\eta_D = 0} = \alpha - 1 \qquad (2.2.27)$$

Similarly, if we consider potentials reasonably close to the reversible potential, then (2.2.17) and (2.2.21) may be combined to give:

$$\theta A = \frac{RT}{z^2F^2k^oC_O^b} \exp\{zF\alpha(E-E^{\ominus})/RT\} \qquad (2.2.28)$$

whence a plot of $\ln\{\theta A\}$ versus E is expected to be linear and:

$$\frac{\partial \ln\{\theta A\}}{\partial E} = \frac{zF\alpha}{RT} \qquad (2.2.29)$$

Hence, α may be determined.

2.3 Mass Transport

It is often the case that an electrochemical reaction is limited by the supply of reactant to the electrode rather than by kinetic factors. Any study of electrode kinetics must, therefore, take full account of mass transport processes.

The flux of a species j to an electrode is given, in its most general form, by the Nernst-Planck Equation[89]:

$$\underline{J}_j = - D_j \nabla c_j - \frac{z_j F}{RT} \cdot D_j c_j \nabla \phi + c_j \underline{v} \qquad (2.3.1)$$

where $\underline{J}$ is the flux, D the diffusion coefficient and $\underline{v}$ the velocity profile, the other symbols having their usual meanings. The operator ∇ is defined:

$$\nabla = \underline{i} \frac{\partial}{\partial x} + \underline{j} \frac{\partial}{\partial y} + \underline{k} \frac{\partial}{\partial z} \qquad (2.3.2)$$

where $\underline{i}$, $\underline{j}$ and $\underline{k}$ are the unit vectors.

The three terms of (2.3.1) represent the three generally accepted modes of mass transfer, namely diffusion, migration and convection.

2.3.1 Migration

The movement of ions under the influence of an electrical potential gradient is known as migration. The majority of electrical current passing through the bulk of the solution does so by this

process. In order to minimise the contribution of migration to the flux of the electroactive species, solutions containing an excess of an inert supporting electrolyte are frequently encountered. Under these conditions, a considerable simplification of (2.3.1) accrues from the neglection of the second term of the equation.

2.3.2 Diffusion

Diffusion is the movement of ions under the influence of a concentration gradient. This is simply expressed in Fick's First Law[90]:

$$\underline{J}_j = - D_j \nabla c_j \qquad (2.3.3)$$

for the diffusional flux, $\underline{J}_j$. The time dependence of the concentration profile is given by Fick's Second Law[90]:

$$\frac{\partial c_j}{\partial t} = D_j \nabla^2 c_j \qquad (2.3.4)$$

where t is the time and ∇^2 is the Laplacian operator defined by:

$$\nabla^2 = \frac{\partial^2}{\partial x^2} + \frac{\partial^2}{\partial y^2} + \frac{\partial^2}{\partial z^2} \qquad (2.3.5)$$

The solution of Fick's Laws is a common problem in electrochemistry, and clearly depends on the choice of boundary and initial conditions. Consider, for the moment, diffusion to a plane electrode. In this case (2.3.3) reduces to:

$$J_j = - D_j \frac{dc_j}{dx} \qquad (2.3.6)$$

In order to obtain a solution to this equation the relationship between c_j and x must first be established. This relationship has been the cause of some controversy.

According to Nernst[91], the concentration varies as a linear function of distance within a stagnant layer of electrolyte of thickness δ. The quantity δ is known as the Nernst diffusion layer thickness, and is an arbitrary quantity defined by Fig. 2.3.1. Clearly, using this artifice:

$$\frac{dc_j}{dx} = (c_j^b - c_j^s)/\delta \qquad (2.3.7)$$

where c_j^b is the bulk concentration of species j. Hence:

$$J_j = - D_j(c_j^b - c_j^s)/\delta \qquad (2.3.8)$$

Where the supply of reactant controls the reaction, the surface concentration of that reactant falls to zero. It is then possible to define the limiting current density, i_L, as:

$$i_L = - z_j F D_j c_j^b/\delta \qquad (2.3.9)$$

Unfortunately, the Nernst diffusion layer thickness cannot be calculated. Indeed, for unstirred solutions δ has no steady state value, but the diffusion layer grows with time until disturbed by convective processes. The diffusion layer is, however, often assumed to be constant for experiments of short duration.

2.3.3 Convection

Convection is generally held to arise in two distinct ways.

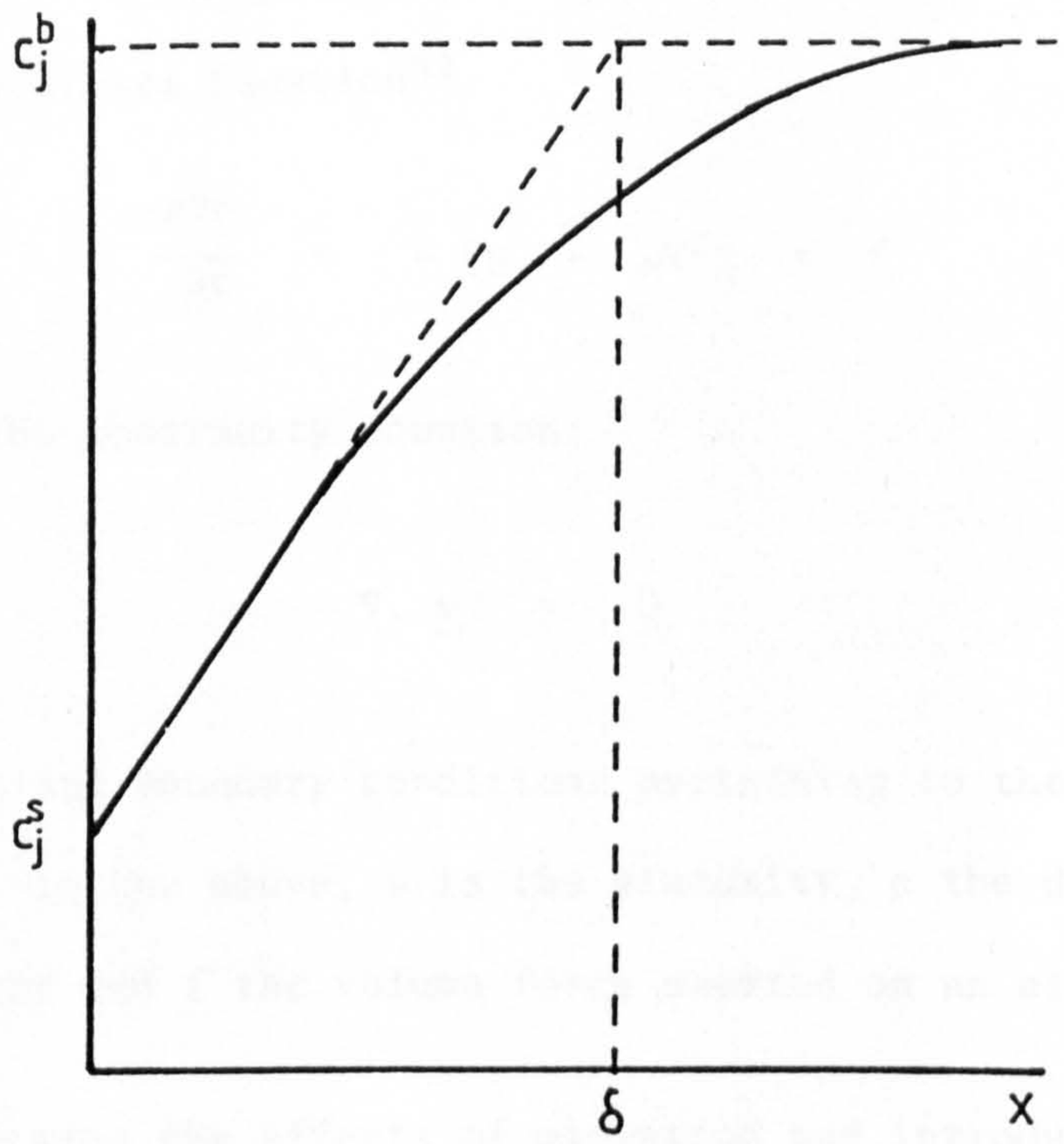

Fig. 2.3.1 Definition of the Nernst Diffusion Layer Thickness

It may be free (natural) or forced. Natural convection, the movement of a fluid under the influence of local density or temperature gradients is impossible to formulate precisely and equally impossible to prevent. Its effects may, however, be minimised by the introduction of a forced convective régime.

The process of forced convection is concerned with the transportation of solution by agitation or stirring, resulting in thorough mixing with a concomitant reduction of local density and temperature gradients. Where the hydrodynamics and cell geometry are well-defined it is often possible to obtain the velocity profile $\underline{v}$ from the Navier-Stokes Equation[92]:

$$\frac{\rho \partial \underline{v}}{\partial t} = - \nabla p + \mu \nabla^2 \underline{v} + \underline{f} \qquad (2.3.10)$$

together with the continuity equation:

$$\nabla . \underline{v} = \underline{0} \qquad (2.3.11)$$

and the initial and boundary conditions pertaining to the system under consideration. In the above, μ is the viscosity, ρ the density, p the pressure gradient and $\underline{f}$ the volume force exerted on an element of fluid.

Neglecting the effects of migration and introducing the mass balance condition:

$$\nabla . J_j = - \frac{\partial c_j}{\partial t} \qquad (2.3.12)$$

(2.3.1) becomes:

$$\frac{\partial c_j}{\partial t} = D_j \nabla^2 c_j - \underline{v} . \nabla c_j \qquad (2.3.13)$$

Clearly, when considering the steady state (2.3.13) reduces to:

$$D_j \nabla^2 c_j - \underline{v} \cdot \nabla c_j = 0 \qquad (2.3.14)$$

which is the familiar equation of convective diffusion. The exact solution of this equation is rarely possible. Indeed, the rotating disc electrode (q.v.) is one of the few systems for which the boundary conditions allow this.

The Nernst diffusion layer theory, despite its usefulness, is of little help in the solution of (2.3.14). A more realistic and quantitative theory is that of the hydrodynamic boundary layer, as developed by Levich.[93] In this theory, a fluid in motion relative to some surface is divided into two regions. In the region adjacent to the surface the fluid velocity rises from zero at the surface to the value attained by the bulk solution, and viscous forces are present. Outside of this hydrodynamic layer the fluid is essentially inviscid. Clearly, the viscous boundary layer is not stagnant as in the Nernst theory. The main change in concentration also occurs within this layer.

An appropriate relation exits for the thickness of the Prandtl layer, according to which:

$$\delta_o = 5.2\sqrt{\{\nu x/U_o\}} \qquad (2.3.15)$$

ν being the kinematic viscosity and U_o the fluid velocity. Consideration of (2.3.14) together with the Navier-Stokes Equation leads to an expression for the thickness of the diffusion boundary layer in terms of δ_o. Hence:

$$\delta \sim \delta_o \, Pr^{-\frac{1}{3}} \qquad (2.3.16)$$

where Pr, the Prandtl Number, is a dimensionless quantity characterising the physical properties of the fluid. In fact:

$$Pr_j = \nu/D_j \qquad (2.3.17)$$

Hence:

$$\delta_j \sim D_j^{\frac{1}{3}} \nu^{\frac{1}{6}} \sqrt{\{x/U_o\}} \qquad (2.3.18)$$

A consequence of the form of (2.3.17) is that (2.3.18) admits a different boundary layer thickness for each species.

2.4 Rotating Disc Electrode

The Rotating Disc Electrode (RDE) is one of the most useful tools available to the electrochemist. It has been noted (§2.3.2) that the value of the Nernst diffusion layer thickness lacks a steady state value in unstirred solutions. In order to obtain reproducible results from an electrochemical experiment it is necessary, at least for experiments in the steady state, to arrange for a well-defined diffusion layer. This condition is met by the RDE, the hydrodynamics of which have been rigorously treated by Levich.[93,94] The review of Filinovsky and Pleskov[95] is noteworthy.

If we consider a general charge transfer reaction such as (2.2.1) then from the solution of Fick's First Law (2.3.8) we write:

$$c_j^s = c_j^b + \frac{i\delta_j}{zFD_j} \qquad (2.4.1)$$

whereupon substitution into (2.2.4) gives:

$$i[1-\vec{k}\delta_o/D_o+\overleftarrow{k}\delta_R/D_R] = zF[\vec{k}c_o^b-\overleftarrow{k}c_R^b] \qquad (2.4.2)$$

We note that the right hand side is merely the current density in the absence of diffusion, which we shall write as i_∞.

The Levich Equation,[93] which is an exact solution to the convective diffusion problem for a rotating disc electrode, may be written:

$$\delta_j = 1.62\ \nu^{\frac{1}{6}}\ D_j^{\frac{1}{3}}\ \omega^{-\frac{1}{2}} \qquad (2.4.3)$$

Introducing (2.4.3) into (2.4.2) gives, on division by $i.i_\infty$ and rearranging:

$$i^{-1} = i_{\infty}^{-1} + \frac{1.62\ \nu^{\frac{1}{6}}(\overleftarrow{k}D_R^{-\frac{2}{3}} - \overrightarrow{k}D_O^{-\frac{2}{3}})\ \omega^{-\frac{1}{2}}}{zF(\overrightarrow{k}c_O^b - \overleftarrow{k}c_R^b)} \qquad (2.4.4)$$

whence a plot of i^{-1} versus $\omega^{-\frac{1}{2}}$ is expected to be linear with slope:

$$\frac{\partial i^{-1}}{\partial \omega^{-\frac{1}{2}}} = \frac{1.62\ \nu^{\frac{1}{6}}(\overleftarrow{k}D_R^{-\frac{2}{3}} - \overrightarrow{k}D_O^{-\frac{2}{3}})}{zF(\overrightarrow{k}c_O^b - \overleftarrow{k}c_R^b)} \qquad (2.4.5)$$

and intercept:

$$i^{-1}(\omega^{-\frac{1}{2}} = 0) = i_{\infty}^{-1} \qquad (2.4.6)$$

When the reaction is entirely controlled by charge transfer it can be shown that the current is independent of rotation speed. For a reversible reaction, however, $i_{\infty}^{-1} \rightarrow 0$ and the plots of i^{-1} versus $\omega^{-\frac{1}{2}}$ pass through the origin. In this case a plot of i versus $\omega^{\frac{1}{2}}$ will also be linear. In the case of mixed kinetic and mass transport control, the full form of (2.4.4) must be used.

When using this equation it is useful to remember that the rate constants are potential dependent according to (2.2.14) and (2.2.15). Introducing these dependencies into (2.4.5) we obtain, on multiplication by $\exp\{-zF(1-\alpha)(E-E^{\ominus})/RT\}$:

$$\frac{\partial i^{-1}}{\partial \omega^{-\frac{1}{2}}} = \frac{1.62\nu^{\frac{1}{6}}}{zF}\left[\frac{D_R^{-\frac{2}{3}} - D_O^{-\frac{2}{3}}\exp\{-zF(E-E^{\ominus})/RT\}}{-c_R^b + c_O^b\exp\{-zF(E-E^{\ominus})/RT\}}\right] \qquad (2.4.7)$$

If we consider the special case when R is a solid metal, then:

$$c_R^b >> c_O^b\exp\{-zF(E-E^{\ominus})/RT\} \qquad (2.4.8)$$

and,
$$D_R^{-\frac{2}{3}} << D_O^{-\frac{2}{3}}\exp\{-zF(E-E^{\ominus})/RT\} \qquad (2.4.9)$$

whence,

$$\frac{\partial i^{-1}}{\partial \omega^{-\frac{1}{2}}} = \frac{1.62\nu^{\frac{1}{6}}}{zFc_R^b} D_O^{-\frac{2}{3}} \exp\{-zF(E-E^{\Theta})/RT\} \qquad (2.4.10)$$

A plot of $\log\{\frac{\partial i^{-1}}{\partial \omega^{-\frac{1}{2}}}\}$ versus E is therefore expected to be linear with slope:

$$\frac{\partial \log\{\frac{\partial i^{-\frac{1}{2}}}{\partial \omega^{-\frac{1}{2}}}\}}{\partial E} = -2.303 \frac{RT}{zF} \qquad (2.4.11)$$

and intercept:

$$\log\{(\frac{\partial i^{-1}}{\partial \omega^{-\frac{1}{2}}})_{E=E^{\Theta}}\} = \log\{1.62\nu^{\frac{1}{6}} D_O^{-\frac{2}{3}}/zFc_R^b\} \qquad (2.4.12)$$

Hence z is available from (2.4.11) and D_O from (2.4.12).

Thus, in theory, the RDE is capable of distinguishing between charge transfer and mass transfer control of a reaction. Where the reaction is not completely dominated by charge transfer control, the method is capable of obtaining the current density due to the charge transfer process in the absence of diffusion and this current may be used in the Tafel Equation, (2.2.24) in order to determine the true electrochemical kinetics. Where the reaction is reversible and the reduced species is a solid metal, the charge transfer valence and diffusion coefficient may be obtained.

2.5 Linear Sweep Voltammetry

Linear sweep voltammetry (LSV) is a technique which is often used for the preliminary investigation of an unknown electrochemical system. The technique has been considered by Delahay[96] and others.[169] Whilst the experimental technique is fairly simple, the underlying theory is quite complex. The derivation of this theory will not be given here - indeed, it would not be appropriate to do so. It will suffice to state the relevant equations.

The experiment concerns the observation of the current response to a linear sweep of the electrode potential from an initial value, E_i, at a rate of ν. At any time t, therefore, the electrode potential is given by:

$$E = E_i - \nu t \qquad (2.5.1)$$

As the electrode potential departs from E_i, which is chosen such that the substance O is not reduced, the electron transfer (2.2.1) is accelerated until the concentration of species O at the electrode surface falls from its initial value (i.e. the bulk concentration) to zero when the reaction becomes diffusion controlled. A peak is observed in the current response.

It may be shown, on application of the appropriate boundary conditions that, for a reversible reaction, the peak current density is given by:

$$i_p = 2.72 \times 10^5 \cdot z^{\frac{3}{2}} D^{\frac{1}{2}} c^b \nu^{\frac{1}{2}} \qquad (2.5.2)$$

and also that the observed peak has a characteristic shape defined by:

$$E_p - E_{p/2} = - 1.109 \cdot RT/zF \qquad (2.5.3)$$

where E_p is the potential at which i_p occurs and $E_{p/2}$ is the potential at $i = i_p/2$. The potential E_p is independent of sweep rate. Where diffusion is unimportant, i.e. for a solid-state reaction, the peak current varies with the sweep rate rather than with $\nu^{\frac{1}{2}}$. Where a return sweep is made, the separation between the cathodic peak and its anodic counterpart is indicative of the number of electrons transferred according to:

$$\Delta E_p = 0.058/z \qquad (2.5.4)$$

Where the reaction is intrinsically irreversible, the quantity E_p may be shown to depend on the sweep rate. For the cathodic process:

$$E_p = E_i + \frac{RT}{\alpha z_\alpha F}\left[-0.78 + \ln\{\vec{k}^i(\beta D)^{\frac{1}{2}}\} - 0.5\ln\{\frac{\alpha z_\alpha F\nu}{RT}\}\right] \qquad (2.5.5)$$

whence,

$$\frac{\partial E_p}{\partial \ln\{\nu\}} = - 0.5\frac{RT}{\alpha z_\alpha F} \qquad (2.5.6)$$

where $\vec{k}^i$ is the value of the rate constant at $E = E_i$ and β is some function. Note that for the irreversible anodic process, the cathodic charge transfer coefficient α should be replaced by $1-\alpha$ in (2.5.6). The peak current density is given by:

$$i_p = 3.01 \times 10^5 \cdot z(\alpha z_\alpha)^{\frac{1}{2}} D^{\frac{1}{2}} c^b \nu^{\frac{1}{2}} \qquad (2.5.7)$$

Thus linear sweep voltammetry offers the possibility of determining the reversibility of a reaction, the number of electrons involved in the charge transfer and the charge transfer coefficient. It is usually only possible to obtain this information for fairly simple systems. Where more complex systems are involved, the method may be useful in a more qualitative way, in determining the various reactions which may possibly occur in a given potential range.

2.6 Faradaic Impedance

2.6.1 The definition and representation of impedance

The method of faradaic impedance was first used to investigate electrochemical processes by Ershler[97] and Randles.[98] The method has been reviewed, notably by Grahame[99] and by Sluyters-Rehbach and Sluyters[100] and extensions to the theory have been made by Armstrong, Bell and Metcalfe.[101]

A small sinuosoidal perturbation in potential is applied to an electrode, superimposed onto a d.c. polarisation. The resultant current response contains an alternating component. If the voltage is given by:

$$V = V_m \sin\{\omega t\} \qquad (2.6.1)$$

and the current by:

$$I = I_m \sin\{\omega t - \phi\} \qquad (2.6.2)$$

then the impedance is defined as the vector:

$$\underline{Z} = \frac{V_m}{I_m} \cdot \arg(\phi) \qquad (2.6.3)$$

V_m and I_m are the amplitudes of the alternating voltage and current respectively, ω the angular frequency, t the time and ϕ the phase angle.

The impedance is conveniently represented in the complex plane as:

$$\underline{Z} = Z' - jZ'' \qquad (2.6.4)$$

where:

$$Z' = \frac{V_m}{I_m} \cos\{\phi\} \qquad (2.6.5)$$

$$Z'' = \frac{V_m}{I_m} \sin\{\phi\} \qquad (2.6.6)$$

and $j = \sqrt{-1}$. The impedance is generally measured as a function of frequency, concentration or d.c. polarisation. A plot of Z'' versus Z' in these cases is referred to as a 'Sluyters Plot'. The alternative Z'' versus $\omega^{-\frac{1}{2}}$ and Z' versus $\omega^{-\frac{1}{2}}$ plots, known as 'Randles Plots' are perhaps less used.

2.6.2 The Randles Equivalent Circuit

The impedance of an electrode was considered by Randles[98], who proposed the equivalent circuit of Fig. 2.6.1a as an analogue model of it. The circuit is a relatively simple one, allowing for the effects of the charge transfer resistance, θ, the double layer capacitance, C_L, the solution resistance, R_Ω, and the Warburg impedance, $\underline{Z}_W$. In essence the circuit allows only for the effects of simple charge transfer and of diffusion on the electrode impedance. The circuit, despite its lack of sophistication, adequately models a large number of electrode reactions. It will therefore be described in some detail.

Fick's Second Law, with the appropriate boundary conditions, has been solved by Warburg[102] to yield the impedance due to diffusion. This impedance, known as the 'Warburg impedance', $\underline{Z}_W$, may be expressed as:

$$\underline{Z}_W = (\sigma_O + \sigma_R)\omega^{-\frac{1}{2}} - j(\sigma_O + \sigma_R)\omega^{-\frac{1}{2}} \qquad (2.6.7)$$

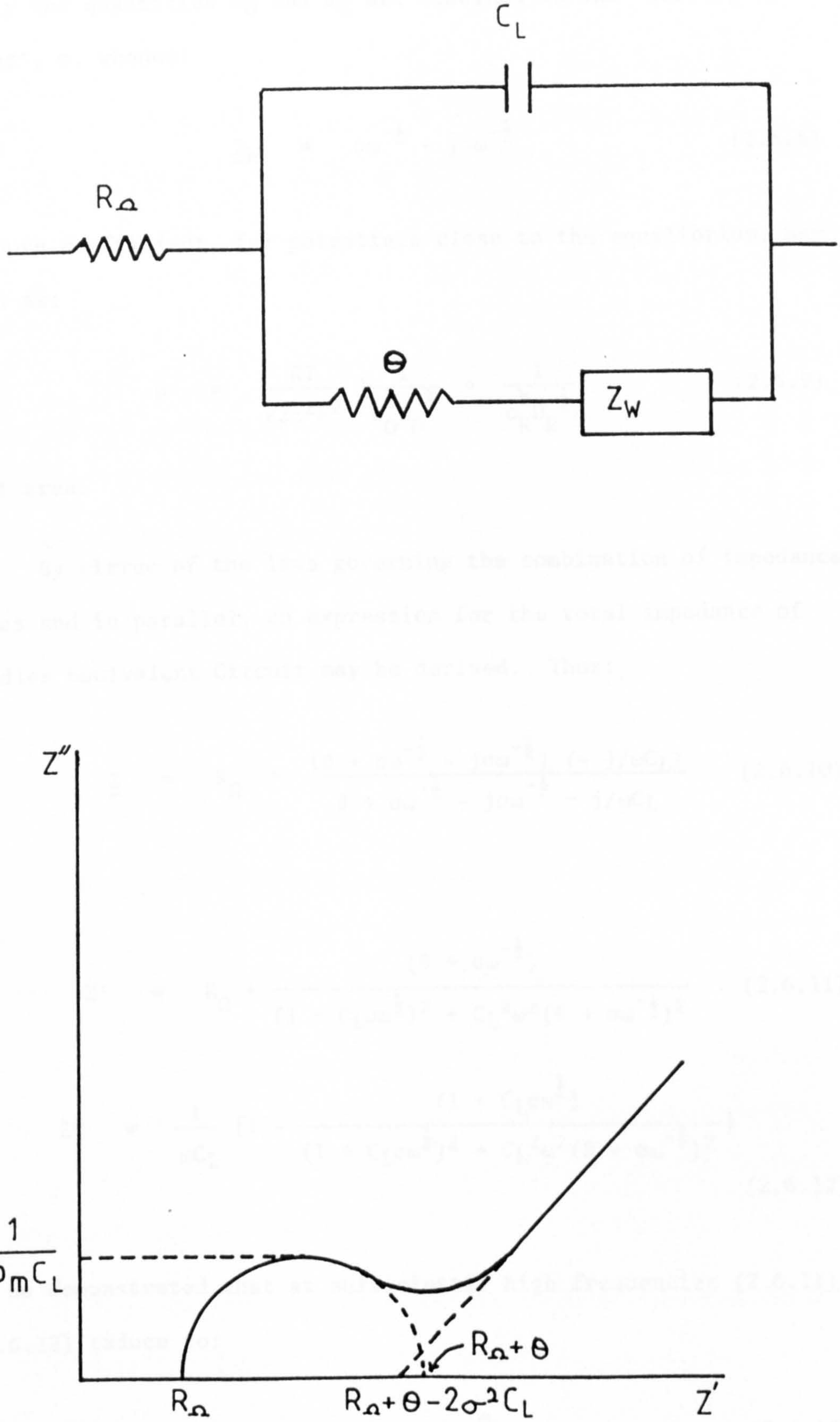

Fig. 2.6.1 The Randles Model

(a) The Equivalent Circuit

(b) Sluyters Plot for (a)

Generally the quantities σ_O and σ_R are combined in the 'Warburg coefficient', σ, whence:

$$\underline{Z}_W = \sigma\omega^{-\frac{1}{2}} - j\sigma\omega^{-\frac{1}{2}} \qquad (2.6.8)$$

The Warburg coefficient, for potentials close to the equilibrium, may be given as:

$$\sigma = \frac{RT}{\sqrt{2}z^2F^2}\left[\frac{1}{c_O^b D_O^{\frac{1}{2}}} + \frac{1}{c_R^b D_R^{\frac{1}{2}}}\right] \qquad (2.6.9)$$

per unit area.

By virtue of the laws governing the combination of impedances in series and in parallel, an expression for the total impedance of the Randles Equivalent Circuit may be derived. Thus:

$$\underline{Z} = R_\Omega + \frac{(\theta + \sigma\omega^{-\frac{1}{2}} - j\sigma\omega^{-\frac{1}{2}})(-j/\omega C_L)}{\theta + \sigma\omega^{-\frac{1}{2}} - j\sigma\omega^{-\frac{1}{2}} - j/\omega C_L} \qquad (2.6.10)$$

whence:

$$Z' = R_\Omega + \frac{(\theta + \sigma\omega^{-\frac{1}{2}})}{(1 + C_L\sigma\omega^{\frac{1}{2}})^2 + C_L^2\omega^2(\theta + \sigma\omega^{-\frac{1}{2}})^2} \qquad (2.6.11)$$

$$Z'' = \frac{1}{\omega C_L}\left[1 - \frac{(1 + C_L\sigma\omega^{\frac{1}{2}})}{(1 + C_L\sigma\omega^{\frac{1}{2}})^2 + C_L^2\omega^2(\theta + \sigma\omega^{-\frac{1}{2}})^2}\right] \qquad (2.6.12)$$

It may be demonstrated that at sufficiently high frequencies (2.6.11) and (2.6.12) reduce to:

$$Z' = R_\Omega + \frac{\theta}{1 + C_L^2\omega^2\theta^2} \qquad (2.6.13)$$

and:

$$Z'' = \frac{\omega C_L \theta^2}{1 + C_L^2 \omega^2 \theta^2} \qquad (2.6.14)$$

respectively. Eliminating ω and rearranging leads to:

$$[Z' - R_\Omega - \frac{\theta}{2}]^2 + [Z'']^2 = \theta^2/4 \qquad (2.6.15)$$

which is the equation of a circle whose centre lies on the Z' axis at $Z' = R_\Omega + \theta/2$ and whose radius is equal to $\theta/2$. Thus, the Slüyters Plot at high frequencies often reveals a semi-circular locus of frequency. Conversely, the frequency may be sufficiently low for (2.6.11) and (2.6.12) to reduce to:

$$Z' = R_\Omega + \theta + \sigma\omega^{-\frac{1}{2}} - 2\sigma^2 C_L \qquad (2.6.16)$$

and:

$$Z'' = \sigma\omega^{-\frac{1}{2}} \qquad (2.6.17)$$

whence the Sluyters Plot becomes a straight line of 45° slope, intersecting the Z' axis at $Z' = R_\Omega + \theta - 2\sigma^2 C_L$ ($\omega=\infty$). At intermediate frequencies the semi-circle bends upwards to meet the 45° line.

For systems which are completely analogous to the Randles Equivalent Circuit, the values of R_Ω, θ, σ and C_L may be determined from the Sluyters Plot, using a graphical method. Fig. 2.6.1b shows the graphical method for such an ideal case.

It is possible, however, to obtain impedance spectra which are not of this form and where the Randles Circuit is not appropriate. In such cases, even where it is possible to design an equivalent

circuit which adequately models the data, there may be no graphical method capable of recovering the values of the circuit parameters. In such cases a numerical method must be used; indeed, such a method may prove advantageous even when the simple Randles Circuit is used.

2.6.3 A numerical method for the analysis of impedance data

The analysis of experimental values of the impedance $\underline{Z}(Z',Z'')$ as a function of angular frequency ω may be achieved using the following numerical method and a mainframe computer. The following method is quite general to any chosen equivalent circuit. We consider an equivalent circuit composed of n elements, whose values are $P_i (i=1,n)$.

The first step is to derive a relation for the total impedance of the equivalent circuit, analogous to (2.6.10). It is assumed that the computer is capable of manipulating complex numbers, so that it is not necessary to derive expressions, such as (2.6.11) and (2.6.12), for the real and imaginary parts of the impedance; these are directly available. Given approximate values of P_i it is clearly possible for the computer to calculate values for these components from the equation for the total impedance. In general, the values calculated in this way will differ from the true (experimental) values, reflecting the use of approximate values of P_i. Thus:

$$Z' = Z'_{cal} + \Delta Z' \qquad (2.6.18)$$

$$Z'' = Z''_{cal} + \Delta Z'' \qquad (2.6.19)$$

We note that the experimental data consists of values of both Z' and Z'' at N different frequencies. The application of the numerical method is equally valid for (2.6.18) as to (2.6.19) and in the following the use of the distinguishing superscripts will be suppressed. The quantity Z will, therefore, represent either Z' or Z'' as required.

We assume that our approximate values of P_i differ from their

true values by an amount ΔP_i. If this amount is small then the quantity ΔZ may be expressed in terms of Taylor expansions about P_i. For sufficiently small values of ΔP_i it is valid to truncate the Taylor expansions after the first term to yield the linear expression:

$$Z = Z_{cal} + \sum_{i=1}^{n} D_i \Delta P_i = Z_{cal} + \Delta Z \qquad (2.6.20)$$

where:

$$D_i = \left(\frac{\partial Z_{cal}}{\partial P_i}\right)_{P_i = \Delta P_i} \qquad (2.6.21)$$

Equation (2.6.20) has n unknowns ΔP_i and therefore at least n values of Z (i.e. n frequencies) must be considered. In general the number of frequencies, N, is much larger than the number of unknowns, n, and it is desirable to derive maximum likelihood estimates of ΔP_i by performing a multiple regression analysis on the data.

For any particular frequency and a given set of P_i:

$$Z - Z_{cal} - \Delta Z = \varepsilon \qquad (2.6.22)$$

whence:

$$\varepsilon^2 = (Z - Z_{cal})^2 - 2(Z - Z_{cal})\Delta Z + (\Delta Z)^2 \qquad (2.6.23)$$

$$\Rightarrow \quad \varepsilon^2 = (Z - Z_{cal})^2 - 2(Z - Z_{cal}) \sum_{i=1}^{n} D_i \Delta P_i + \sum_{i=1}^{n} (D_i \Delta P_i)^2 + \sum_{i=1}^{n} \sum_{j=1}^{n} D_i \Delta P_i D_j \Delta P_j \delta_{ij} \qquad (2.6.24)$$

where $\delta_{ij} = 0 (i=j)$ and $\delta_{ij} = 1$ otherwise. The sum of errors squared is then:

$$\sum_{k=1}^{N} \epsilon^2 = \sum_{k=1}^{N} [(Z - Z_{cal})_k - 2(Z - Z_{cal})_k \sum_{i=1}^{n} D_{i,k}\Delta P_i + \sum_{i=1}^{n} (D_{i,k}\Delta P_i)^2 + \sum_{i=1}^{n} \sum_{j=1}^{n} D_{i,k}\Delta P_i D_{j,k}\Delta P_j \delta_{ij}] \quad (2.6.25)$$

The normal equations for linear regression require that:

$$\frac{\partial \sum_{k=1}^{n} \epsilon^2}{\partial \Delta P_i} = 2 \sum_{k=1}^{N} [D_{i,k}(\Delta P_i + \sum_{j=1}^{n} D_{j,k}\Delta P_j \delta_{ij} - (Z - Z_{cal})_k)] = 0 \quad (2.6.26)$$

At this point it is convenient to express the n normal equations in matrix form. To illustrate the method, we choose the Randles Circuit for which n=4. The method is valid for all n, however.

We define a matrix of differential coefficients:

$$\underline{A}_k = \begin{bmatrix} D_{1,k} & D_{1,k}D_{2,k} & D_{1,k}D_{3,k} & D_{1,k}D_{4,k} \\ D_{2,k}D_{1,k} & D_{2,k} & D_{2,k}D_{3,k} & D_{2,k}D_{4,k} \\ D_{3,k}D_{1,k} & D_{3,k}D_{2,k} & D_{3,k} & D_{3,k}D_{4,k} \\ D_{4,k}D_{1,k} & D_{4,k}D_{2,k} & D_{4,k}D_{3,k} & D_{4,k} \end{bmatrix} \quad (2.6.27)$$

so that:

$$\sum_{k=1}^{N} \underline{A}_k \begin{bmatrix} \Delta P_1 \\ \Delta P_2 \\ \Delta P_3 \\ \Delta P_4 \end{bmatrix} = \sum_{k=1}^{N} [(Z - Z_{cal})_k \begin{bmatrix} D_{1,k} \\ D_{2,k} \\ D_{3,k} \\ D_{4,k} \end{bmatrix}] \quad (2.6.28)$$

It remains only to calculate $(Z - Z_{cal})_k$ and $D_{i,k}$. We have already seen that $(Z - Z_{cal})_k$ is available. The differential coefficients,

$D_{i,k}$, are also capable of calculation. The original equation is used, with the approximation:

$$D_{i,k} = [(Z_{cal}(1.01\ P_i) - Z_{cal}(P_i))_k]/.01\ P_i \quad (2.6.29)$$

The values of ΔP_i are now available from (2.6.28) via the matrix inversion of $\underline{A}_k$. This is easily achieved using computer methods.

Because of the errors introduced in linearising the Taylor expansions, the new values of $P_i (= P_i + \Delta P_i)$ are substituted and the entire process repeated. This iterative procedure continues until the value of $\Sigma\varepsilon^2$ becomes constant. The true values of P_i result.

CHAPTER THREE

A SELECTIVE REVIEW OF THE RELEVANT LITERATURE

3.1 The electrochemistry of cadmium in aqueous solution

3.1.1 Introduction

The electrochemistry of cadmium in various electrolytes has been comprehensively reviewed by Latham and Hampson[103]; and in alkaline solution by Armstrong et al.[104] This latter review has been extended by Barnard[105] recently.

The purpose of this review is to summarise the literature pertaining to the electrochemical kinetics of solid cadmium metal in aqueous solution.

3.1.2 Standard and Formal Potentials

The data of Harned and Fitzgerald[106] is regarded as the most comprehensive. Values have also been reported by Burnett and Zirin[107] and by Getman.[108] The generally accepted value for the standard electrode potential of cadmium is -0.402 V.

The potential-pH diagram for the aqueous cadmium system (Fig. 3.1.1) has been obtained by Deltcombe, Pourbaix and de Zoubov.[109] A simplified active-passive diagram has also been given.[109]

3.1.3 Double Layer Properties

The point of zero charge, E_z, has been determined in several electrolytes (Table 3.1.1).

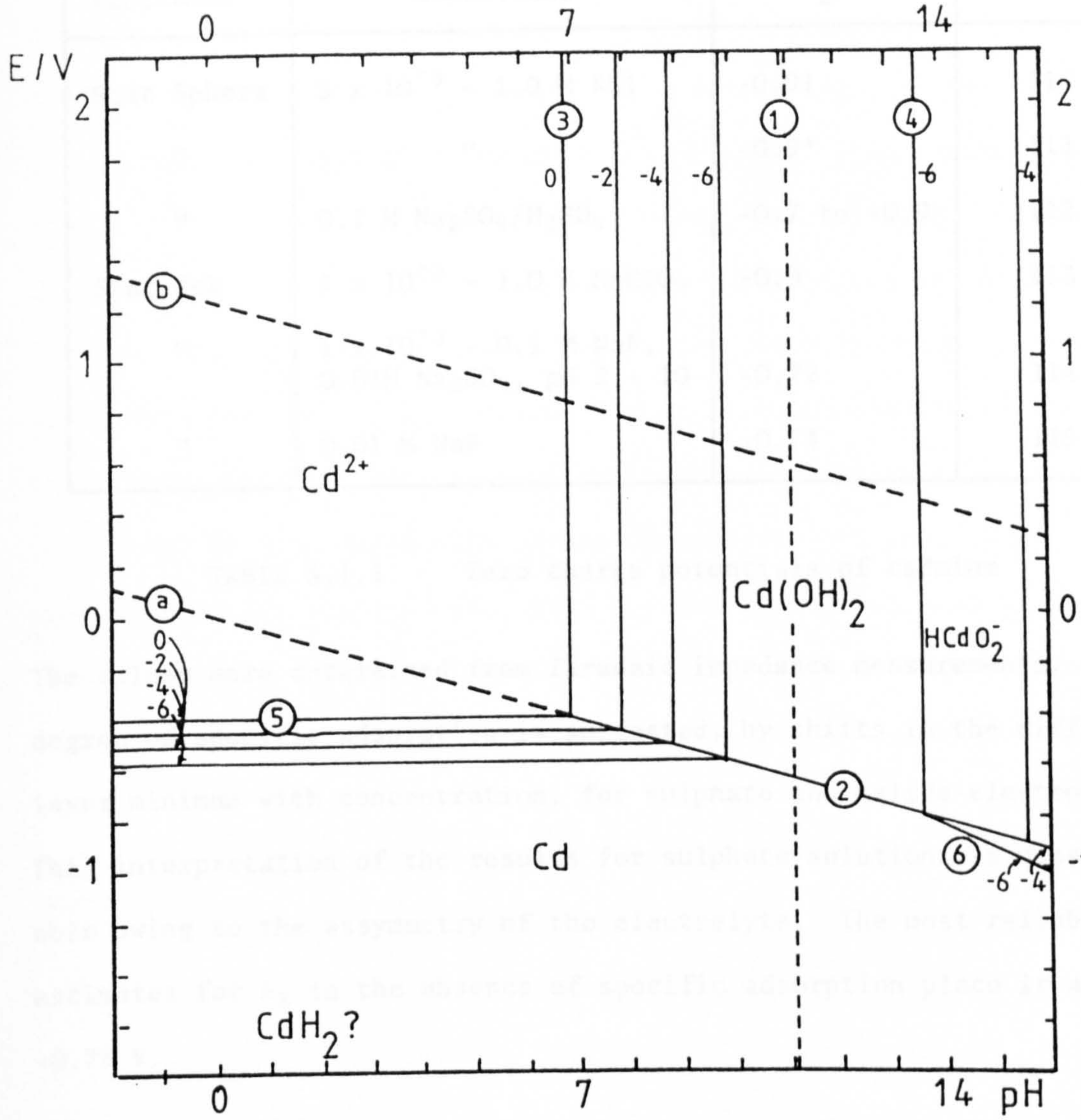

Fig. 3.1.1 Potential-pH Diagram for the Cadmium Aqueous System[109]

(1) $Cd^{2+} + 2H_2O = HCdO_2^- + 3H^+$; $Cd^{2+}/HCdO_2^-$, pH = 11.1;

(2) $CdO + 2H^+ + 2e = Cd + H_2O$; (3) $Cd^{2+} + H_2O = CdO + 2H^+$;

(4) $CdO + H_2O = HCdO_2^- + H^+$; (5) $Cd^{2+} + 2e = Cd$;

(6) $HCdO_2^- + 3H^+ + 2e = Cd + 2H_2O$; (7) $Cd + H^+ + e = CdH$.

ELECTRODE	CONDITIONS	E_z/V	REFERENCE
Stat Sphere	5×10^{-3} - 1.0 M KCl	-0.91	110
"	"	-0.9*	111
"	0.1 M Na_2SO_4/H_2SO_4	-0.7 to -0.9	112
Stat dsk	1×10^{-3} - 1.0 M $NaClO_4$	-0.9	113
"	1×10^{-3} - 0.1 M NaF, 0.01N Na_2SO_4, pH 2 - 10	-0.72	114
"	0.01 M NaF	-0.74	115

TABLE 3.1.1 Zero charge potentials of cadmium

The values were determined from faradaic impedance measurements. Some degree of specific adsorption is suggested, by shifts in the diffuse layer minimum with concentration, for sulphate and halide electrolytes. This interpretation of the results for sulphate solutions is questionable owing to the assymmetry of the electrolyte. The most reliable estimates for E_z in the absence of specific adsorption place it around -0.73 V.

3.1.4 Kinetics

Compared with the amalgam electrode, the electrode kinetics of cadmium metal have received little attention. There is, as yet, no unambiguous mechanism for the cadmium electrode. The fact that the zero charge potential is positive of the equilibrium potential means that equilibrium measurements are often subject to the adsorption of OH^-. The development of electrode films is frequently observed.

---

*by electroreduction of anions.

Lorenz[116] has studied the kinetics of the exchange reaction in neutral sulphate solution. The galvanostatic pulse method was applied in the Tafel region; the results were interpreted in terms of a rate determining two electron charge transfer step. A cathodic charge transfer coefficient of 0.45 was obtained. The exchange current density, for 5×10^{-3} M Cd^{2+} in 0.4 M K_2SO_4, was 1.5×10^{-3} Acm^{-2}, indicating an extremely fast reaction. A value of 0.5 was obtained for the apparent charge transfer coefficient in 0.75 M K_2SO_4, from the slope of a plot of $\log\{i_o\}$ versus $\log\{c\}$. A determination of the transfer coefficient was also made using the transition time for the deposition of cadmium at high current densities. At long times, a plot of E versus $\log\{1 - \sqrt{t/\tau}\}$ gave a value of $\alpha = 0.5$. At short times, however, values as low as $\alpha = 0.25$ were found. The faradaic impedance data of Brodd[117] largely supports the conclusions of Lorenz.[116]

According to Heusler and Gaiser[118], however, a two-step mechanism:

$$Cd^{2+} + e \rightleftharpoons Cd^{+}_{ad} \qquad (3.1.1)$$

$$Cd^{+}_{ad} + e \rightleftharpoons Cd \qquad (3.1.2)$$

cannot be dismissed. Their data, and indeed that of Lorenz[116], is consistent with this mechanism. The rate constants of (3.1.2) were found to be always greater than those of (3.1.1) which is, therefore, the rate determining step. The second step is not necessarily always in equilibrium. The observed kinetics are in agreement with this mechanism as long as each step has a charge transfer coefficient of 0.5 and the adsorbed intermediate is well-defined and weakly bound to the electrode, via a water bridge, say. The rate determining step,

(3.1.1), is a typical redox reaction; (3.1.2) represents a metal/ion reaction.

Amosse et al[119] have also studied the cadmium exchange reaction in sulphate solution. Using a double potential step technique, they found exchange current densities, (in a solution of 2.5×10^{-3} M $CdSO_4$/0.5 M Na_2SO_4), of 1.65×10^{-2} A cm^{-2} in agreement with those of Lorenz.[116] A Tafel slope of 58 mV was obtained, consistent with a charge transfer valence of 2 and a transfer coefficient of 0.5.

Hampson and Latham[120] have measured exchange current densities and obtained a value of $\alpha = 0.23$ for the apparent charge transfer coefficient. Their values for i_o lie within an order of magnitude of those of Lorenz.[116] Their experiments were conducted in 2.0 M $NaClO_4$ in a range of cadmium concentrations from 0.0617 - 0.452 M. The galvanostatic pulse technique was used. In a later paper[121], they employed the method of faradaic impedance to confirm their earlier results. The apparent transfer coefficient was found to be 0.35. No evidence for the Cd^+_{ad} species postulated by Heusler and Gaiser[118] was deduced, but, working close to the equilibrium, the two step mechanism could not be rejected. They note that their values of αz support the latter mechanism if the transfer coefficient for each step is 0.5.

It is now generally accepted that the mechanism of Heusler and Gaiser[118] is correct, although its unambiguous deduction remains to be sought, despite the recent work of Harrison et al.[135]

Largely as a result of its application to the nickel-cadmium battery, the cadmium electrode in alkaline solutions has been more extensively studied. Despite this work, the system remains even less clearly defined than was the case for sulphate or perchlorate electrolytes.

It has been shown[122-4] that the adsorption of the hydroxyl ion is important to the anodic oxidation process, and it is difficult to avoid the intrusion of oxide/hydroxide films.

Casey and Lake[125] concluded that the anodic oxidation of cadmium proceeded in two stages, viz:

$$Cd \xrightarrow{\text{electrochemical}} CdO \xrightarrow{\text{chemical}} Cd(OH)_2 \qquad (3.1.3)$$

and indeed evidence for CdO has been given.[126]

There has, however, been some dispute as to the sequence of the two reactions. Croft[127] considered the oxidation to follow the mechanism:

$$Cd + 2OH^- \rightleftharpoons Cd(OH)_2 + 2e \qquad (3.1.4)$$

having established the presence of $Cd(OH)_2$ but not crystalline CdO.

Lange and Ohse[128] and Ohse[129] pointed out the thermodynamic unlikelihood of the primary formation of CdO. It was suggested[129] that $Cd(OH)_2$ was formed initially and subsequently dehydrated to CdO, viz:

$$Cd(OH)_2 \rightleftharpoons CdO + H_2O \qquad (3.1.5)$$

Breiter and Weininger[130] have carried out voltammetric experiments in an attempt to distinguish between the two mechanisms. They suggested that the primary oxidation product, formed below the passivation potential, consisted of $Cd(OH)_2$. Strong passivation was thought to be due to a thin layer of CdO. At more anodic potentials, thickening of the $Cd(OH)_2$ layer was said to occur. The thin passivating

layer was reduced first.

Devanathan and Lakshmanan[131], from galvanostatic transient experiments, concluded that passivation on cadmium occurred by way of the following dissolution-precipitation mechanism:

$$Cd + OH^- \rightarrow CdOH^+ + 2e \qquad (3.1.6)$$

$$CdOH^+ + OH^- \rightleftharpoons Cd(OH)_2 \qquad (3.1.7)$$

$$CdOH^+ \rightarrow CdO + H^+ \qquad (3.1.8)$$

The analysis of these results, however, has been questioned.[132]

L'vova et al[133] have studied the impedance of the cadmium electrode in concentrated KOH solution. The frequency spectrum of the impedance was characteristic of diffusion. The diffusing species was shown to be neither the hydroxyl ion nor the cadmate ion. It was suggested instead that the electrochemical adsorption of hydroxyl ions was responsible and the frequency dependence due to either the surface diffusion of OH^-, or some surface inhomogeneity. There is, however, no quantitative basis for either of these explanations. The movement of the species has been demonstrated by other methods.[122-3] The equivalent circuit was consistent with the mechanism:

$$OH^- \rightarrow OH_{ad} + e \qquad (3.1.9)$$

$$OH_{ad} + OH^- \rightarrow O^-_{ad} + H_2O \qquad (3.1.10)$$

$$Cd + O^-_{ad} \rightarrow CdO + e \qquad (3.1.11)$$

The rate of (3.1.11) is sensitive to temperature, and is diminished, as expected, by the application of more cathodic potentials and the accumulation of CdO at the electrode.

The work of Okinaka[134] at the rotating ring disc electrode also supports the dissolution-precipitation mechanism over the solid-state alternative, in the active range of potential. Passivation was found to be due to a thin layer of CdO.

Later work by Armstrong and West[132] criticised the work of Devanathan[131] and of Okinaka.[134] The authors presented results from potentiostatic pulse, rotating ring disc, linear sweep and impedance experiments. These results revealed a region of active dissolution prior to film formation. The mechanism of film formation was thought to be a solid-state one. Film thickening followed an approximately parabolic law at short times. These results support the claims of Croft[127] and Farr and Hampson[136] for the solid-state mechanism.

Hampson and Latham[137] have examined the cadmium electrode in alkaline solution by double pulse galvanostatic and faradaic impedance techniques. Their attempts to determine the kinetic parameters were complicated by film formation. They reported a very fast exchange reaction, certainly faster than that in perchlorate electrolytes, and the process was found to be independent of $[Cd^{2+}]$. It was postulated that a neutral or complexed species be transferred. This would explain, if $Cd(OH)_2$ were the species transferred, the enhanced value of the rate constant in alkaline solution. Their unexpected lack of variation in the results with temperature was explained in terms of control of the reaction by film growth.

3.2 The electrochemistry of nickel in aqueous solution

3.2.1 Introduction

The electrochemistry of nickel has been exhaustively reviewed by Arvia and Posadas[138] and this is the major source consulted.

The present survey considers the kinetic parameters and other relevant work concerning the mechanisms of dissolution and deposition of nickel metal in aqueous solution. There is an immense body of literature pertaining to nickel and the present review seeks only to summarise this. Much of the data pertains to the dissolution reaction and this will not be considered here.

3.2.2 Standard and Formal Potentials

It is, as yet, not possible to quote with great accuracy the standard electrode potential of the Ni/Ni(II) couple. This is due to the fact that a truly reversible equilibrium appears difficult to obtain. Values have been determined by several researchers. The generally accepted value, $E^{\ominus} = -0.23$ V, has been found by several independent methods[139-142], but values approaching -0.25 V have also been reported.[143-5]

The potential-pH diagram for the aqueous system has been constructed by Pourbaix et al.[109] The diagram is considerably more complicated than that for cadmium.

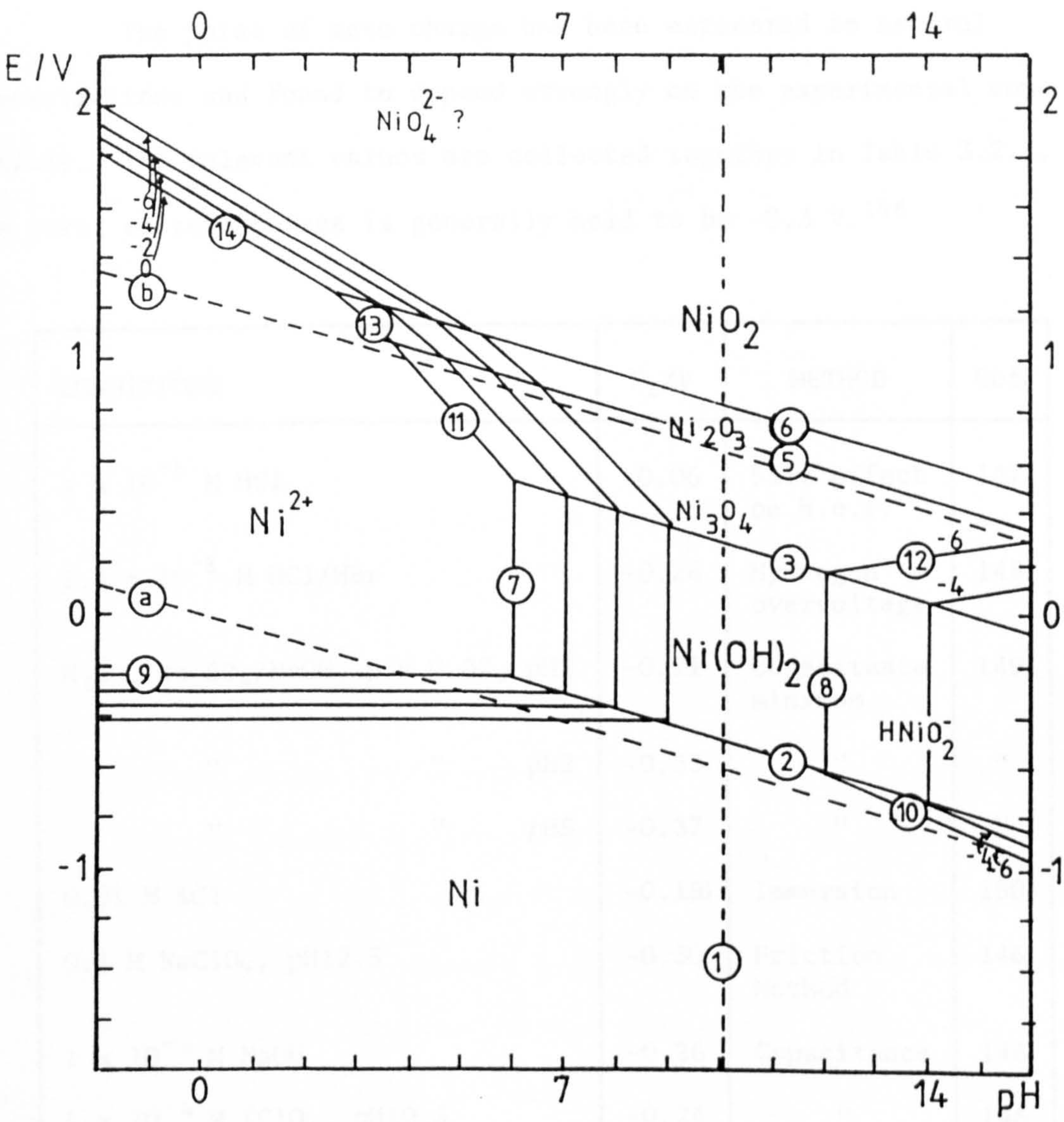

Fig. 3.2.1 Potential-pH Diagram for the Nickel Aqueous System[109]

(2) $Ni(s) + H_2O(l) = NiO(s) + 2H^+ + 2e$; (3) $3NiO(s) + H_2O(l) = Ni_3O_4(s) + 2H^+ + 2e$; (5) $2Ni_3O_4(s) + H_2O(l) = 3Ni_2O_3(s) + 2H^+ + 2e$; (6) $Ni_2O_3(s) + H_2O(l) = 2NiO_2(s) + 2H^+ + 2e$; (7) $Ni^{2+} + H_2O(l) = NiO(s) + 2H^+$; (9) $Ni(s) = Ni^{2+} + 2e$; (10) $Ni(s) + 2H_2O(l) = HNiO_2^- + 3H^+ + 2e$; (11) $3Ni^{2+} + 4H_2O = Ni_3O_4(s) + 8H^+ + 2e$; (12) $3HNiO_2^- + H^+ = Ni_3O_4(s) + 2H_2O(l) + 2e$; (13) $2Ni^{2+} + 3H_2O(l) = Ni_2O_3(s) + 6H^+ + 2e$; (14) $Ni^{2+} + 2H_2O(l) = NiO_2(s) + 4H^+ + 2e$; (a) $H_2 = 2H^+ + 2e$; (b) $2H_2O = O_2 + 4H^+ + 4e$; (1') $Ni^{2+}/HNiO_2^-$, pH = 10.13.

3.2.3 Double Layer Properties

The point of zero charge has been estimated in several investigations and found to depend strongly on the experimental conditions. The relevant values are collected together in Table 3.2.1. The point of zero charge is generally held to be -0.3 V.[146]

CONDITIONS	E_z/V	METHOD	Ref.
1×10^{-3} M HCl	-0.06	Salt effect on h.e.r.	147
1.5×10^{-3} M HCl/HBr	-0.28	Hydrogen overvoltage	148
$H_2SO_4/Na_2SO_4/NaOH$, μ = 0.02, pH1	-0.21	Capacitance minimum	149
" " pH2	-0.33	"	"
" " pH5	-0.37	"	"
0.01 M KCl	-0.193	Immersion	150
0.1 M $NaClO_4$, pH12.5	-0.30	Friction Method	146
1×10^{-4} M NaOH	-0.26	Capacitance	146
5×10^{-4} M $KClO_4$, pH10.3	-0.24	"	146

TABLE 3.2.1 Zero Charge Potentials of Nickel

3.2.4 Kinetics

The available kinetic data is summarised in Table 3.2.2 for the reduction of Ni^{2+}.

CONDITIONS	pH	i_o/Acm^{-2}	α	Ref.
1 M $NiSO_4$	-	2×10^{-9}	0.5	151
2 N H_2SO_4/0.01 N $NiSO_4$	0.00	8.3×10^{-10}	0.35 - 0.4	152
0.2 N H_2SO_4/0.01 N $NiSO_4$	0.83	2.4×10^{-9}	"	"
2 N Na_2SO_4/0.01 N $NiSO_4$	5.86	4.2×10^{-8}	-	"
2 N HCl/1.0 N $NiCl_2$	0.28	1.1×10^{-8}	0.35 - 0.4	"
1 N HCl/1.0 N KCl/ 0.01 M $NiCl_2$	0.01	6.9×10^{-9}	"	"
0.2 N HCl/1.5 N KCl/ 0.01 M $NiCl_2$	0.60	1.7×10^{-9}	"	"
0.2 N HCl/0.01 M $NiCl_2$	0.67	3.9×10^{-9}	"	"
2 N KCl/0.01 M $NiCl_2$	5.96	1×10^{-8}	"	"

Piatti, Arvia and Podesta[153-4] have studied the behaviour of nickel in acid aqueous solution. They found that in nickel ion solutions at pH > 4, a Tafel slope of 60 mV was observed. Correction of the results for the simultaneous evolution of hydrogen resulted in a slope of 120 mV. The exchange current density (extrapolated to the reversible potential) was 2×10^{-6} Acm^{-2}. These experiments were carried out in 2 M $NaClO_4$. In chloride solutions the system was less amenable to analysis, presumably due to the specific adsorption demonstrated by several workers.[147-8,155]

Tafel plots, again corrected for the hydrogen evolution reaction, were obtained by Ovari and Rotinyan[156] using solutions of $NiSO_4/H_2SO_4$. The nickelous ion concentration was varied from 0.25 M to 2 M and the pH from 0.55 to 3. The observed Tafel slopes, which were independent of the nickelous ion concentration, were between 124 and 130 mV. Other studies[157], in nickel chloride solution, had

shown that the cathodic process was first order with respect to $[Ni^{2+}]$, the anodic reaction being independent of the nickelous ion concentration. They were able to propose the following mechanism:

$$Ni^{2+} + e \rightleftharpoons Ni^{+} \qquad (3.2.1)$$

$$Ni^{+} + e \rightleftharpoons Ni \qquad (3.2.2)$$

of which the first step is rate determining. This mechanism may be seen to adequately fit the data of Table 3.2.2.

Of particular relevance to the present work are the experiments of Epelboin.[158] Results obtained using a Watts solution, at varying pH and nickelous ion concentration, indicated that the NiOH species was involved as an intermediate in the charge transfer process, although it did not fulfil a catalytic rôle.

Certain of the recently reported investigations of the nickel electrode have revealed details of the mechanism of metal deposition in electrolytes more closely associated with the present work.

In chloride electrolytes the involvement of a NiCl intermediate has been suggested[159], viz:

$$Ni^{2+} + Cl^{-} \rightleftharpoons (NiCl)^{+} \qquad (3.2.3)$$

$$(NiCl)^{+} + e \rightleftharpoons NiCl \qquad (3.2.4)$$

$$NiCl + e \rightleftharpoons Ni + Cl^{-} \qquad (3.2.5)$$

The nickel ion concentration ranged from $\sim$ 0.01 to $\sim$ 0.1 M.

It has also been proposed[160] that, in all-chloride electrolytes, the chemical reduction of electrogenerated hydrogen was involved.

The following scheme could apply:

$$H^+ + e \longrightarrow H_{ad} \qquad (3.2.6)$$

$$\left.\begin{array}{l} 2H_{ad} \rightleftharpoons H_2 \uparrow \qquad (3.2.7) \\ 2H_{ad} + Ni^{2+} \rightleftharpoons Ni + 2H^+ \qquad (3.2.8) \end{array}\right\{$$

The choice of second step, i.e. (3.2.7) or (3.2.8), would be expected to depend on the pH. The involvement of $NiOH^+$ is suggested for the reduction (3.2.8), possibly via:

$$Ni^{2+} + H_2O \rightleftharpoons NiOH^+ + H^+ \qquad (3.2.9)$$

$$NiOH^+ + 2H_{ad} \rightleftharpoons Ni + H_2O + H^+ \qquad (3.2.10)$$

Ovari[161] has suggested the possibility of enhancement by hydrogen ions according to:

$$[Ni(H_2O)_4]^{2+} + H_3O^+ \rightleftharpoons [Ni(H_3O)(H_2O)_3]^{3+} + H_2O \qquad (3.2.11)$$

$$[Ni(H_3O)(H_2O)_3]^{3+} + 2e \longrightarrow Ni + H_3O^+ + 3H_2O \qquad (3.2.12)$$

Equation (3.2.12) may be expanded as:

$$[Ni(H_3O)(H_2O)_3]^{3+} + e \rightleftharpoons [Ni(H_3O)(H_2O)_3]^{2+} \qquad (3.2.13)$$

$$[Ni(H_3O)(H_2O)_3]^{2+} + e \rightleftharpoons Ni + H_3O^+ + 3H_2O \qquad (3.2.14)$$

Perhaps the most widely accepted mechanism[153,162-3] is one resembling that proposed for the deposition of iron:

$$Ni^{2+} + H_2O \rightleftharpoons (NiOH)^+ + H^+ \qquad (3.2.15)$$

$$(NiOH)^+ + 2e \longrightarrow Ni + OH^- \qquad (3.2.16)$$

{

$$(NiOH)^+ + e \longrightarrow NiOH_{ad} \qquad (3.2.17)$$

If (3.2.17) occurs rather than (3.2.16) then one of the following steps may be envisaged for the reduction of the adsorbed NiOH:

$$NiOH_{ad} + H^+ + e \rightleftharpoons Ni + H_2O \qquad (3.2.18)$$

{

{ $NiOH_{ad} + NiOH^+ + 2e \longrightarrow NiOH_{ad} + Ni + OH^-$

{ (3.2.19)

$$NiOH_{ad} + NiOH^+ + 3e \longrightarrow 2Ni + 2OH^- \qquad (3.2.20)$$

An alternative mechanism, also involving NiOH, is[164]:

$$Ni + [Ni(H_2O)_4]^{2+} + e \rightleftharpoons (NiOH)^+ \cdot 3H_2O + Ni - H_{ad} \qquad (3.2.21)$$

$$(NiOH)^+ + e \rightleftharpoons NiOH_{ad} \qquad (3.2.22)$$

$$NiOH_{ad} + Ni - H_{ad} \rightleftharpoons 2Ni + H_2O \qquad (3.2.23)$$

The presence of a monolayer of $(NiOH)^+$ (at small cathodic potentials) has been claimed.[165]

CHAPTER FOUR

EXPERIMENTAL TECHNIQUES

4.1 Techniques for kinetic investigations

All experiments of this type were conducted in an electrolytic cell (in house) similar to that illustrated in Plate I. The three electrode cell was constructed from borosilicate glass with unlubricated ground glass joints, facility being made for the passage of nitrogen gas both through and (in later designs) over the electrolyte. White spot nitrogen, further purified by passage over copper turnings at ∿ 400°C, was used in this way in all experiments. The reference electrode compartment was terminated by a Luggin capillary, the tip of which was positioned 0.5 - 1.0 mm from the surface of the working electrode. The counter electrode compartment was separated from the main body of the cell by a porous frit. The facility of circulating the electrolyte over purified charcoal was provided, but not found to be beneficial and was not utilised.

All glassware was steeped in ∿ 50:50 (vol:vol) H_2SO_4/HNO_3 for 24 h. and then thoroughly rinsed with tri-distilled water before use. All solutions were prepared from AnalaR grade reagents where possible; tri-distilled water was used throughout.

The working electrodes were metal rods (Cd; Specpure, JMC 170, Johnson Matthey Chemicals Ltd.) machined to a diameter of 3.0 mm and pressed into a Teflon shroud. A one piece construction (Fig. 4.1.1b) was favoured over the two piece design (Fig. 4.1.1a) on account of the improved corrosion resistance afforded. Electrical contact was established via a compression spring soldered onto the electrode thence to the stainless steel shaft of the rotating disc assembly and a mercury

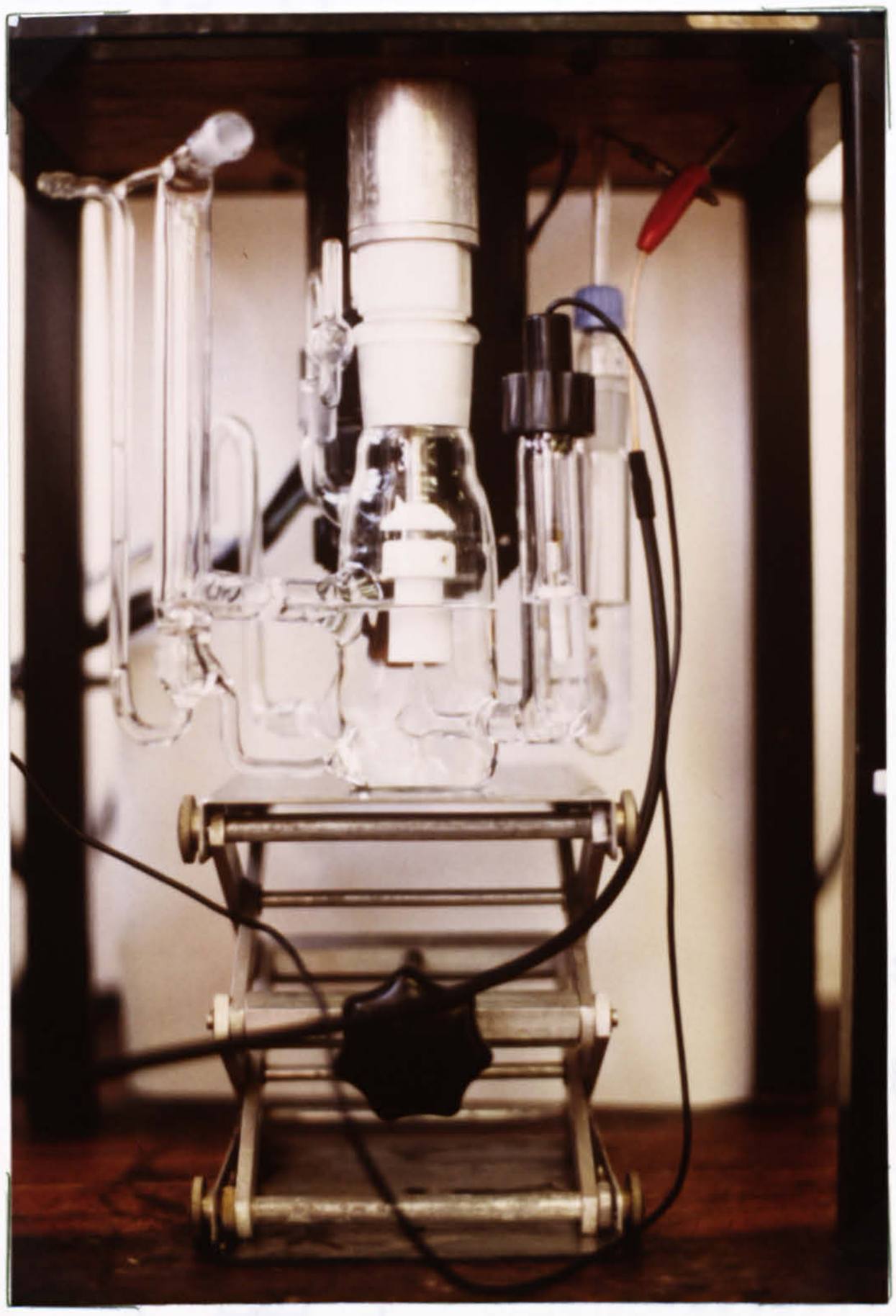

PLATE I The electrochemical cell

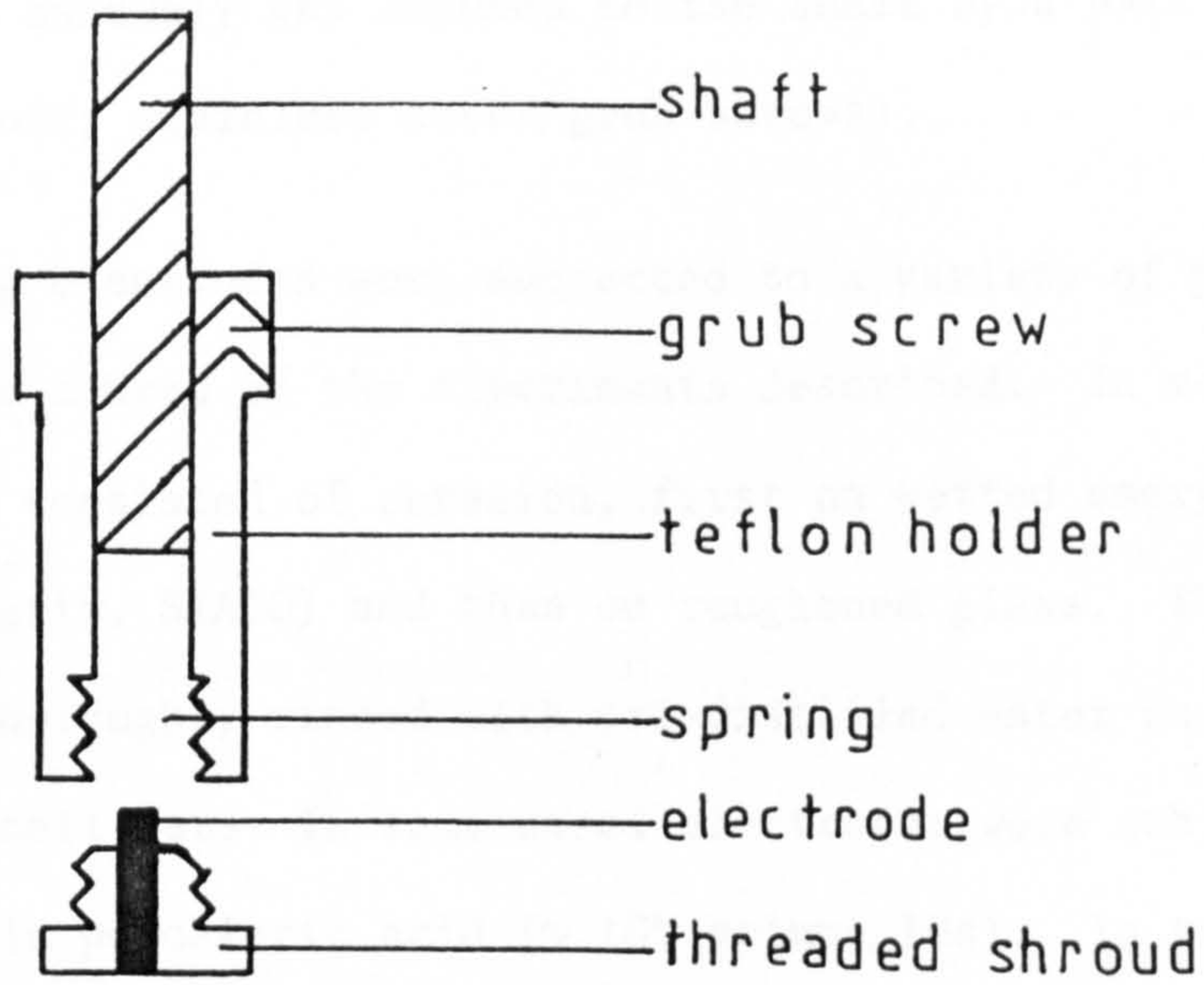

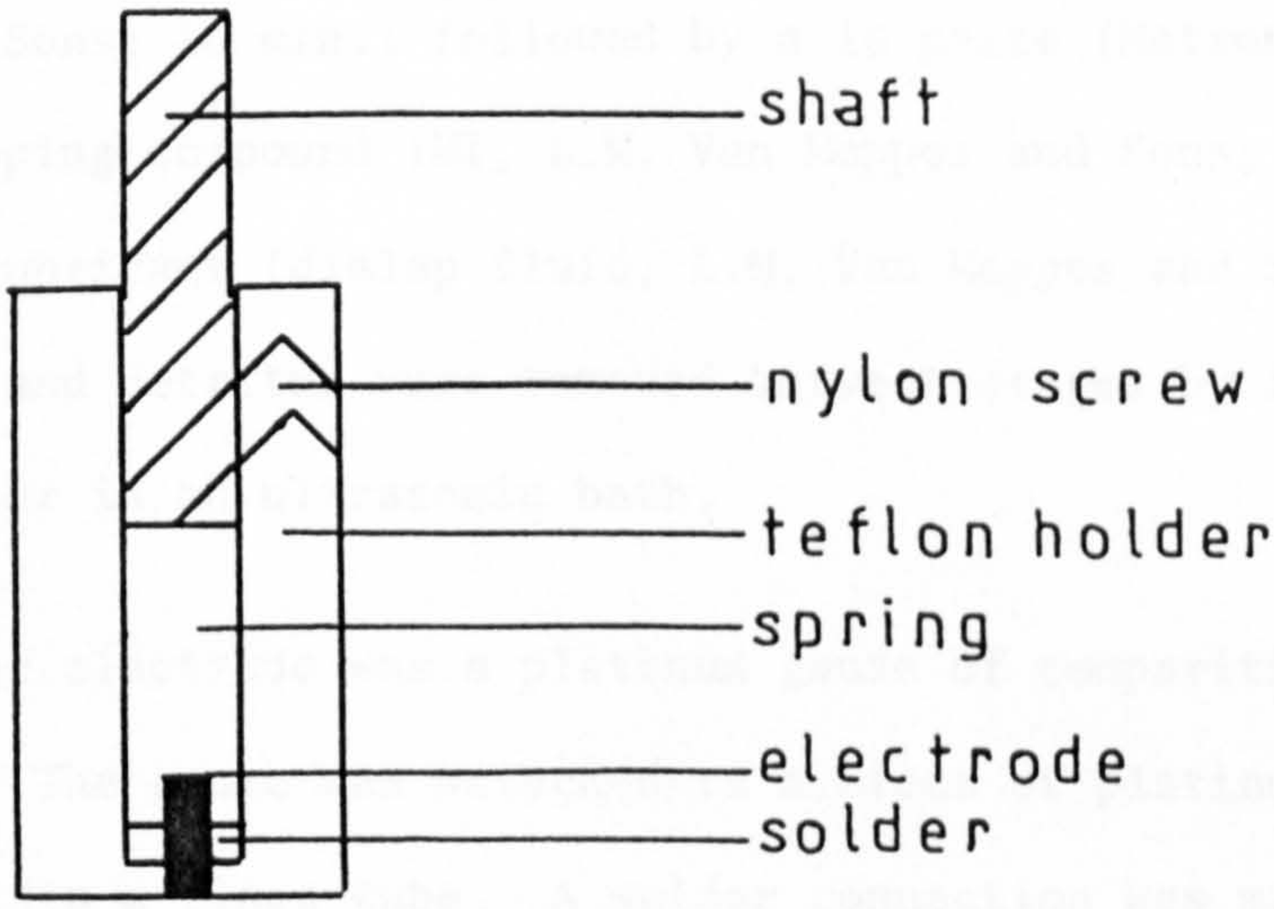

Fig. 4.1.1 Working Electrode designs

(a) Two piece construction

(b) One piece construction

pool. The electrode assembly was secured to the shaft by a pair of nylon screws (previously stainless steel grub screws).

The working electrodes were subjected to a variety of pre-treatments during the course of the experiments described. In most cases, pre-treatment consisted of abrasion, first on wetted emery paper (600 and 1200 grit, SIACO) and then on roughened glass. The electrode was then thoroughly rinsed with tri-distilled water and introduced into the cell wet. In some cases electrodes were subjected to chemical etching in perchloric acid (∿ 10% volume, 10s). In an attempt to produce working electrodes of a more reproducible surface state, abrasion on roughened glass was replaced by the following procedure. The electrodes were roughly dried and polished on an automatic polishing and lapping machine (Kent 2A, Engis Ltd.) using a 6μ diamond paste (Padamet cloth, Metaserv; dialap lapping compound 6M3, L.M. Van Moppes and Sons; 10 min.) followed by a 1μ paste (Metron cloth, Metaserv; dialap lapping compound 1M1, L.M. Van Moppes and Sons; 5 min.) with a recommended lubricant (dialap fluid, L.M. Van Moppes and Sons). Traces of lubricant and detritus were removed between stages by immersion in tri-distilled water in an ultrasonic bath.

The counter electrode was a platinum gauze of comparitively large surface area. The gauze was attached to a piece of platinum wire which was let into a glass tube. A solder connection was made, at the bottom of the tube, between the platinum and a length of copper wire.

The reference electrode was a wick-type sodium calomel electrode (Beckman RIIC, reference solution: saturated sodium chloride).

4.1.1 Experiments at the Rotating Disc Electrode

The electrical circuitry, in schematic form, is shown in Fig. 4.1.2. For experiments at the rotating disc, however, there was no need for the x-y recorder or the function generator.

The potential of the working electrode was maintained against that of the reference electrode (measured at the tip of the Luggin capillary) using a potentiostat (Ministat 251 (I.R.), H.B. Thompson and Associates). For each electrode potential the steady-state current was measured with a digital multimeter (Sinclair DM450, Sinclair Radionics Ltd.) as a potential drop across a sense resistor (1.00 kΩ) in series with the working electrode. The current-time profile was recorded using a y-t chart recorder (Omniscribe B5116-7, Houston Instrument) to determine the attainment of the steady-state. The electrode was rotated at a series of angular velocities (in house RDE assembly) in the range $50<\omega<1000$ r.p.m. and the steady-state current determined for each.

4.1.2 Linear/Cyclic Sweep Voltammetry

The same electrical circuit (Fig. 4.1.2) as used for rotating disc experiments was employed, this time utilising the x-y recorder and function generator.

The function generator (in house) was capable of producing a triangular waveform of various amplitudes and frequencies. The triangular waveform of the generator was superimposed upon the d.c. potential of a potentiostat (Ministat 251 (I.R.), H.B. Thompson and

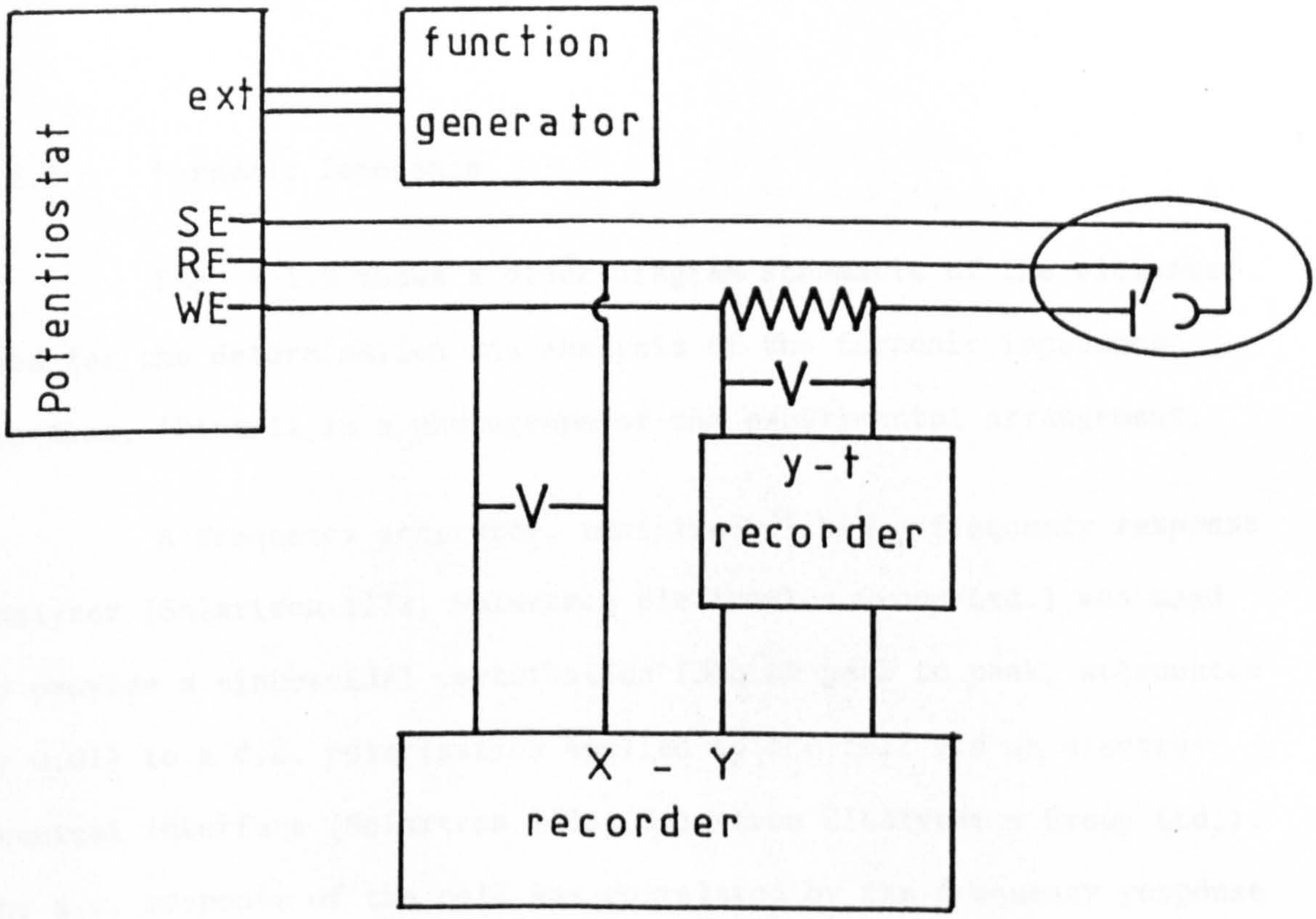

Fig. 4.1.2 Electrical circuit (block diagram) for LSV/RDE experiments

Associates). The voltammograms were recorded with a x-y recorder (Omnigraphic 2011, Houston Instrument) at a series of sweep rates. The first sweep was made, in the cathodic direction, at a clean electrode and subsequent sweeps carried out until a steady-state voltammogram was achieved. Both the initial and equilibrium sweeps could be obtained from the same experiment. The sweep limits were generally from the onset of oxygen evolution to that of hydrogen evolution.

4.1.3 Faradaic Impedance

Fig. 4.1.3 shows a block diagram schematic of the elements used for the determination and analysis of the faradaic impedance spectrum. Plate II is a photograph of the experimental arrangement.

A frequency generator, contained within a frequency response analyser (Solartron 1172, Solartron Electronics Group Ltd.) was used to provide a sinuosoidal perturbation (300 mV peak to peak, attenuated by 0.01) to a d.c. polarisation applied to the cell via an electrochemical interface (Solartron 1186, Solartron Electronics Group Ltd.). The a.c. response of the cell was correlated by the frequency response analyser and output, via a data transfer unit, to a teletype printer and paper-tape punch (Data Dynamics 390, Data Dynamics Ltd.). The frequency response analyser also allowed for the programming of a frequency scan anywhere between the limits 10 kHz>ω>1 mHz in either direction. The number of frequencies per decade may also be programmed. When required, a Sluyters Plot, could be obtained directly on an x-y recorder (Bryans 26000) via a plotter interface (Solartron 1182, Solartron Electronics Group Ltd.). The data was subsequently transferred to a Prime 400 mainframe computer equipped with graphics terminals.

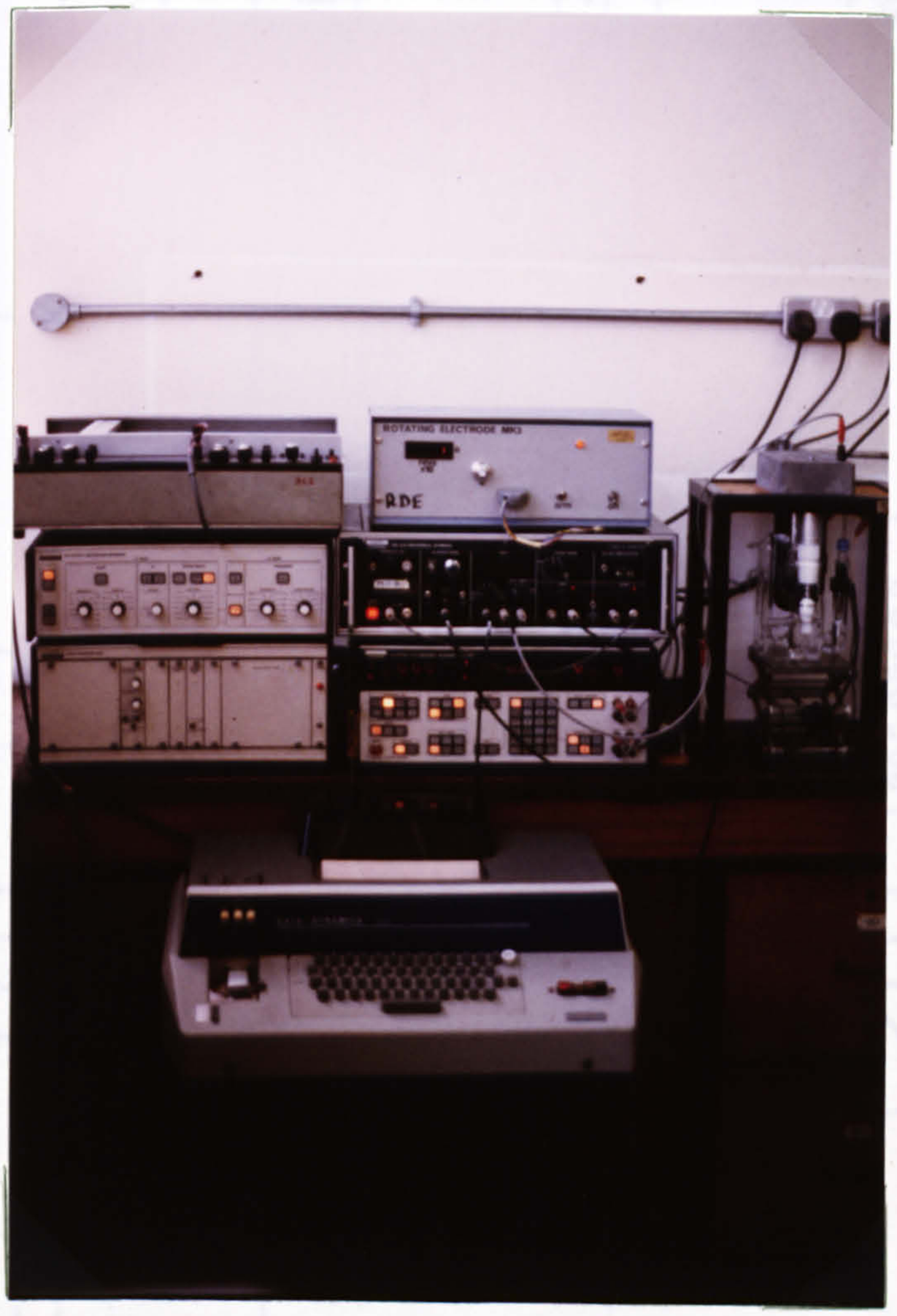

PLATE II The experimental arrangement for the measurement of faradaic impedance

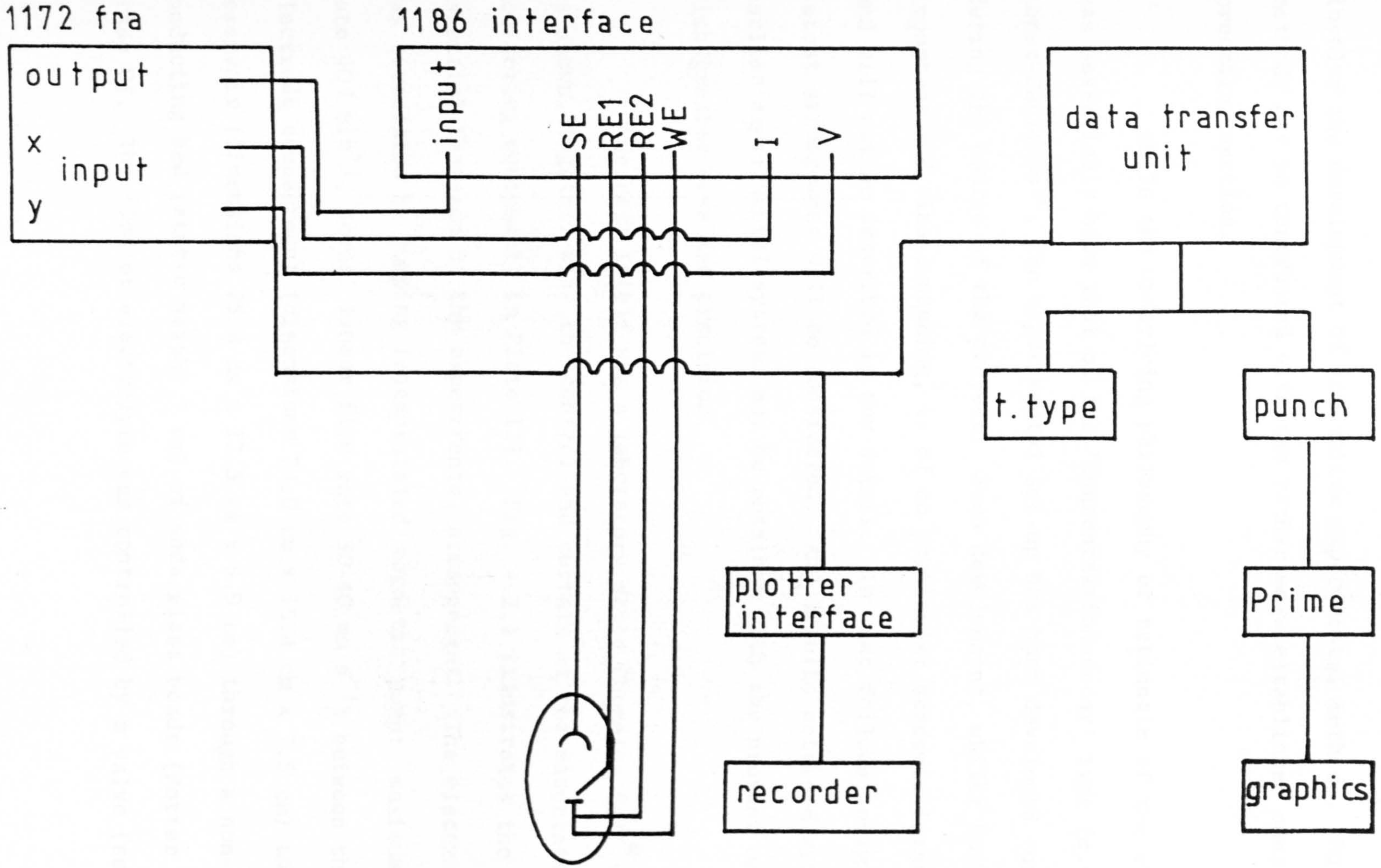

Fig. 4.1.3 Electrical circuit (block diagram) for impedance experiments

4.2 Experiments in the Chemelec Cell®

The Chemelec Cell® is a comparatively recent development in electrochemical technology. It is to be expected, therefore, that the scientific investigation of aspects of its electrochemistry will involve the development of innovative experimental methods. Such methods may be contrasted with the rather more established ones of the preceding section.

While the underlying philosophy or rationale of the experiments has essentially been that of the 'concentration-decay' type (q.v.) of Lopez-Cacicedo[30], the experimental set-up has been developed continuously during the course of the project. Such development, whilst both important and time-consuming, is of no particular academic interest and will not be described in any detail. In what follows, only the latest arrangement will be considered. Any results obtained with earlier experimental systems may be obtained with the present one, and with greater ease and precision.

The cell itself was a laboratory scale Chemelec Cell® which is shown, together with the control and certain of the associated monitoring equipment, in Plate III. Fig. 4.2.1 illustrates the essential features of the experimental arrangement. The electrolyte was circulated by pumping (encapsulated magnetic pump: maximum flow rate 40 l min^{-1}, actual linear flow rate 30-40 mm s^{-1}) between the electrode compartment (dimensions 24.0 cm x 15.4 cm x 7.5 cm) and the reservoir (dimensions 25.0 cm x 13.3 cm x 9.9 cm) through a non-conducting bed (static height 7 cm) of soda glass beads (Potter Ballutini Grade O). The flow of electrolyte was controlled by a valve (see Plate III)

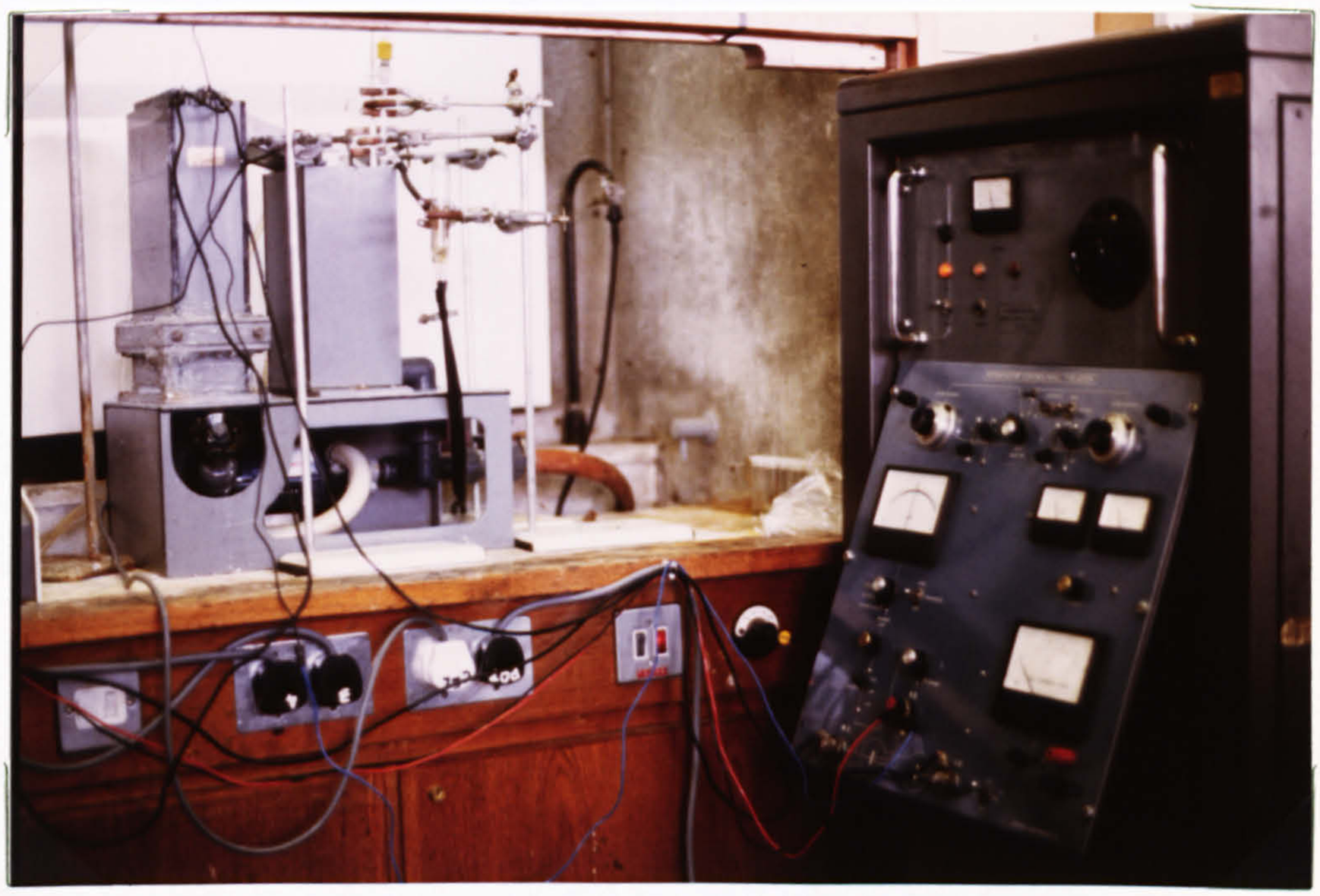

PLATE III The Chemelec Cell and potentiostat

Key to Fig. 4.2.1

1 Hg/Hg_2SO_4 electrode

2 reference electrode assembly

3 RuO_2/Ti anode (mesh)

4 Ti cathode (mesh)

5 Luggin capillary

6 fluidised bed

7 slotted flow distributor

8 encapsulated magnetic pump

9 weir

10 bead catcher

11 thermometer

12 pH electrode

13 reservoir

14 heating coil

15 water outlet

16 water inlet

17 constant head device

18 from peristaltic pump

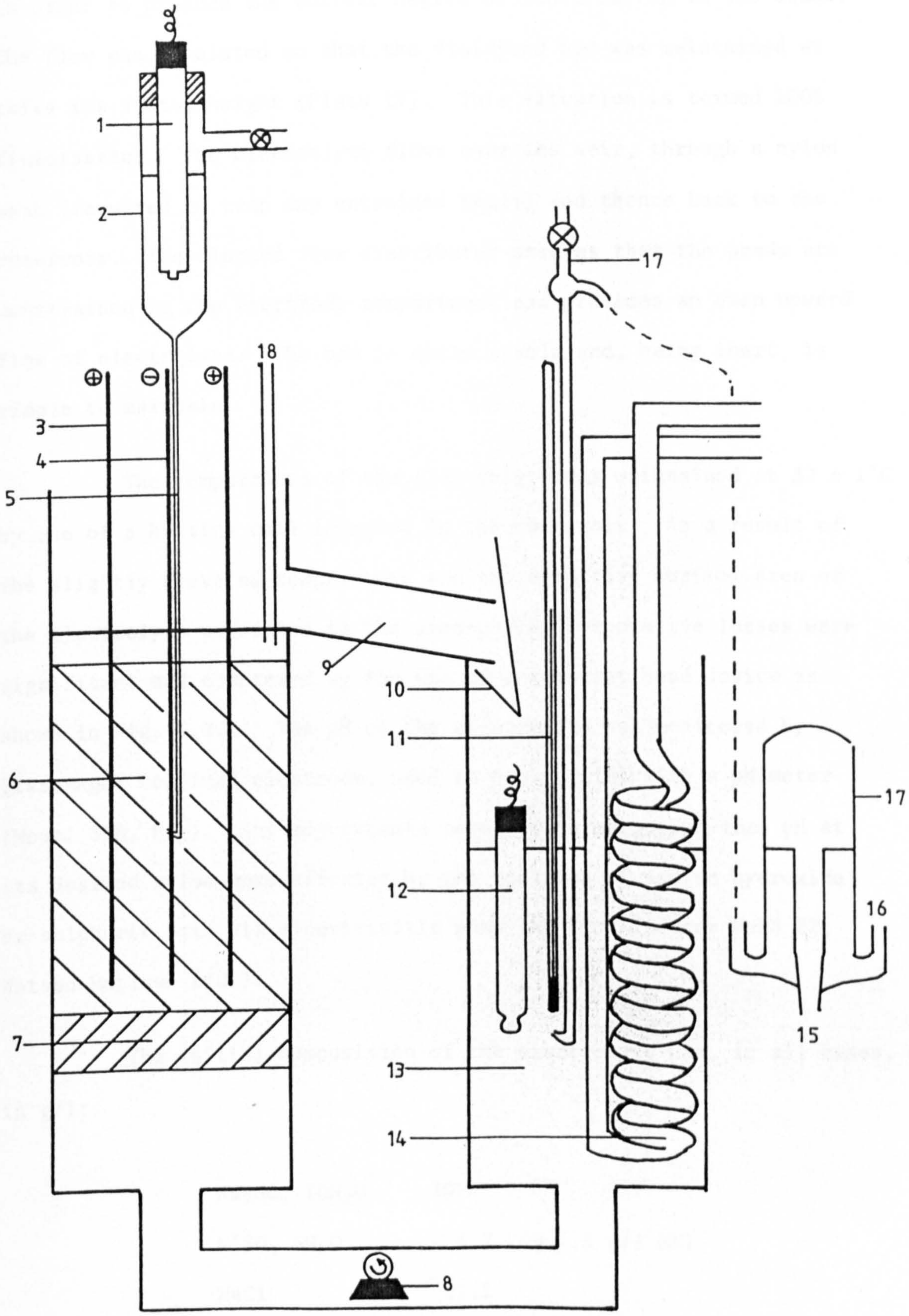

Fig. 4.2.1 Essential features of the Chemelec Cell® experimental arrangement

in order to produce the correct degree of fluidisation in the beads. The flow was regulated so that the fluidised bed was maintained at twice its static height (Plate IV). This situation is termed 100% fluidisation. The electrolyte flows over the weir, through a nylon mesh (required to trap any entrained beads) and thence back to the reservoir. The slotted flow distributor ensures that the beads are constrained to the electrode compartment and provides an even upward flow of electrolyte. The bed is quite stable and, being inert, is simple to maintain.

The temperature of the electrolyte was maintained at 32 ± 1°C by use of a heating coil immersed in the reservoir. As a result of the slightly elevated temperature and the effective surface area of the electrolyte presented to the atmosphere, evaporative losses were significant and countered by the use of a constant head device as shown in Fig. 4.2.1. The pH of the electrolyte was monitored by a glass-AgCl combined electrode, used in conjunction with a pH meter (Model 38B, EIL). Any adjustments required to maintain the pH at its desired value were effected by the addition of sodium hydroxide or sulphuric acid via a peristaltic pump (HR Flow Inducer MHRE 22, Watson-Marlowe Ltd.).

The initial composition of the electrolyte was, in all cases, in g/l:

$Na_2SO_4.10H_2O$	397	
$NiSO_4.6H_2O$	6.7	(≡ 1.5 g/l Ni)
NaCl	22.2	
H_3BO_3	39.6	

PLATE IV The electrode compartment of the Chemelec Cell showing 100% fluidisation of the bed

This composition was thought to adequately model that of a typical drag-out solution after many months of use*.

The cathode was an expanded titanium mesh, whose nominal working surface area was restricted by the use of a stopping-off medium (Fortolac, Wm. Canning & Co.) to a central area consistent with the output limitations of the potentiostat. The cathode was flanked by a pair of RuO_2/Ti anodes; the inter-electrode separation was 2.45 cm. The reference electrode (Hg/Hg_2SO_4, ceramic junction, EIL) was housed in a reference electrode assembly allowing a Luggin capillary to penetrate the approximate centre of the cathode working area. The tip of the capillary contained an asbestos fibre to guard against its becoming blocked by glass beads.

The electrical circuit is shown, in block schematic form, in Fig. 4.2.2 (see also Plate V). The potential of the cathode was maintained with respect to the potential of the reference electrode at the tip of the Luggin capillary by a potentiostat (Chemical Electronics 10/50A), and measured with a digital voltmeter (DPM 300, Advance). A network of resistors, interposed in the secondary electrode circuit, allowed for the measurement of the current as a potential drop displayed on a further digital multimeter. An attenuated voltage (derived from the resistor network as shown in Fig. 4.2.2) was grounded via a differential amplifier (151-BD, Fylde) and used to drive a y-t recorder (Omniscribe B5116-7, Houston Instrument). The same attenuated voltage was integrated (Mark IV Volt-Time Integrator, Lintronic Systems) over time to provide the charge passed.

All experiments were of the 'concentration-decay' type. The cell was operated potentiostatically in batch recycle mode at constant

---

* the nickel ion concentration falls continuously during the course of the experiment.

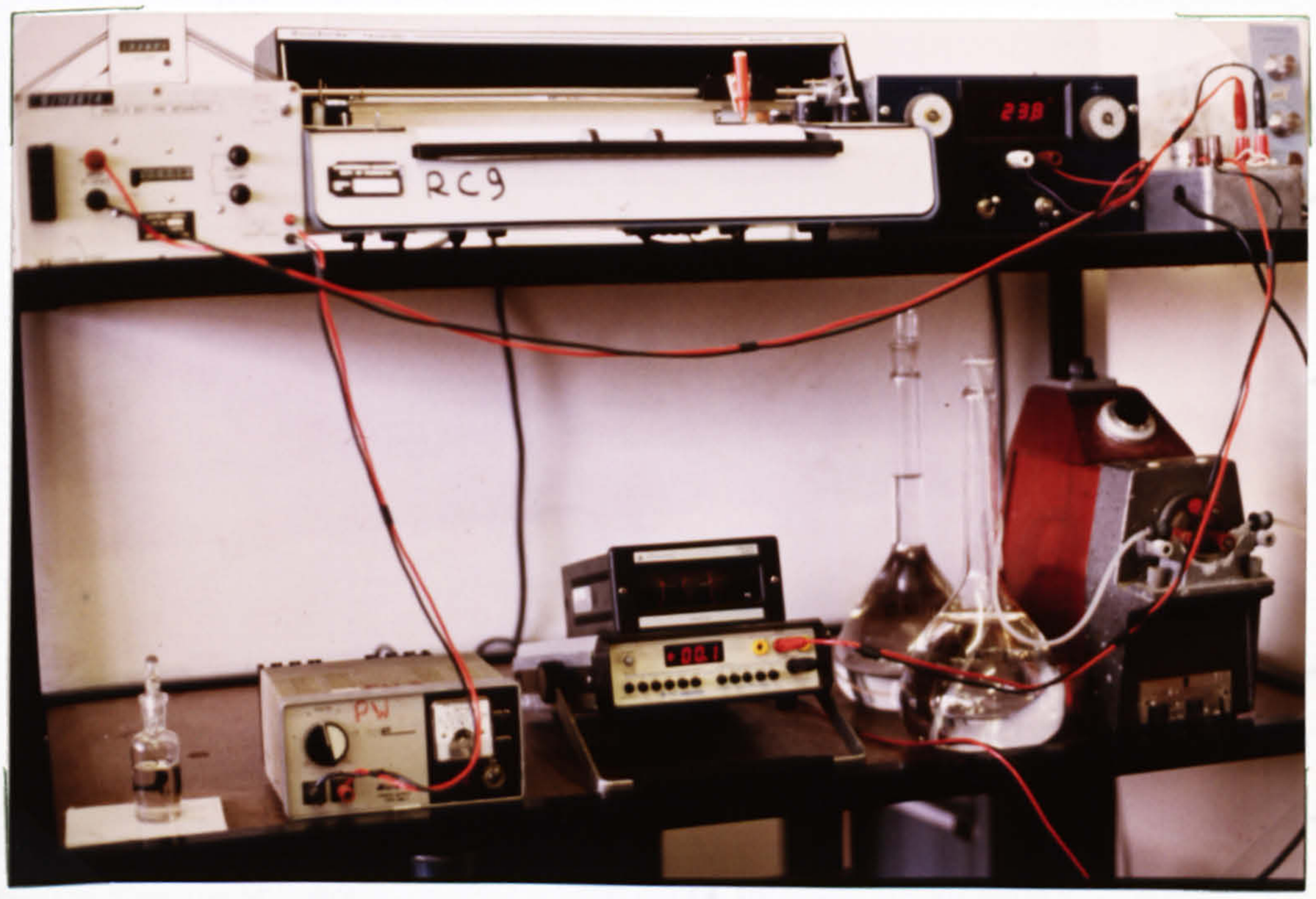

PLATE V Monitoring equipment used in Chemelec experiments

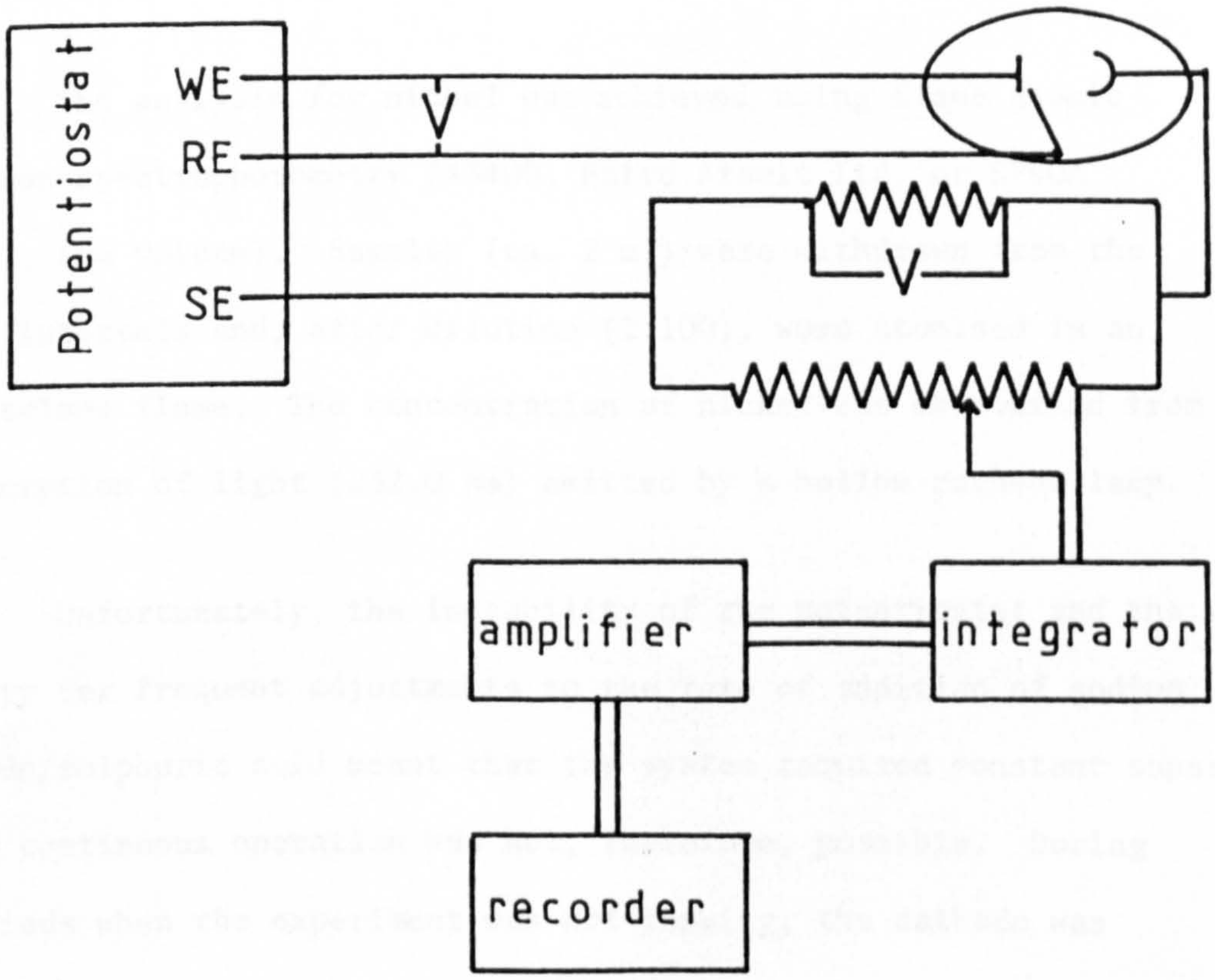

Fig. 4.2.2 Electrical circuit (block diagram) for Chemelec experiments

temperature, pH and fluidisation. The metal ion concentration was allowed to fall continuously and both it and the charge passed were obtained as functions of time.

Polarisation data was obtained at various concentrations (i.e. at various times during the experiment) by interrupting the experiment and manually step scanning the potential, observing the resulting steady-state currents. The potential scans were from the most cathodic in all cases.

The analysis for nickel was achieved using flame atomic absorption spectrophotometry (A3400, Baird Atomic Ltd. or SP90A Series 2, Pye Unicam). Samples (ca. 2 ml) were withdrawn from the cell at intervals and, after dilution (1:100), were atomised in an air-acetylene flame. The concentration of nickel was determined from the absorption of light (232.0 nm) emitted by a hollow cathode lamp.

Unfortunately, the instability of the potentiostat and the necessity for frequent adjustments to the rate of addition of sodium hydroxide/sulphuric acid meant that the system required constant supervision; continuous operation was not, therefore, possible. During the periods when the experiment was not running, the cathode was removed from the cell and stored under water.

Likewise, between experiments, the glass beads were kept wet. It was found that if the beads were allowed to dry then aggregation would occur and it would no longer be possible to produce an evenly fluidised bed. This situation could be remedied by treating the glass beads with hot sodium hydroxide ($\sim$ 5 M), followed by hot sulphuric acid ($\sim$ 4 M) with copious washing with water between.

CHAPTER FIVE

CADMIUM IN PERCHLORIC ELECTROLYTES

5.1 Introduction

Before attempting to determine impedance spectra for cadmium in alkaline cyanide solutions, it was decided to test the procedure on a system for which impedance data was already available. The choice of a perchloric electrolyte was thought to exclude the possibility of encountering film formation and associated problems. Experiments with electrolytes similar to those studied by Harrison et al[135] afforded results of interest in their own right, as well as verifying the method.

5.2 Experimental

The solution was composed of the following electrolytes:

$CdSO_4$	0.005M
$HClO_4$	0.001M
$NaClO_4$	1.000M

The impedance spectrum of the system was determined at a range of electrode potentials on either side of the equilibrium. For each potential, the frequency of the alternating perturbation was scanned from 9.9 kHz to 1.0 mHz (or until the system became unstable) in steps of ten frequencies per decade.

5.3 Results

The resulting impedance spectra were analysed by computer according to the model of Randles.[98] The previously described numerical method (§2.6.3) was used to find maximum likelihood estimates of the four parameters R_Ω, Θ, C_L and $\dot{\sigma}$. The computer then calculated the impedance spectrum from the values of the parameters thus determined. In the spectra of Figs. 5.1 to 5.8 the points represent the experimental values, the solid lines are the calculated computer fits. In all cases the analysis was performed using both the so-called 'R-' and 'C-equations', (2.6.11) and (2.6.12). Noting in passing that R_Ω cannot be determined from (2.6.12), being purely resistive in nature, the values of the other parameters should be the same whether calculated from (2.6.11) or (2.6.12). In fact, there is generally a small discrepancy between the two values calculated for any given parameter. This discrepancy may be ascribed to the fact that the equivalent circuit does not exactly model the experimental system.

5.3.1 The cathodic process

Figs. 5.1 to 5.4 show the impedance spectra for the given system, at four different electrode potentials, as calculated from the 'R-equation'. Figs. 5.5 to 5.8 show the corresponding fits calculated from the 'C-equation'. The upper figure in each is the Sluyters Plot and the lower one the Randles Plot.

The agreement between experimental and calculated data is excellent and extends to frequencies of 1 Hz in some cases. This is a significant achievement in itself for the study of solid metal electrodes.

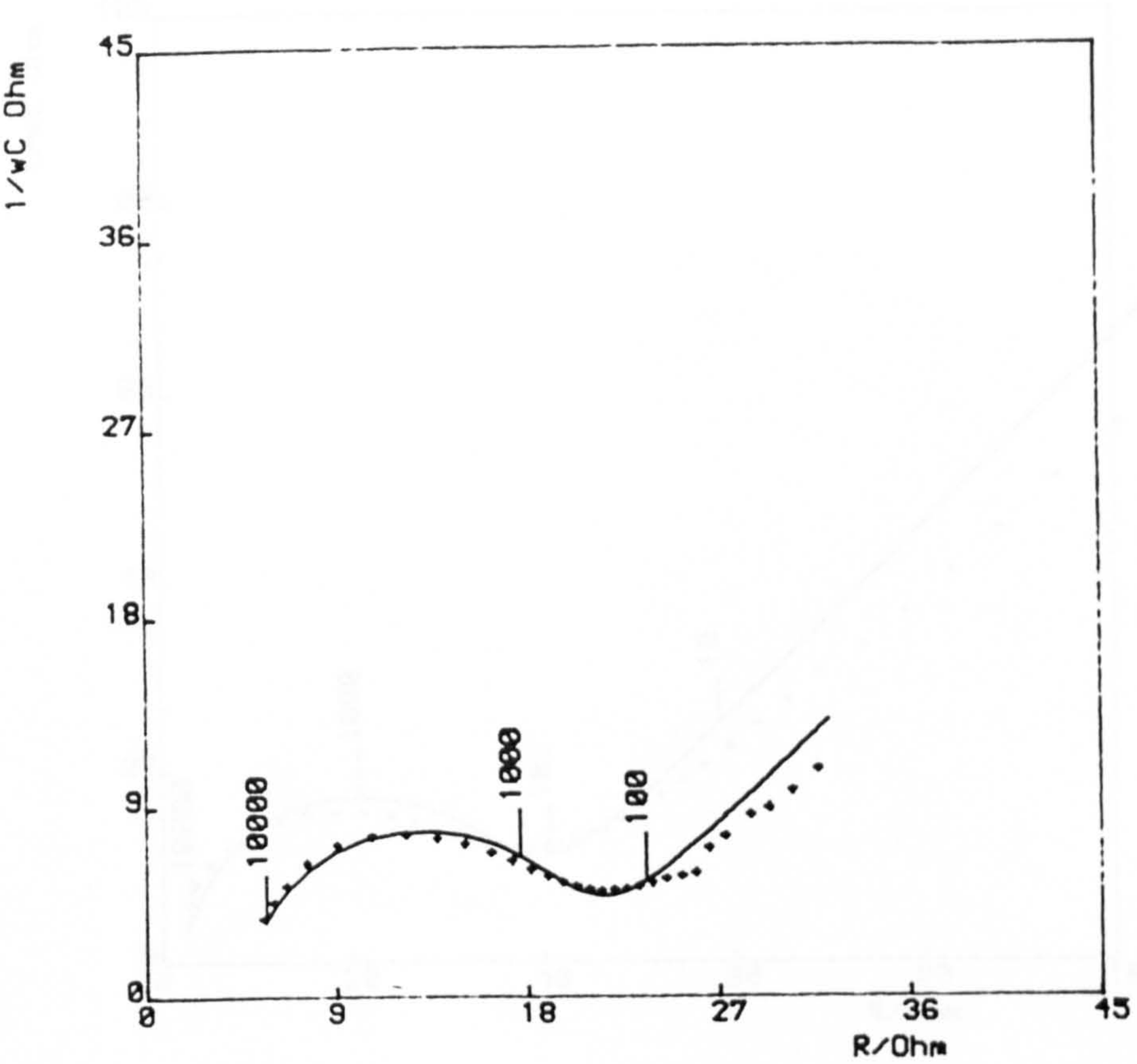

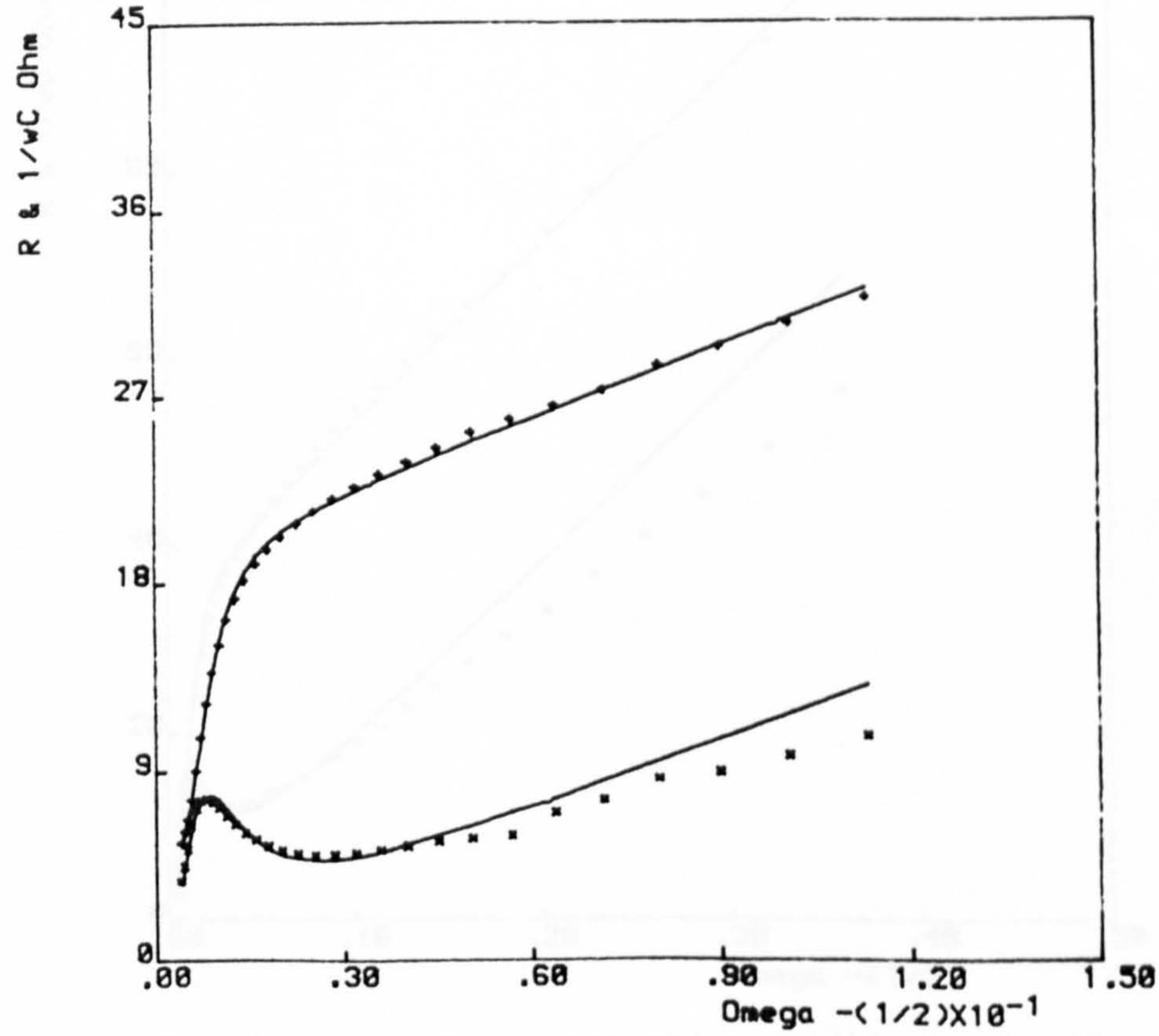

Fig. 5.1 Impedance spectrum analysed according to the 'R-equation', E = - 0.721 V

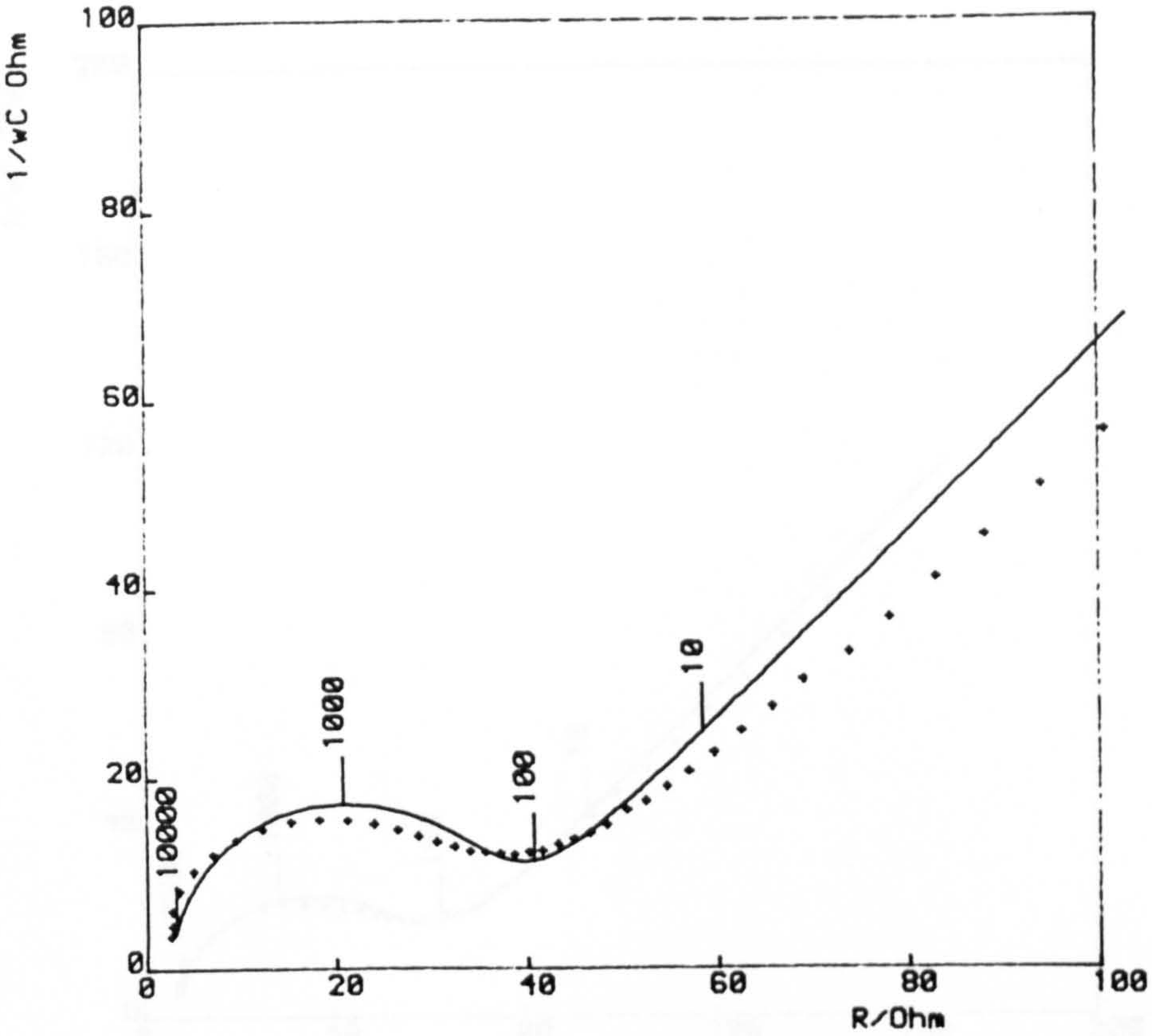

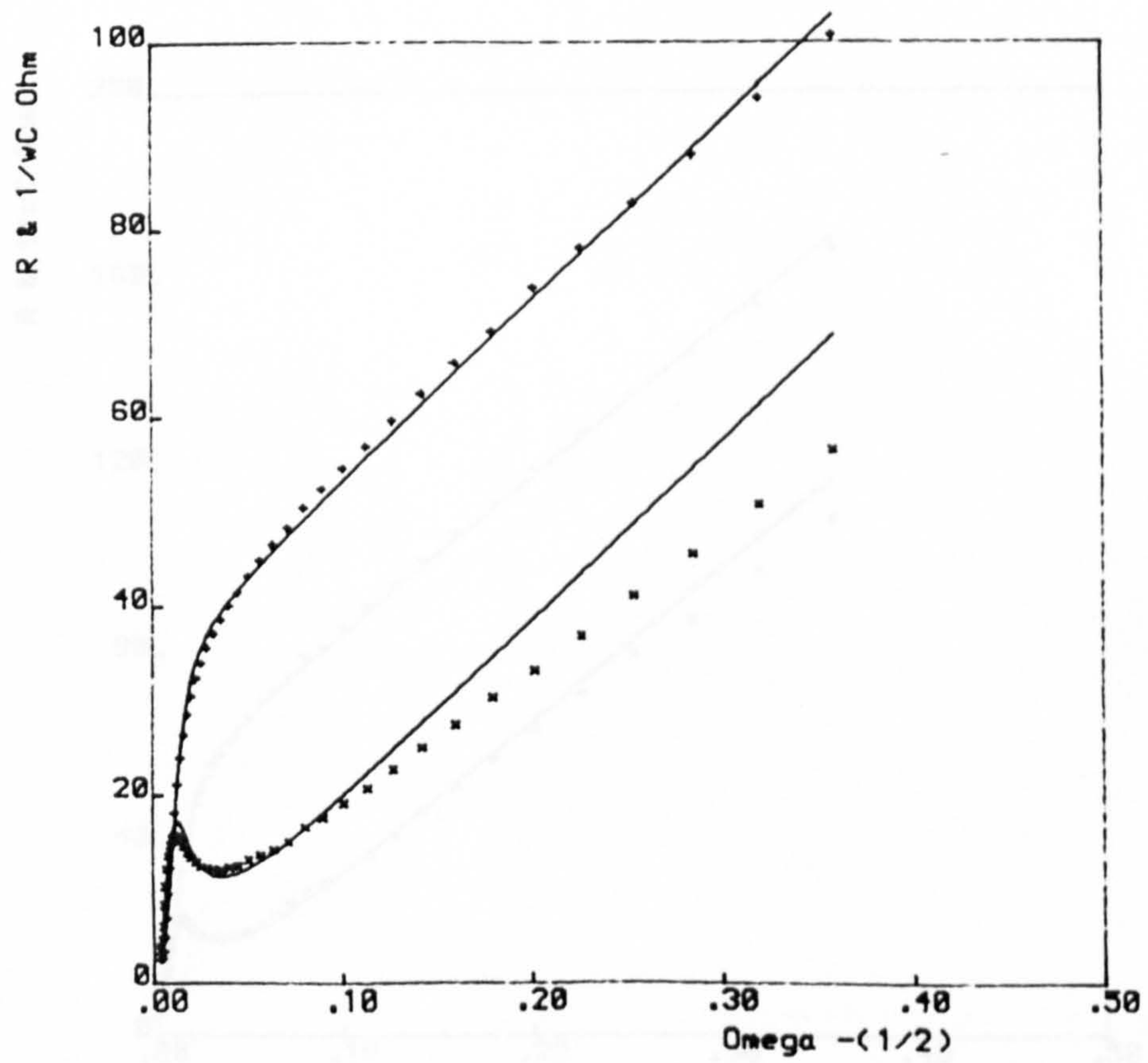

Fig. 5.2 Impedance spectrum analysed according to the 'R-equation', E = - 0.731 V

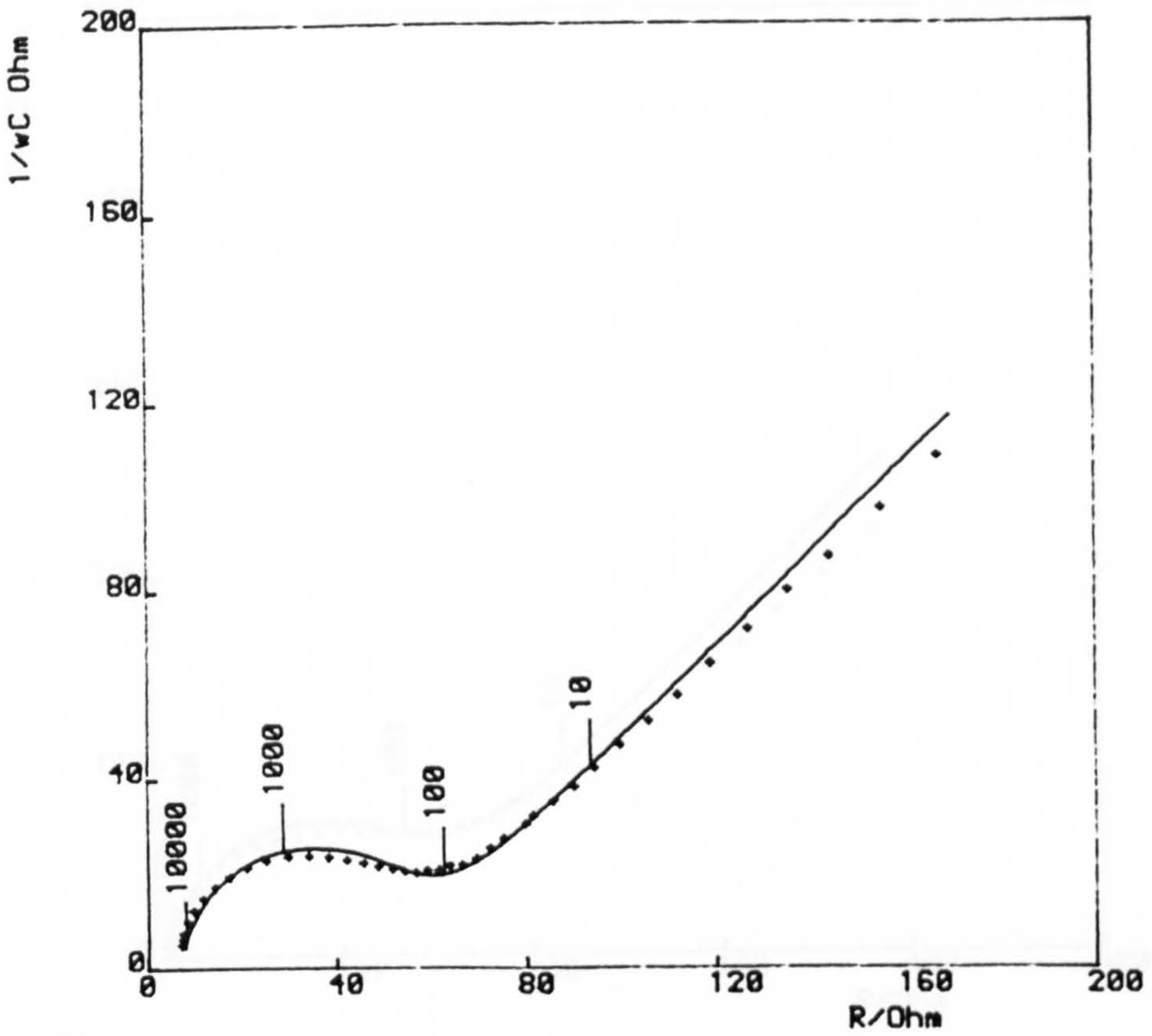

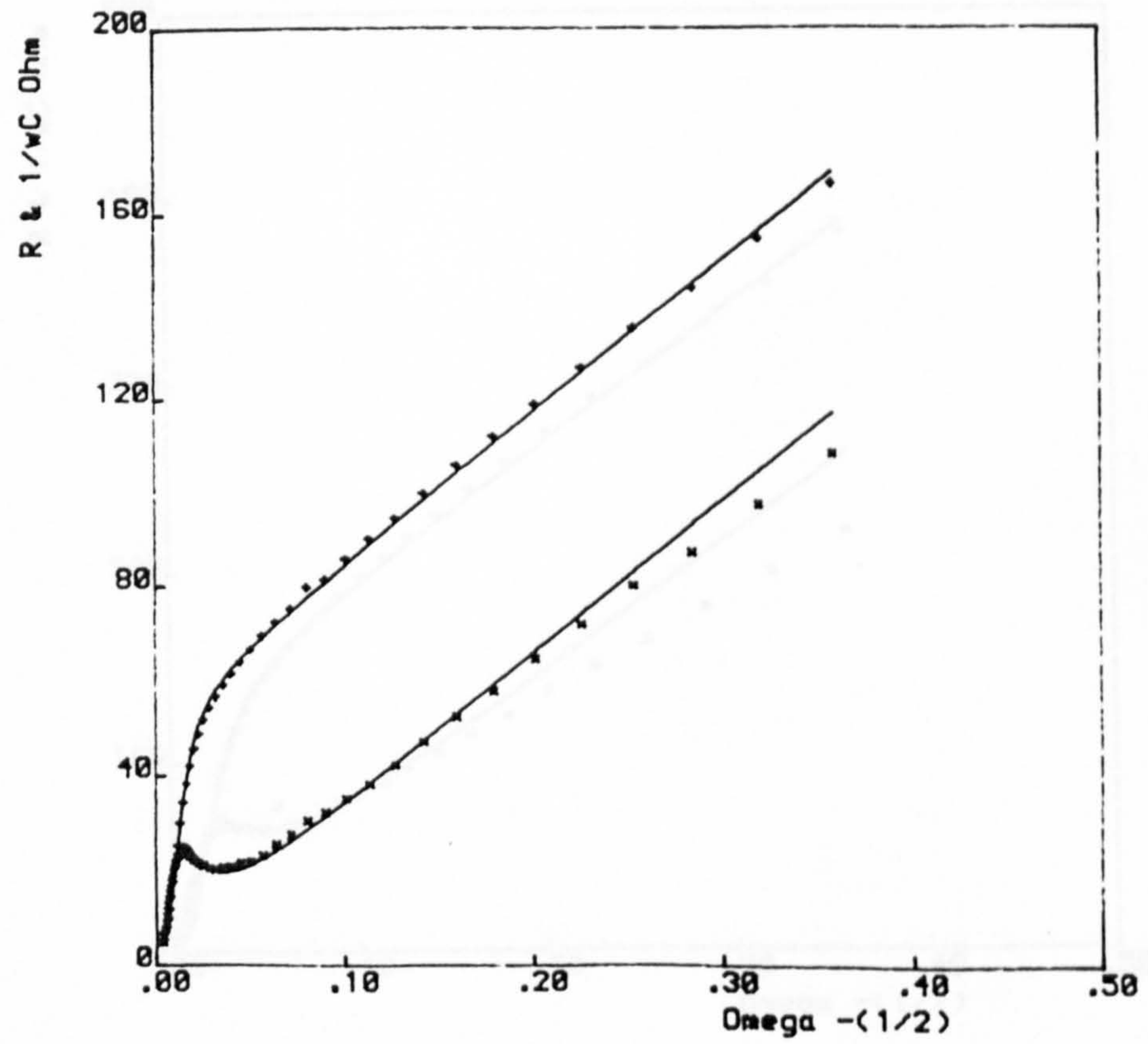

Fig. 5.3 Impedance spectrum analysed according to the 'R-equation', E = - 0.737 V

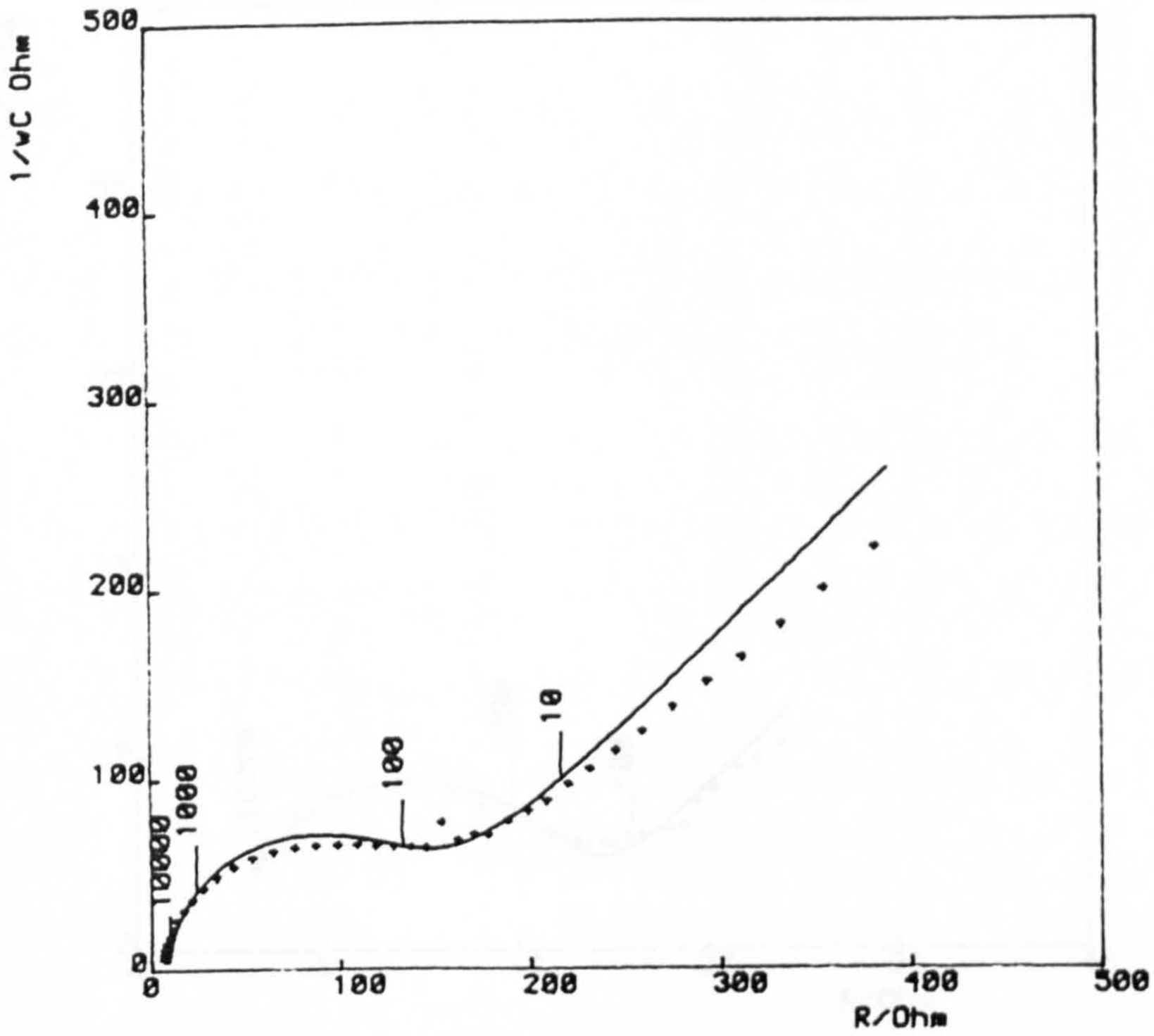

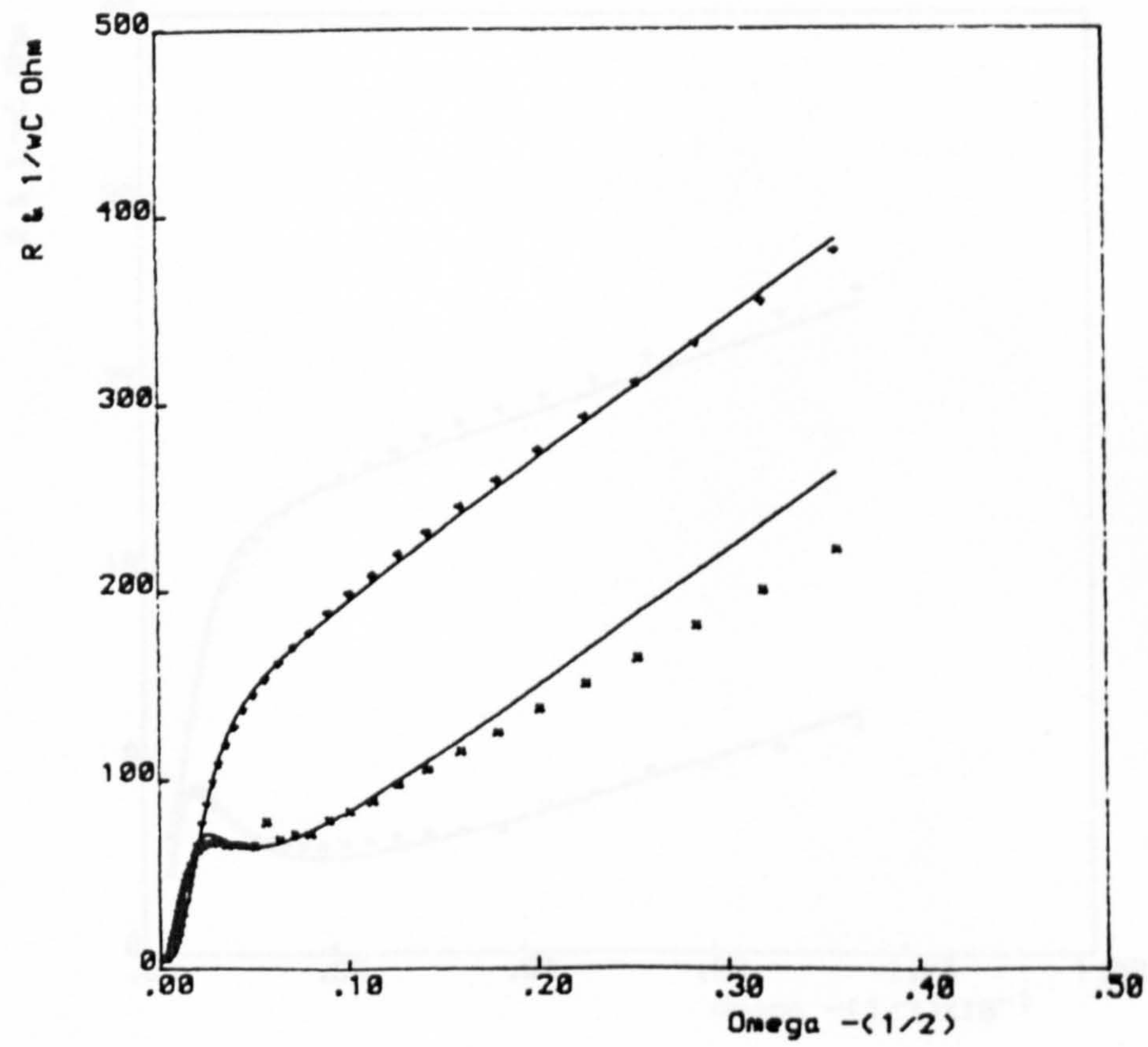

Fig. 5.4 Impedance spectrum analysed according to the 'R-equation', E = - 0.745 V

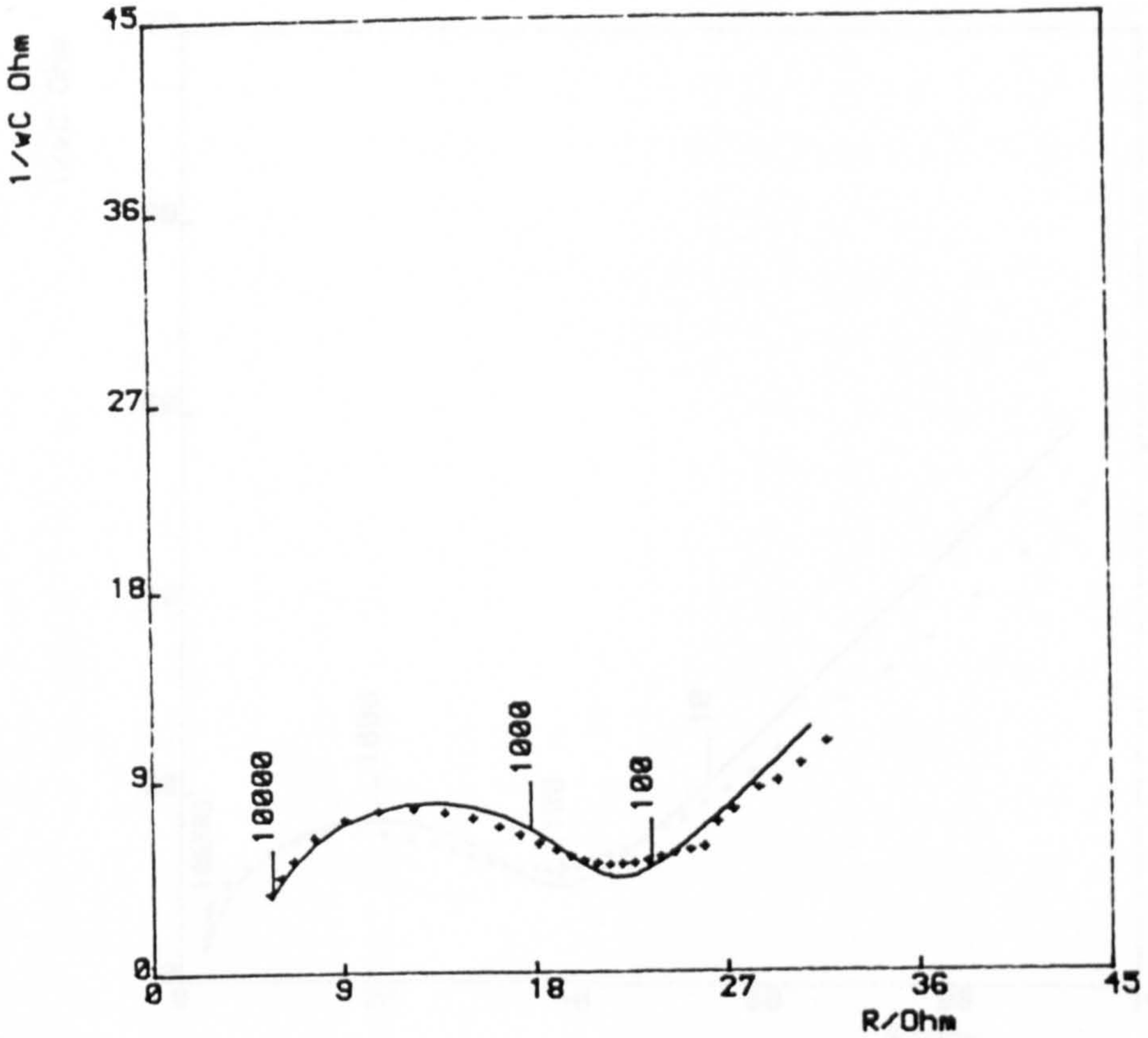

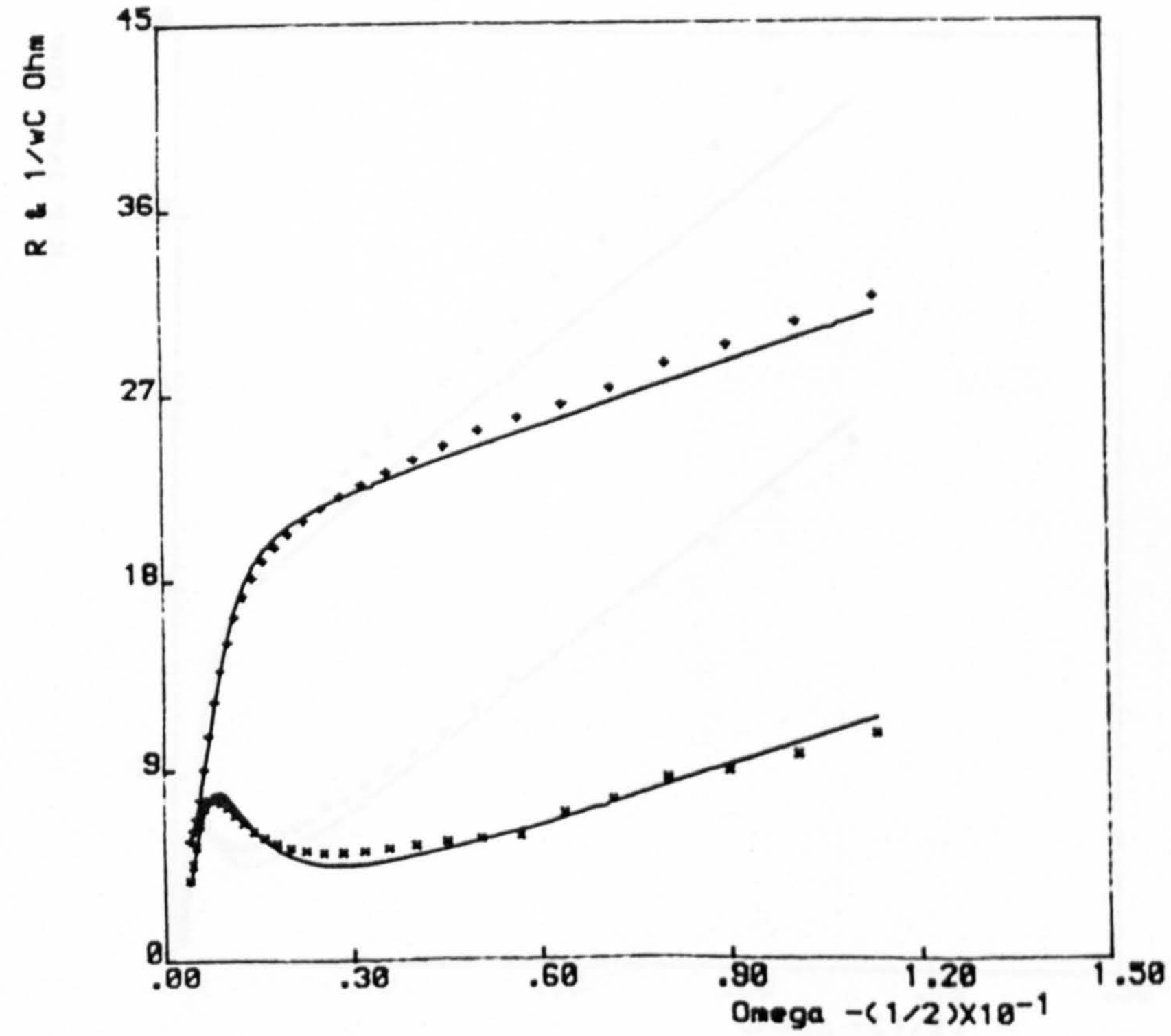

Fig. 5.5 Impedance spectrum analysed according to the 'C-equation', E = - 0.721 V

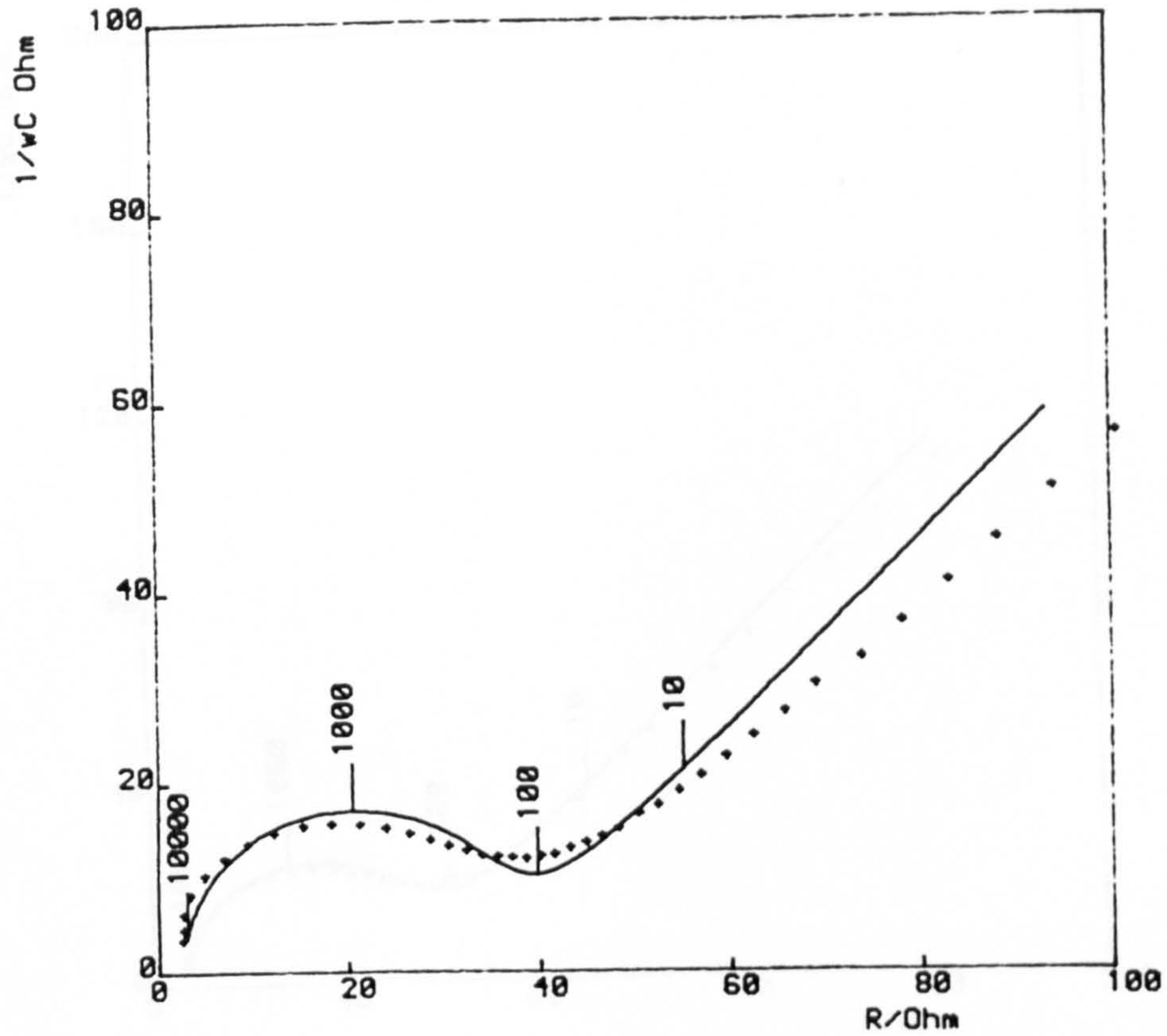

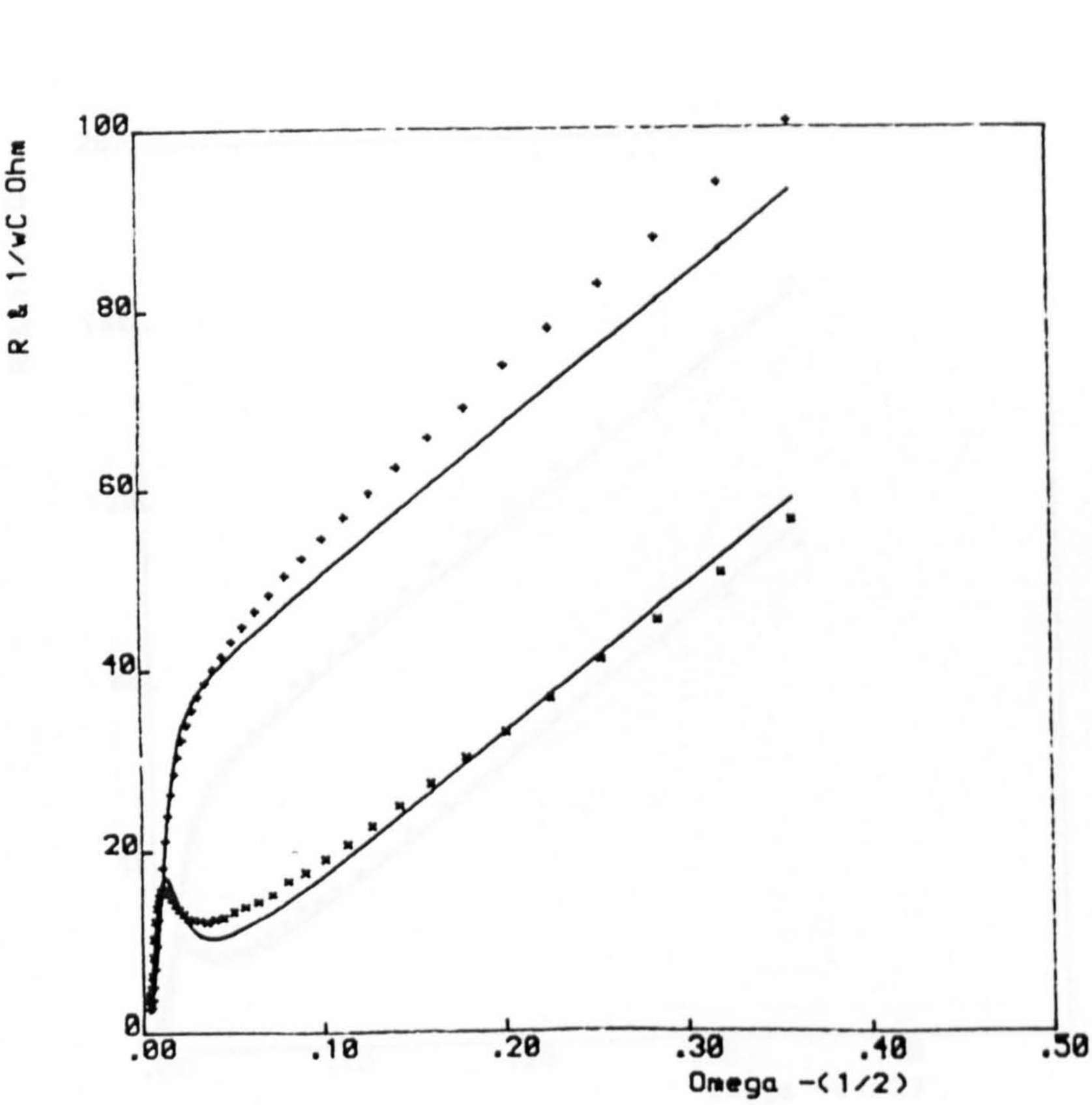

Fig. 5.6 Impedance spectrum analysed according to the 'C-equation', E = - 0.731 V

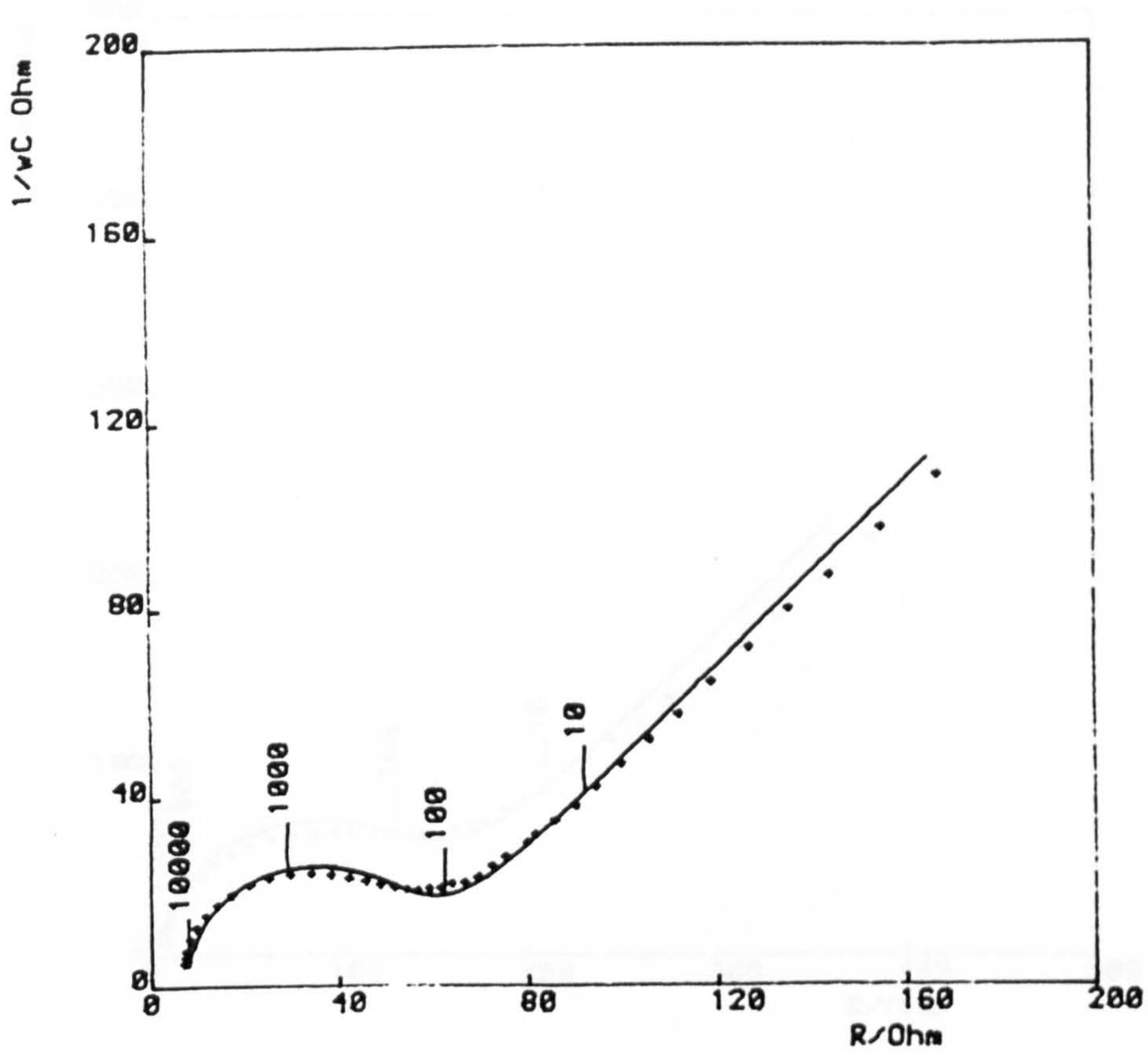

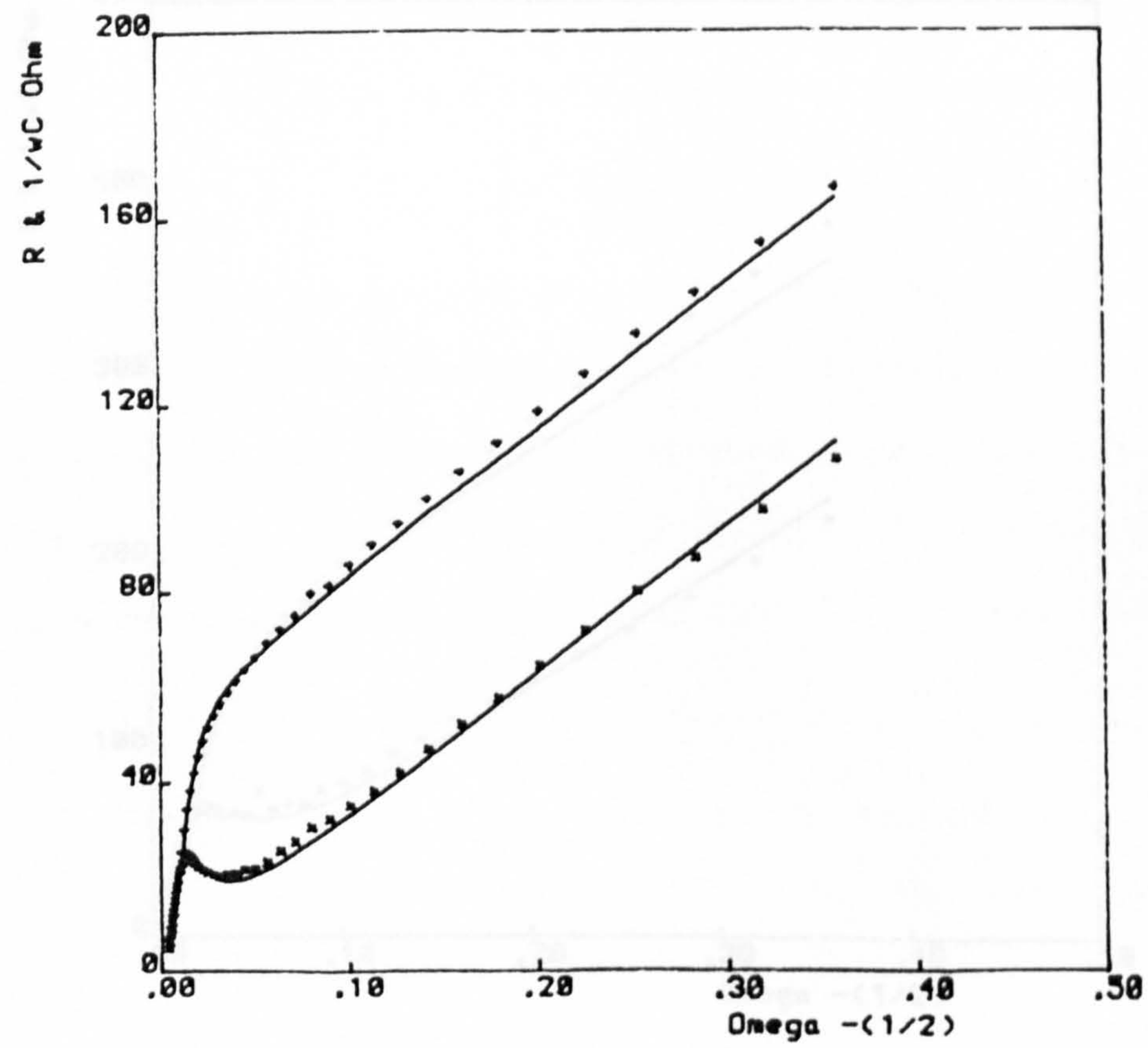

Fig. 5.7 Impedance spectrum analysed according to the 'C-equation', E = - 0.737 V

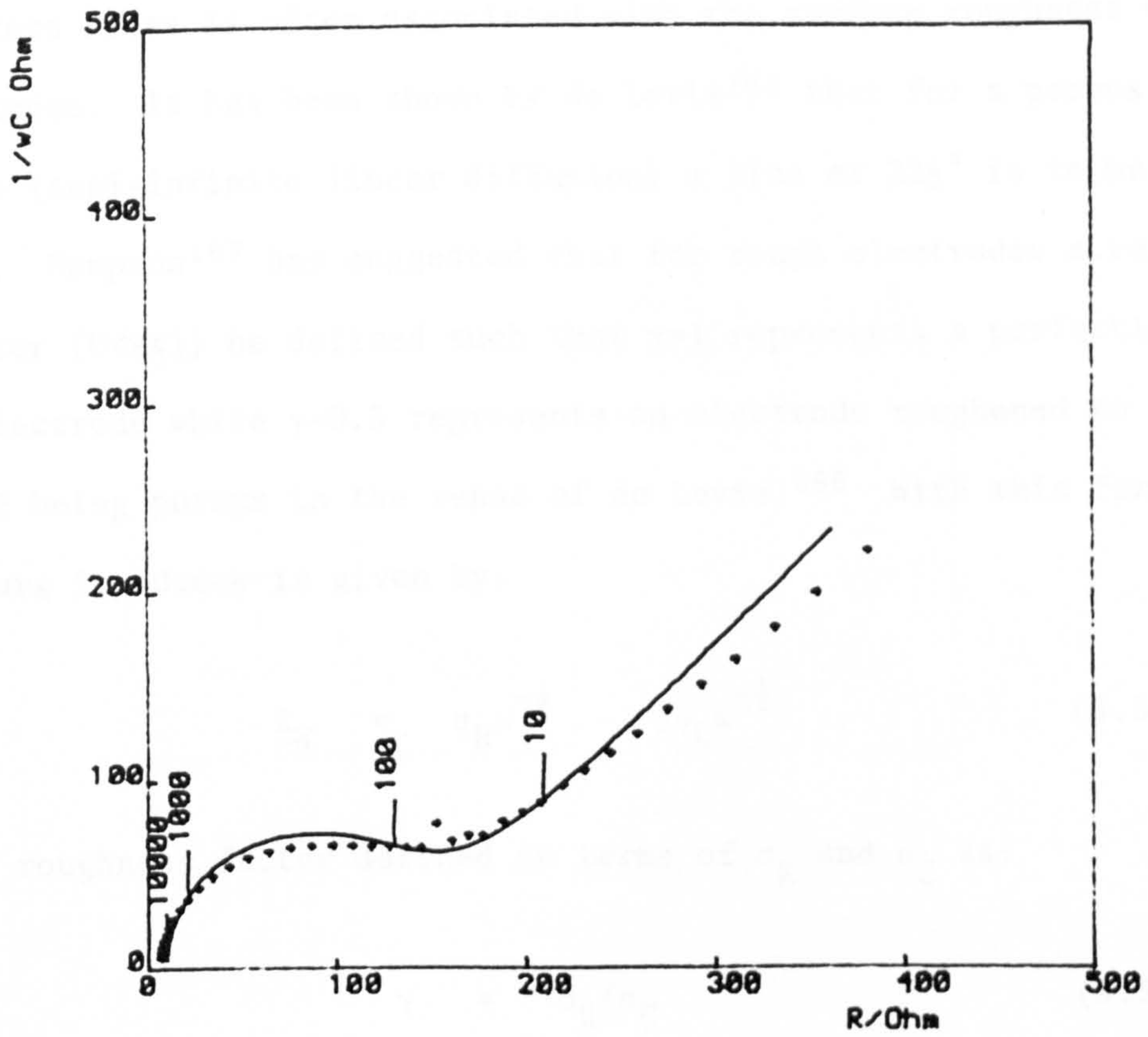

Fig. 5.8 Impedance spectrum analysed according to the 'C-equation', E = - 0.745 V

The departure of the experimental data from the 45° line in the Sluyters Plots is often associated with the surface roughness of the electrode. It has been shown by de Levie[166] that for a porous electrode (semi-infinite linear diffusion) a line at 22½° is to be expected. Hampson[167] has suggested that for rough electrodes a roughness factor ($0<\gamma\leq 1$) be defined such that $\gamma=1$ represents a perfectly smooth electrode while $\gamma=0.5$ represents an electrode roughened to the extent of being porous in the sense of de Levie.[166] With this formalism, the Warburg impedance is given by:

$$\underline{Z}_W = \sigma_R \omega^{-\frac{1}{2}} - j\sigma_C \omega^{-\frac{1}{2}} \qquad (5.3.1)$$

with the roughness factor defined in terms of σ_R and σ_C as:

$$\gamma = \sigma_R/\sigma_C \qquad (5.3.2)$$

The effect of such a modification on the Sluyters Plot is twofold. At low frequencies the slope of the Warburg line may vary from 22½° to 45°. Concomitant with this is a flattening of the high frequency semicircle.

A model for the Randles Circuit with a roughened electrode was used to try and improve the fit between the theoretical values of the impedance at low frequencies. Any improvement gained, however, was outweighed by the effects on the high frequency part of the spectrum and a better overall fit was obtained from the original Randles Circuit.

The average values of the parameters at each of the four electrode potentials are given in Table 5.1 below. The magnitudes

of the double layer capacitance are consistent with a film-free solid metal surface.

E V	θA $10^4 \Omega m^2$	C_L/A Fm^{-2}	$\dot{\sigma}$ $\Omega s^{-\frac{1}{2}}$
-0.721	1.056	0.597	107
-0.731	2.289	0.588	178
-0.737	3.280	0.487	319
-0.745	8.035	0.442	835

TABLE 5.1 Values of θA, C_L and σ as a function of E-cathodic process

The Warburg coefficient increases with the degree of d.c. polarisation and a plot of log{$\dot{\sigma}$} versus E (fig. 5.9) is consistent with a linear relationship of - 29 mV/decade slope, indicating a two electron reversible process.

The charge transfer resistance also varies with electrode potential. The corresponding semi-logarithmic plot (fig. 5.10) is also consistent with a - 29 mV/decade slope. From examination of (2.2.29) a value of $z\alpha = 1$ is deduced and this is confirmatory evidence for the two electron reversible process.

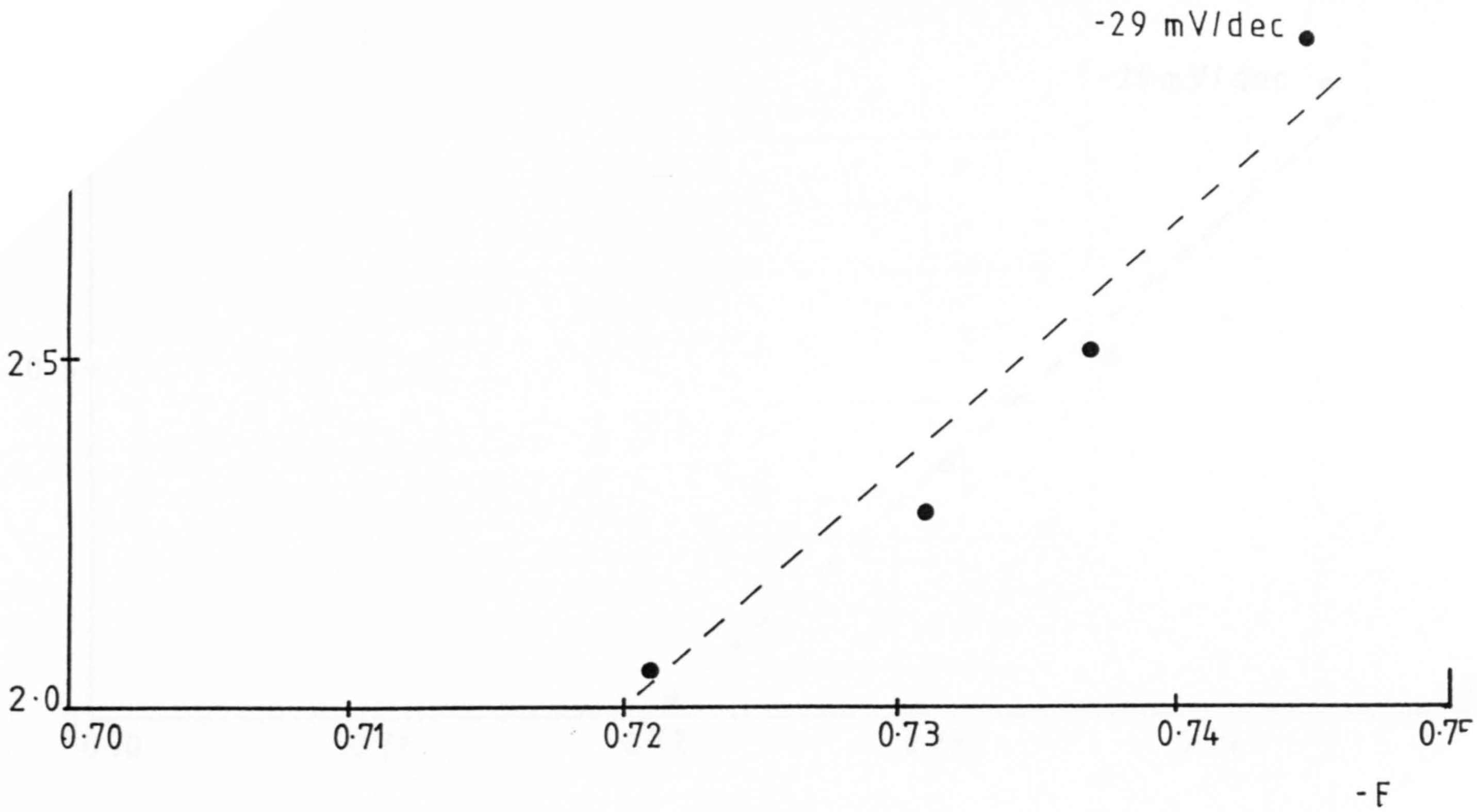

Fig. 5.9 log{σ} versus E (cathodic)

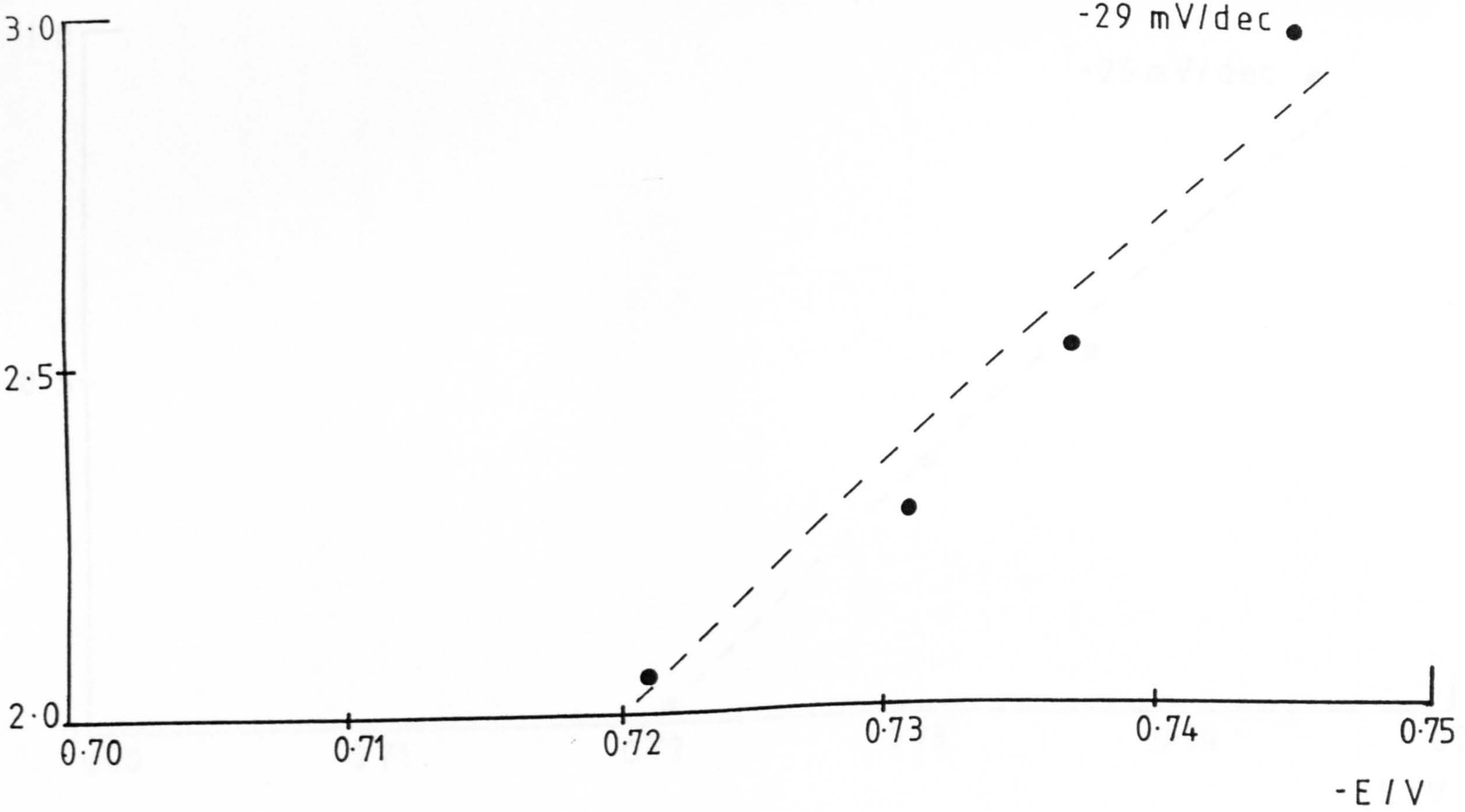

Fig. 5.9 log{σ} versus E (cathodic)

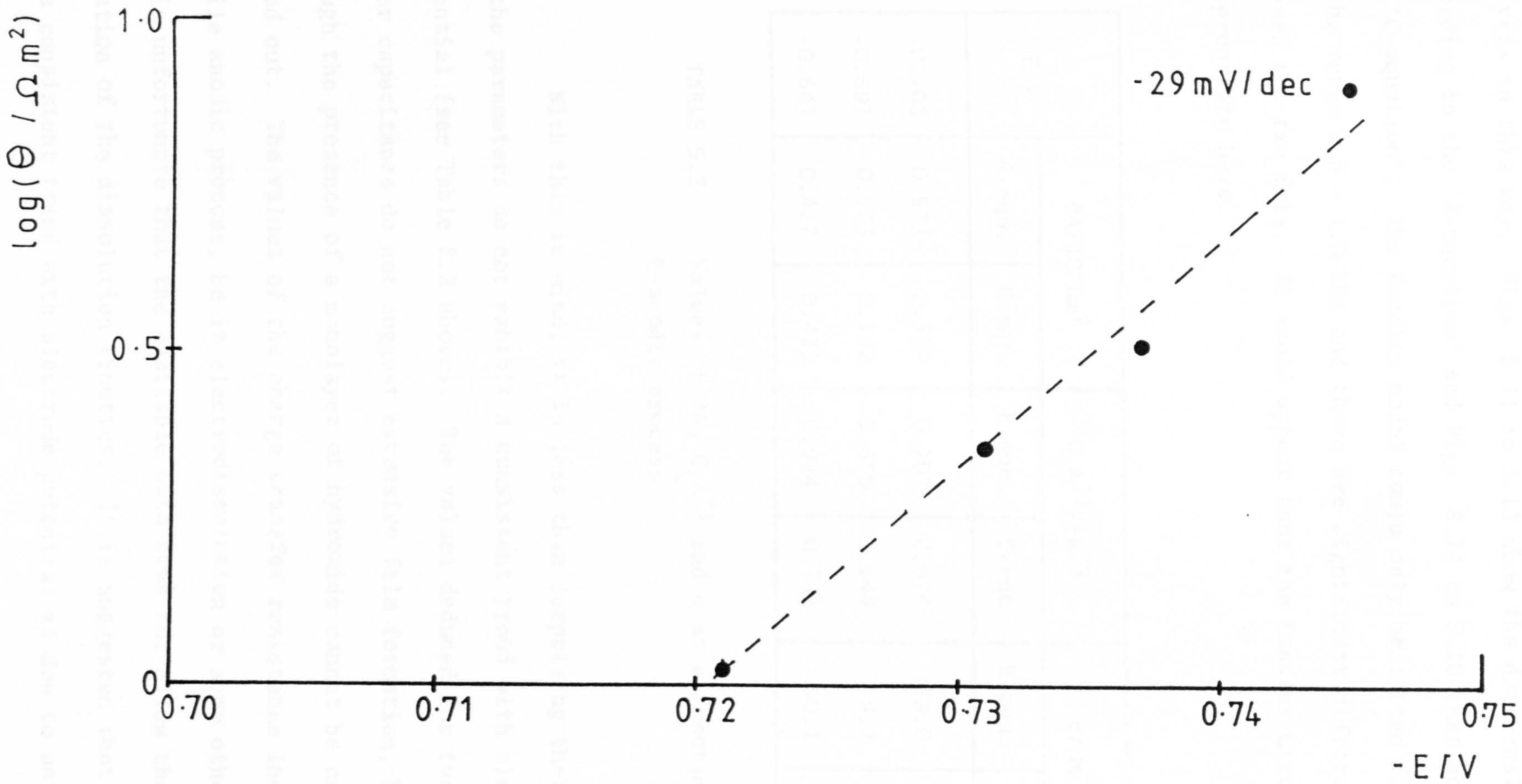

Fig. 5.10 log{θA} versus E (cathodic)

5.3.2 The anodic process

The data obtained for the anodic process is less amenable to analysis in this way. Figs. 5.11 to 5.13 show the data analysed according to the 'R-equation' and Figs. 5.14 to 5.16 that according to the 'C-equation'. The Randles model could only be fitted for frequencies in the range 9.9 - 1.0 kHz and there are significant differences between the two fits. It would appear that the Randles Circuit is inappropriate here.

E/V	$\theta A/10^4 \Omega m^2$		$C_L A^{-1}/Fm^{-2}$		$\sigma/\Omega s^{-\frac{1}{2}}$	
	R-eqn.	C-eqn.	R-eqn.	C-eqn.	R-eqn.	C-eqn.
-0.703	0.573	0.519	0.707	0.674	119.0	117.0
-0.691	0.173	0.182	2.659	1.648	9.2	53.6
-0.647	0.427	0.421	0.924	0.701	90.1	129.1

TABLE 5.2 Values of θA, $C_L A^{-1}$ and σ as a function of E-anodic process

With this in mind, it is less than surprising that the values of the parameters do not exhibit a consistent trend with electrode potential (see Table 5.2 above). The values deduced for the double layer capacitance do not suggest extensive film formation, however, though the presence of a monolayer of hydroxide cannot be completely ruled out. The values of the charge transfer resistance indicate a facile anodic process, be it electrodissolution or some other process. It is unfortunate that the available data does not allow the determination of the dissolution kinetics. It is suggested that the lack of a consistent trend with electrode potential is due to an ill-defined

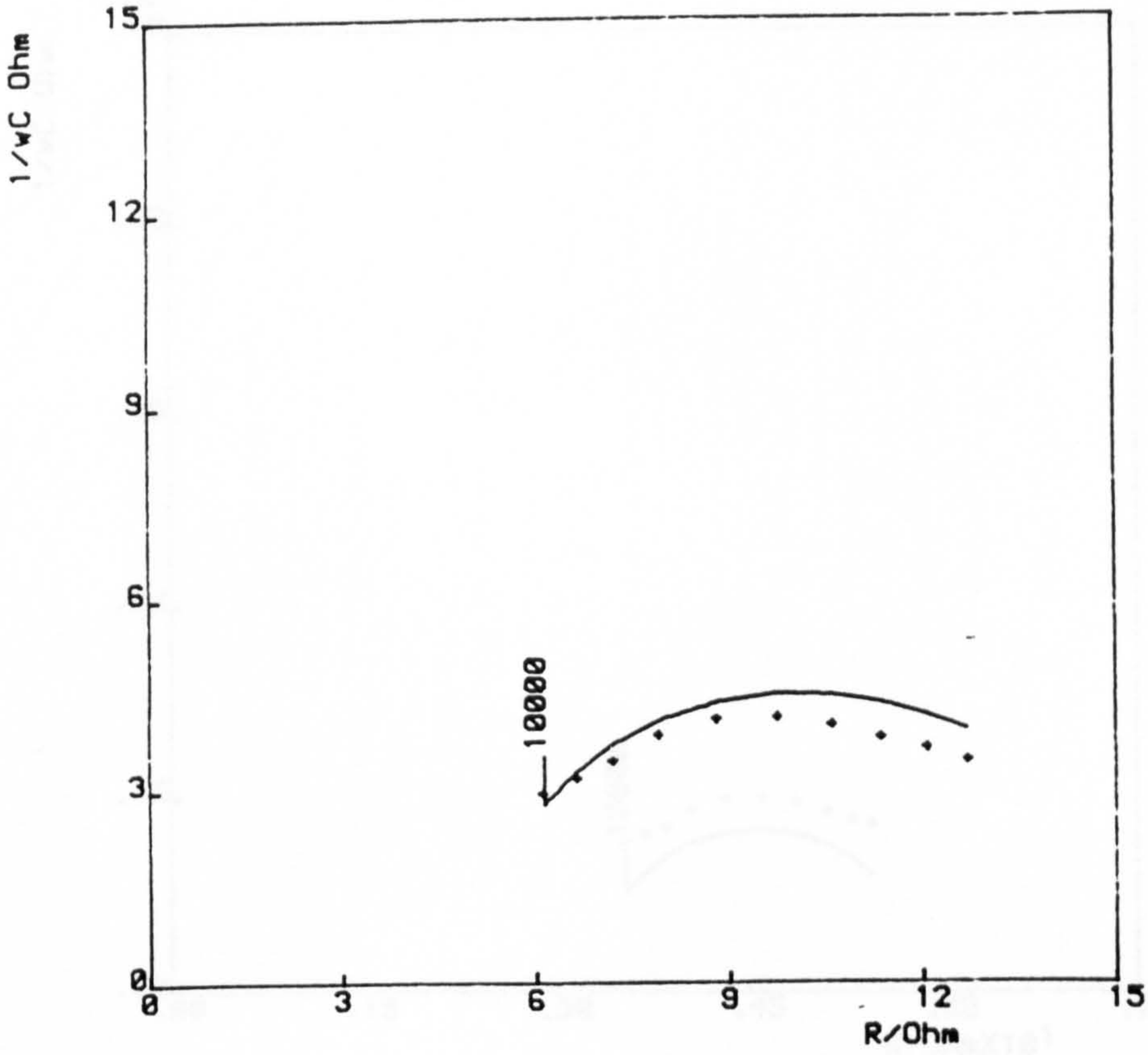

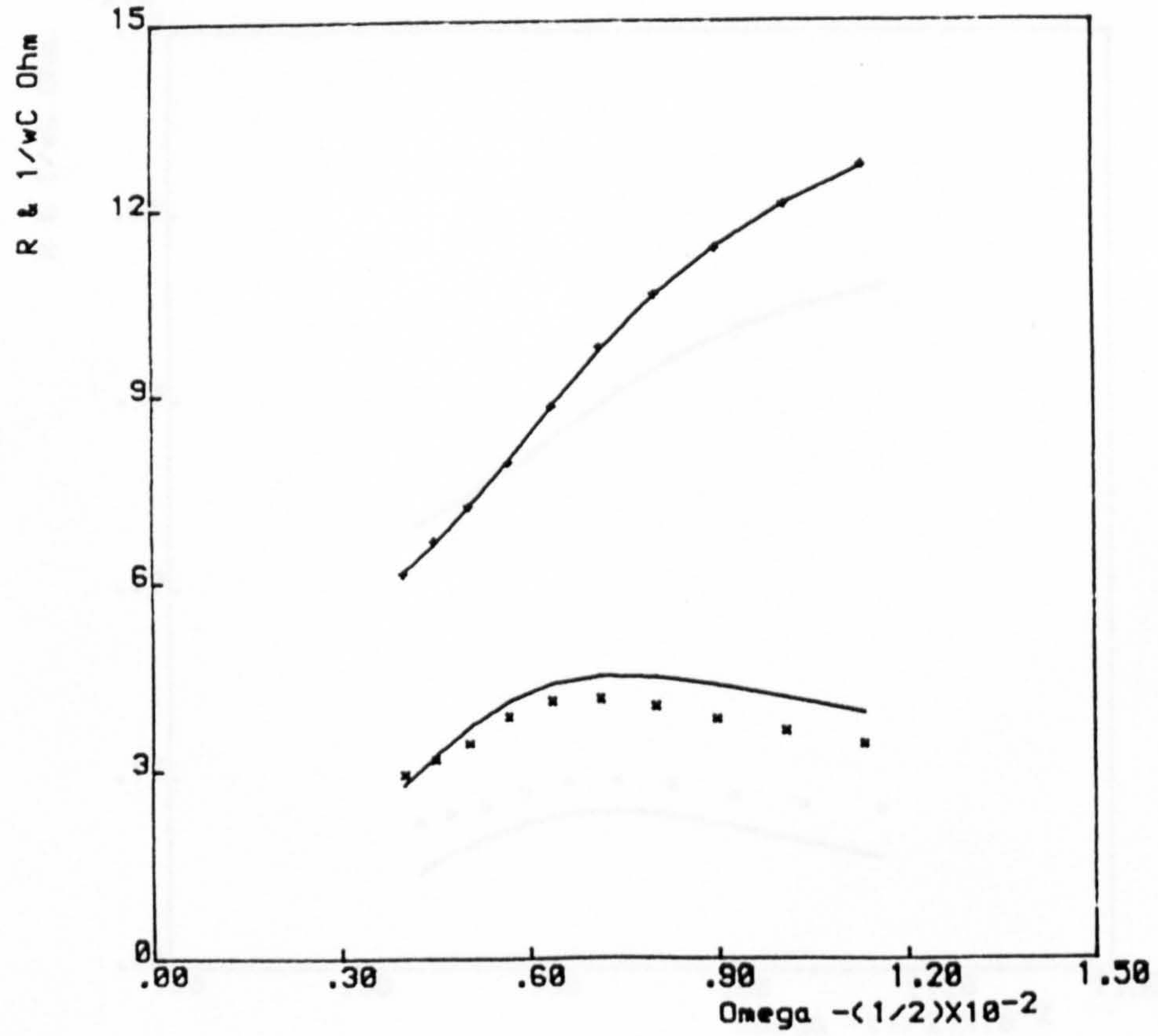

Fig. 5.11 Impedance spectrum analysed according to the 'R-equation', E = - 0.703 V

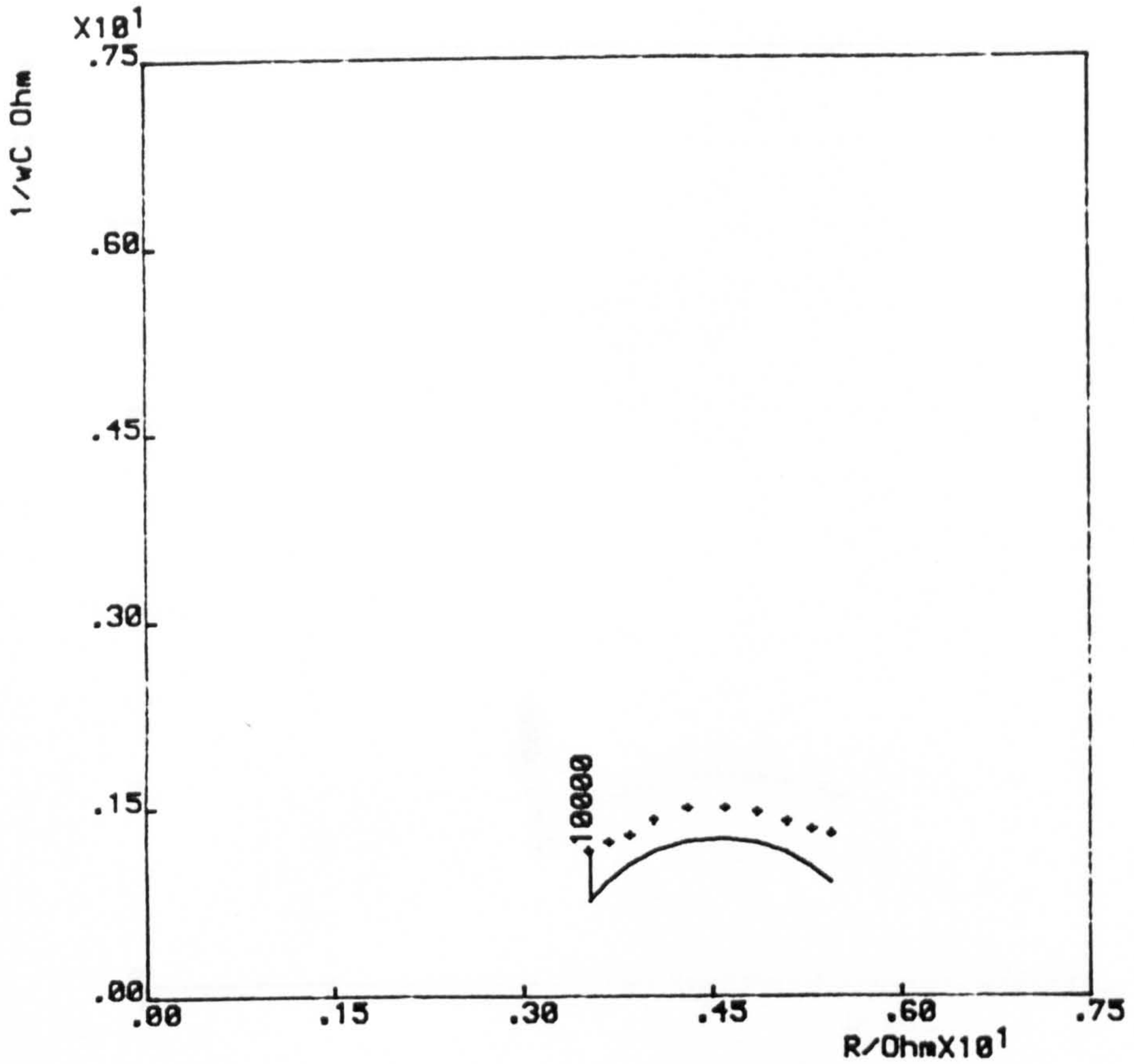

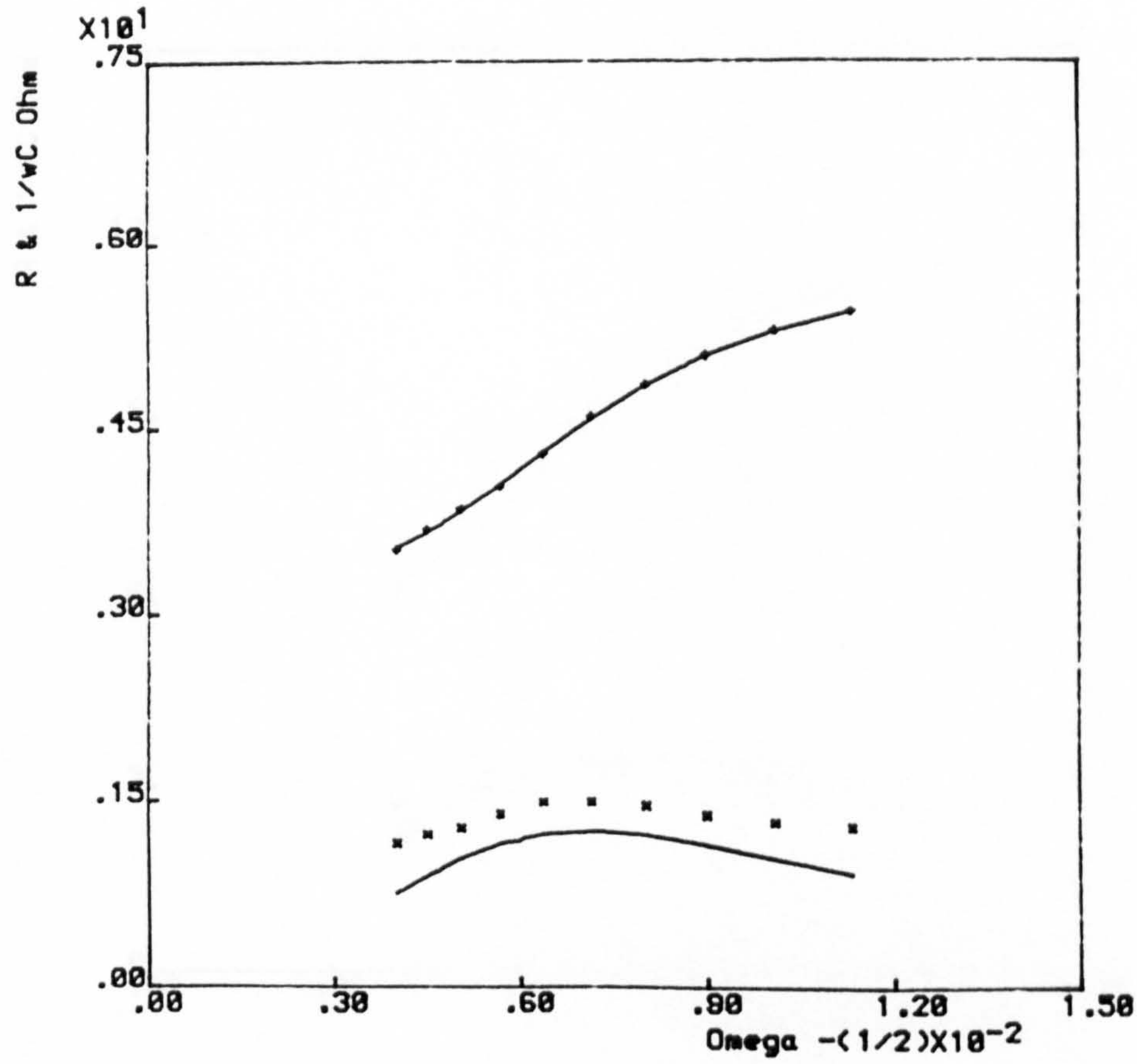

Fig. 5.12 Impedance spectrum analysed according to the 'R-equation', E = - 0.691 V

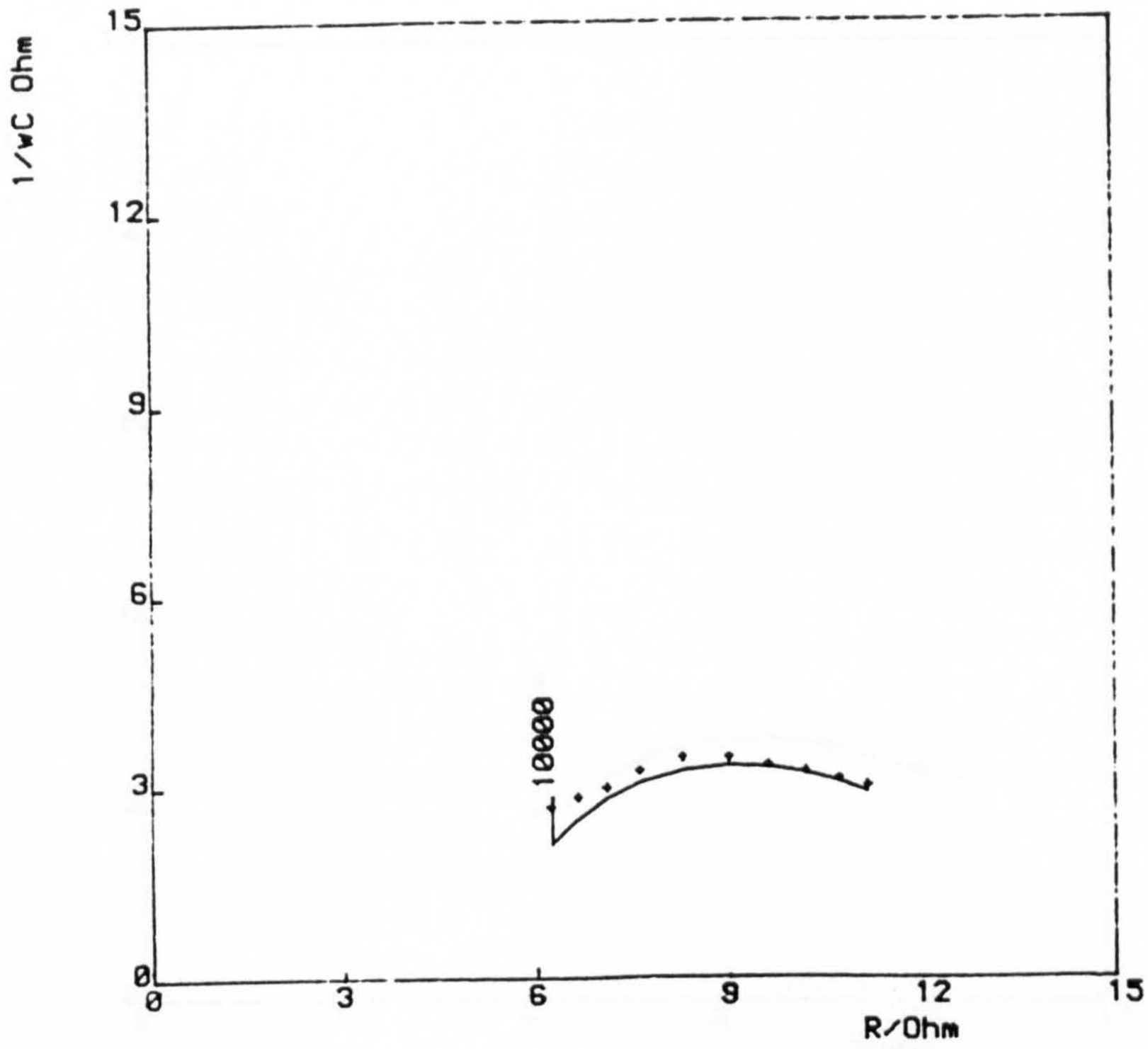

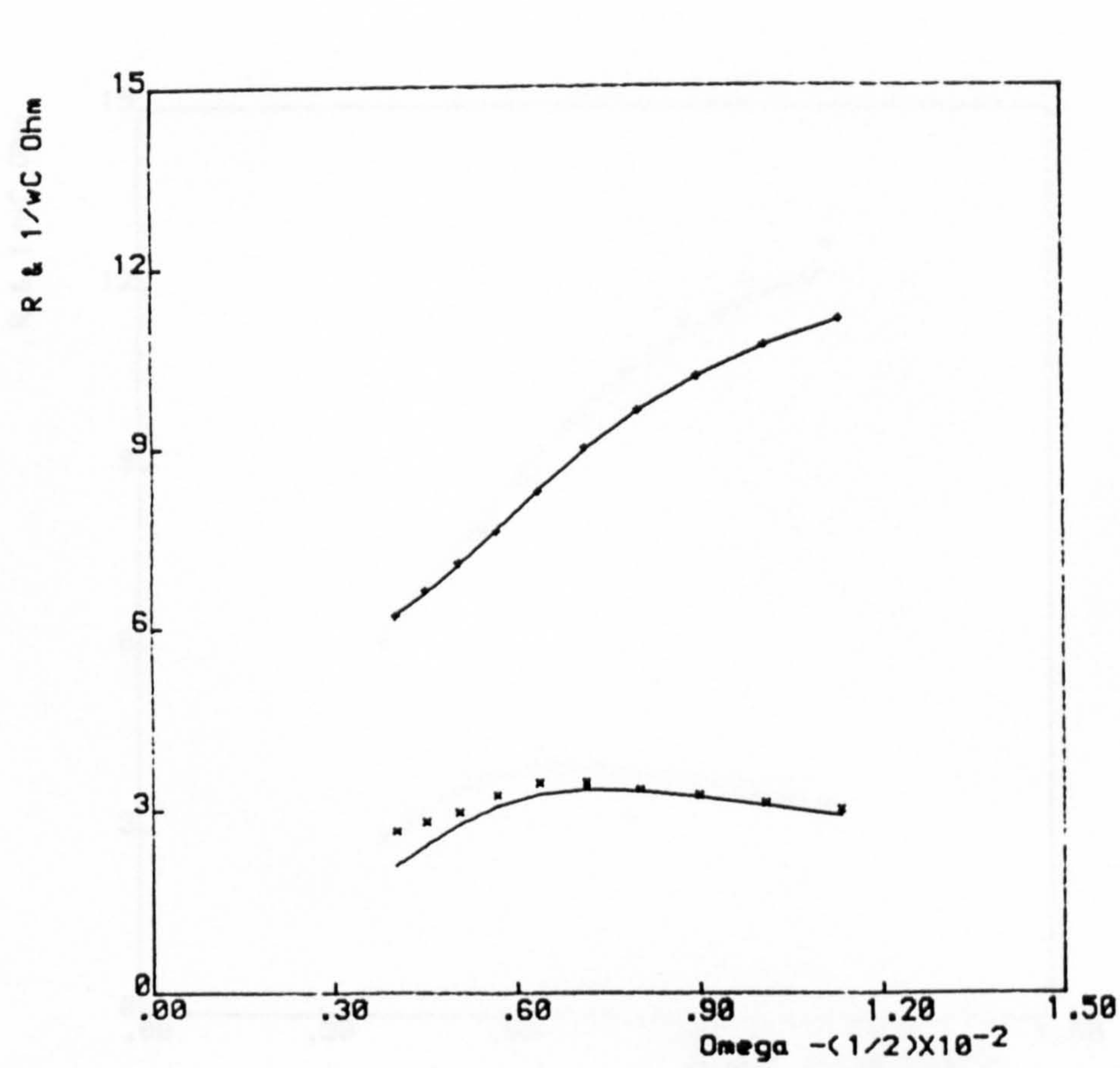

Fig. 5.13 Impedance spectrum analysed according to the 'R-equation',
E = - 0.647 V

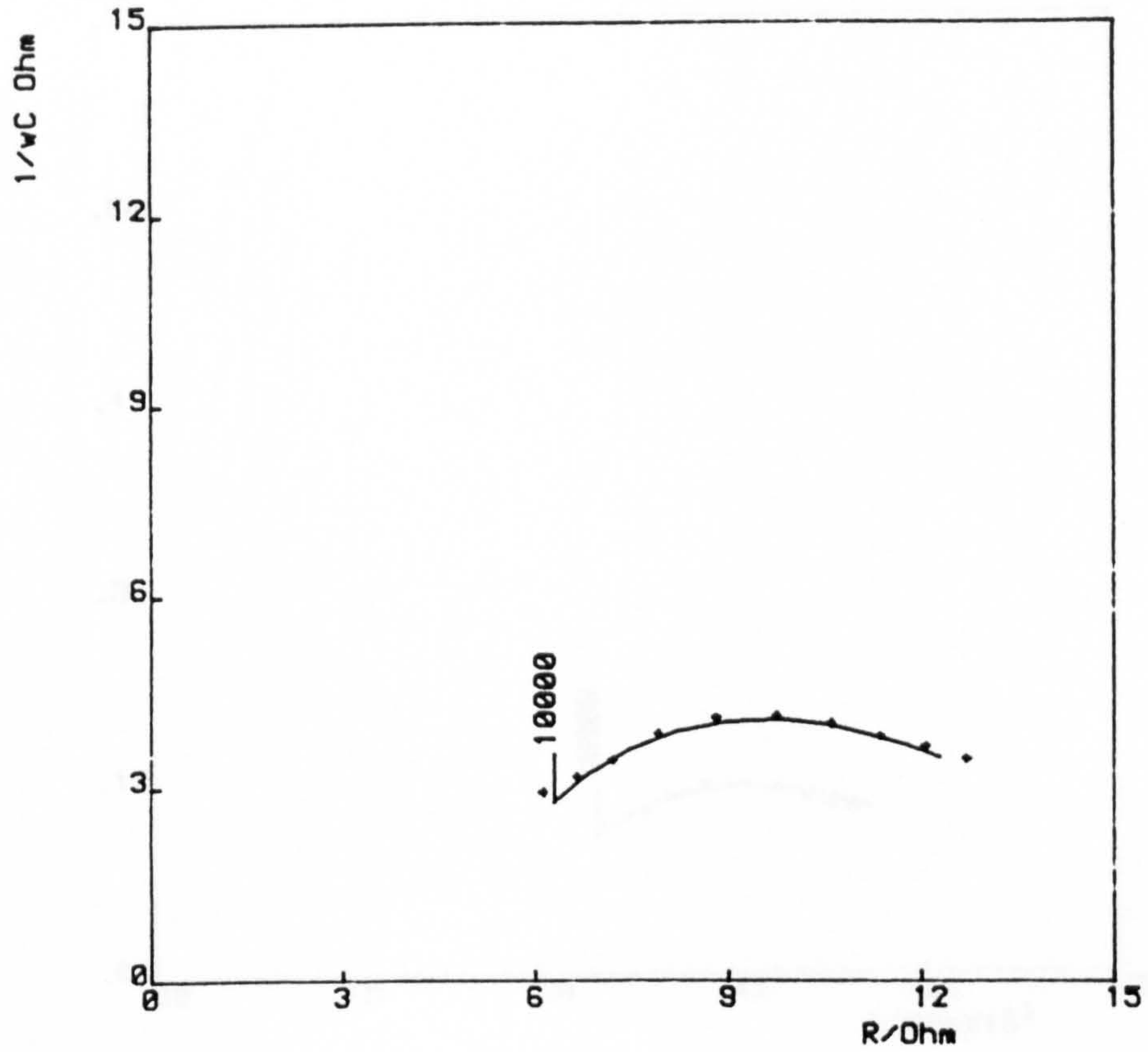

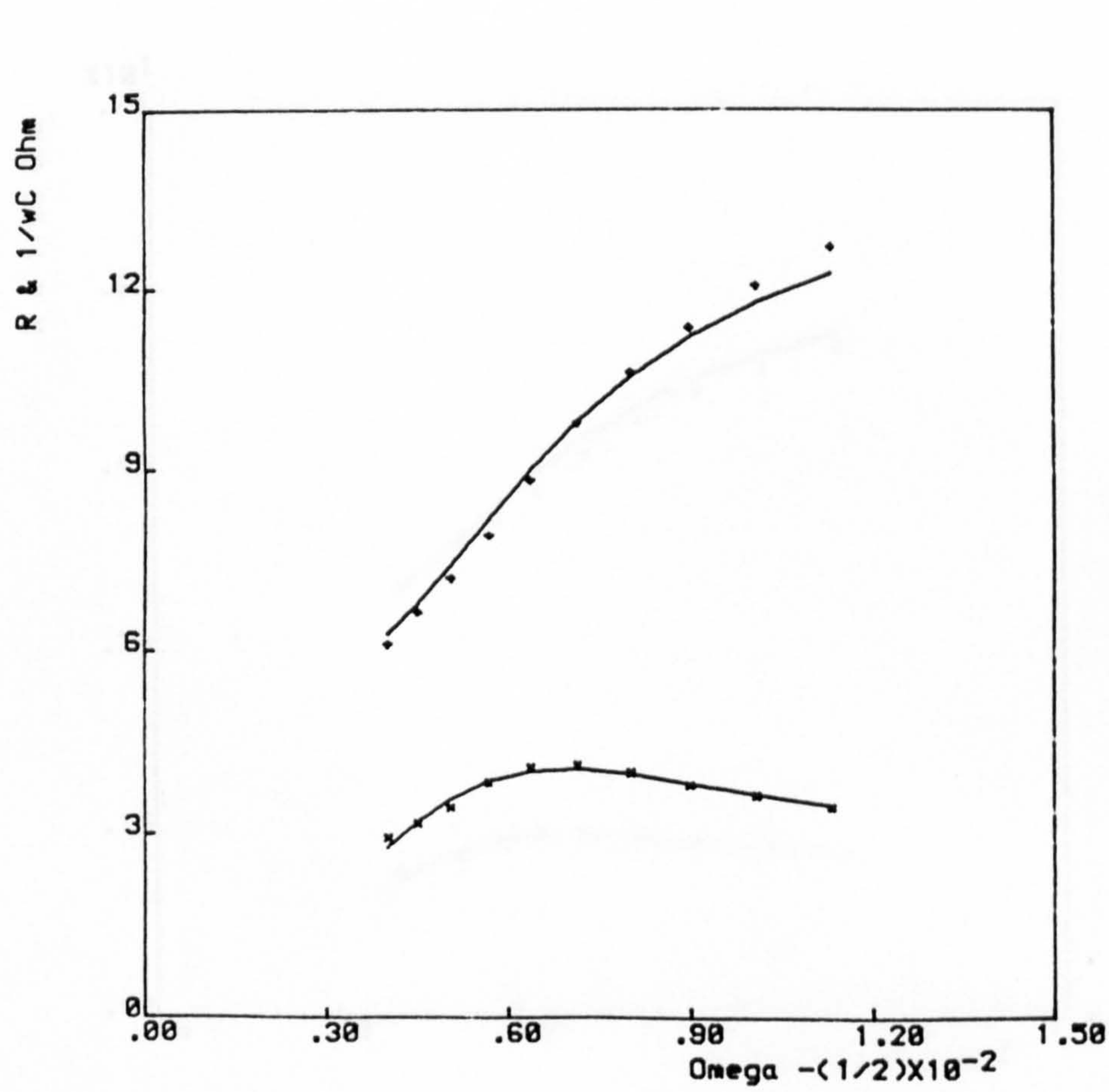

Fig. 5.14 Impedance spectrum analysed according to the 'C-equation',
E = - 0.703 V

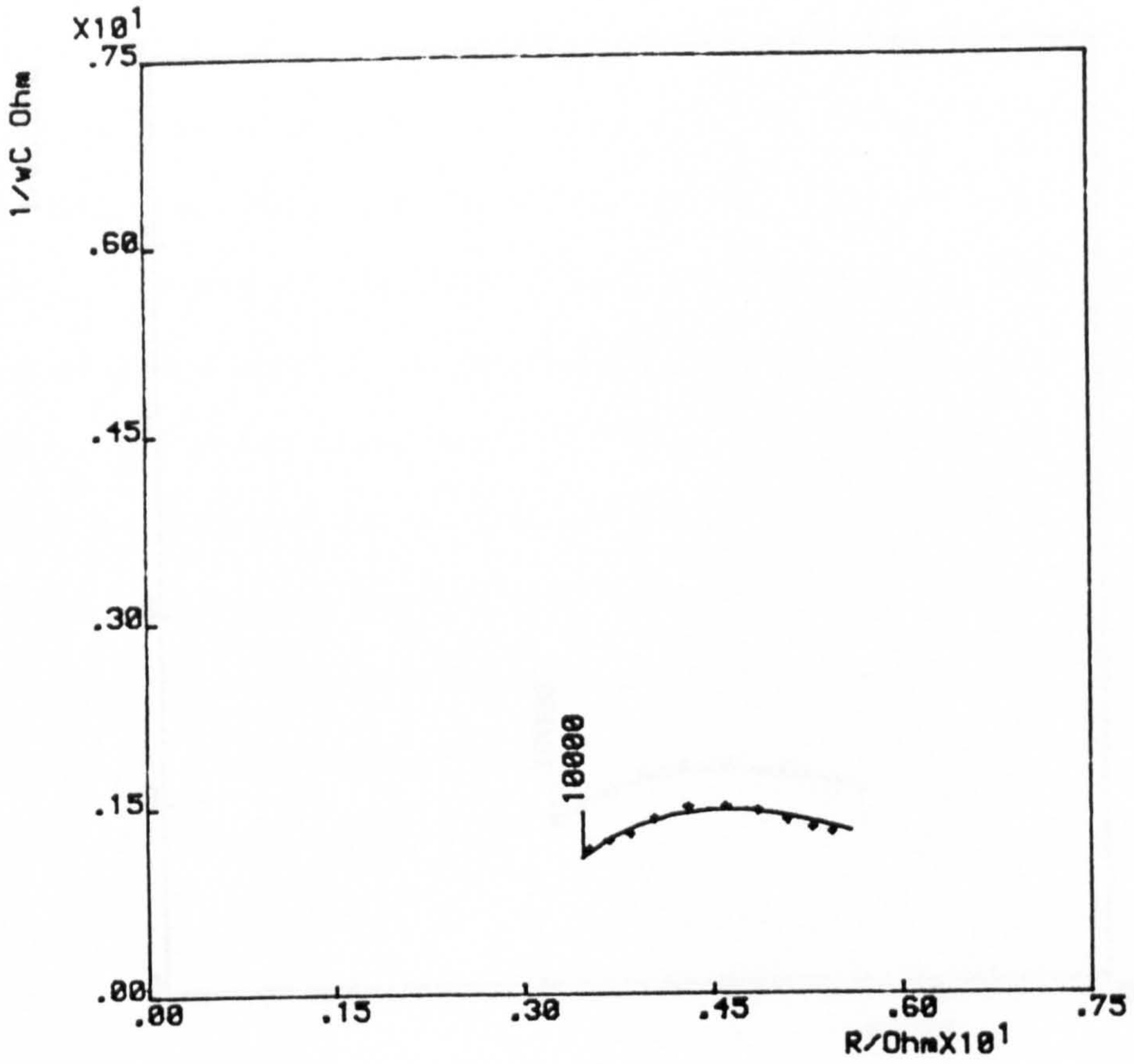

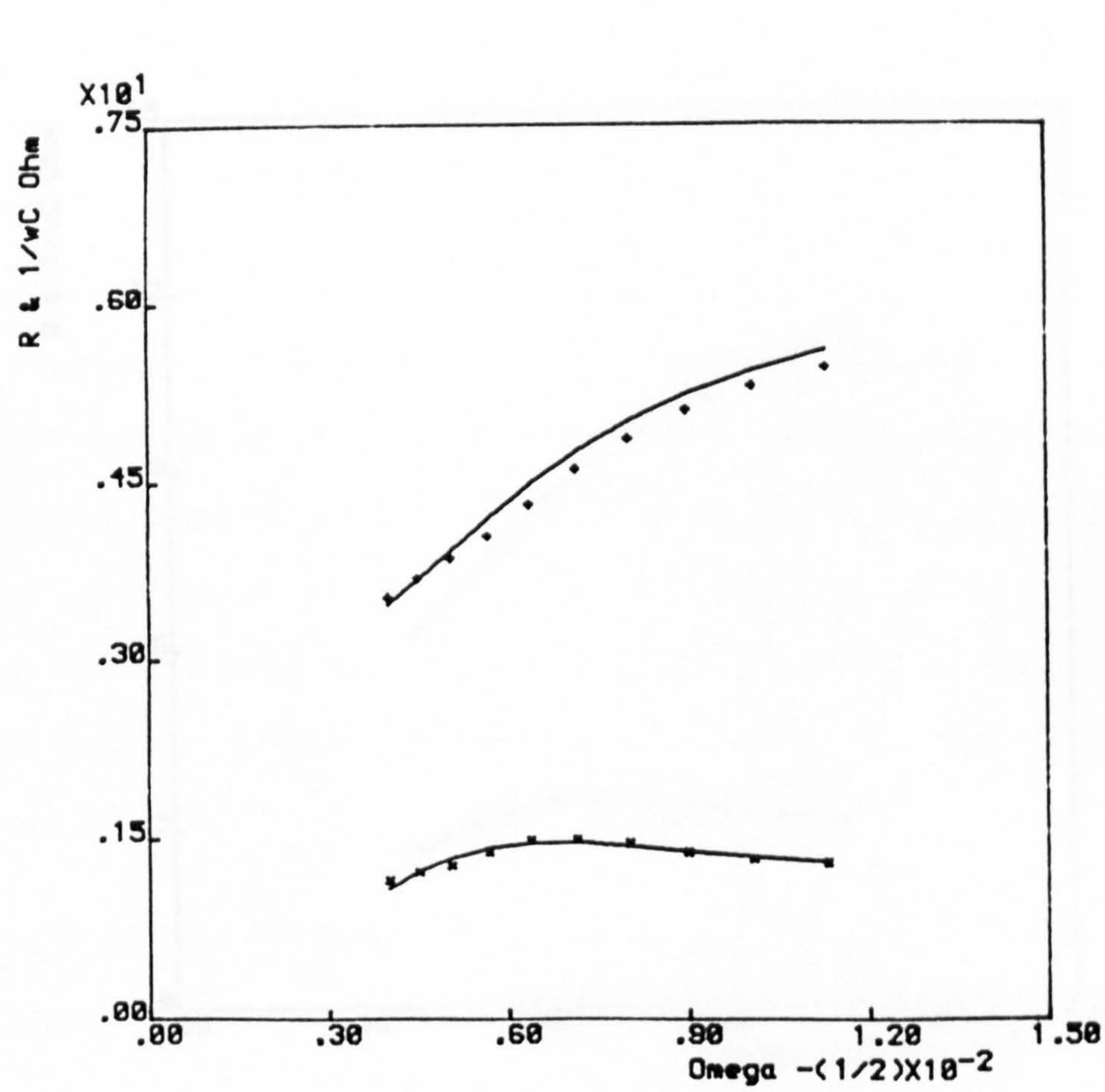

Fig. 5.15 Impedance spectrum analysed according to the 'C-equation', E = - 0.691 V

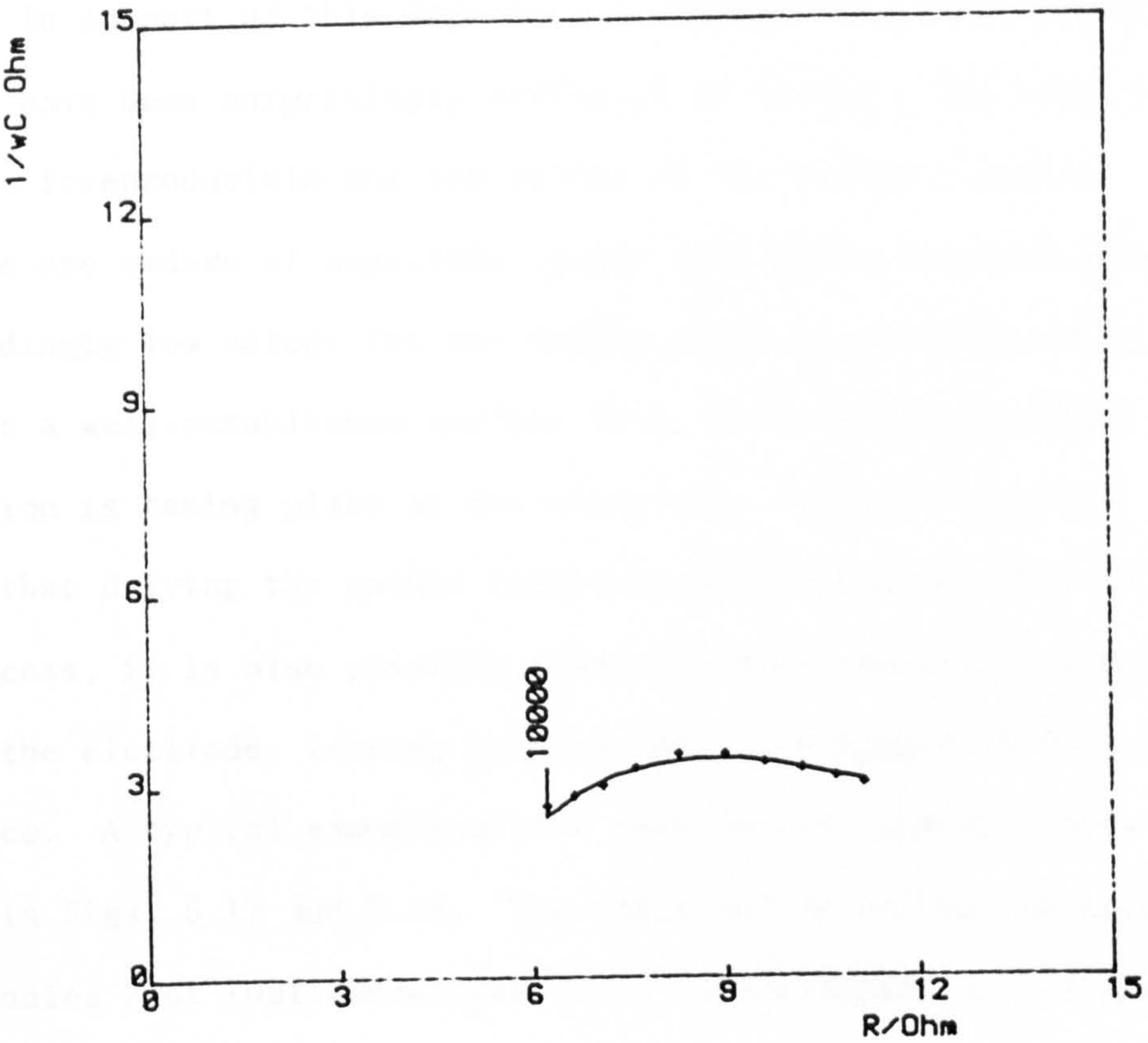

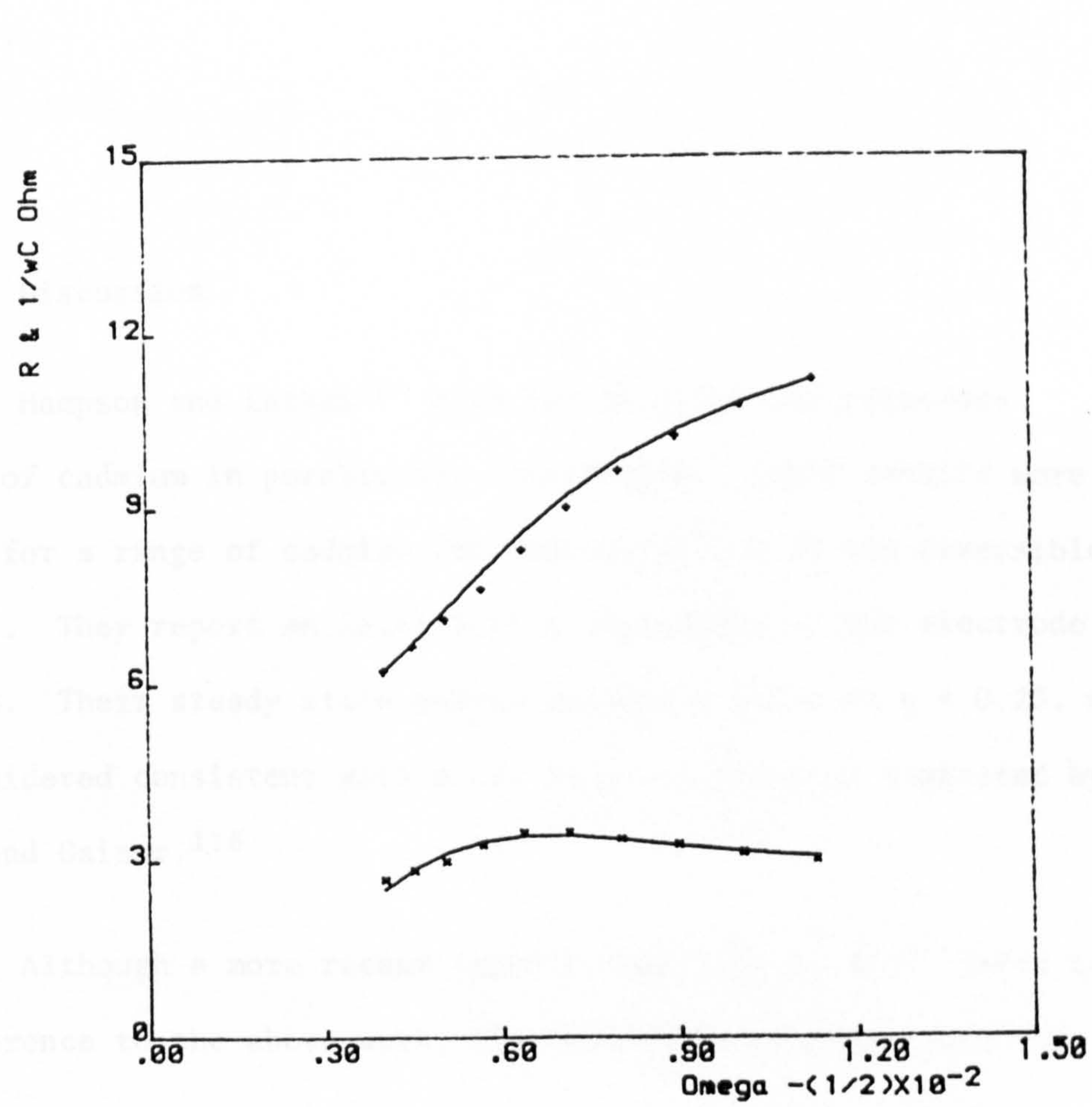

Fig. 5.16 Impedance spectrum analysed according to the 'C-equation', E = - 0.647 V

electrode surface.

In support of this argument, measurements at the equilibrium potential have been surprisingly difficult to obtain. The results tend to be irreproducible and the values of the charge transfer resistance are orders of magnitude larger than those obtained above. Correspondingly low values for the double layer capacitance would tend to suggest a well-established surface film, which develops whilst no net reaction is taking place at the electrode. Whilst it may be imagined that driving the anodic reaction may enhance the film thickening process, it is also possible that the electrodissolution serves to clean the electrode, leaving perhaps only a monolayer of film on the surface. A typical example of the equilibrium impedance spectrum is shown in Figs. 5.17 and 5.18. The intersection of the two curves of the Randles Plot (well-developed here) is characteristic of phase formation.

5.4 Discussion

Hampson and Latham[121] have investigated the electrode kinetics of cadmium in perchlorate electrolyte. Their results were obtained for a range of cadmium ion concentrations at the reversible potential. They report an initial time dependence of the electrode impedance. Their steady state values yielded a value of $\alpha = 0.23$, which they considered consistent with a two step mechanism as suggested by Heusler and Gaiser.[118]

Although a more recent paper by Harrison et al[135] fails to make reference to the above work, its conclusions endorse those of

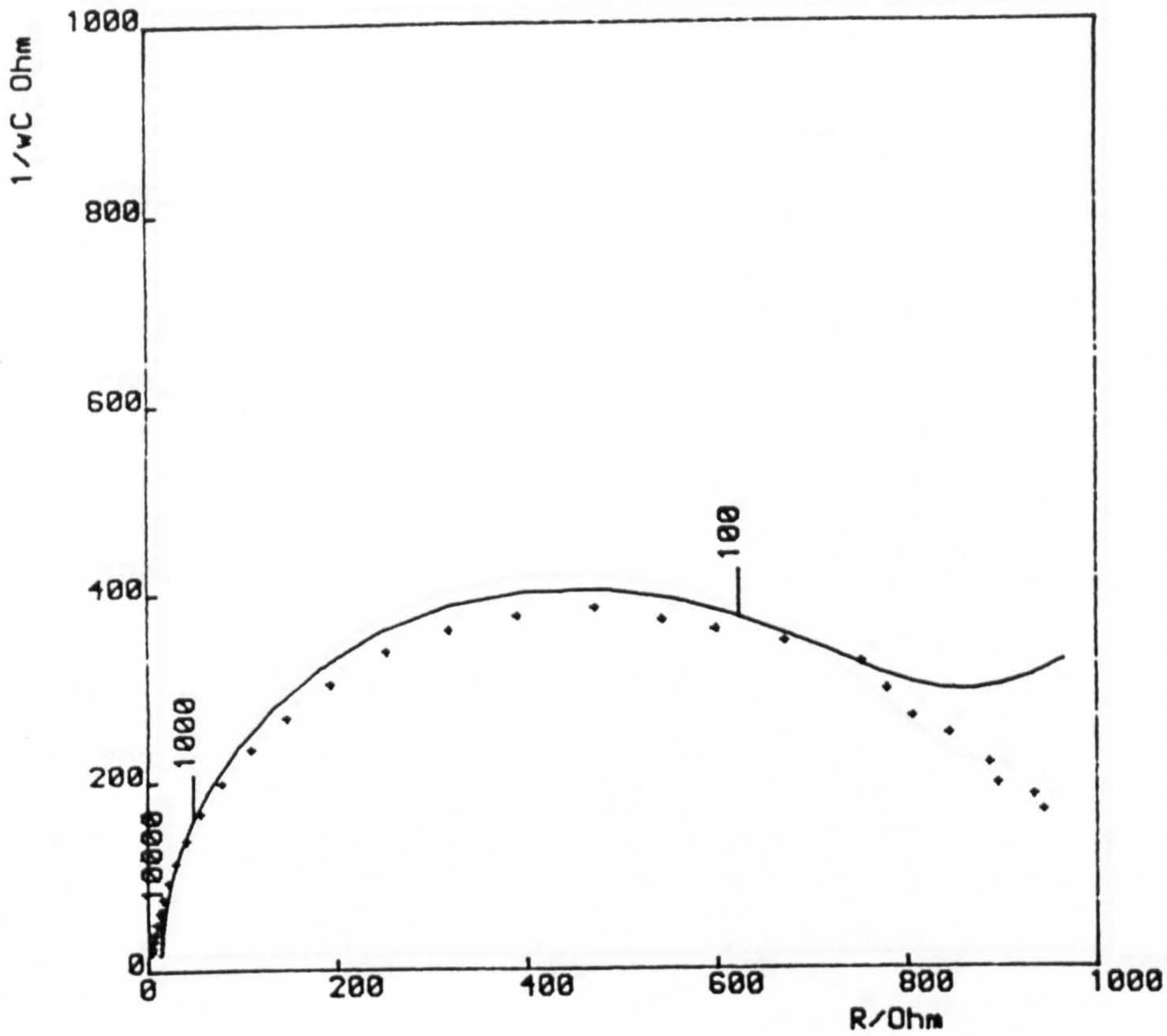

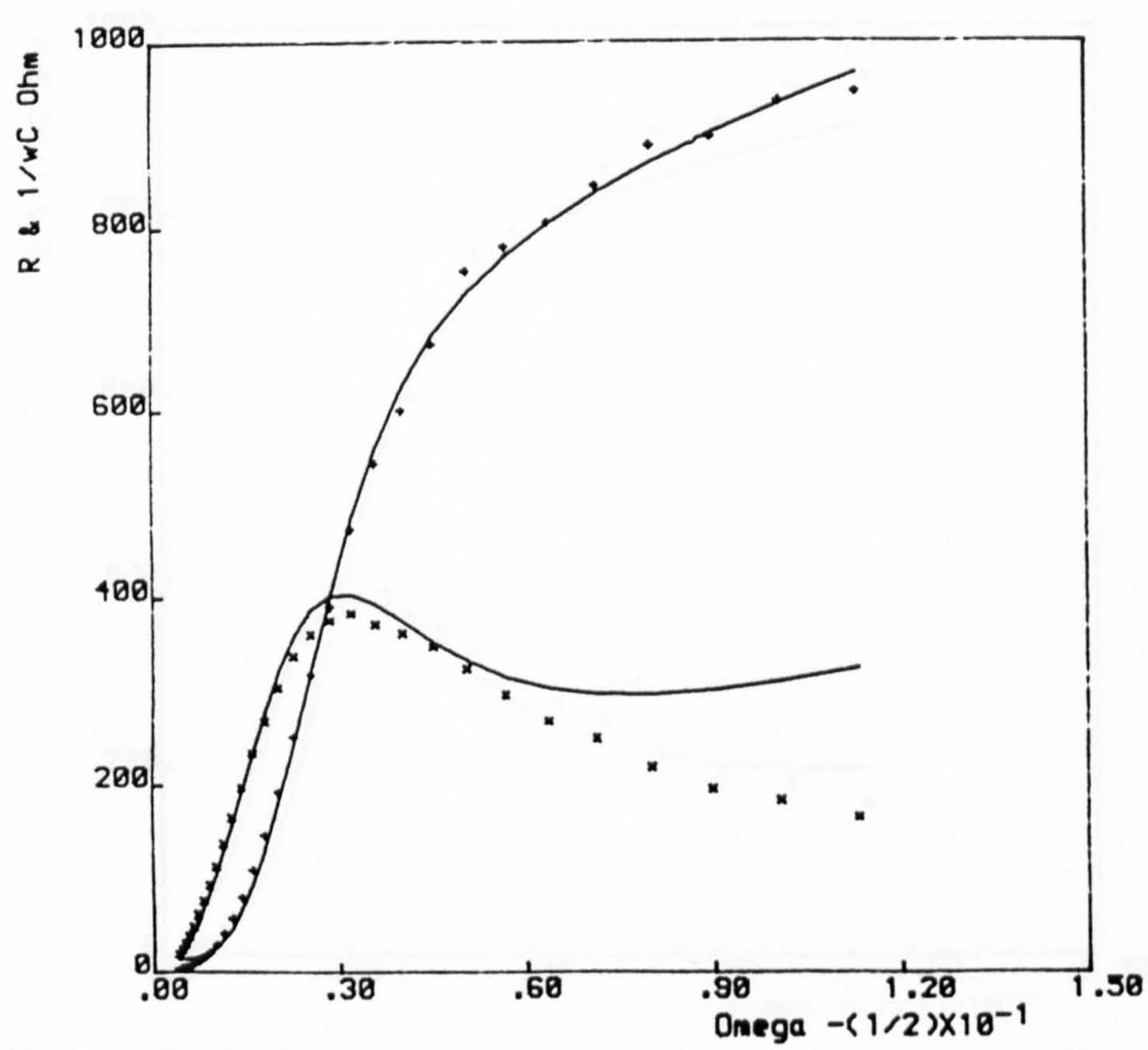

Fig. 5.17 Equilibrium impedance spectrum analysed according to the 'R-equation'. (θA = 0.00522 $\Omega\ m^2$; $C_L A^{-1}$ = 0.136 Fm^{-2}; σ = 2284 $\Omega\ s^{-\frac{1}{2}}$).

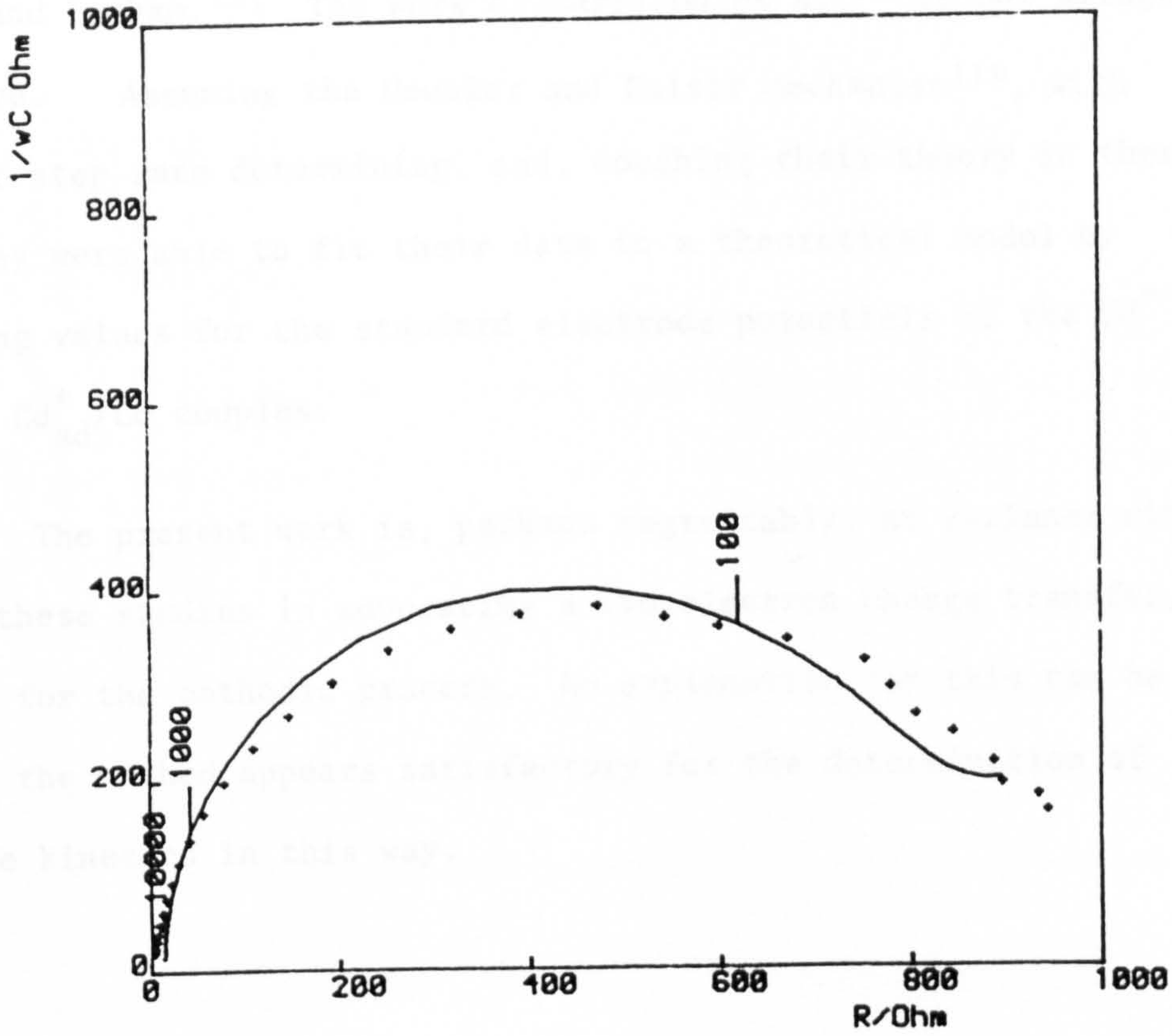

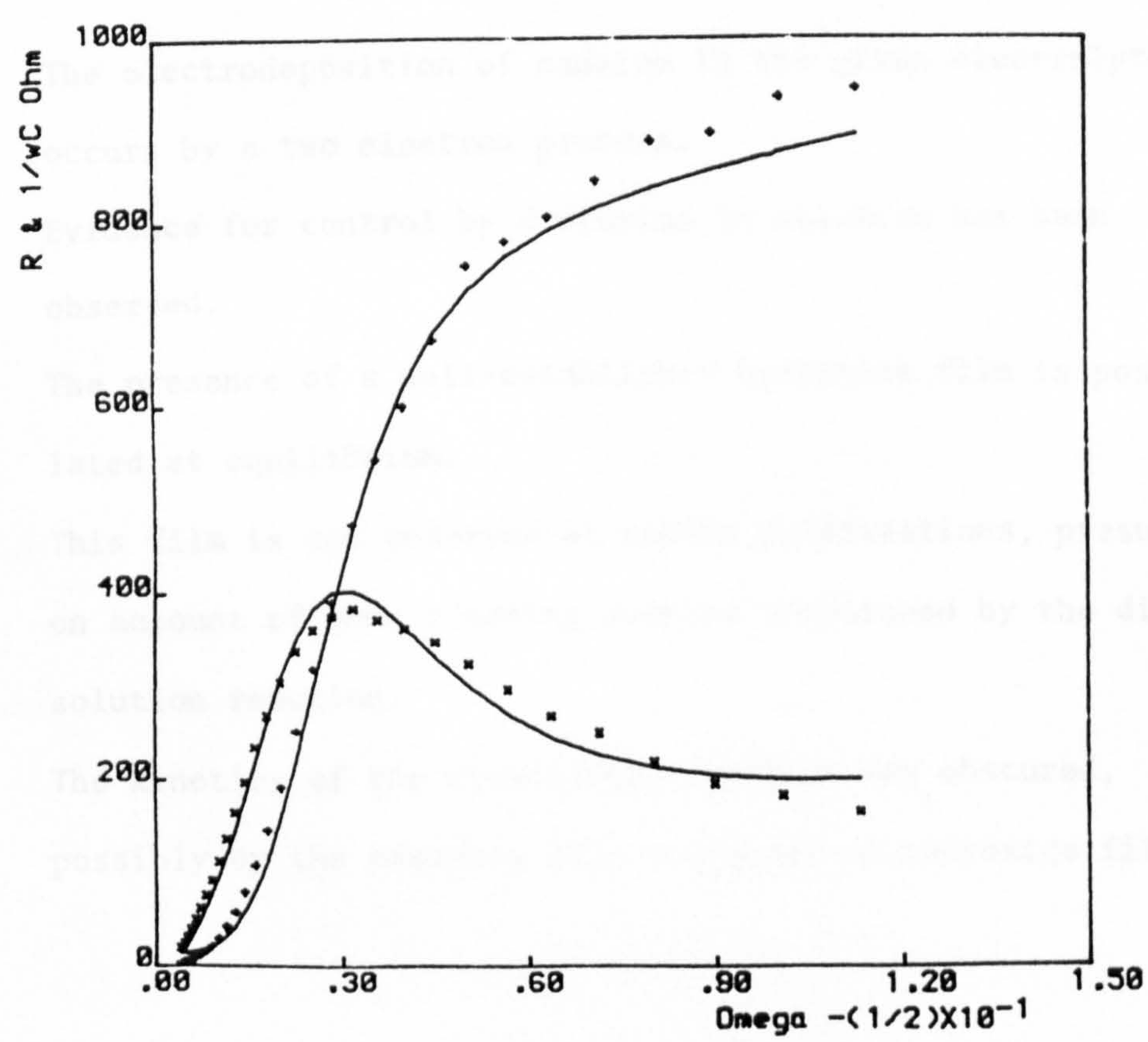

Fig. 5.18 Equilibrium impedance spectrum analysed according to the 'C-equation'. (θA = 0.00547 $\Omega\ m^2$; $C_L A^{-1}$ = 0.149 Fm^{-2}; σ = 1196 $\Omega\ s^{-\frac{1}{2}}$).

Hampson and Latham.[121] The work of Harrison et al[135] is not altogether conclusive. Assuming the Heusler and Gaiser mechanism[118], with the first step rate determining, and, couching their theory in these terms they were able to fit their data to a theoretical model by estimating values for the standard electrode potentials of the Cd^{++}/Cd^{+}_{ad} and Cd^{+}_{ad}/Cd couples.

The present work is, perhaps regrettably, at variance with both of these studies in advocating a two electron charge transfer, at least for the cathodic process. No explanation for this can be given. However, the method appears satisfactory for the determination of electrode kinetics in this way.

5.5 Conclusions

1. The electrodeposition of cadmium in the given electrolyte occurs by a two electron process.
2. Evidence for control by diffusion in solution has been observed.
3. The presence of a well-established hydroxide film is postulated at equilibrium.
4. This film is not observed at anodic polarisations, presumably on account of some cleaning process occasioned by the dissolution reaction.
5. The kinetics of the dissolution reaction are obscured, possibly by the presence of a monolayer of hydroxide film.

CHAPTER SIX

CADMIUM IN CYANIDE/CHLORIDE ELECTRCLYTES

6.1 Introduction

Before attempting a kinetic investigation of the complex system of the next chapter, it was decided to apply the rotating disc method to a slightly simpler system. As in the last chapter it was thought desirable to examine a system for which some data was available. The work of Gerischer[168] has been selected for this purpose. By means of impedance methods, Gerischer was able to propose a mechanism for the discharge of cadmium cyanide complexes at an amalgam electrode.

The present work concerns the electrode kinetics of the dissolution of a solid cadmium electrode in electrolytes similar to those of Gerischer.[168] The technique of the rotating disc has been used for this purpose.

6.2 Experimental

The dissolution of a solid cadmium electrode in the following electrolytes was examined at the rotating disc electrode. The rotation speed of the electrode was varied from 100 to 600 r.p.m. for a series of electrode potentials.

Electrolyte	(a)	(b)	(c)	(d)
NaCl	3.99M	3.95M	3.99M	3.99M
NaCN	0.01M	0.05M	0.01M	0.01M
$CdCl_2$	—	—	2.0mM	1.0mM

6.3 Results and Discussion

6.3.1 Electrolyte (a)

The dependence of the current density on the rotation speed for this electrolyte, at seven different electrode potentials, is shown in Fig. 6.1, plotted in the form i^{-1} versus $\omega^{-\frac{1}{2}}$. These plots are quite linear and the fact that the current density depends on the rotation speed shows that the reaction is controlled, at least partly, by diffusion in solution. All of the curves pass through the origin from which fact (cf. equation (2.4.6.)) it may be concluded that the charge transfer current is extremely high; that is to say the reaction is essentially reversible.

Taking the logarithm of the slopes of these curves and plotting them against electrode potential (Fig. 6.2), a linear relationship is obtained as would be expected on the basis of equation (2.4.10). Consideration of eqn. (2.4.11) and the -29 mV/decade slope indicates that the electrode is in equilibrium with a two electron solution species.

6.3.2 Electrolyte (b)

Keeping the total ionic strength the same as for electrolyte (a), the cyanide ion concentration was increased fivefold. As before, i^{-1} versus $\omega^{-\frac{1}{2}}$ plots (Fig. 6.3) for seven electrode potentials were linear and passed through the origin. In this case, however, the slope of the linear plot of $\log\{\partial i^{-1}/\partial\omega^{-\frac{1}{2}}\}$ versus E (Fig. 6.4) was -415 mV/decade compared to the -29 mV/decade slope obtained for electrolyte (a).

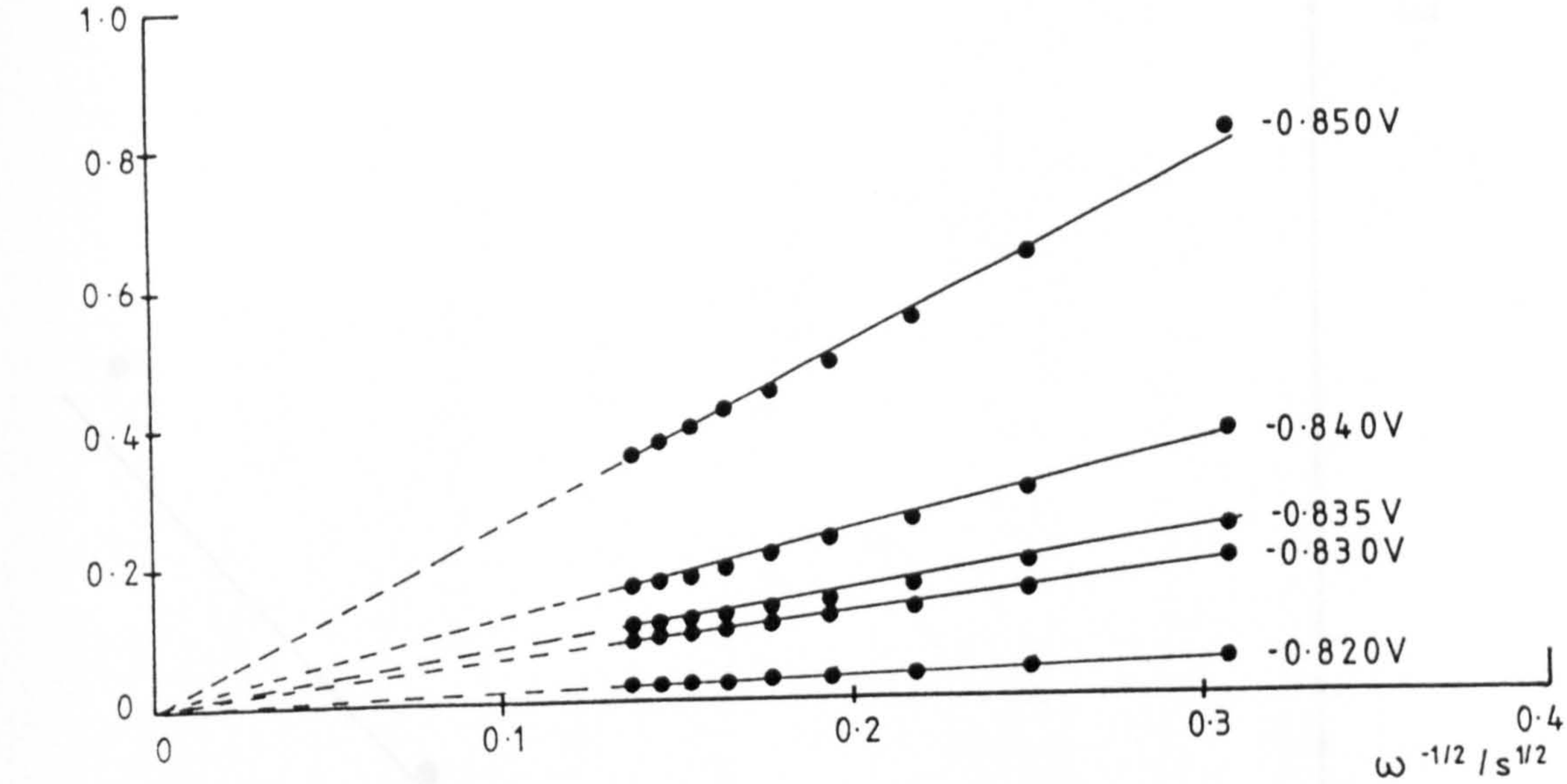

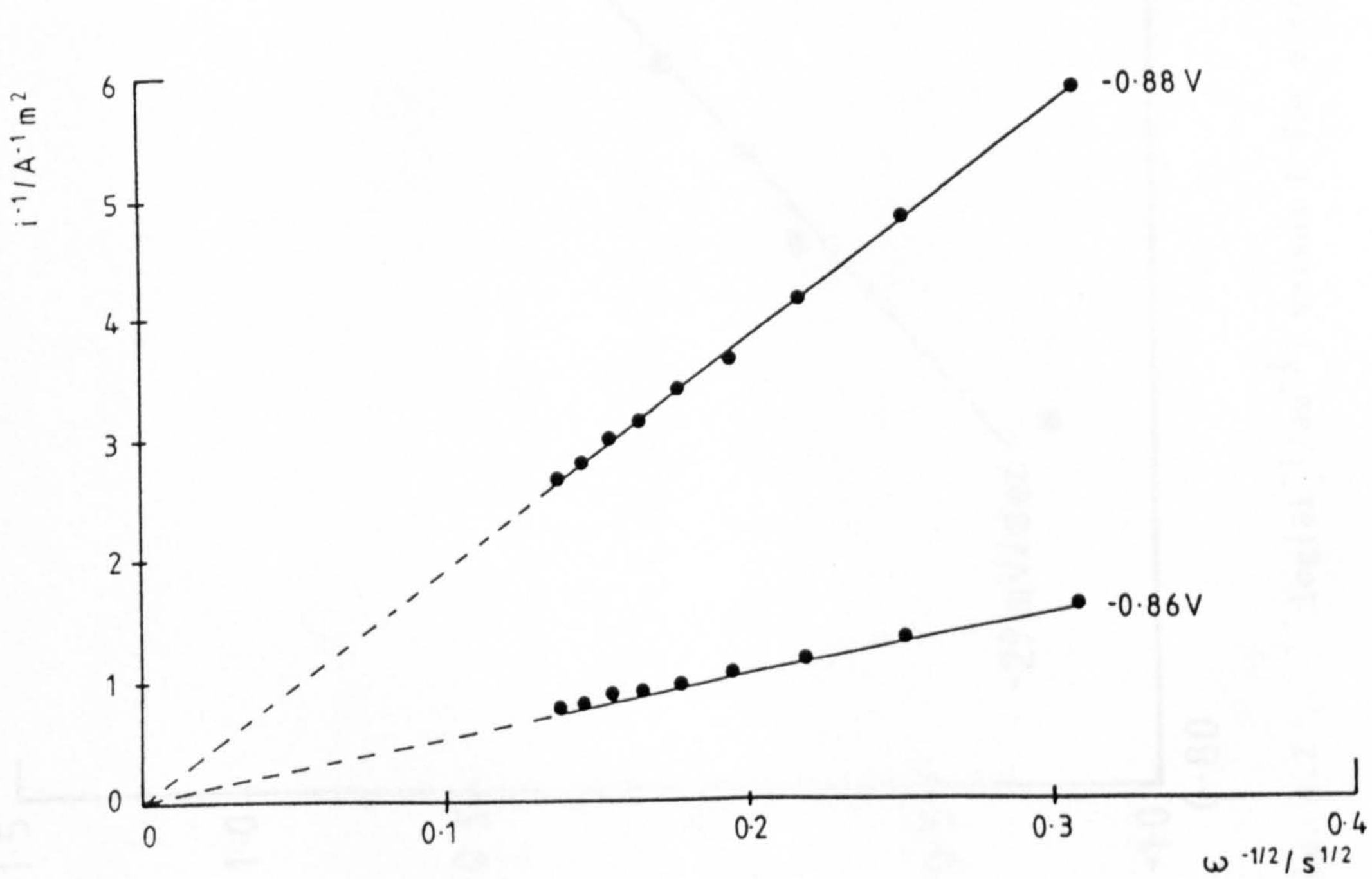

Fig. 6.1 i^{-1} versus $\omega^{-\frac{1}{2}}$ plots for electrolyte (a) at a series of electrode potentials.

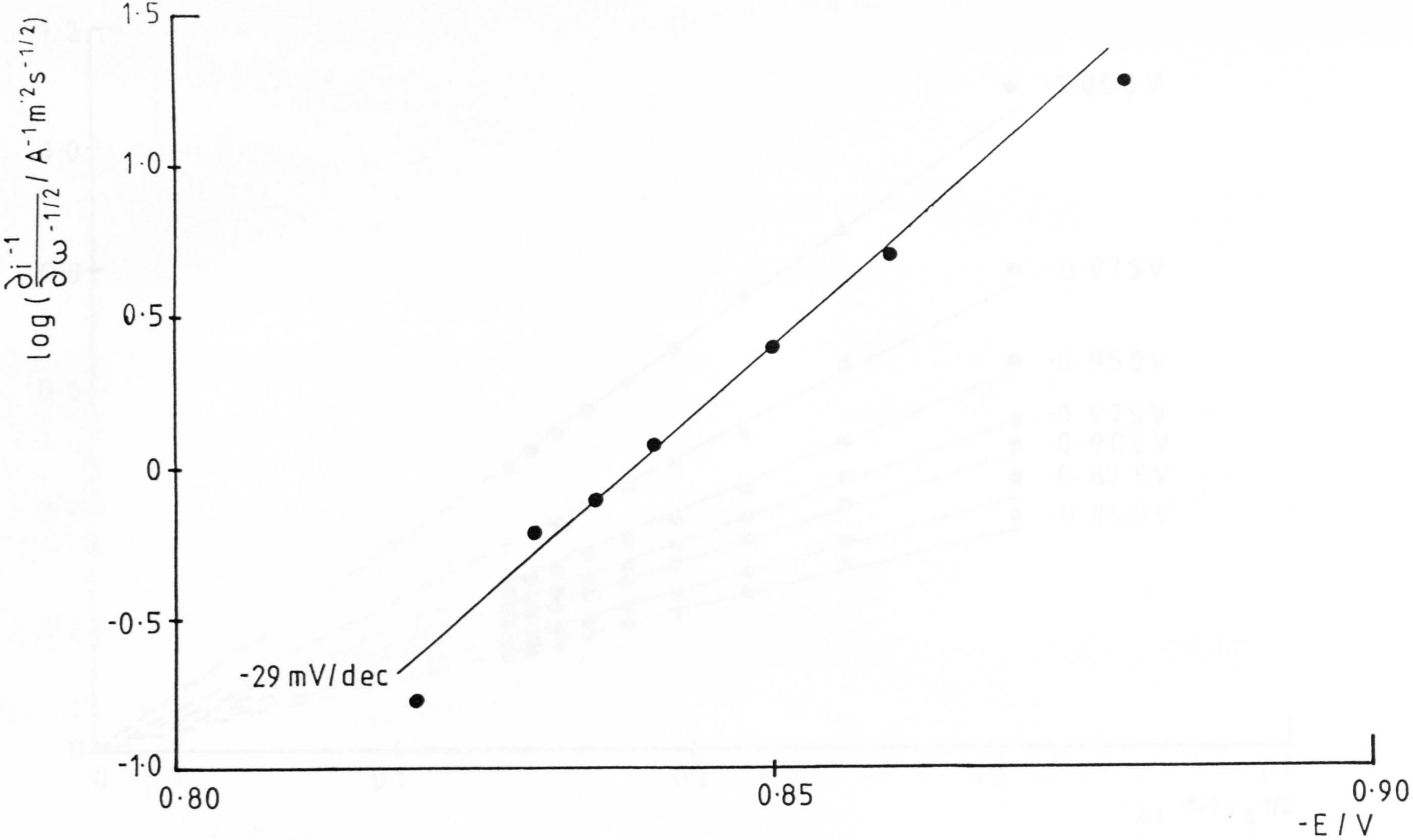

Fig. 6.2 $\log\{\partial i^{-1}/\partial \omega^{-\frac{1}{2}}\}$ versus E for electrolyte (a)

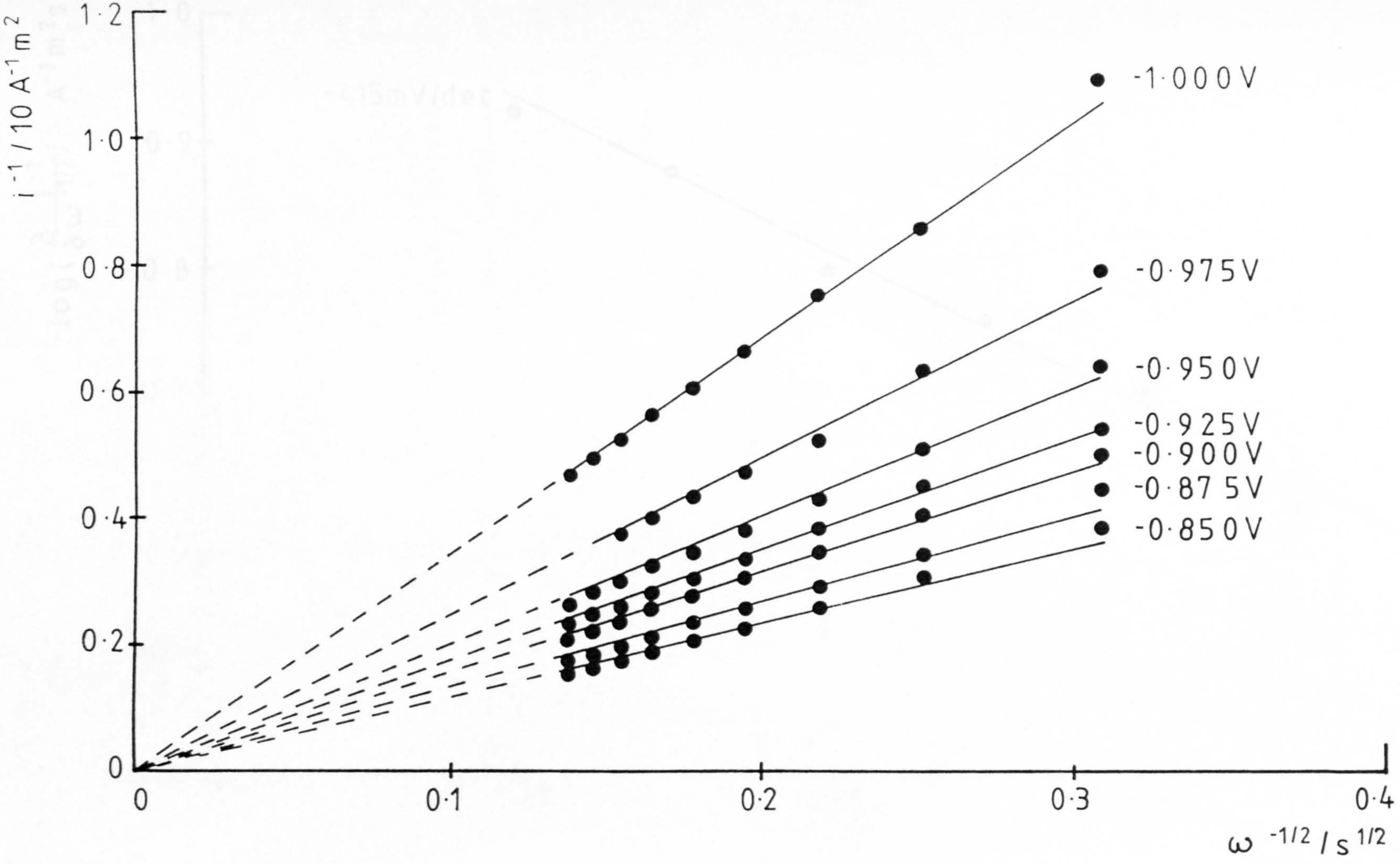

Fig. 6.3 i^{-1} versus $\omega^{-\frac{1}{2}}$ plots for electolyte (b) at a series of electrode potentials

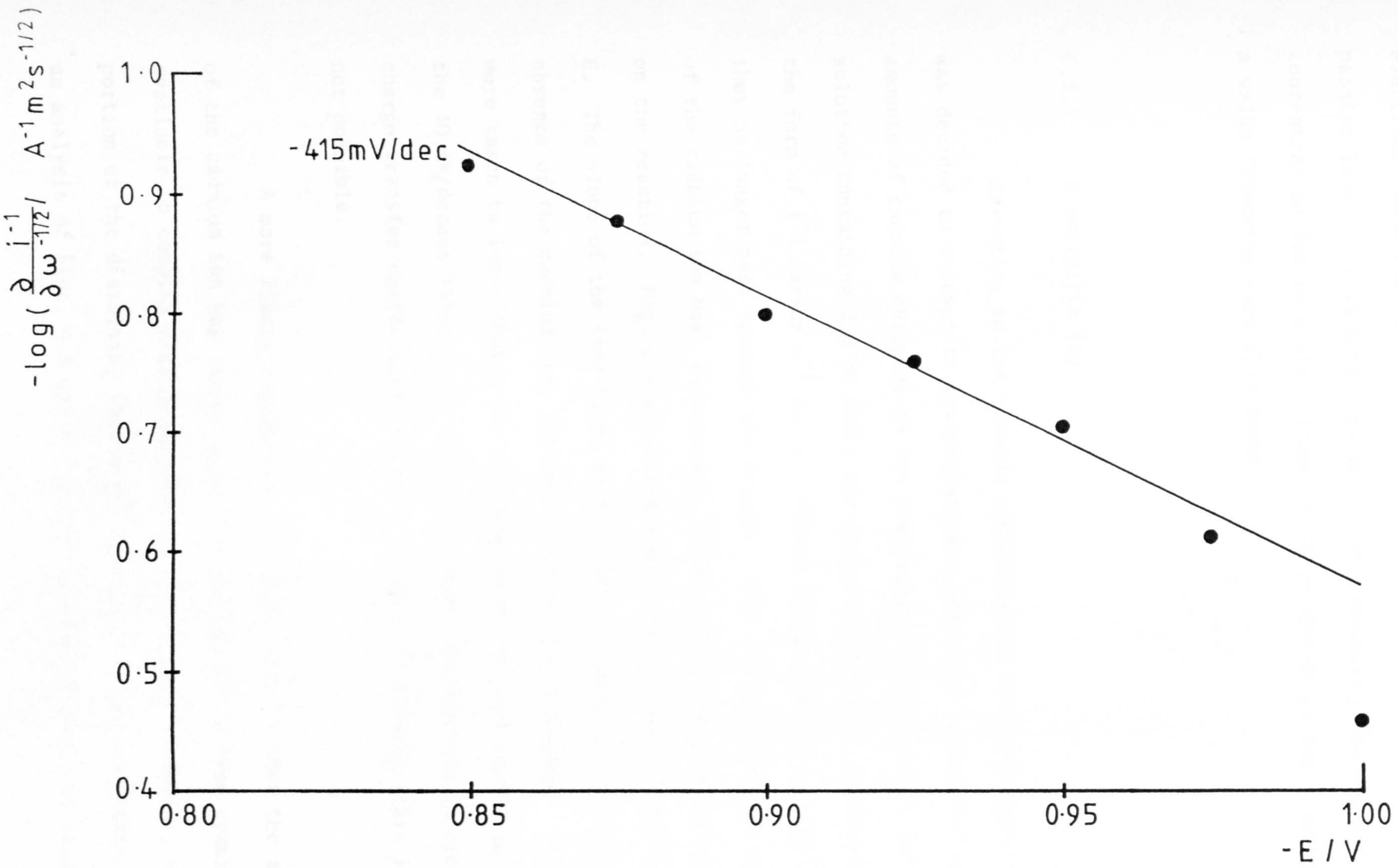

Fig. 6.4 $\log\{\partial i^{-1}/\partial\omega^{-\frac{1}{2}}\}$ versus E for electrolyte (b)

Such a value is usually associated with the presence of a film on the electrode, such that the entire reaction must be pulled through a passive layer. It is quite possible that increasing the cyanide concentration led to a significant shift in the pH of the solution to a value favouring such film formation.

6.3.3 Electrolyte (c)

Reverting to the cyanide concentration of electrolyte (a) it was decided to attempt to investigate the effect of adding various amounts of cadmium chloride to the electrolyte. The results for a solution containing 2.0 mM $CdCl_2$ are shown in Fig. 6.5, as always in the form of i^{-1} versus $\omega^{-\frac{1}{2}}$ plots. Whilst these plots are still linear, they no longer pass through the origin. This implies that the addition of the cadmium ion has, in some way, conferred a degree of irreversibilit on the reaction. Fig. 6.6 shows the variation of $\log\{\partial i^{-1}/\partial\omega^{-\frac{1}{2}}\}$ with E. The slope of the line is no longer -29 mV/decade as it was in the absence of the cadmium ion, but has risen to -55 mV/decade. If this were taken to imply that a one electron transfer were occurring then the 40 mV/decade Tafel slope (Fig. 6.7) would indicate an apparent charge transfer coefficient in excess of unity. Clearly, this is not possible.

A more likely explanation of these facts is that the addition of the cadmium ion has caused a fall in the amount of free cyanide available to complex dissolving cadmium. In such a situation, a proportion of the dissolving ions might be expected to precipitate. Such an analysis of Figs. 6.6 and 6.7 would not then be strictly valid. The

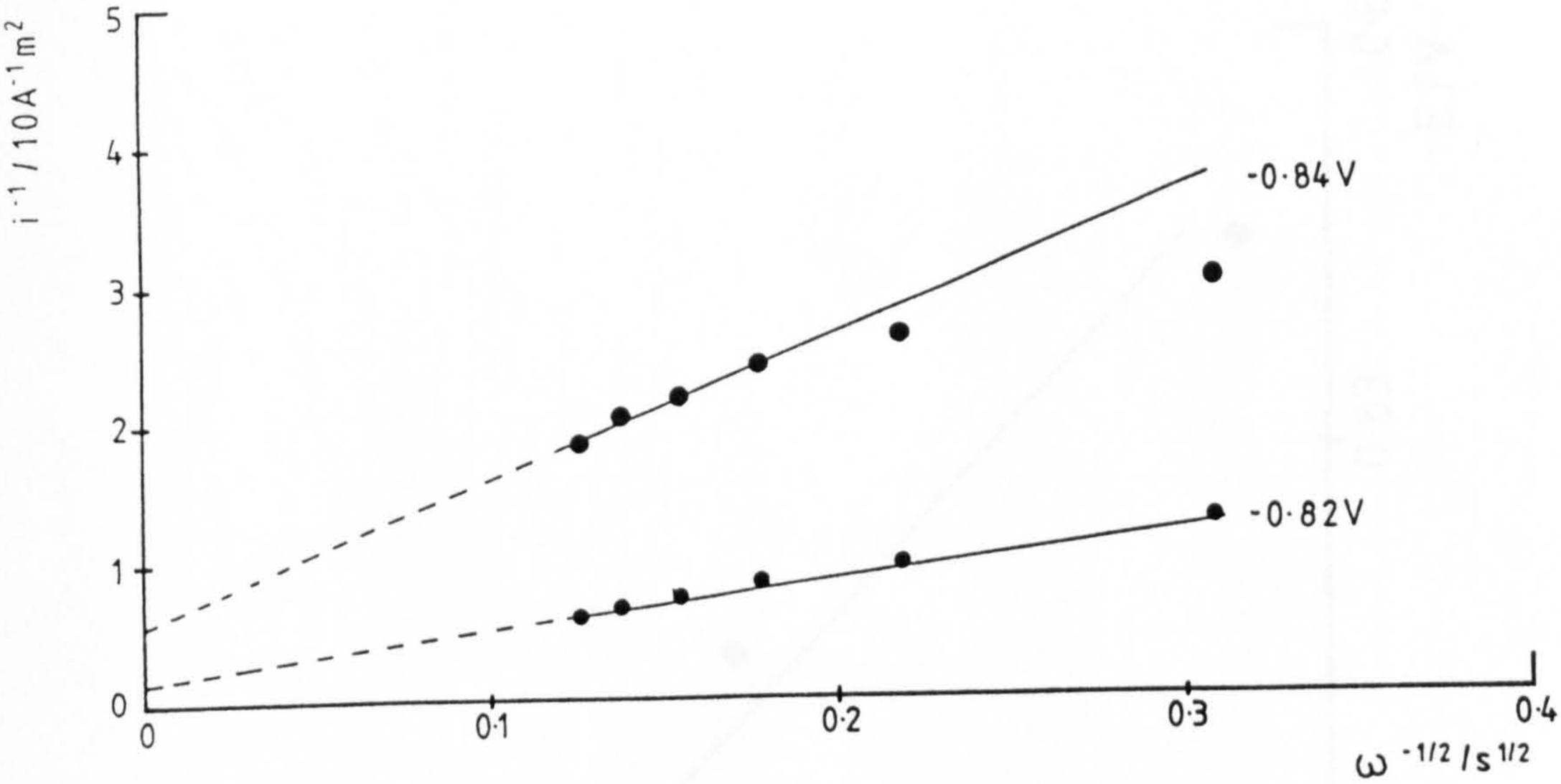

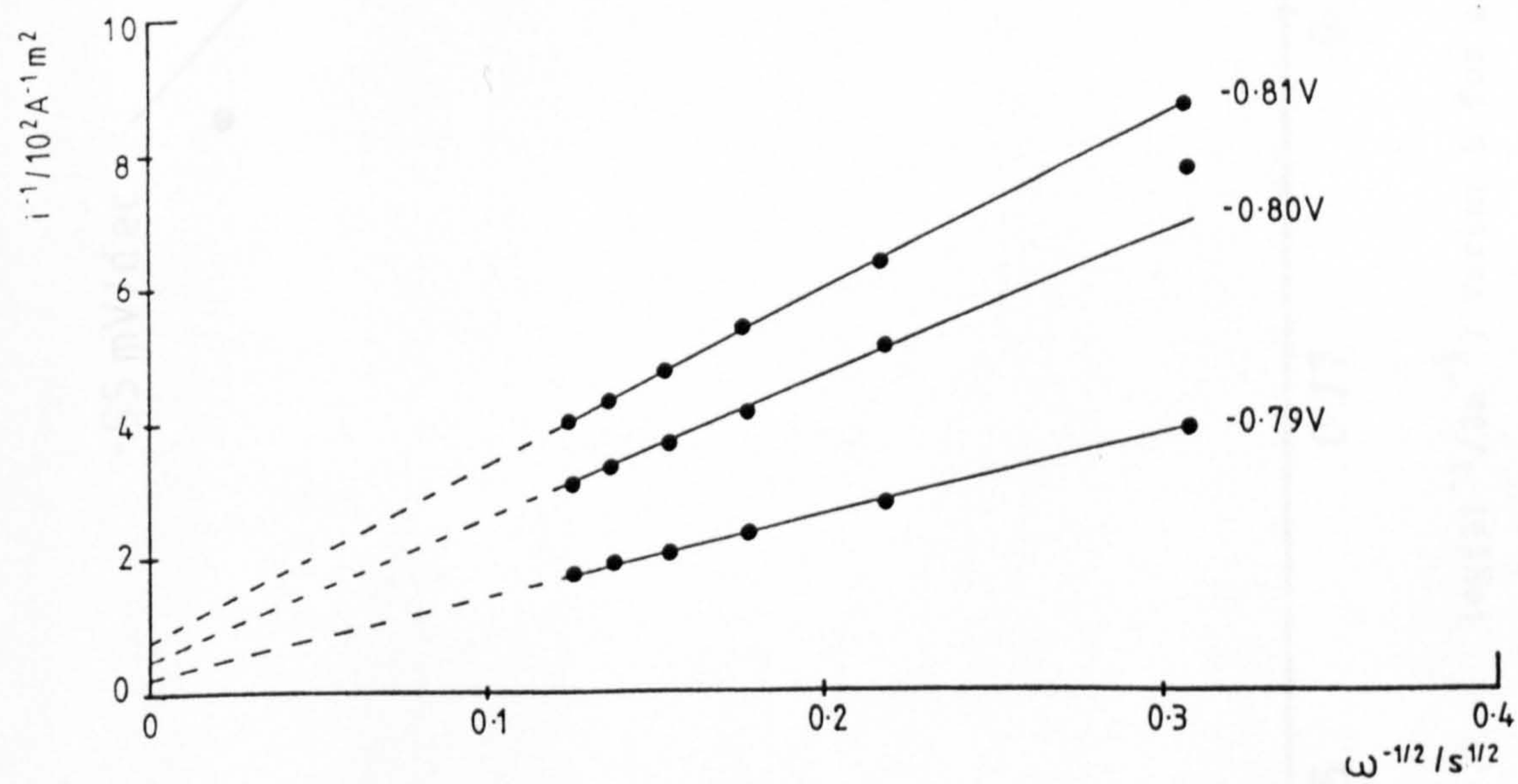

Fig. 6.5 i^{-1} versus $\omega^{-\frac{1}{2}}$ plots for electrolyte (c) at a series of electrode potentials.

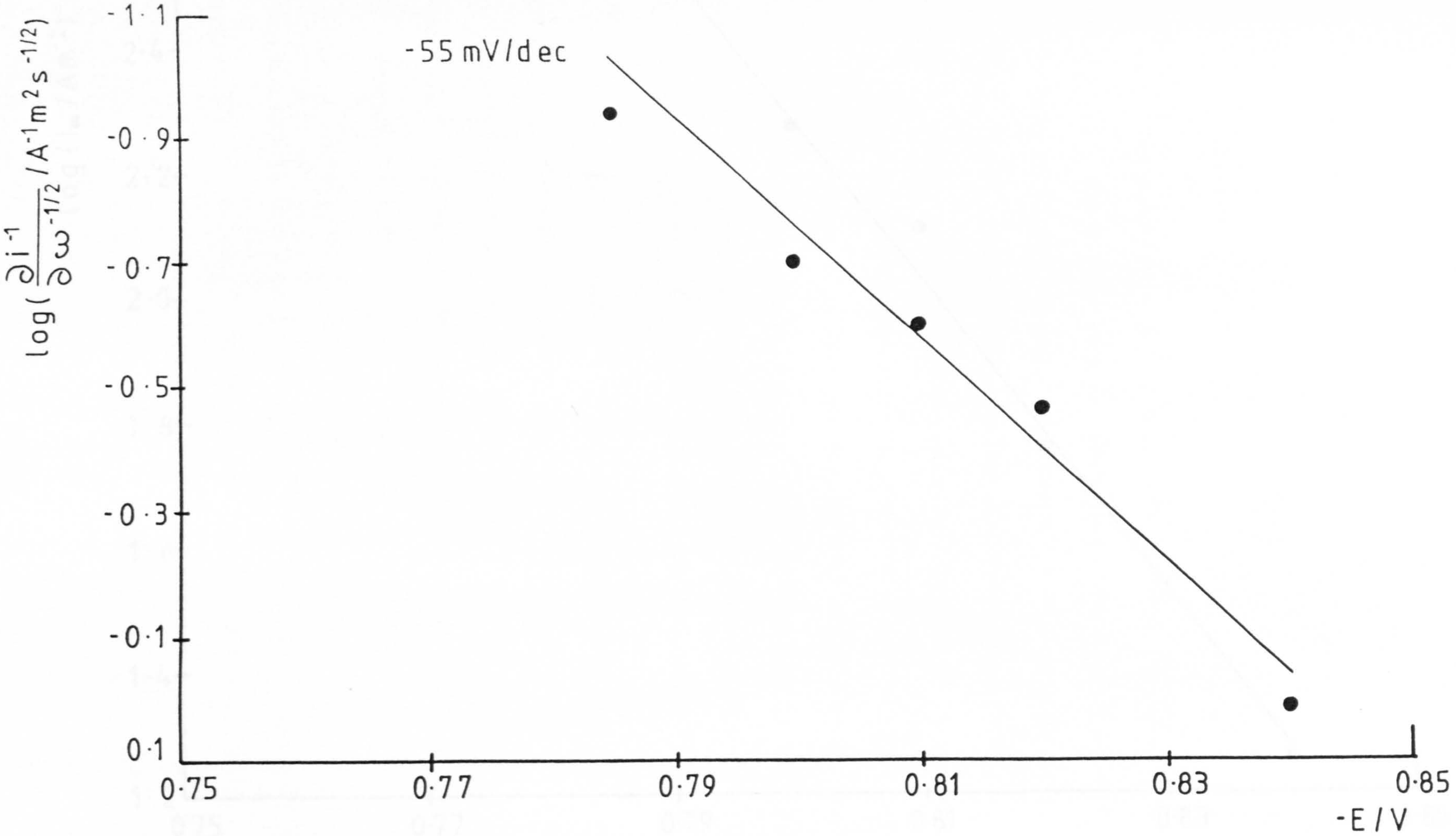

Fig. 6.6 $\log\{\partial i^{-1}/\partial \omega^{-\frac{1}{2}}\}$ versus E for electrolyte (c)

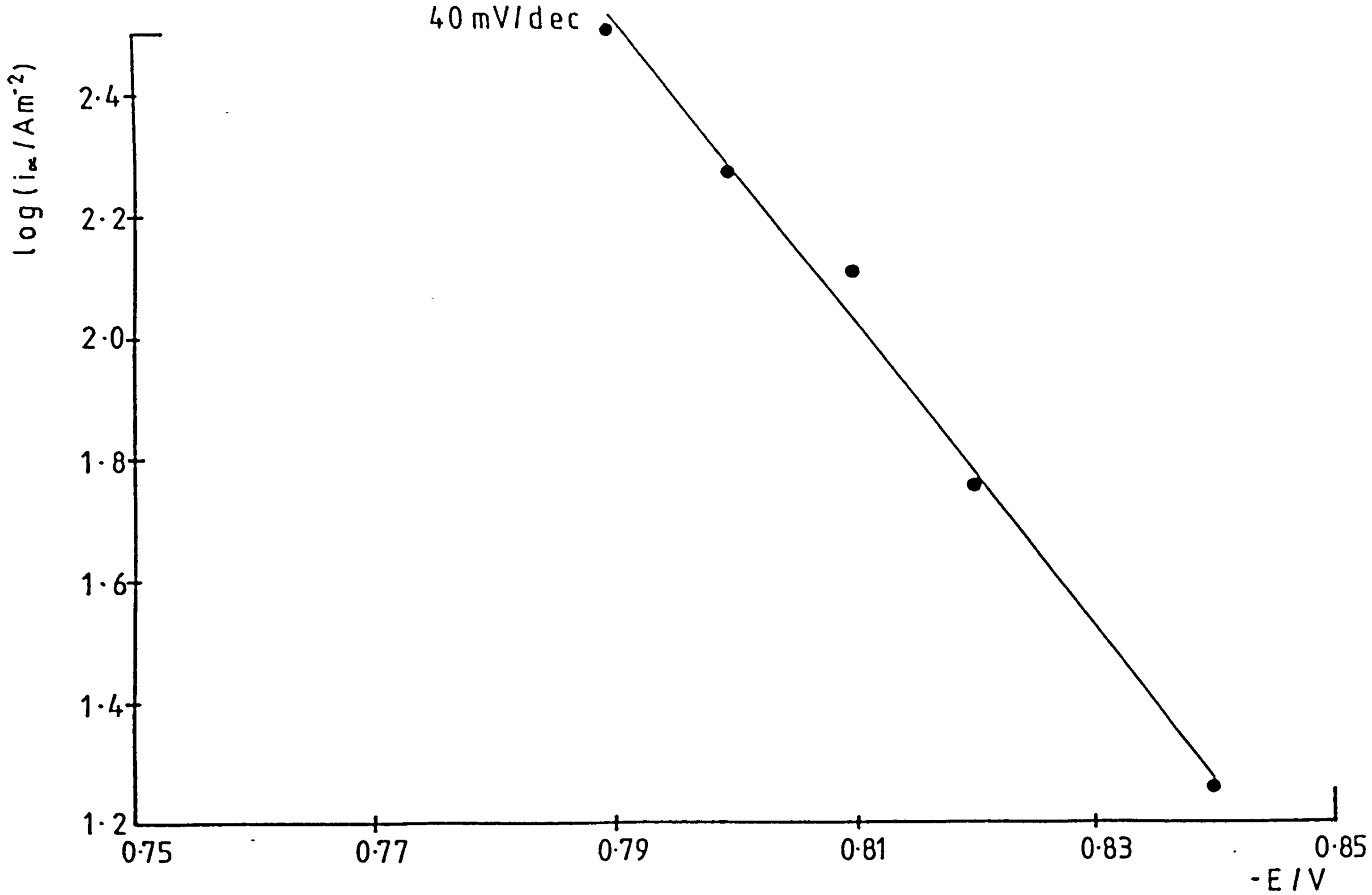

Fig. 6.7 Tafel plot for electrolyte (c)

value of the slope of Fig. 6.6 shows, however, that the precipitated cadmium is far less passivating than the hydroxide film experienced in electrolyte (b).

6.3.4 Electrolyte (d)

The conditions for this experiment were identical to those of 6.3.3 save for a reduction in the concentration of cadmium chloride to 1.0 mM. Yet again linear i^{-1} versus $\omega^{-\frac{1}{2}}$ plots were produced (Fig. 6.8) with intercepts indicating an irreverisble process. The variation of $\log\{\partial i^{-1}/\partial\omega^{-\frac{1}{2}}\}$ with potential (Fig. 6.9) is similar to that of Fig. 6.6 and although insufficient data exists for a line to be drawn, the slope of a line passing through the points at the three most positive potentials exhibits a slope of less than 55 mV/decade. Similarly, the Tafel slope of Fig. 6.10 is increased from its 40 mV/decade value for Fig. 6.7 to 45 mV/decade in the present case.

Whilst the changes in these parameters are too small with regard to the overall accuracy of the experiment to be considered conclusive, it is interesting to note that, if the interpretation of the data is correct, then the effect of a decrease in the concentration of cadmium chloride would be to decrease the competition for free cyanide. Thus is might be expected that the Tafel slope should rise towards its theoretical value of 59 mV/decade and the slope of the $\log\{\partial i^{-1}/\partial\omega^{-\frac{1}{2}}\}$ versus E plot return to its -29 mV/decade value.

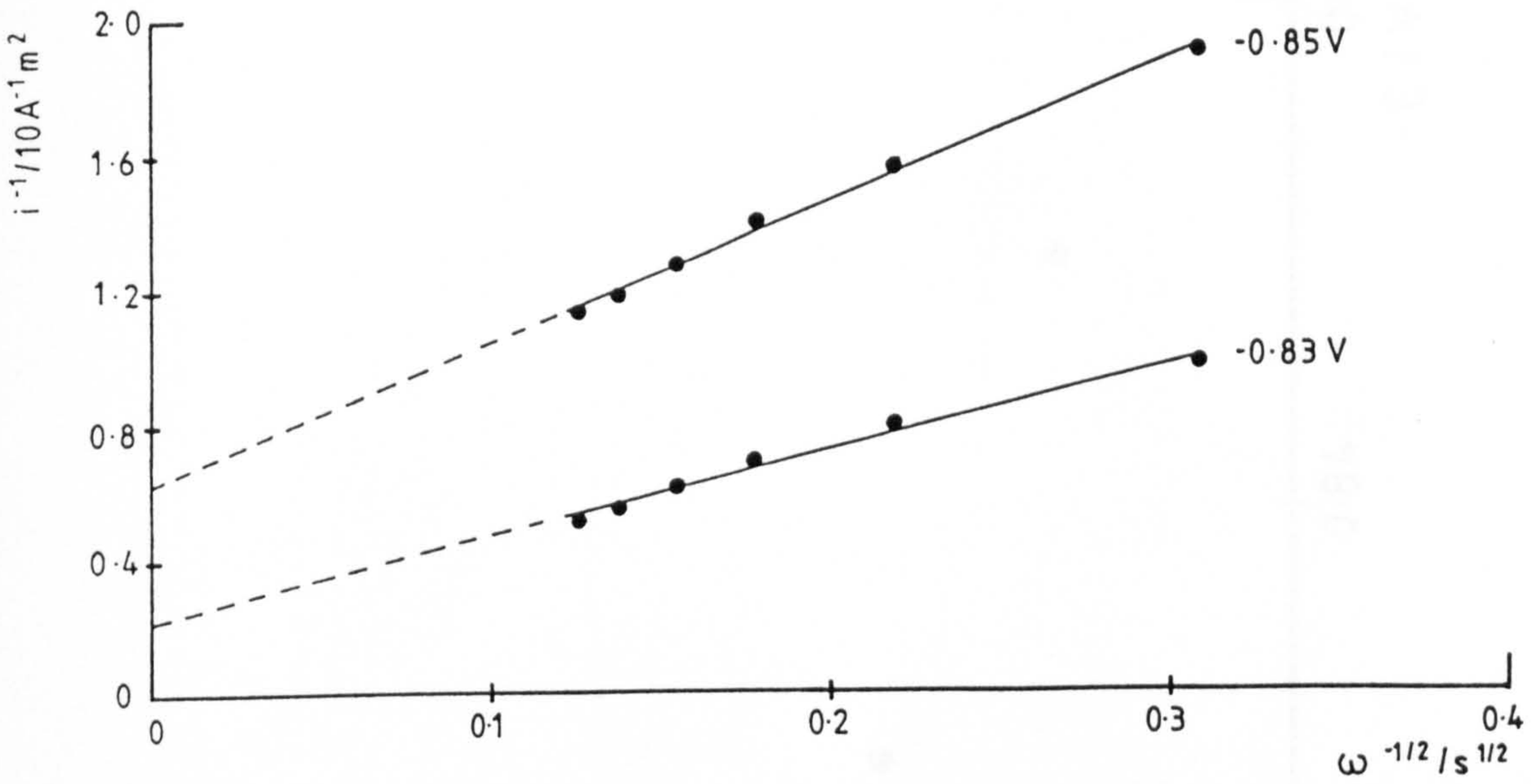

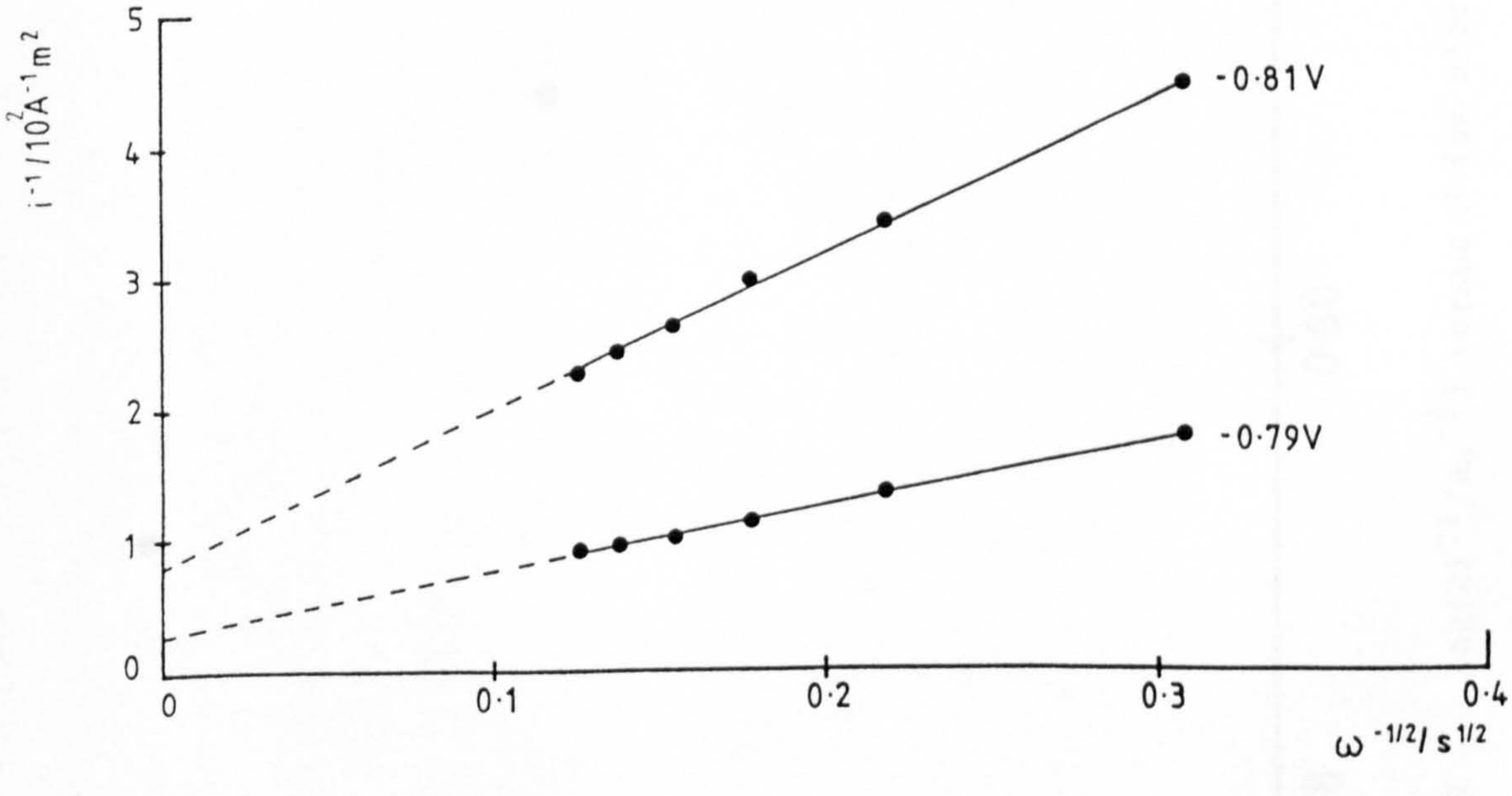

Fig. 6.8 i^{-1} versus $\omega^{-\frac{1}{2}}$ plots for electrolyte (d) at a series of electrode potentials

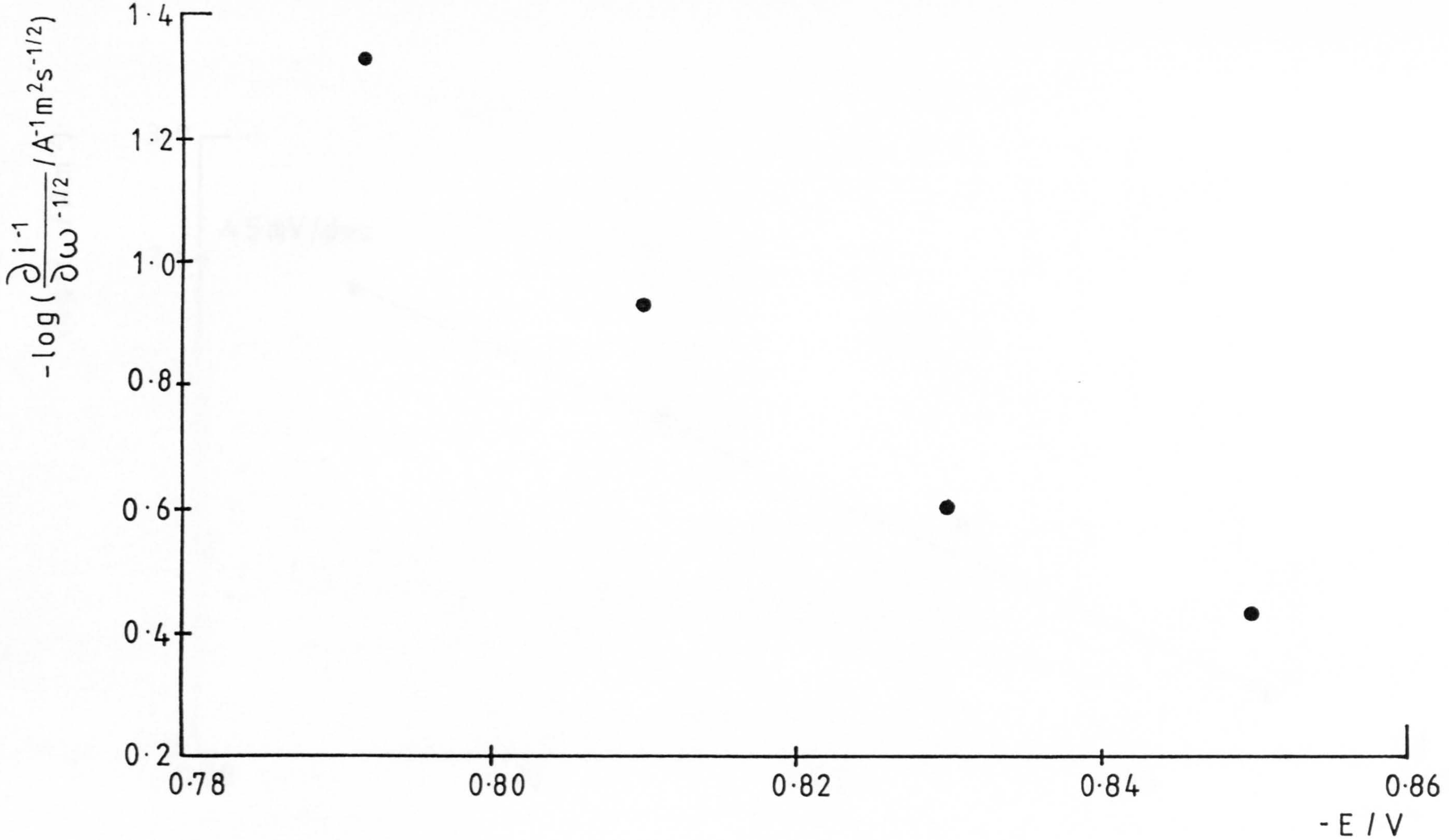

Fig. 6.9 $\log\{\partial i^{-1}/\partial \omega^{-\frac{1}{2}}\}$ versus E for electrolyte (d)

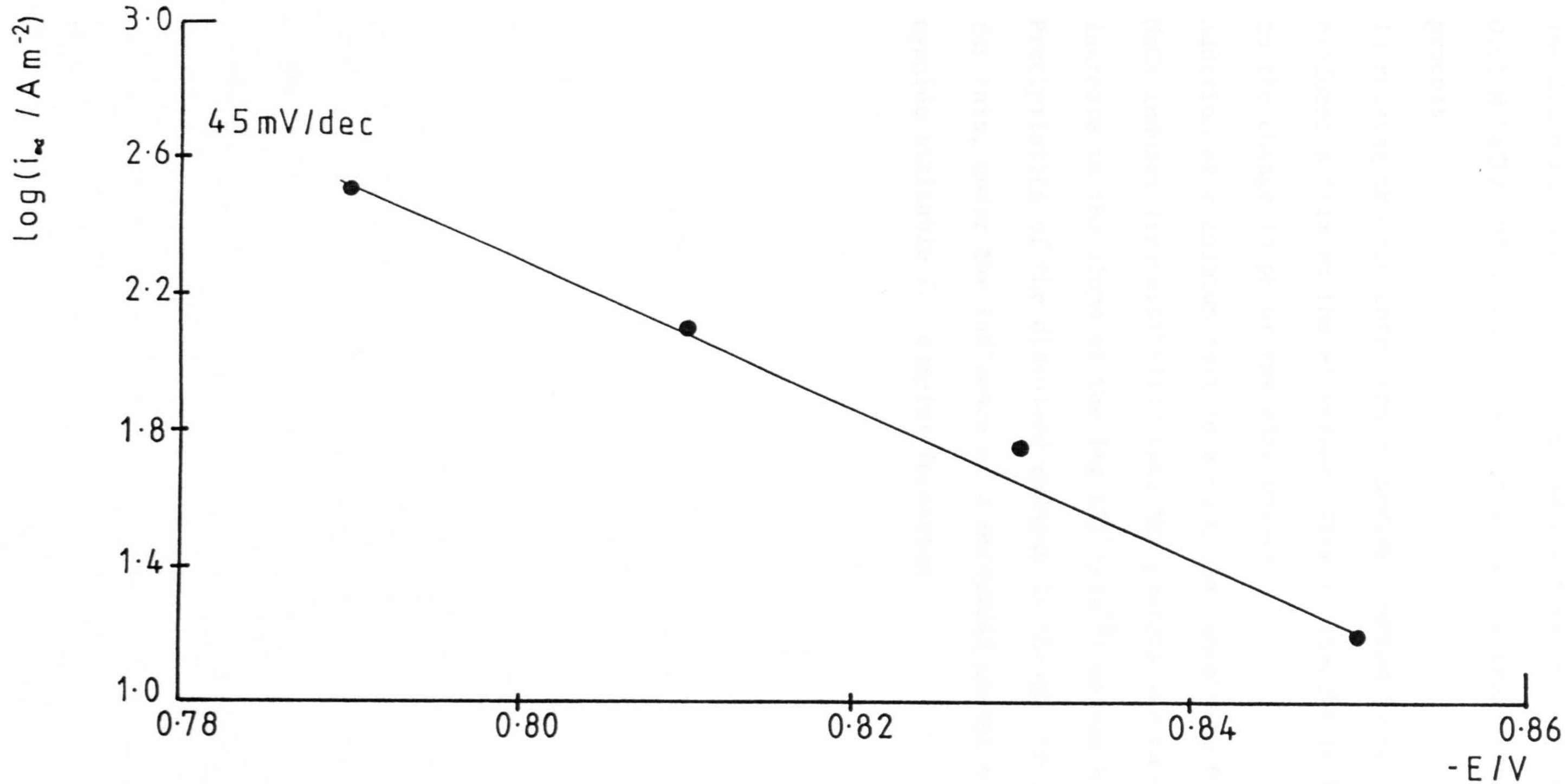

Fig. 6.10 Tafel plot for electrolyte (d)

6.4 Conclusions

1. The dissolution of a solid cadmium electrode in a solution of 0.01 M NaCN/3.99 M NaCl occurs as a two electron reversible process.

2. Increasing the concentration of sodium cyanide to only 0.05 M produces a film on the electrode; this is thought to be due to the change in pH of the electrolyte.

3. Addition of a cadmium salt to a solution containing 0.01 M NaCN induces irreversibility into the process and causes an increase in the slope of the log $\{\partial i^{-1}/\partial \omega^{-\frac{1}{2}}\}$ versus E curve. Precipitation of the dissolved cadmium is thought to account for this, under the influence of a decreased amount of free cyanide available for complex formation.

CHAPTER SEVEN

CADMIUM IN CHEMELEC ELECTROLYTES

7.1 Introduction

As has already been stated (§1.1), the majority of cadmium plating is achieved from cyanide electrolytes. A typical cyanide bath composition might be[103]:

Cd	20 g/l
NaCN	50 g/l
NaOH	15 g/l

A typical drag-out tank might commence operation with a solution containing only 10 g/l of sodium hydroxide. Over a period of months, drag-out from the plating bath will result in the incorporation of plating bath salts with concentrations up to their plating bath values. The metal ion concentration will, however, be depleted to below 1 g/l. In practice, a range of solution compositions will be encountered in operation of the Chemelec Cell®. The probable limits of such solutions are, in g/l:

	Start-up	After many months
Cd	0.2	0.2 - 0.5
NaCN	0.6 - 0.9	50 - 60
NaOH	10	15

and the electrolytes studied in the following sections have been chosen to fall within these values.

A combination of techniques (linear sweep voltammetry, rotating disc and faradaic impedance) has been used in an attempt to elucidate the electrode kinetics of solid cadmium in such electrolytes.

7.2 Linear Sweep Voltammetry

Linear sweep voltammograms were recorded at a series of five different sweep rates for a set of three electrolytes of composition:

	(a)	(b)	(c)
$Cd(CN)_2$	3.0mM	3.0mM	3.0mM
NaCN	1.0M	0.1M	0.01M
NaOH	0.4M	0.4M	0.4M

The electrolytes were typical of the drag-out solution after many months of use, but with sodium cyanide concentrations straddling the range.

The resulting voltammograms are extremely complex and not amenable to a rigorous quantitative interpretation. There are several anodic and cathodic peaks and, often, a considerable fine structure. A semi-quantitative treatment will be attempted where possible.

7.2.1 Electrolyte (a)

Figs. 7.2.1 to 7.2.5 show the voltammograms for the 1.0 M NaCN case. The first quadrant of each shows the oxidation currents, with the reduction currents in the fourth quadrant.

Fig. 7.2.1 is suggestive of a passivated electrode, with the main anodic peak characteristic of classical passivation. The cathodic process, save for the evolution of hydrogen at $\sim$ -2 V is completely inhibited. As the sweep rate is increased (Figs. 7.2.2 through 7.2.5)

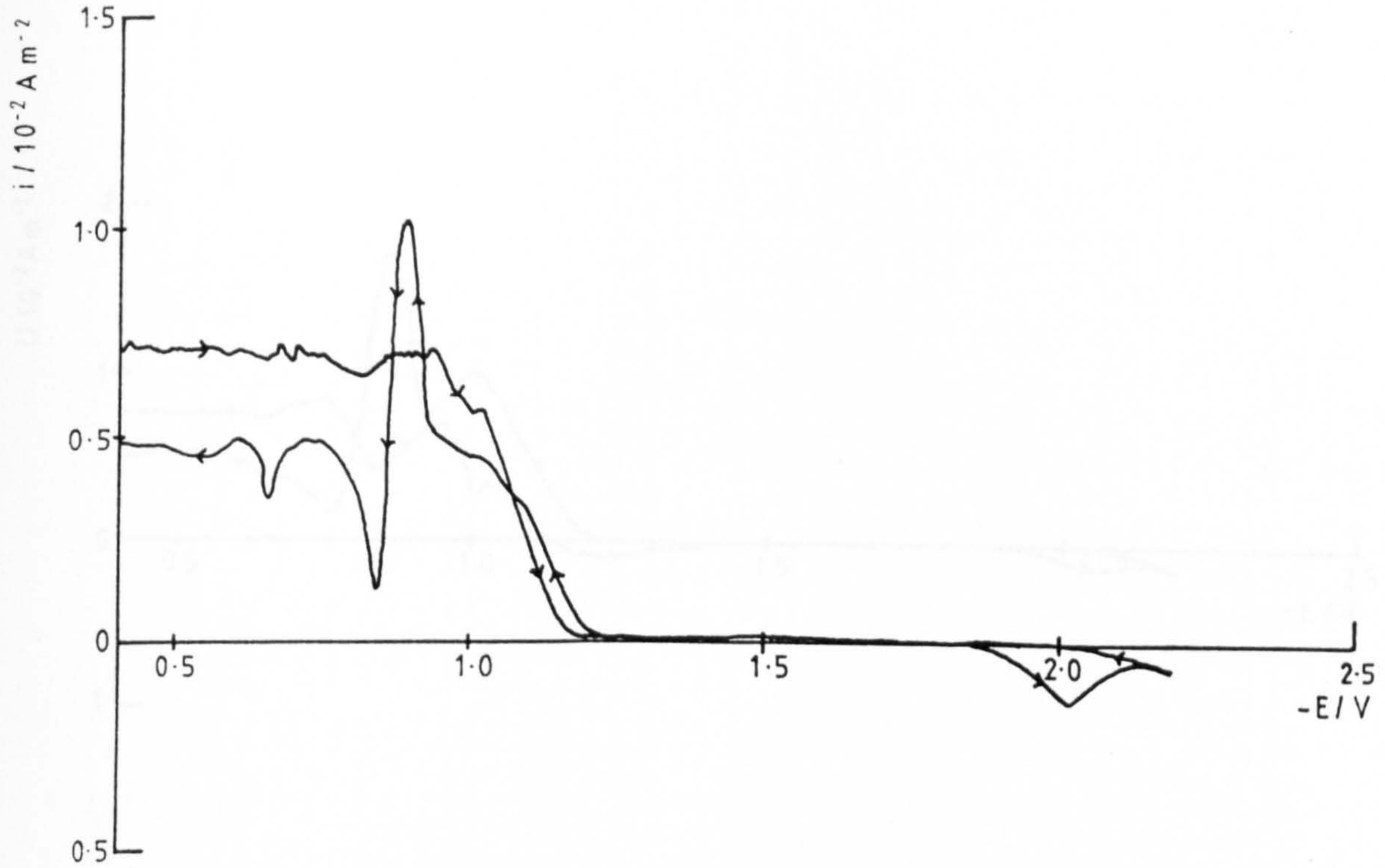

Fig. 7.2.1 LSV in 1.0 M NaCN, ν = 2.96 mV s^{-1}

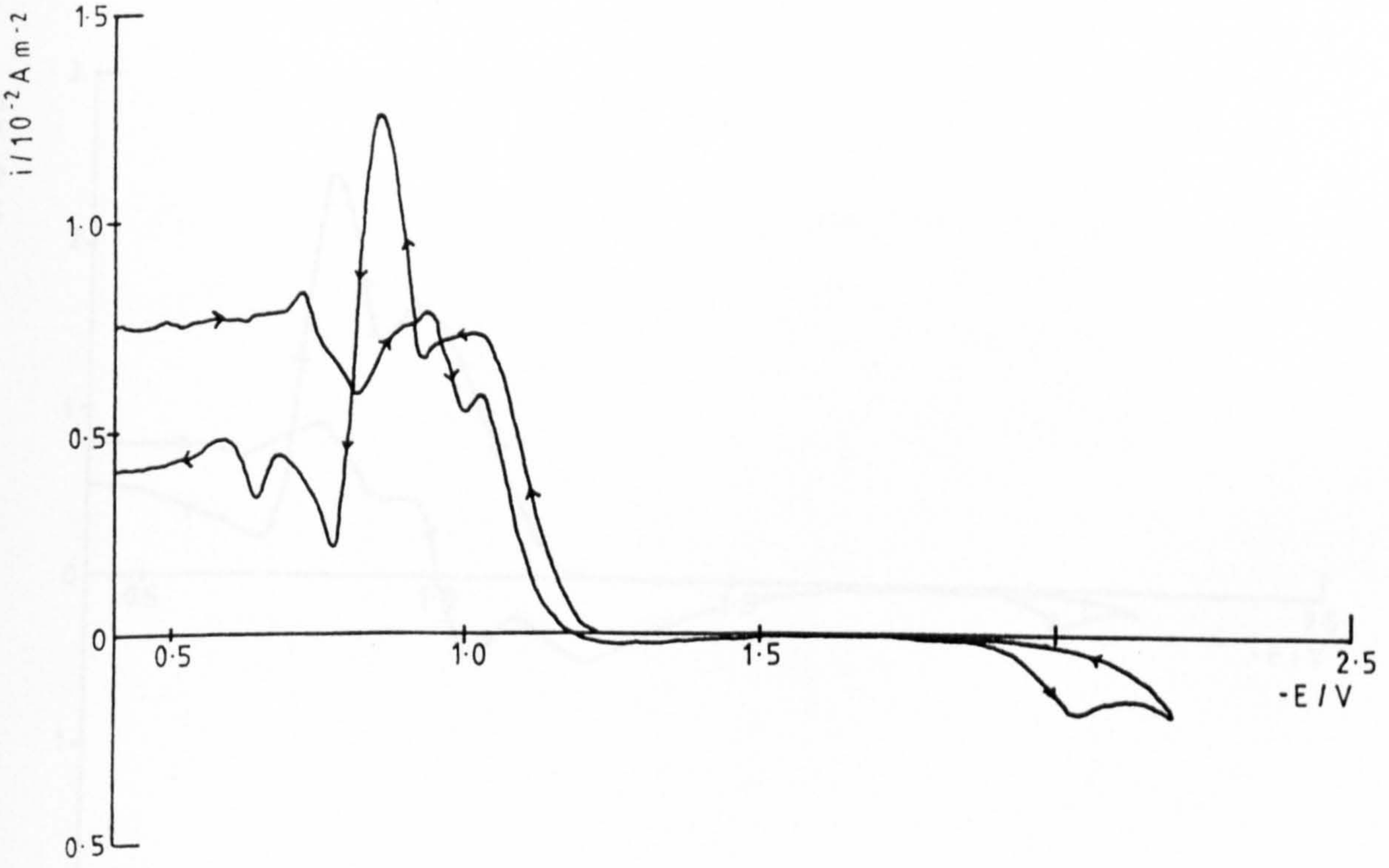

Fig. 7.2.2 LSV in 1.0 M NaCN, ν = 13.2 mV s^{-1}

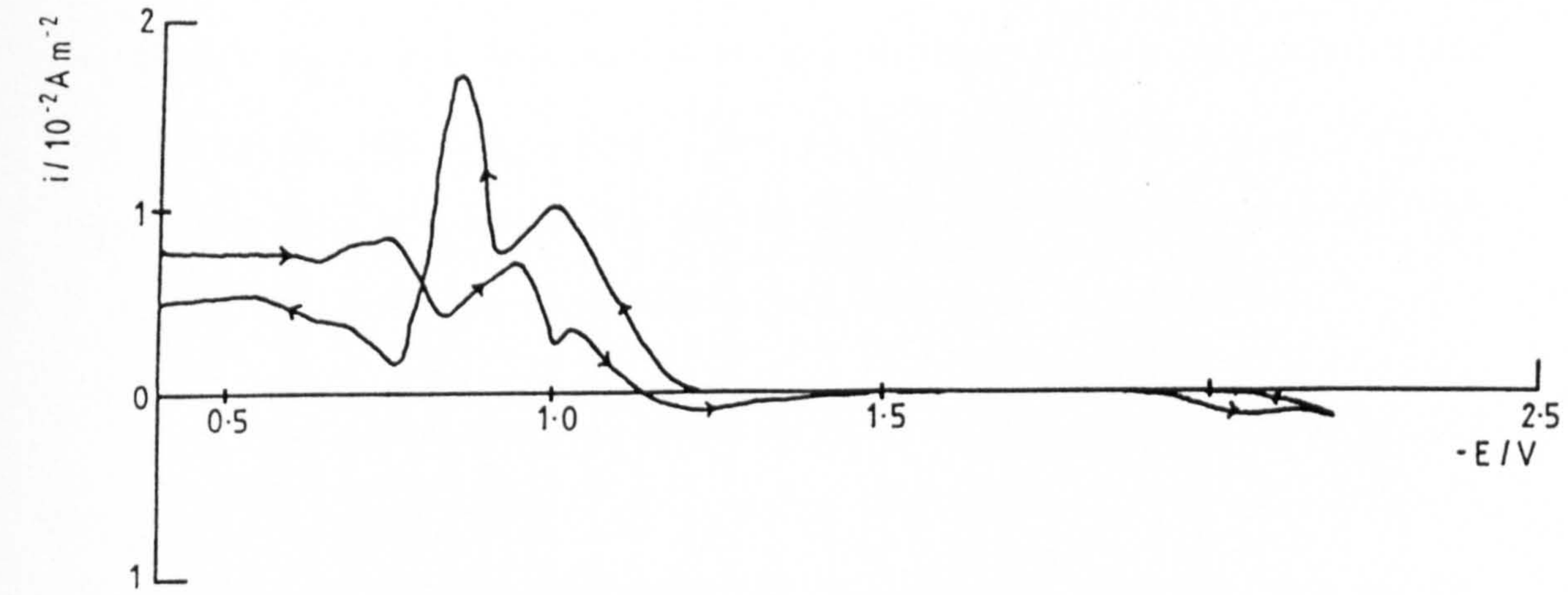

Fig. 7.2.3 LSV in 1.0 M NaCN, ν = 40.9 mV s^{-1}

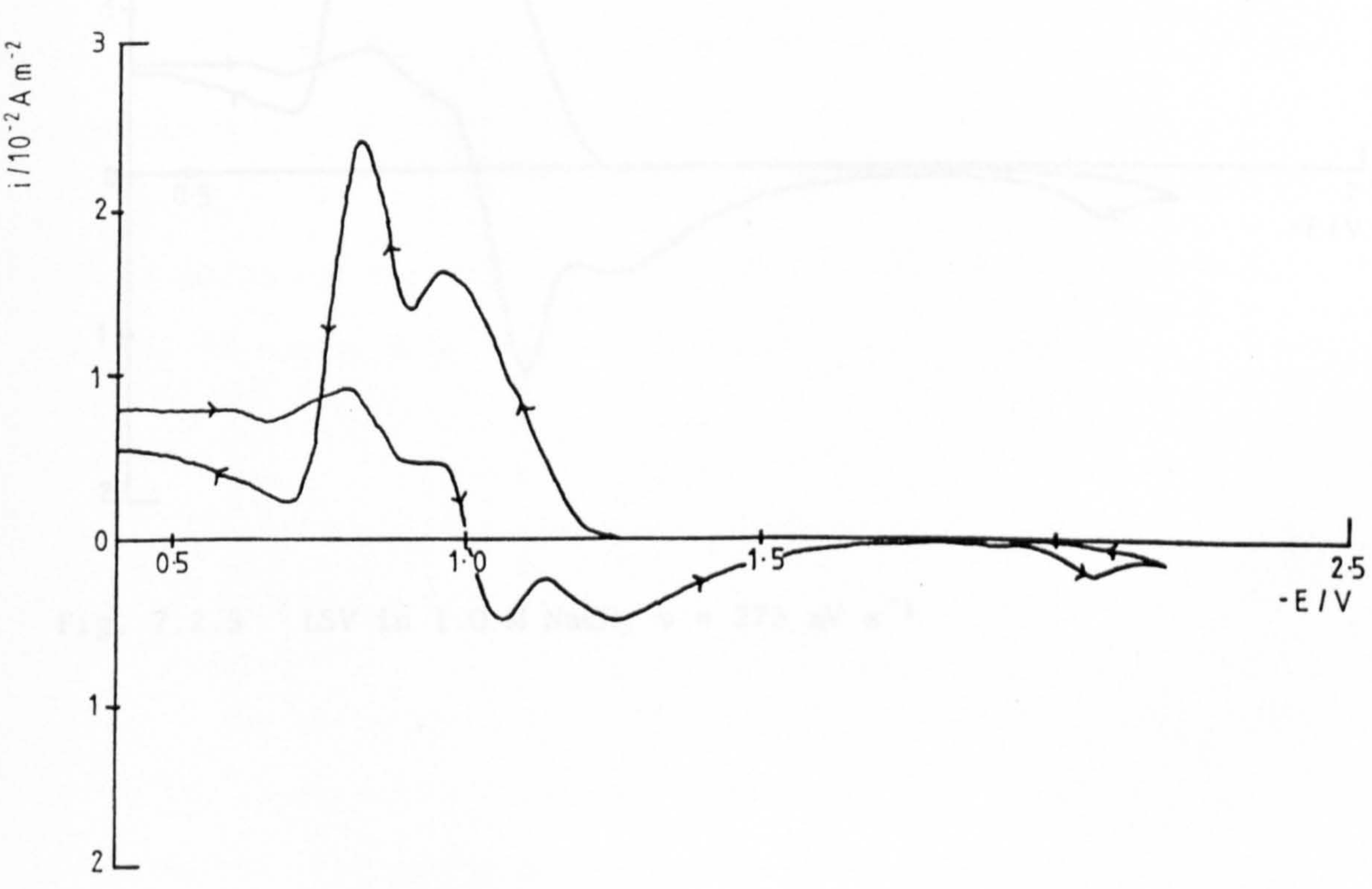

Fig. 7.2.4 LSV in 1.0 M NaCN, ν = 128 mV s^{-1}

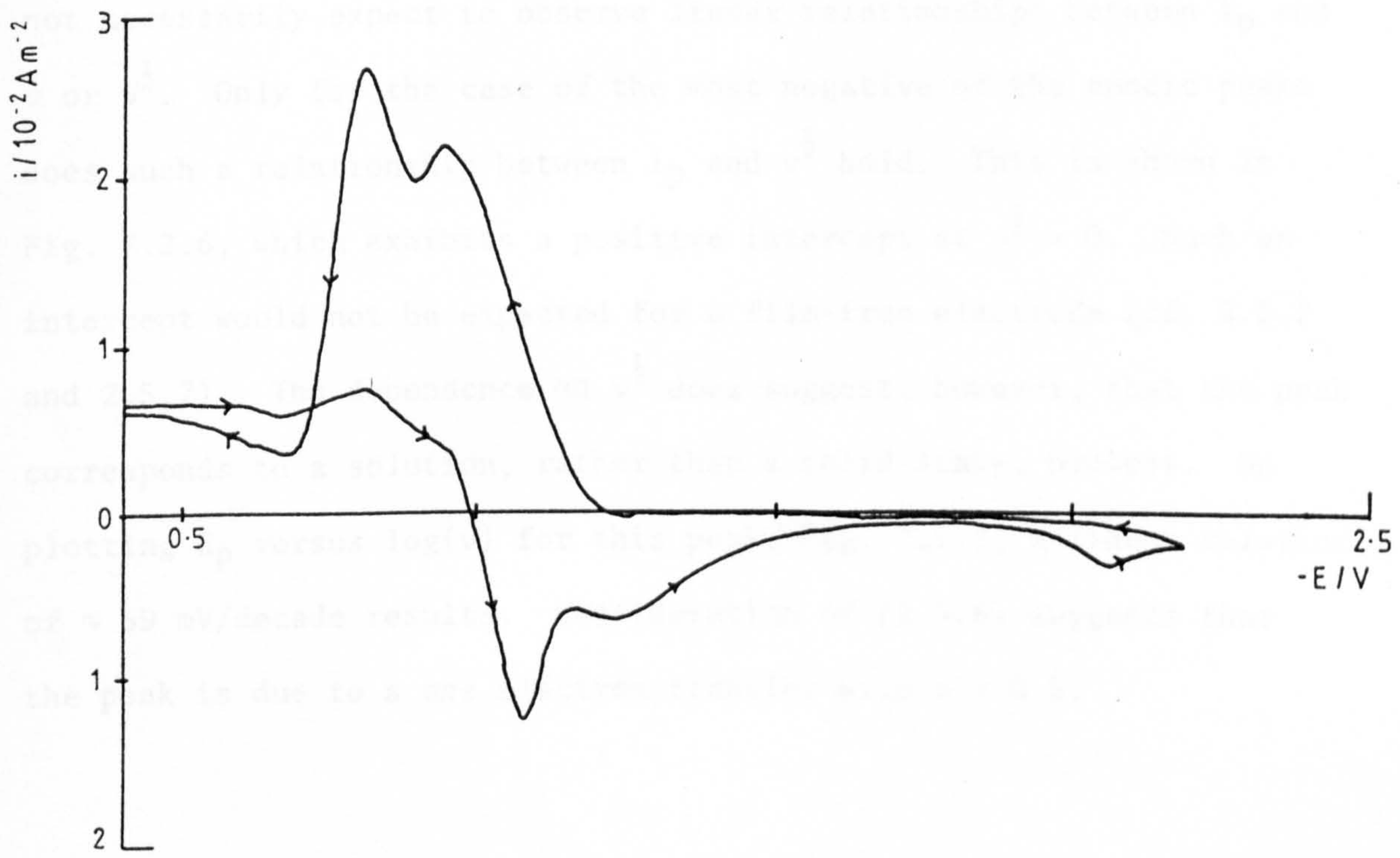

Fig. 7.2.5 LSV in 1.0 M NaCN, ν = 273 mV s^{-1}

the appearance of cathodic peaks is noted. The separations between the anodic and cathodic peaks (and indeed their broadness) are far in excess of the values associated with simply coupled redox processes. The anodic peaks are thought to be due essentially to the solid-state film formation and the cathodic processes are believed to be predominantly associated with the reduction of the film. The cathodic peak at $\sim$ -2 V is due to the hydrogen evolution reaction.

The anomalous peak separations would be rationalised by the existence of a hydroxide film covering the electrode. In view of this interpretation and the complexity of the current response, one would not necessarily expect to observe linear relationships between i_p and ν or $\nu^{\frac{1}{2}}$. Only for the case of the most negative of the anodic peaks does such a relationship between i_p and $\nu^{\frac{1}{2}}$ hold. This is shown in Fig. 7.2.6, which exhibits a positive intercept at $\nu^{\frac{1}{2}} = 0$. Such an intercept would not be expected for a film-free electrode (cf. 2.5.2 and 2.5.7). The dependence on $\nu^{\frac{1}{2}}$ does suggest, however, that the peak corresponds to a solution, rather than a solid state, process. On plotting E_p versus log{ν} for this peak, Fig. 7.2.7, a linear relation of $\sim$ 59 mV/decade results. Consideration of (2.5.6) suggests that the peak is due to a one electron transfer with $\alpha = 0.5$.

7.2.2 Electrolyte (b)

The voltammograms obtained for electrolyte (b), Figs. 7.2.8 to 7.2.12, appear to be of greater simplicity than those of Figs. 7.2.1 to 7.2.5. The values for the peak separations are still too large, however, for simple redox processes. There is less evidence of pass-

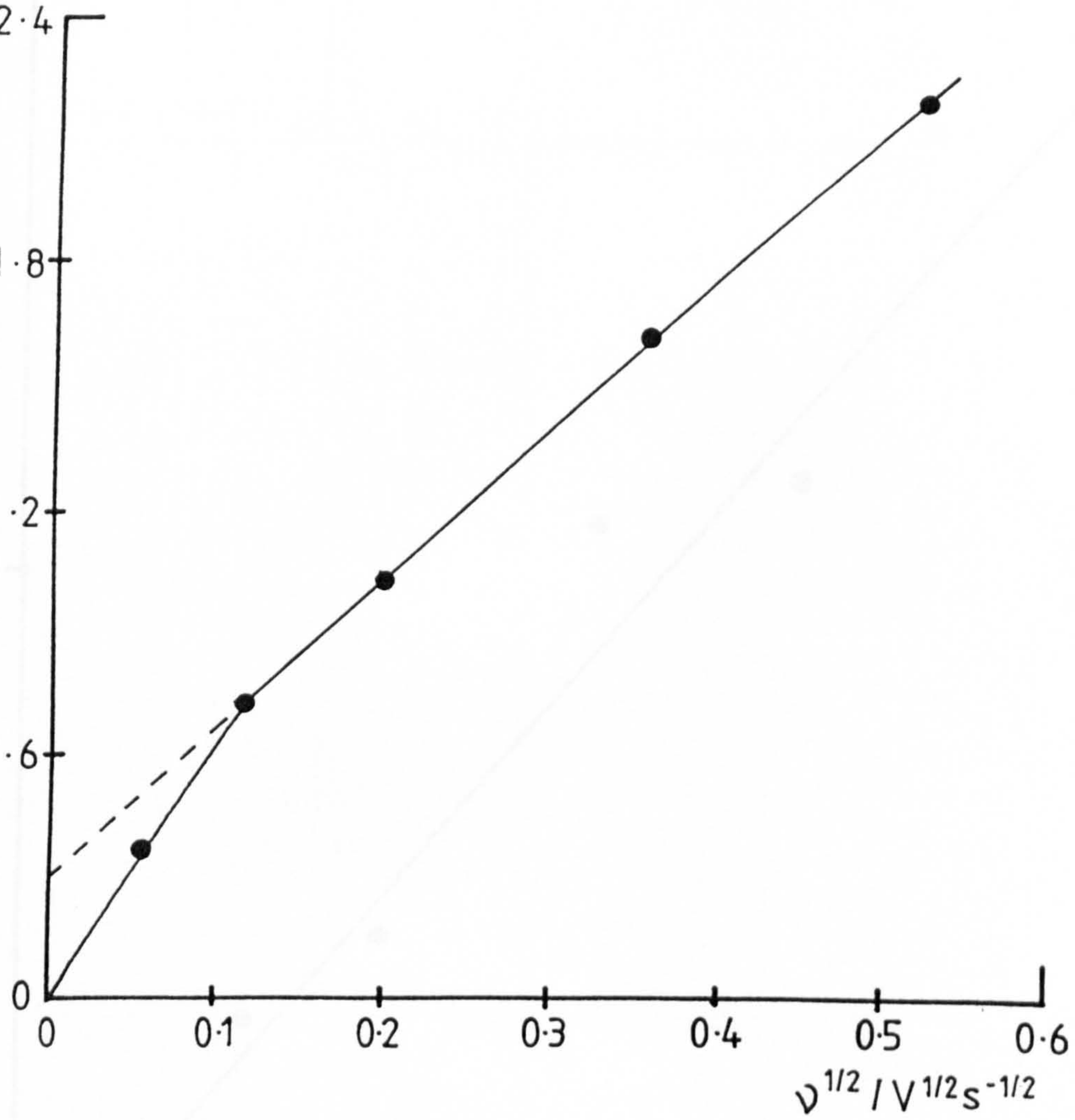

Fig. 7.2.6 i_p versus $\nu^{\frac{1}{2}}$ plot (1.0 M NaCN)

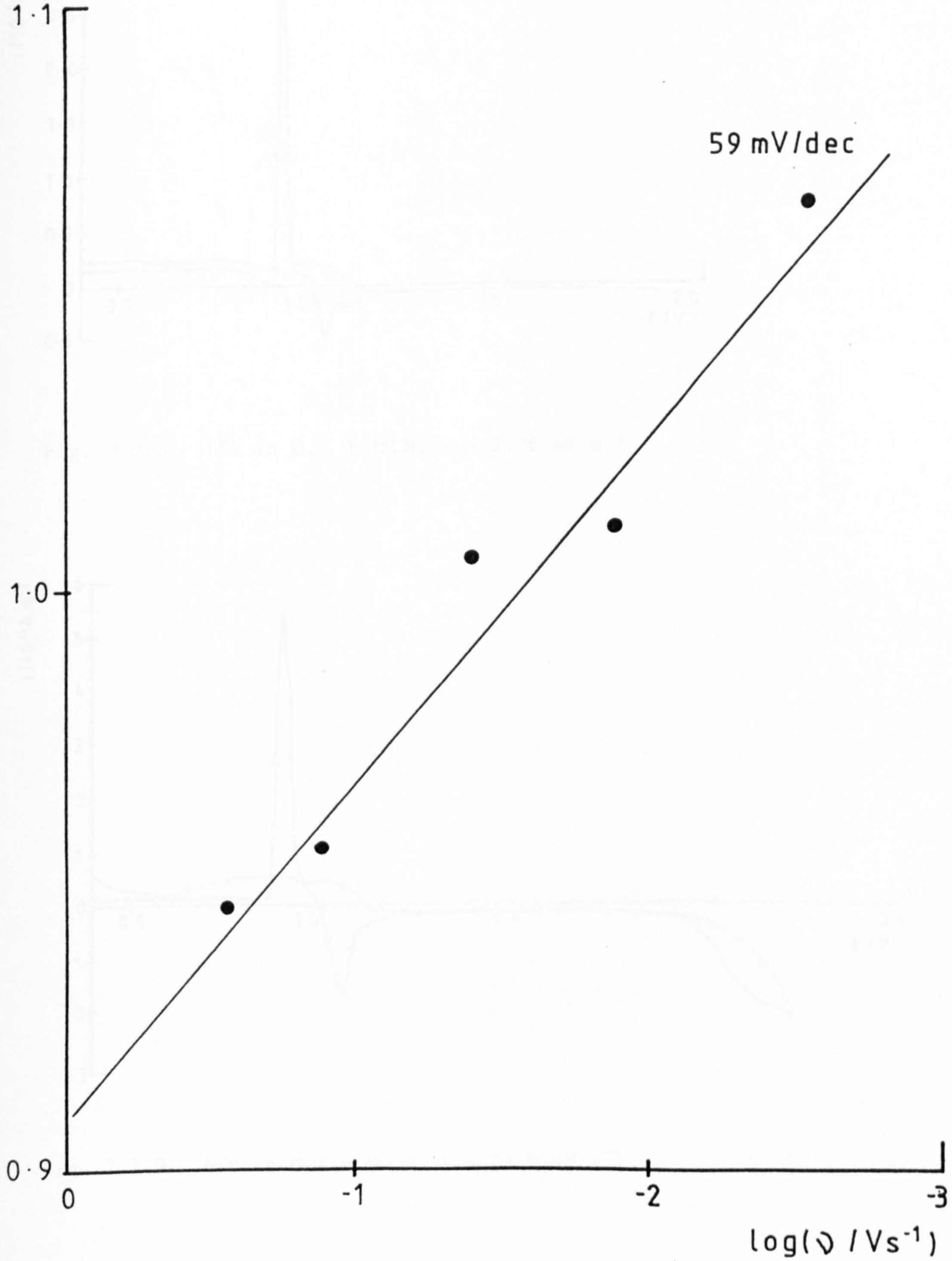

Fig. 7.2.7 E_p versus log{ν} plot (1.0 M NaCN)

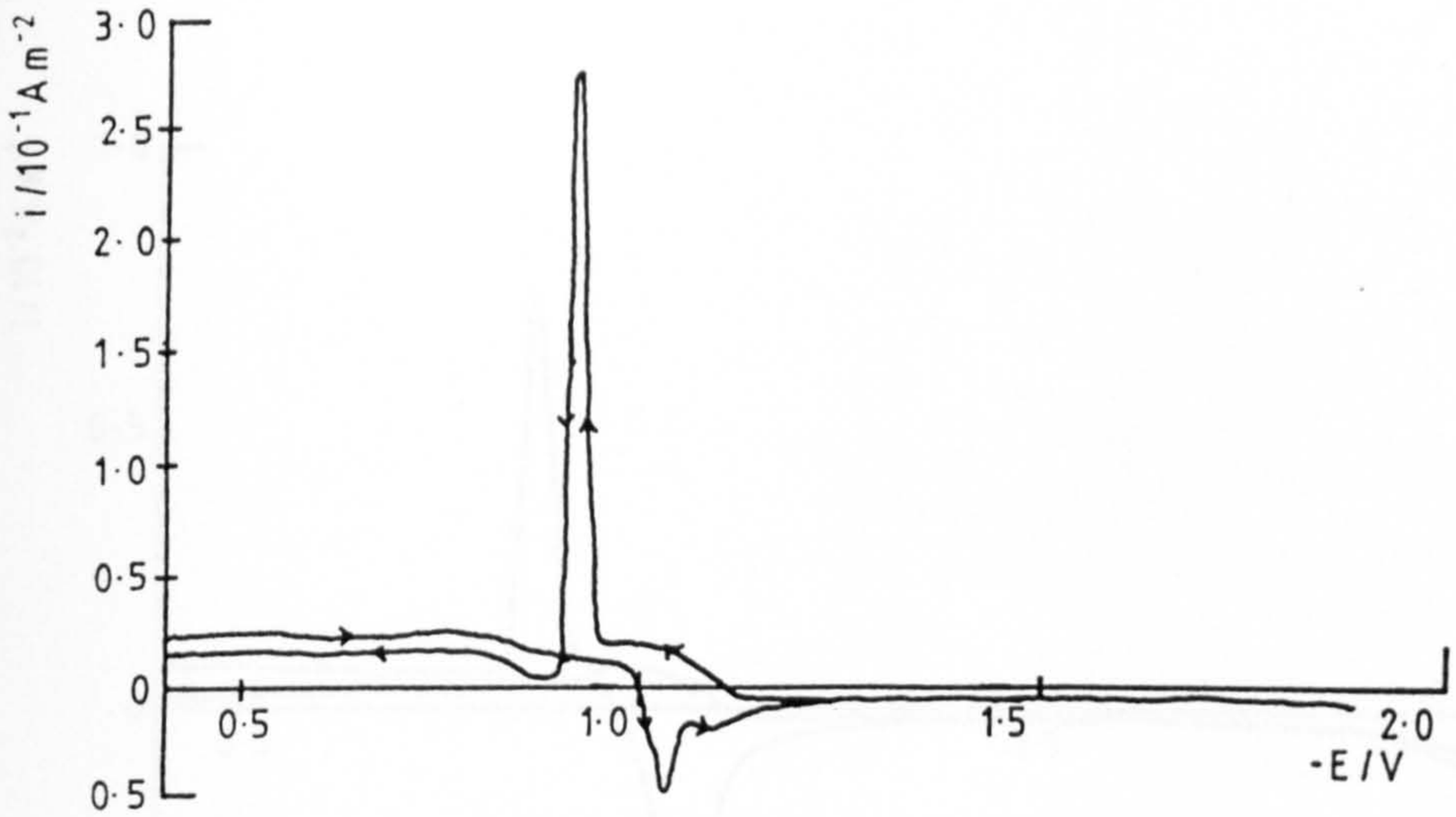

Fig. 7.2.8 LSV in 0.1 M NaCN, ν = 2.96 mV s^{-1}

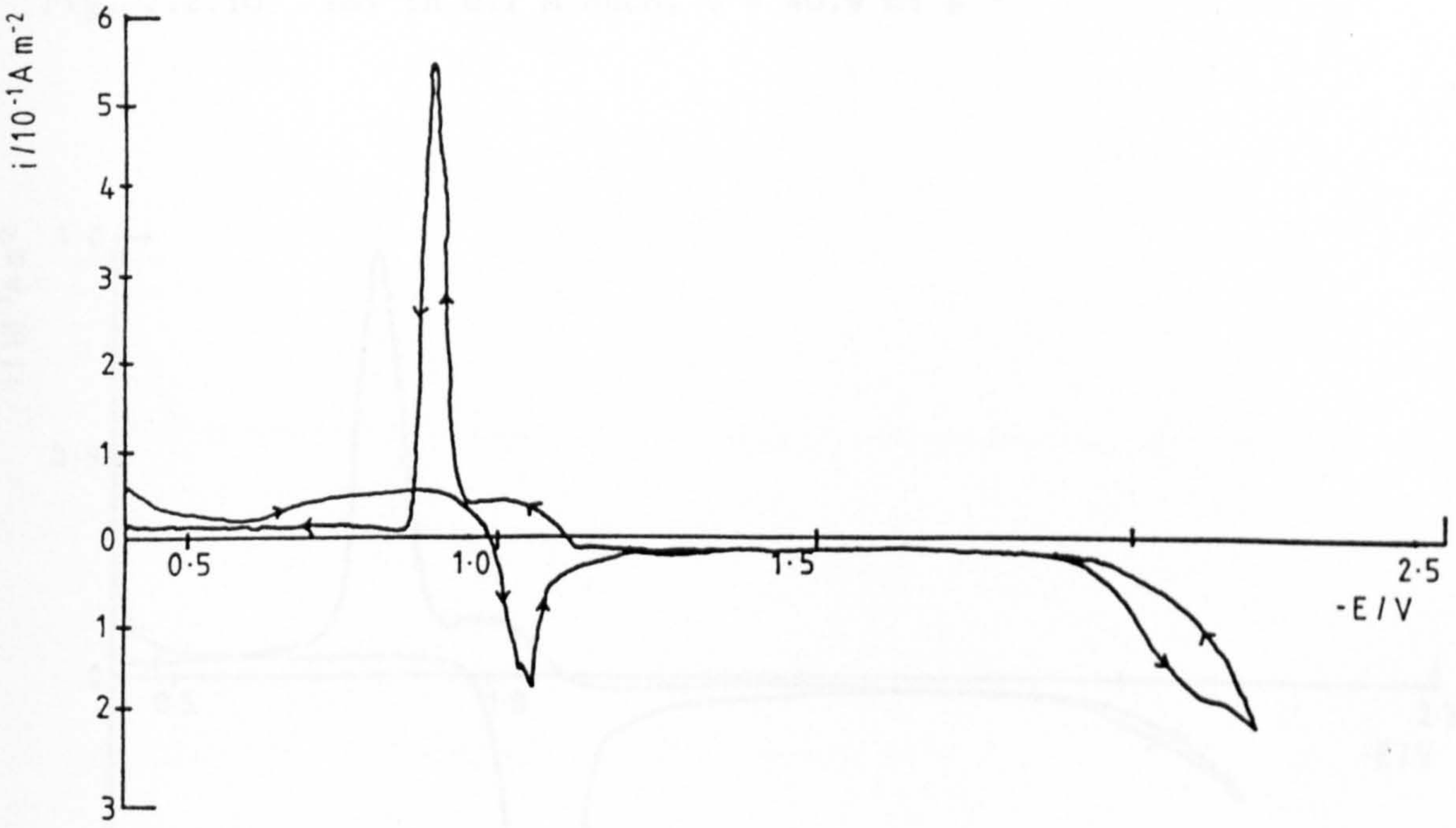

Fig. 7.2.9 LSV in 0.1 M NaCN, ν = 13.2 mV s^{-1}

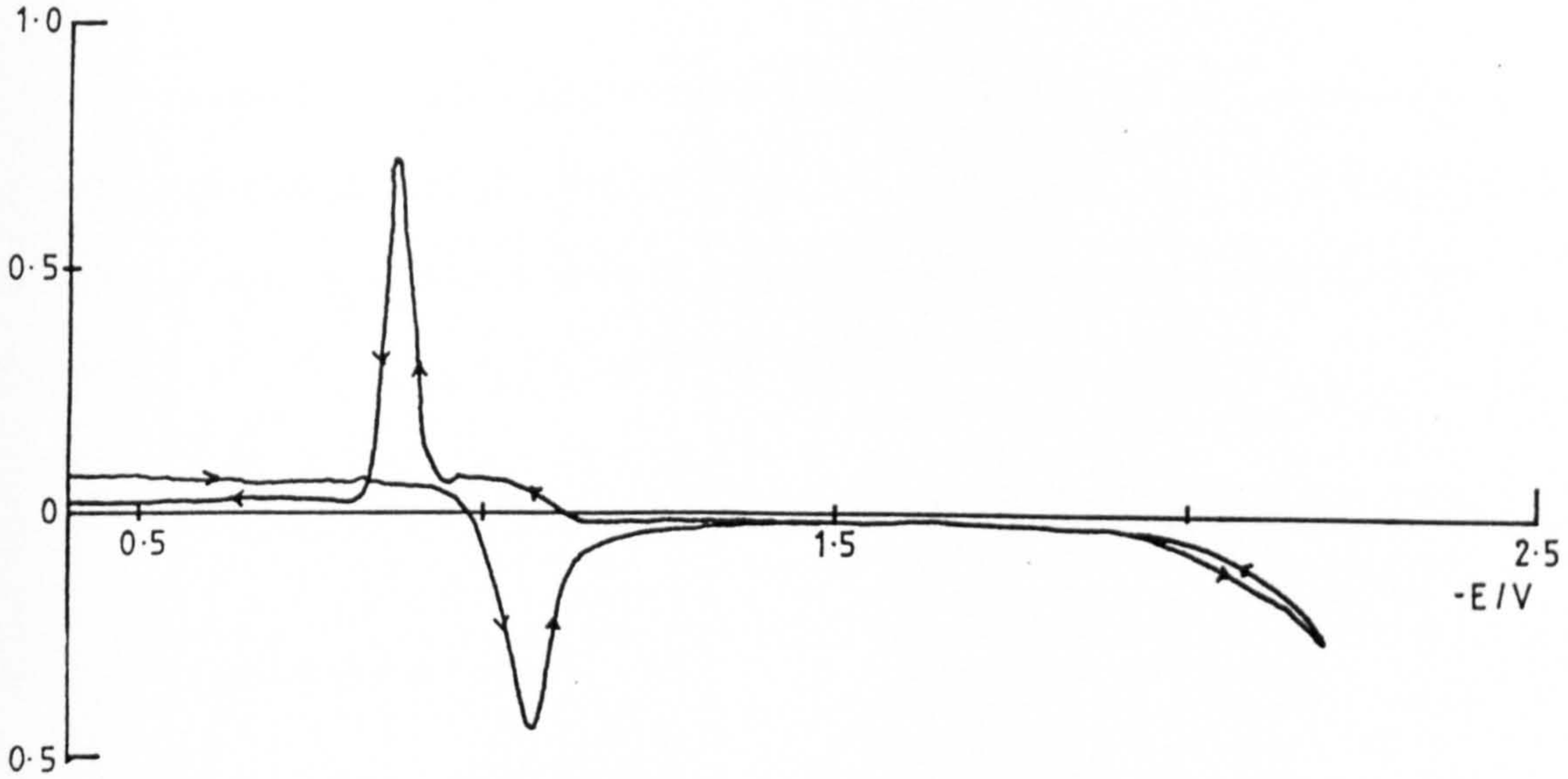

Fig. 7.2.10 LSV in 0.1 M NaCN, ν = 40.9 mV s^{-1}

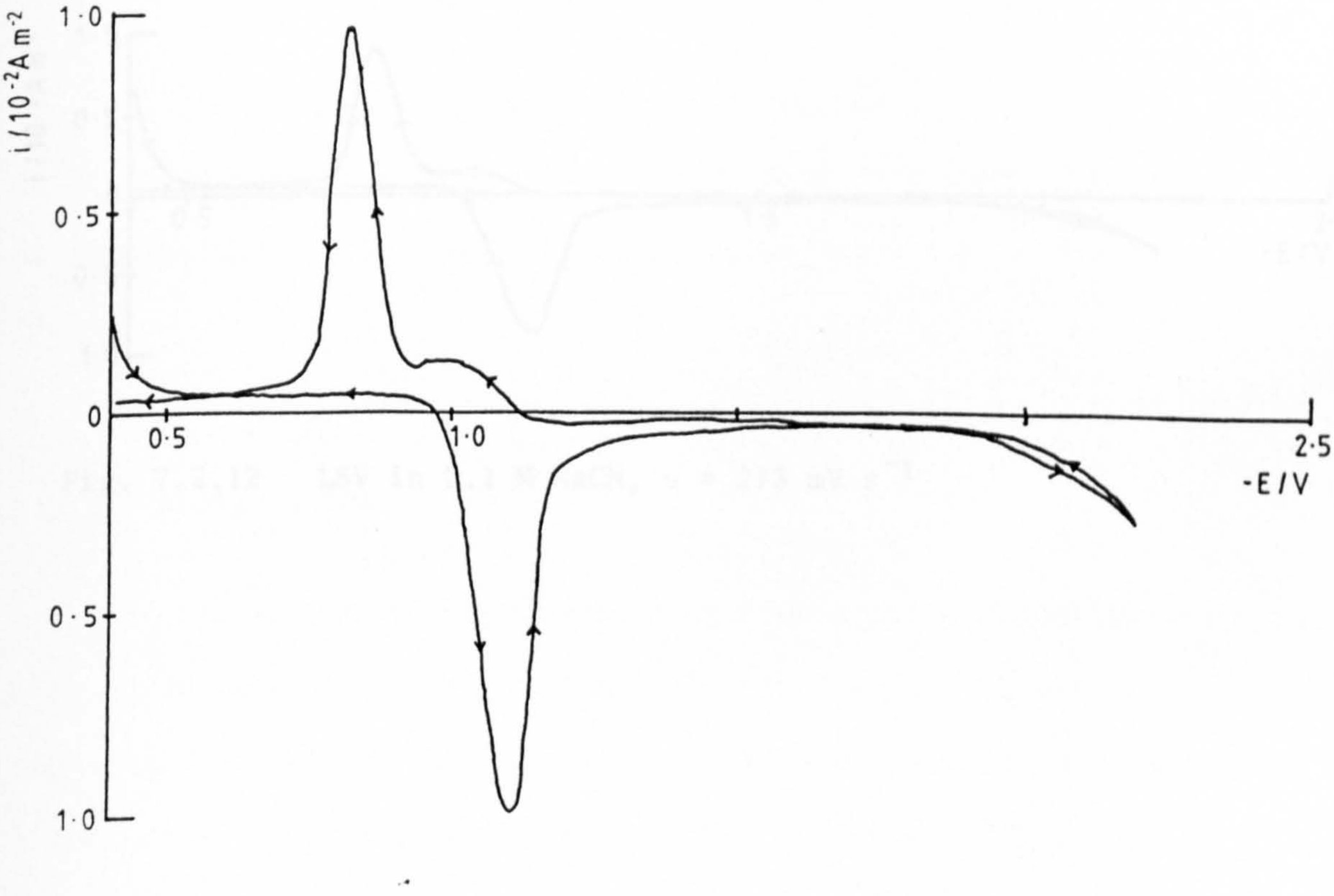

Fig. 7.2.11 LSV in 0.1 M NaCN, ν = 128 mV s^{-1}

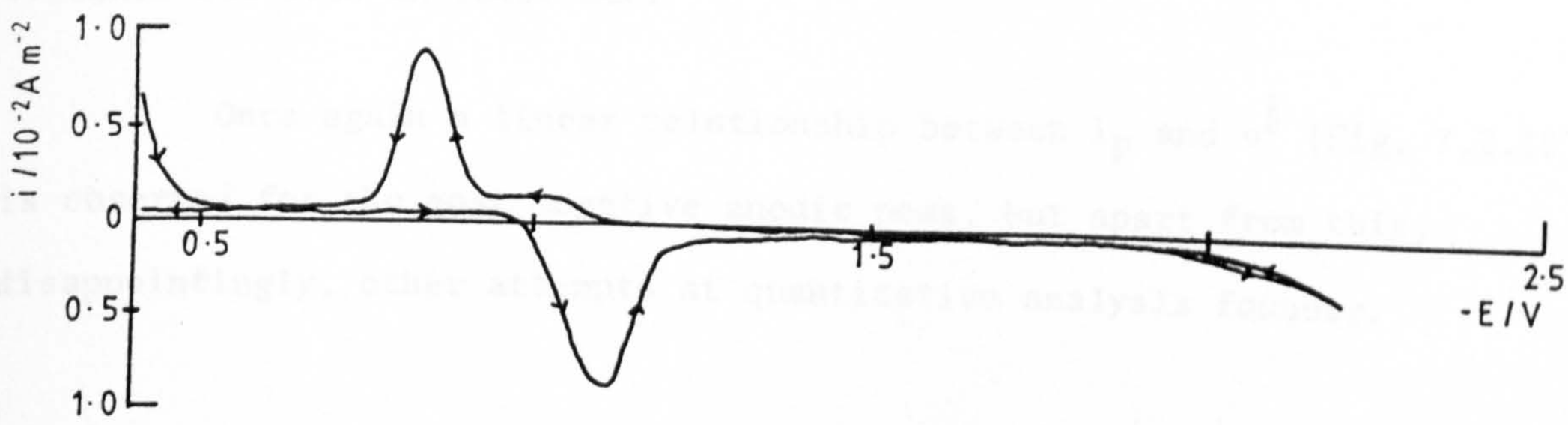

Fig. 7.2.12 LSV in 0.1 M NaCN, ν = 273 mV s^{-1}

ivation here, as might be expected on the basis of the arguments developed in §6.3.

Again, a full quantitative interpretation is not possible. Only one resonably linear relationship is seen- Fig. 7.2.13 shows the plot of i_p versus $\nu^{\frac{1}{2}}$ for the most negative anodic peak. There is no consistent trend in E_p with sweep rate in this case, however.

7.2.3 Electrolyte (c)

Figs. 7.2.14 to 7.2.18 show the voltammograms for the 0.01 M case. It is unfortunate that little additional information can be extracted from these experiments. The presence of multiple cathodic peaks might be interpreted in terms of the discharge of different cadmium cyanide complexes. However, there is really insufficient evidence for such an inference.

Once again a linear relationship between i_p and $\nu^{\frac{1}{2}}$ (Fig. 7.2.19) is observed for the most negative anodic peak, but apart from this, disappointingly, other attempts at quantitative analysis founder.

7.2.4 Discussion

It is indeed regrettable that no kinetic information could be deduced for the deposition process. It would appear, however, that the deposition of cadmium from one or more cyanide complexes occurs through a more or less developed hydroxide film. A feature of the data of Fig. 7.2.1 which may at first sight appear puzzling, is the complete

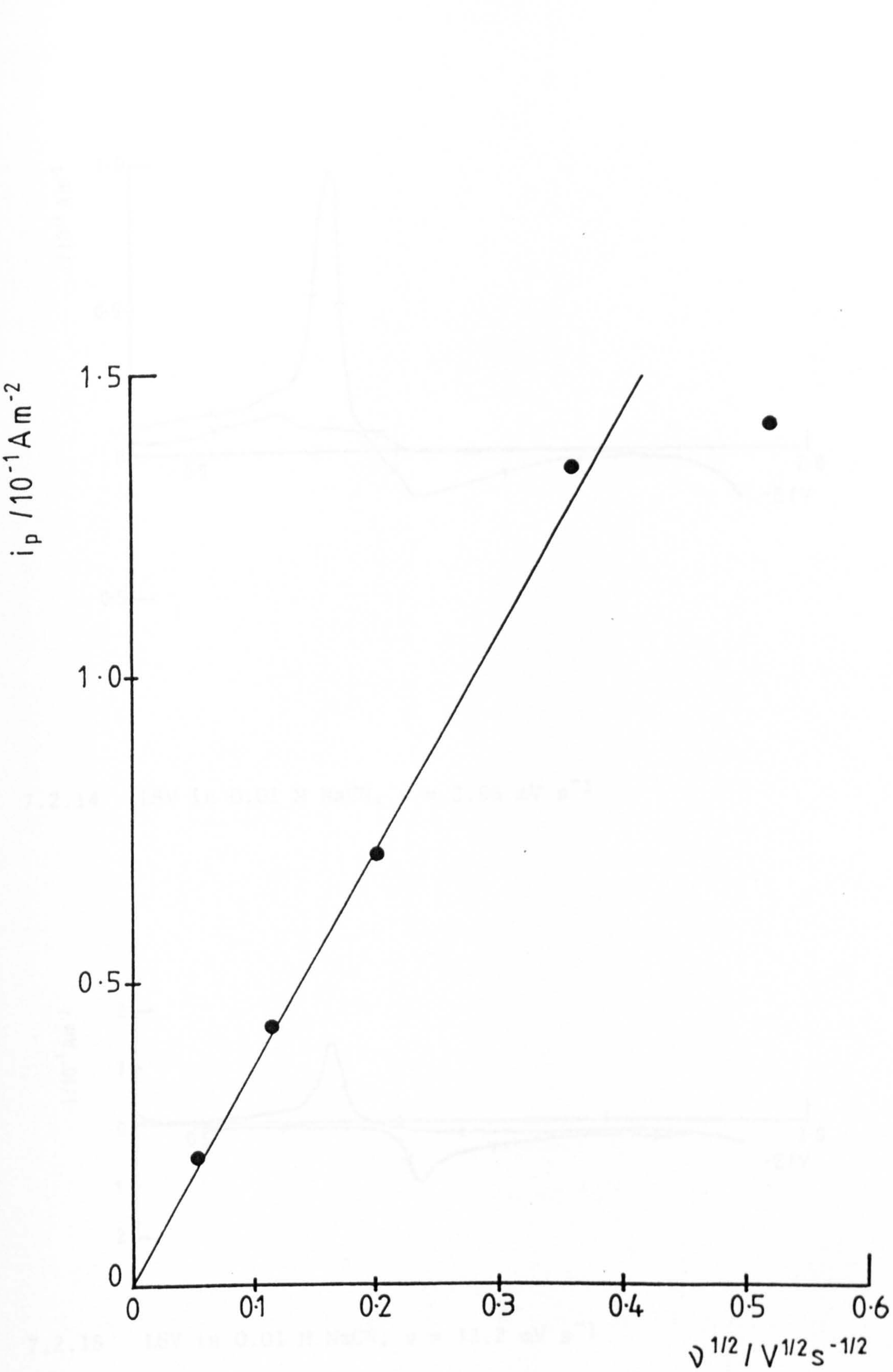

Fig. 7.2.13 i_p versus $\nu^{\frac{1}{2}}$ plot (0.1 M NaCN)

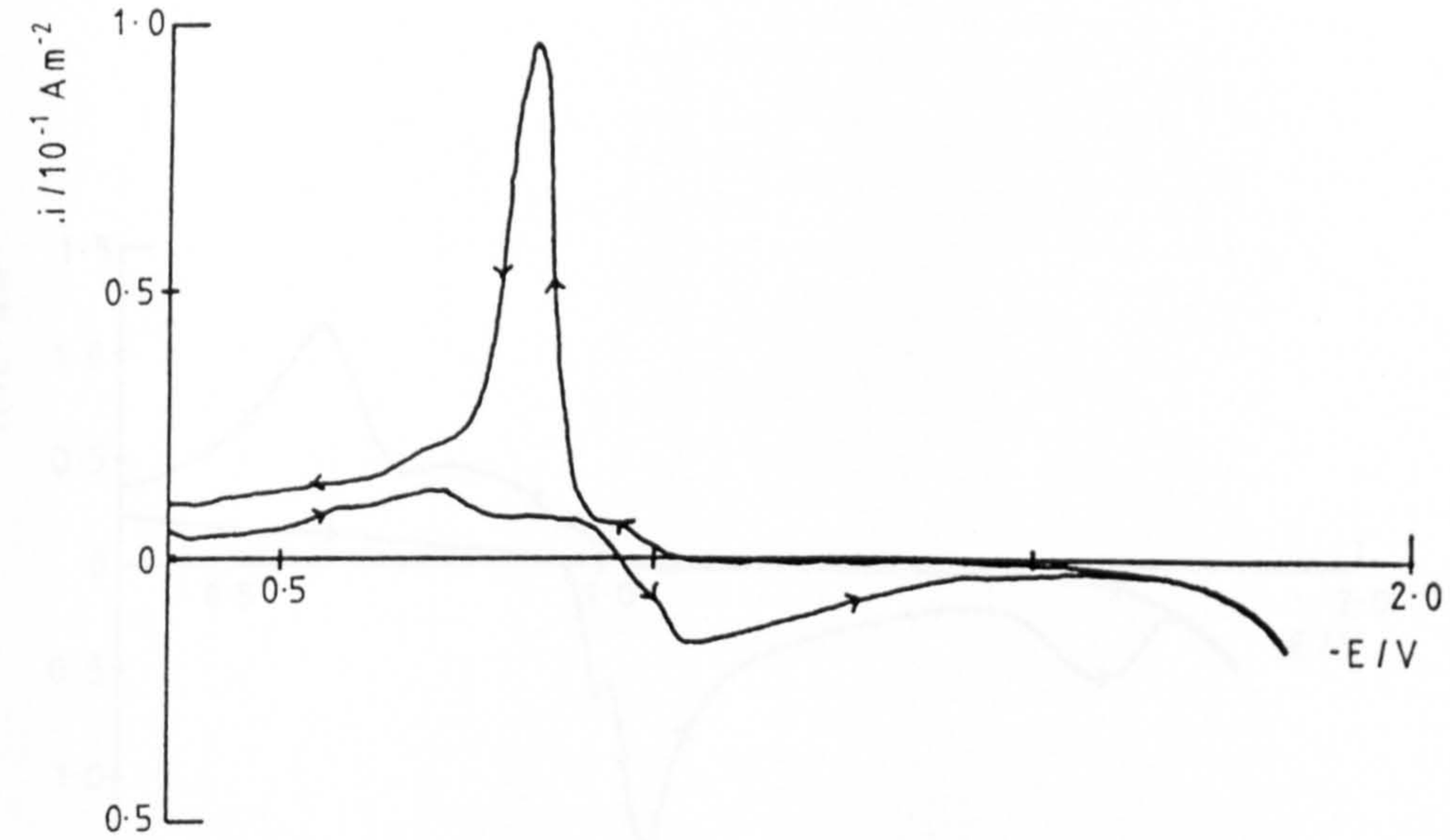

7.2.14 LSV in 0.01 M NaCN, ν = 2.96 mV s^{-1}

7.2.15 LSV in 0.01 M NaCN, ν = 13.2 mV s^{-1}

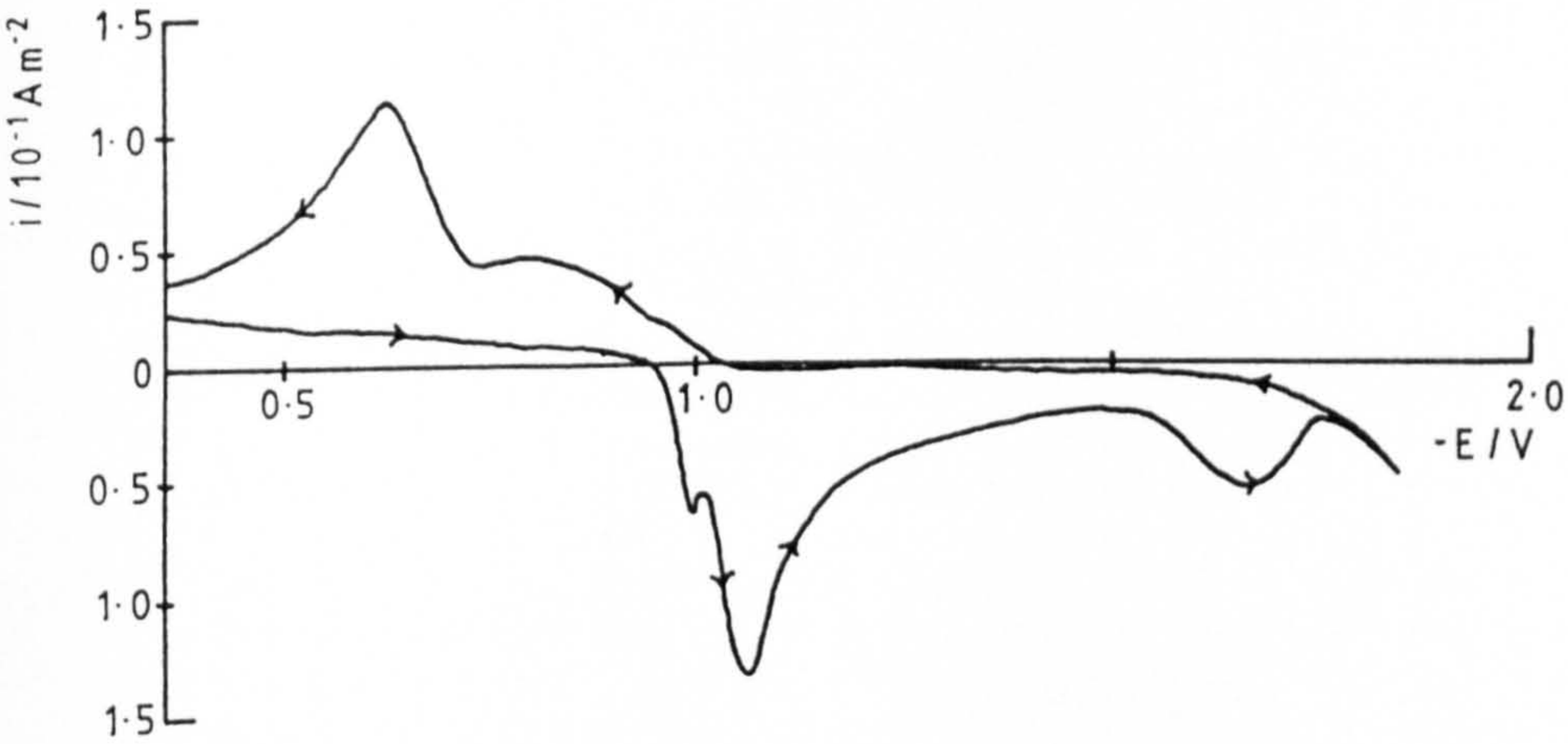

Fig. 7.2.16 LSV in 0.01 M NaCN, ν = 40.9 mV s^{-1}

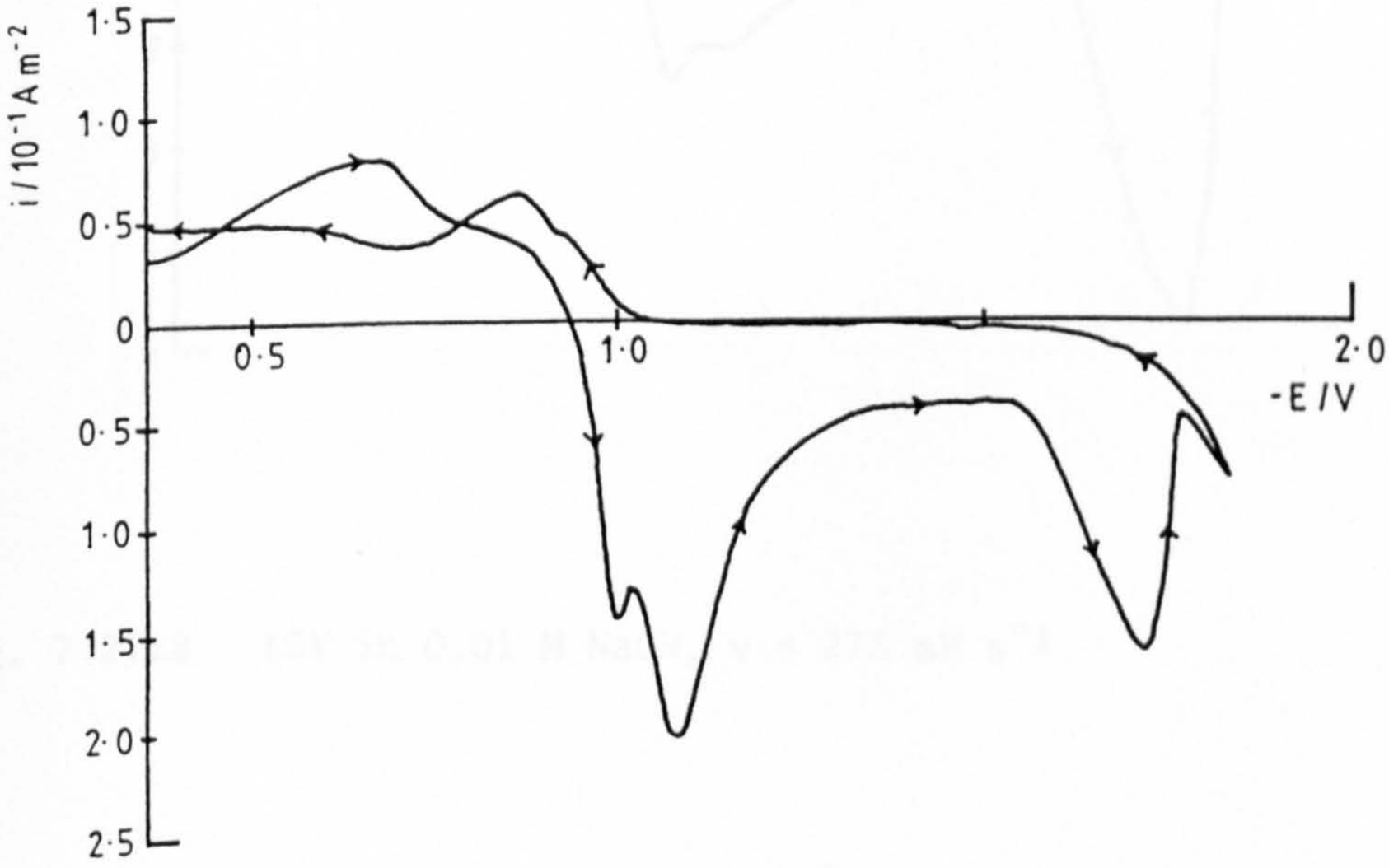

Fig. 7.2.17 LSV in 0.01 M NaCN, ν = 128 mV s^{-1}

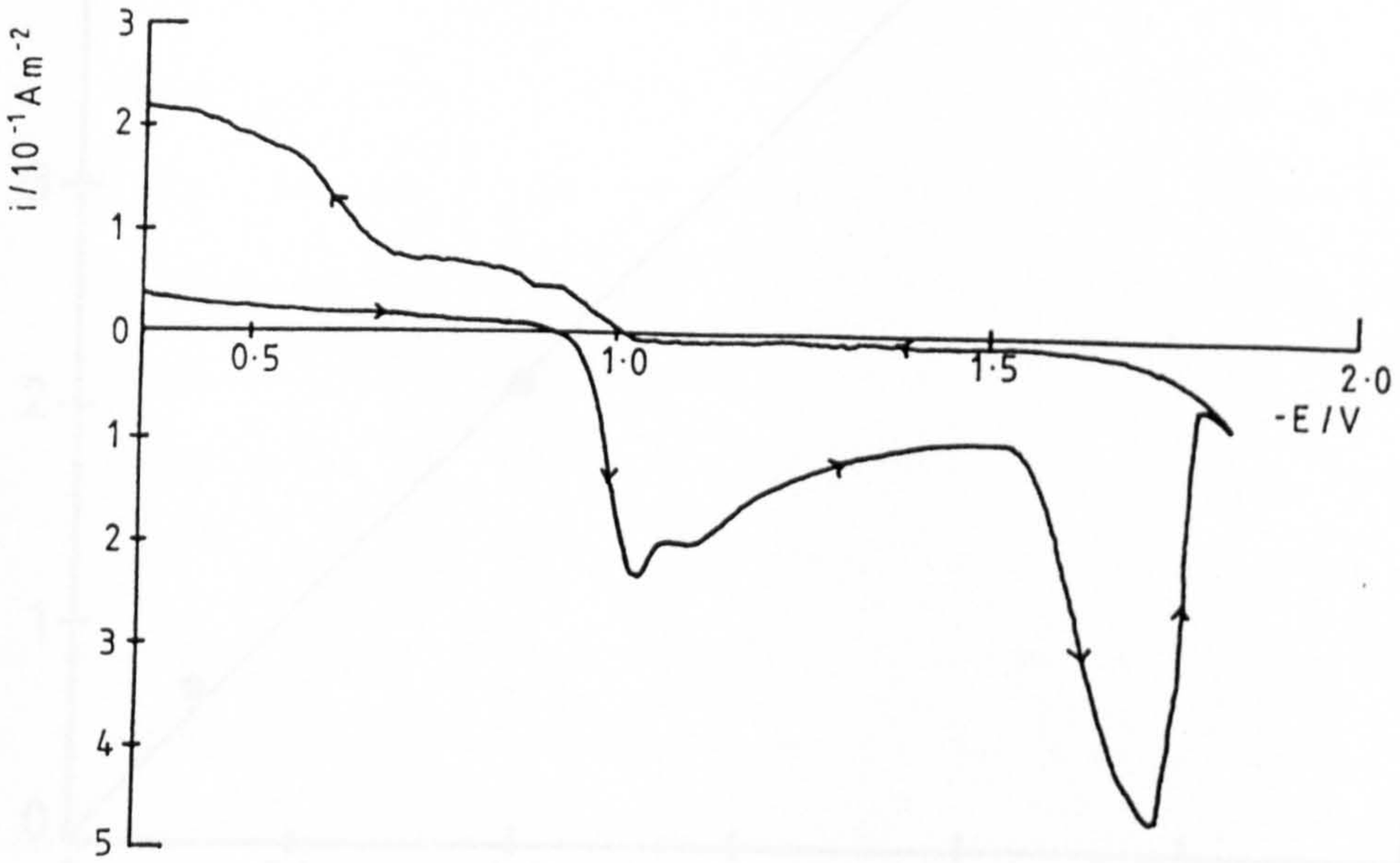

Fig. 7.2.18 LSV in 0.01 M NaCN, ν = 273 mV s^{-1}

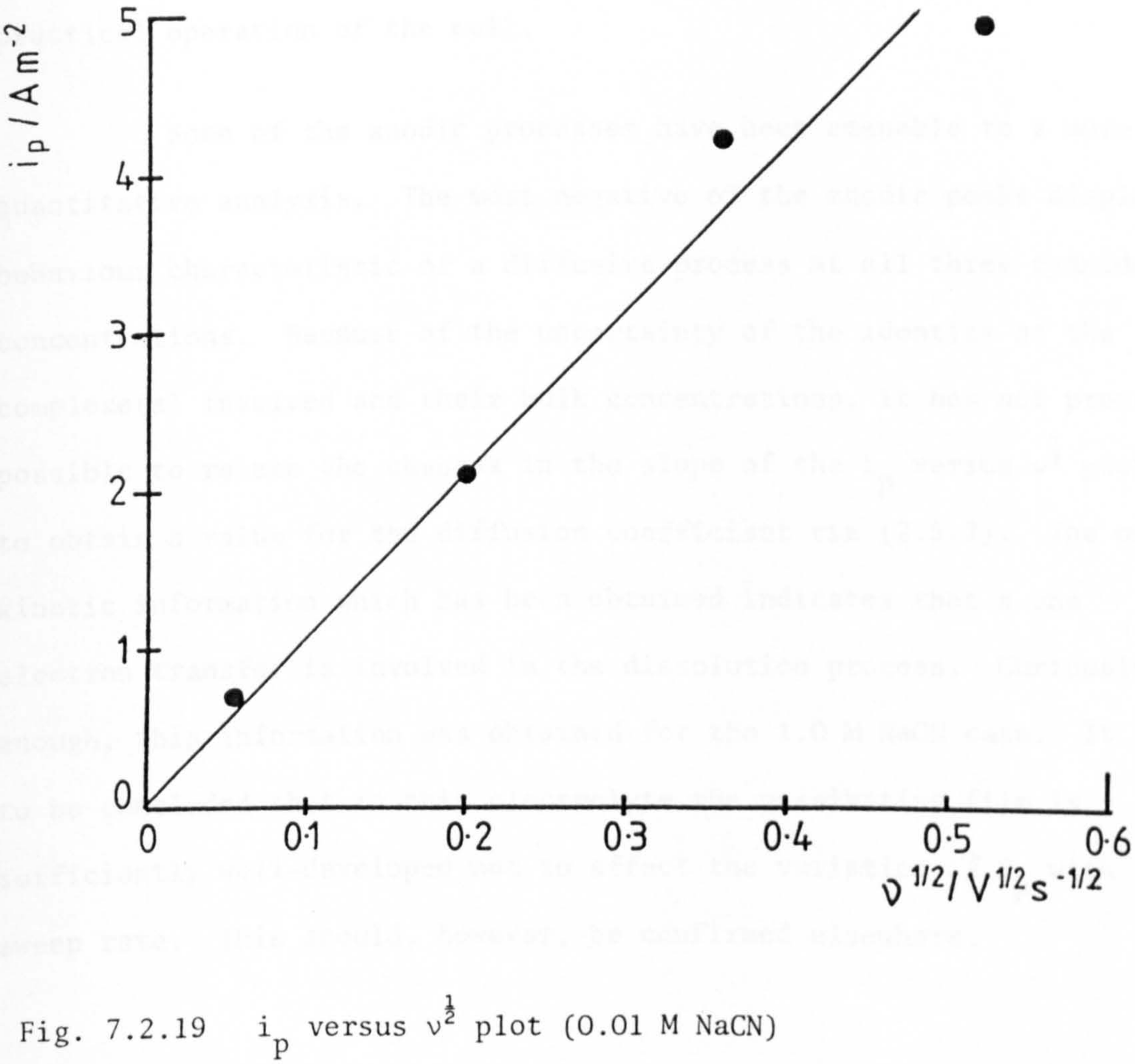

Fig. 7.2.19 i_p versus $\nu^{\frac{1}{2}}$ plot (0.01 M NaCN)

lack of cathodic processes (h.e.r. excepted) in a solution for which satisfactory operation of the Chemelec Cell® occurs. When considering this point, however, it should be borne in mind that the linear sweep experiment spans a very large region of electrode potential. In addition, the sweeps are made from ∿ -0.4 V in a cathodic direction. Especially at low sweep rates, therefore, there will be opportunity for the complete development of a passivating film prior to reaching the region of electrode potential in which electrodeposition occurs. This is a situation which, it is hoped, would never be encountered in practical operation of the cell.

Some of the anodic processes have been amenable to a more quantitative analysis. The most negative of the anodic peaks displays behaviour characteristic of a diffusive process at all three cyanide concentrations. Because of the uncertainty of the identity of the complexe(s) involved and their bulk concentrations, it has not proved possible to relate the changes in the slope of the i_p versus $\nu^{\frac{1}{2}}$ plots to obtain a value for the diffusion coefficient via (2.5.7). The only kinetic information which has been obtained indicates that a one electron transfer is involved in the dissolution process. Curiously enough, this information was obtained for the 1.0 M NaCN case. It is to be concluded that in this electrolyte the passivating film is sufficiently well-developed not to affect the variation of E_p with sweep rate. This should, however, be confirmed elsewhere.

7.3 Experiments at the rotating disc electrode

The rotating disc electrode has been used to investigate the electrode kinetics of the dissolution and deposition of cadmium in the following solutions:

	(a)	(b)	(c)
$Cd(CN)_2$	3.0mM	3.0mM	3.0mM
NaCN	0.03M	0.1M	1.0M
NaOH	0.4M	0.4M	0.4M

7.3.1 The deposition of cadmium from electrolyte (a)

Figs. 7.3.1a and 7.3.1b show the dependence of the current density on the rotation speed for a series of electrode potentials in the deposition region. A linear relationship is found to exist between i^{-1} and $\omega^{-\frac{1}{2}}$ indicating at least partial control of the reaction by diffusion in solution. The extrapolated intercepts at $\omega^{-\frac{1}{2}} = 0$ are close to zero on the i^{-1} axis, but the lines have not been drawn through the origin as it was felt that to do so would impair the determination of $\partial i^{-1}/\partial \omega^{-\frac{1}{2}}$ as a function of E, as plotted semi- - logarithmically in Fig. 7.3.2. A line of 29 mV/decade slope has been drawn through the data and this shows, within a fairly large experimental error, that the data is consistent with a two electron transfer. In view of the rather small and inaccurate values of the intercepts at $\omega^{-\frac{1}{2}} = 0$ the Tafel plot has not been constructed. From this evidence, it appears that the deposition of cadmium from this electrolyte occurs as an essentially reversible two electron process.

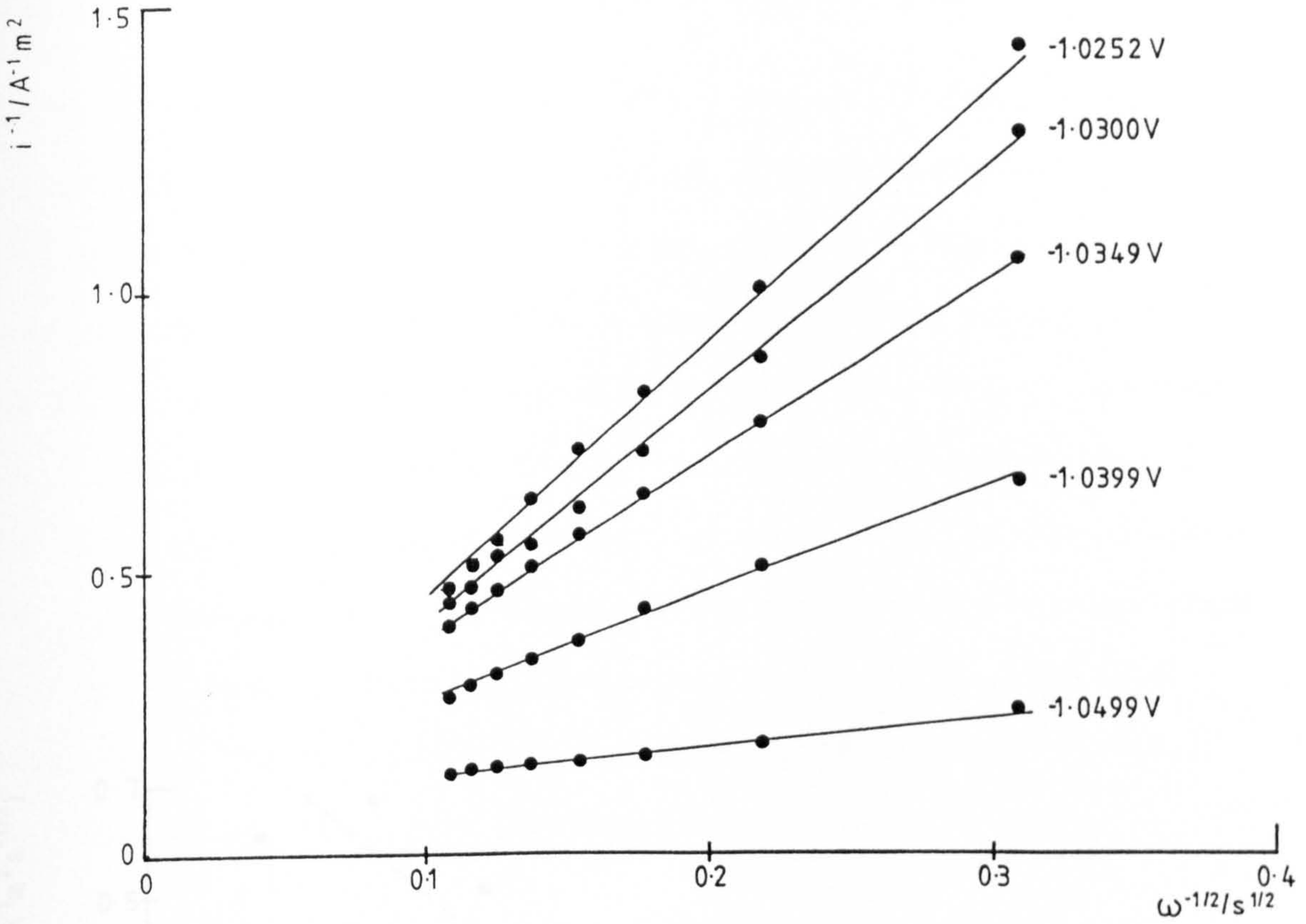

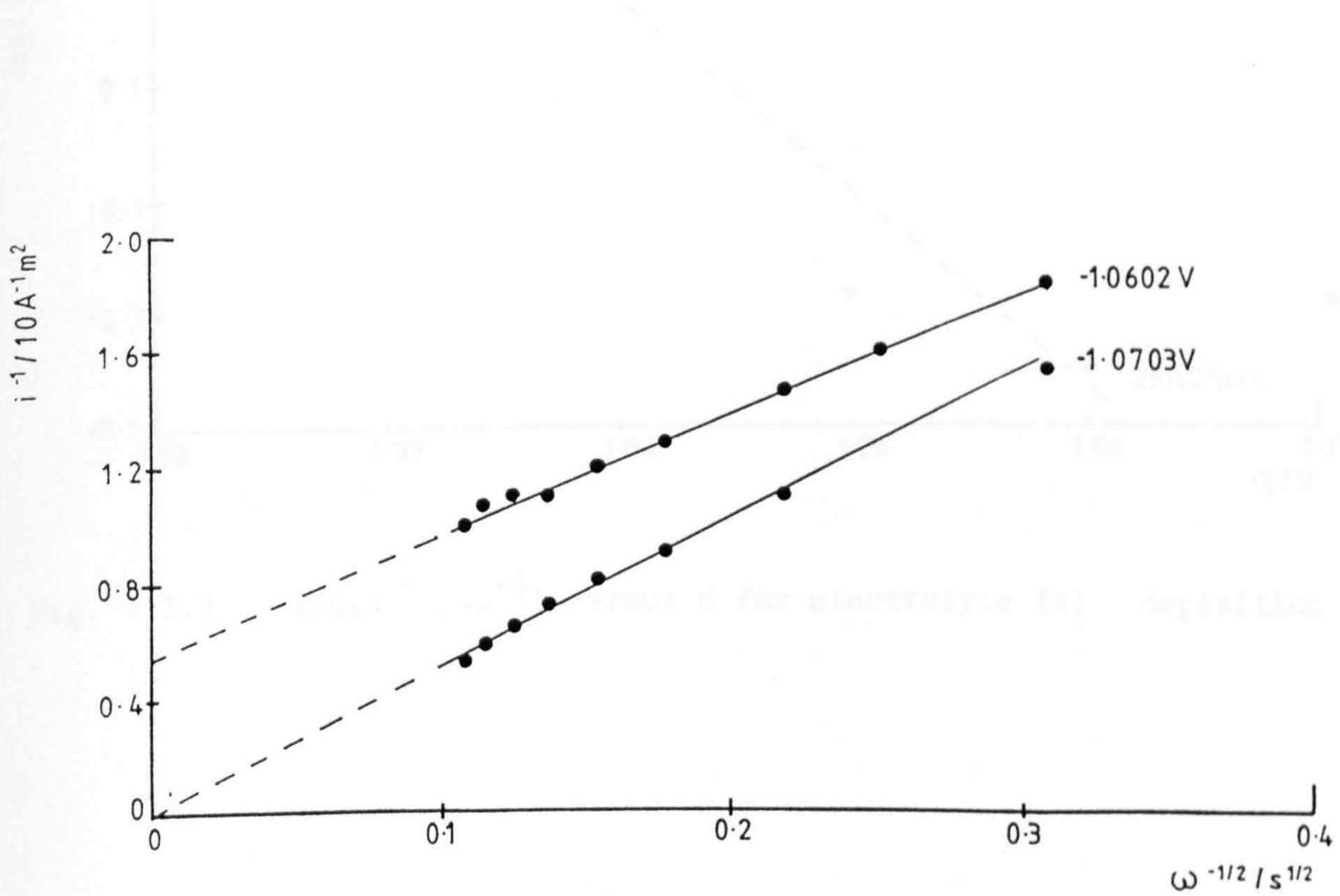

Fig. 7.3.1 i^{-1} versus $\omega^{-\frac{1}{2}}$ plots for electrolyte (a) at a series of electrode potentials - deposition

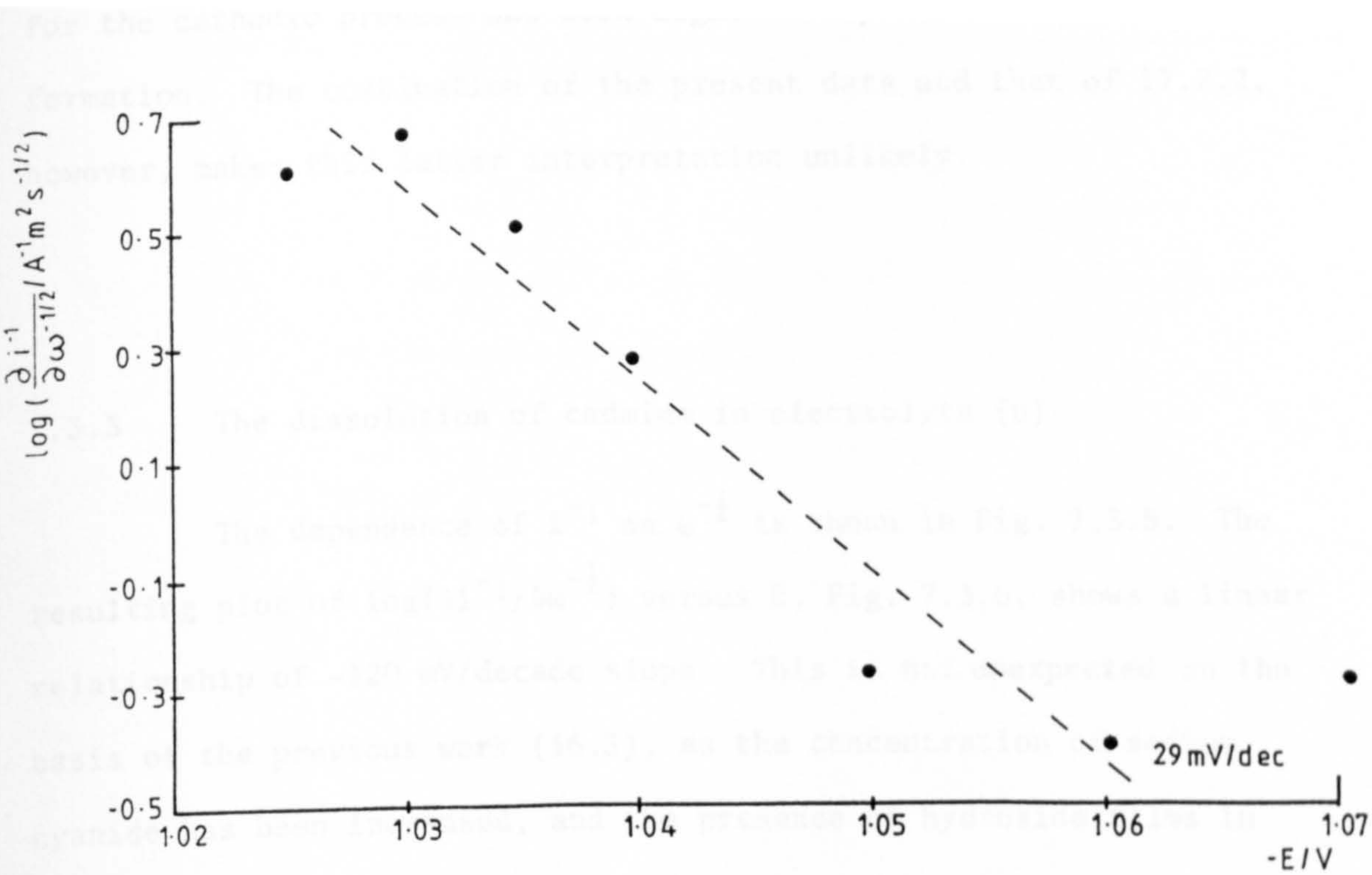

Fig. 7.3.2 $\log\{\partial i^{-1}/\partial\omega^{-\frac{1}{2}}\}$ versus E for electrolyte (a) - deposition

7.3.2 The dissolution of cadmium in electrolyte (a)

The corresponding plots of i^{-1} versus $\omega^{-\frac{1}{2}}$ for the dissolution process are shown in Fig. 7.3.3. Again, a linear relationship is obtained and the extrapolation to $\omega^{-\frac{1}{2}} = 0$ yields unreliable intercepts. The semi-logarithmic plot of $\partial i^{-1}/\partial\omega^{-\frac{1}{2}}$ against electrode potential is shown in Fig. 7.3.4 and a line of -59 mV/decade slope is entirely consistent with this data. This would tend to indicate a one electron transfer in the dissolution step, in complete agreement with the conclusions of §7.2.2. However, it is not inconceivable that the 29 mV/decade slope for the cathodic process has been augmented by the onset of film formation. The combination of the present data and that of §7.2.2, however, makes this latter interpretation unlikely.

7.3.3 The dissolution of cadmium in electrolyte (b)

The dependence of i^{-1} on $\omega^{-\frac{1}{2}}$ is shown in Fig. 7.3.5. The resulting plot of $\log\{\partial i^{-1}/\partial\omega^{-\frac{1}{2}}\}$ versus E, Fig. 7.3.6, shows a linear relationship of -120 mV/decade slope. This is not unexpected on the basis of the previous work (§6.3), as the concentration of sodium cyanide has been increased, and the presence of hydroxide films in such solutions is strongly suspected.

7.3.4 Deposition of cadmium from electrolyte (c)

In the case of 1.0 M NaCN, the dependence of i^{-1} upon $\omega^{-\frac{1}{2}}$ is maintained for the deposition reaction. However, as Fig. 7.3.7 clearly shows, the theory for the rotating disc is not really applicable

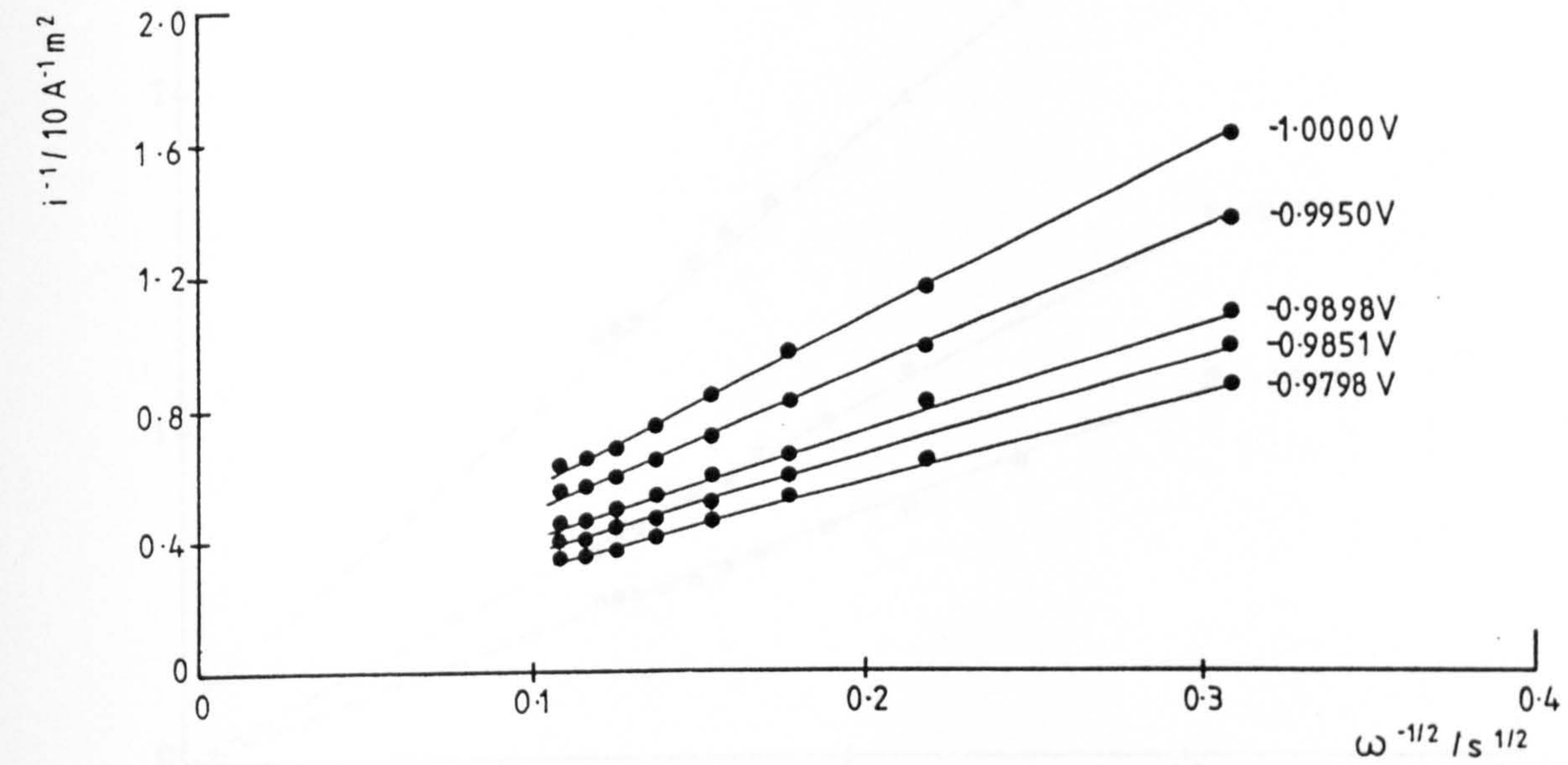

Fig. 7.3.3 i^{-1} versus $\omega^{-\frac{1}{2}}$ plots for electrolyte (a) at a series of electrode potentials - dissolution

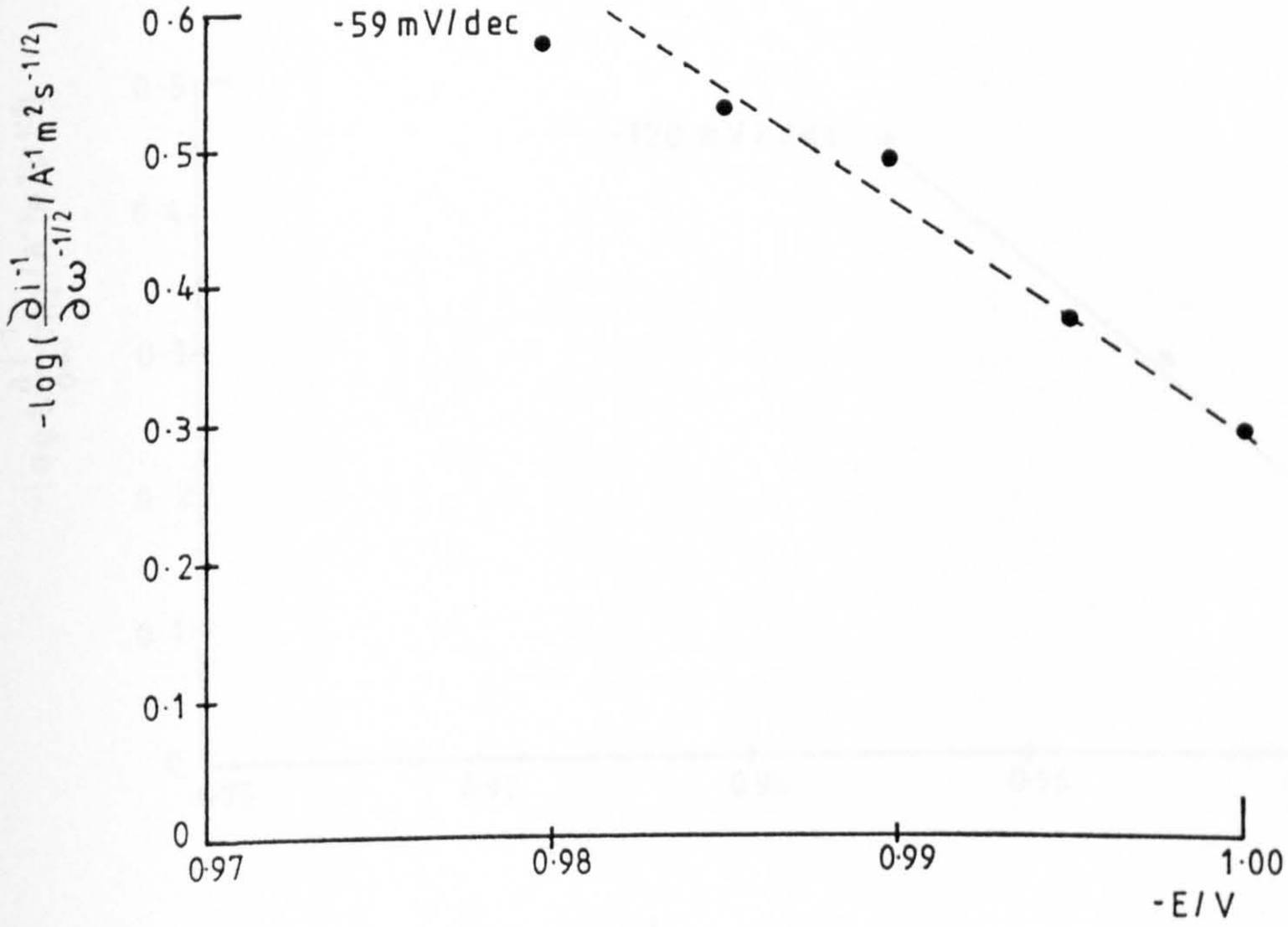

Fig. 7.3.4 $\log\{\partial i^{-1}/\partial \omega^{-\frac{1}{2}}\}$ versus E for electrolyte (a) - dissolution

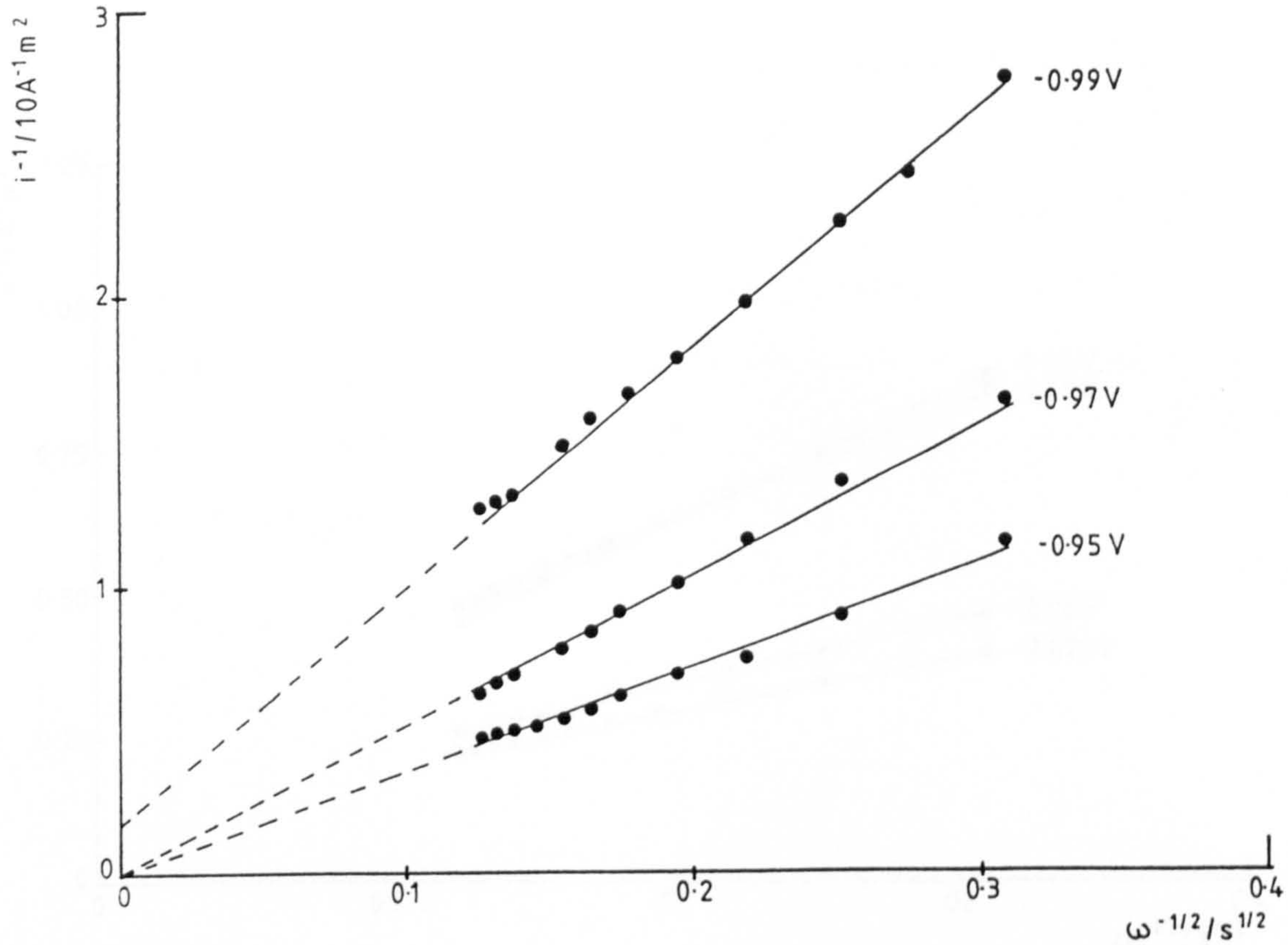

Fig. 7.3.5 i^{-1} versus $\omega^{-\frac{1}{2}}$ plots for electrolyte (b) at a series of electrode potentials - dissolution

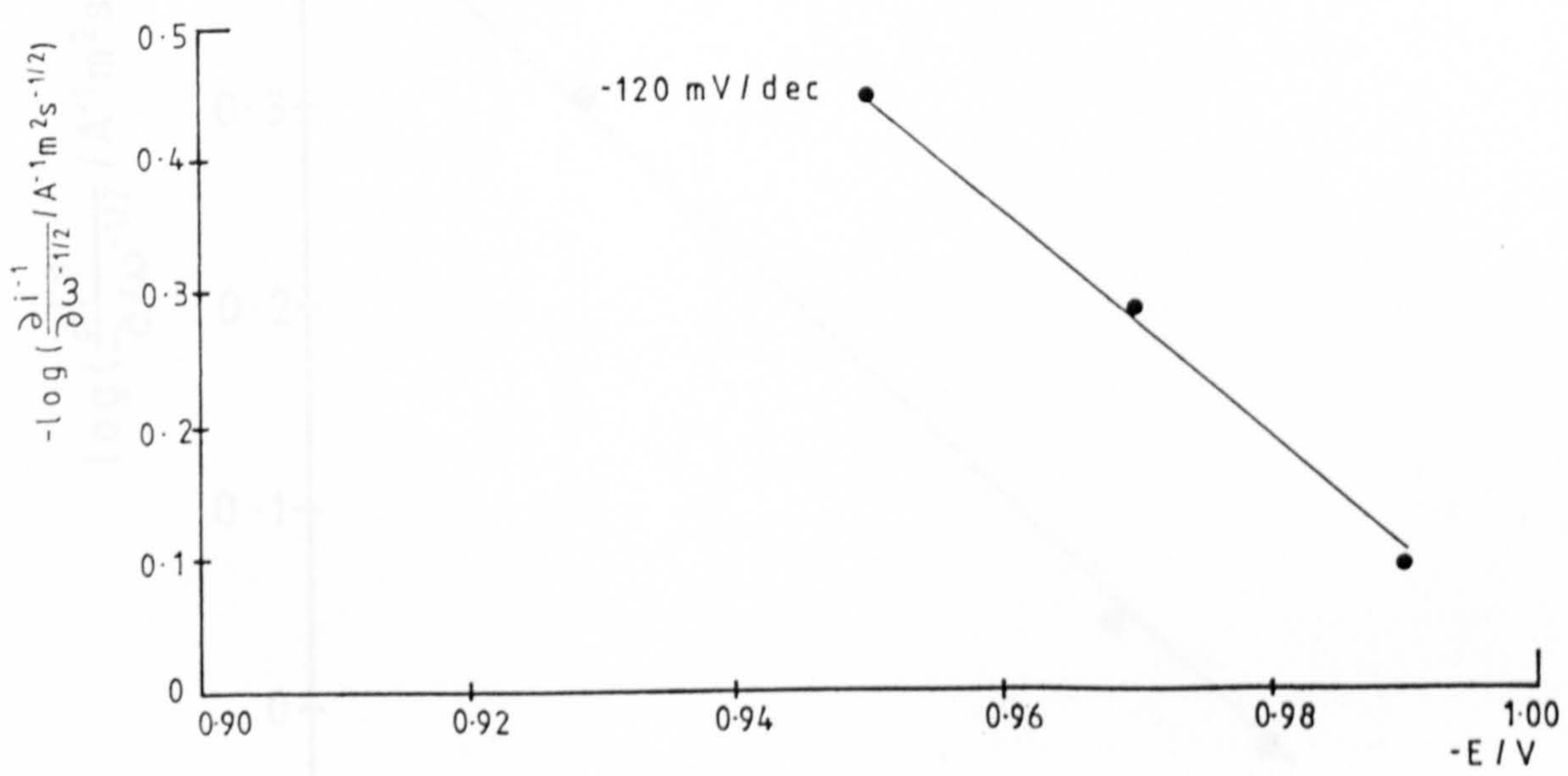

Fig. 7.3.6 $\log\{\partial i^{-1}/\partial \omega^{-\frac{1}{2}}\}$ versus E for electrolyte (b) - dissolution

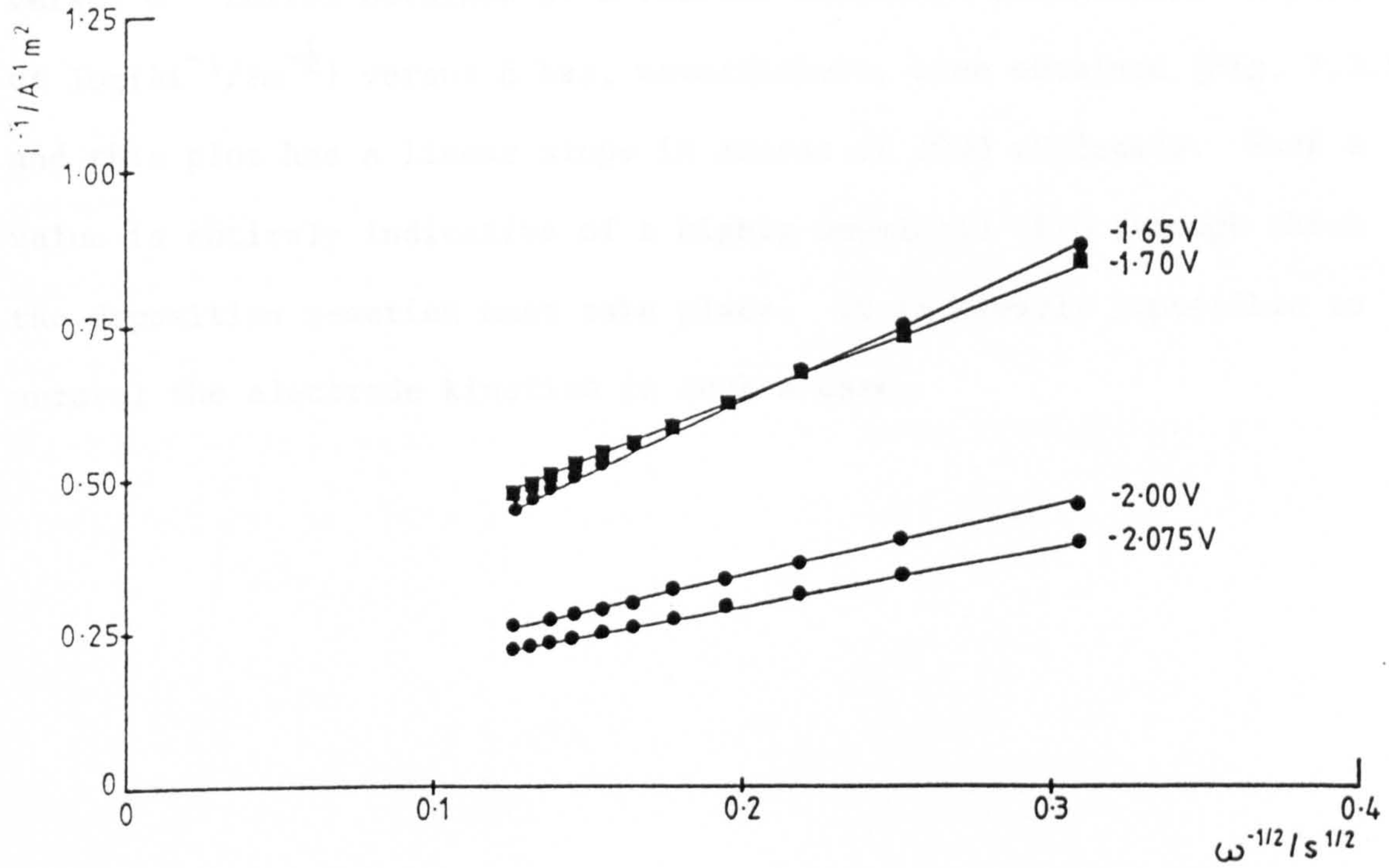

Fig. 7.3.7 i^{-1} versus $\omega^{-\frac{1}{2}}$ plots for electrolyte (c) at a series of electrode potentials - deposition

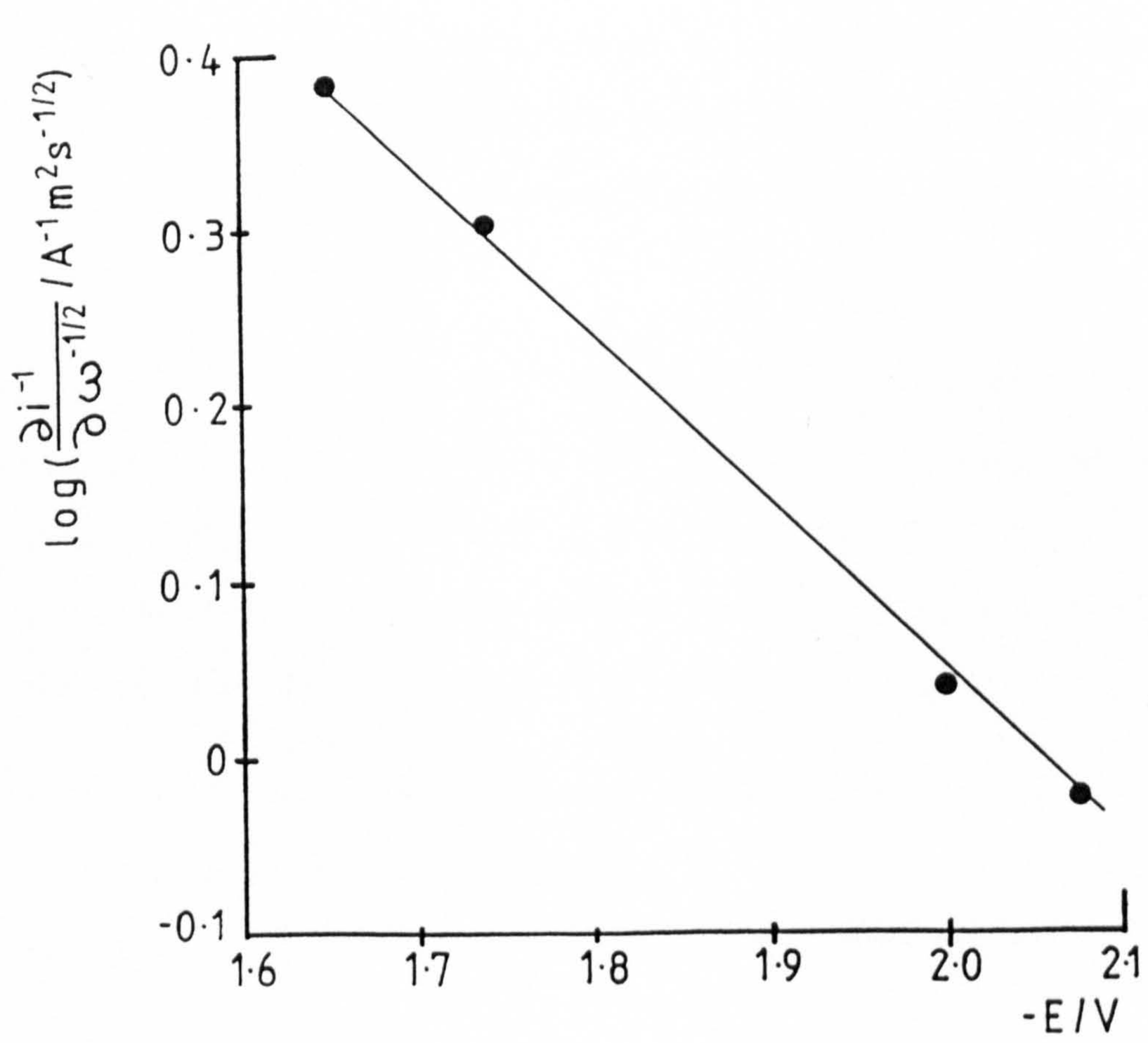

Fig. 7.3.8 $\log\{\partial i^{-1}/\partial \omega^{-\frac{1}{2}}\}$ versus E for electrolyte (c) - deposition

inasmuch as it is incapable of allowing the intersection of two i^{-1} versus $\omega^{-\frac{1}{2}}$ curves obtained at different electrode potentials. A plot of $\log\{\partial i^{-1}/\partial\omega^{-\frac{1}{2}}\}$ versus E has, nevertheless, been obtained (Fig. 7.3.8) and this plot has a linear slope in excess of 1000 mV/decade. Such a value is entirely indicative of a highly developed film, through which the deposition reaction must take place. It is clearly impossible to unravel the electrode kinetics in such a case.

7.4 Faradaic Impedance Studies

The impedance spectrum for cadmium in the electrolytes below was determined both at the equilibrium potential and at electrode potentials on either side of the equilibrium. As has frequently been observed during the course of this work, the attainment of a reproducible and stable equilibrium potential is one of the foremost problems in experiments such as these. Often the rest potential varies with time, presumably due to the thickening of a hydroxide film.

	(a)	(b)
$Cd(CN)_2$	1.0mM	10mM
NaCN	1.0M	1.0M
NaCdOH	0.4M	0.4M

Although an impedance spectrum, Figs. 7.4.1 and 7.4.2, has been obtained for both electrolytes at the equilibrium potential (cf. §5.3.2), and a moderately good fit achieved using the Randles equivalent circuit, the values of the parameters thus obtained defy a quantitative interpretation.

It has also been possible to fit the Randles model to impedance spectra obtained at potentials close to the equilibrium, as shown in Figs. 7.4.3 to 7.4.6. The values of the quantity θA are at least an order of magnitude greater than those observed in §5.3. The values of C_L/A, however, remain high.

At higher overpotentials, both anodic and cathodic, the Randles model becomes inappropriate as the high frequency semicircle elongates along the real axis; a typical example is shown in Figs. 7.4.7

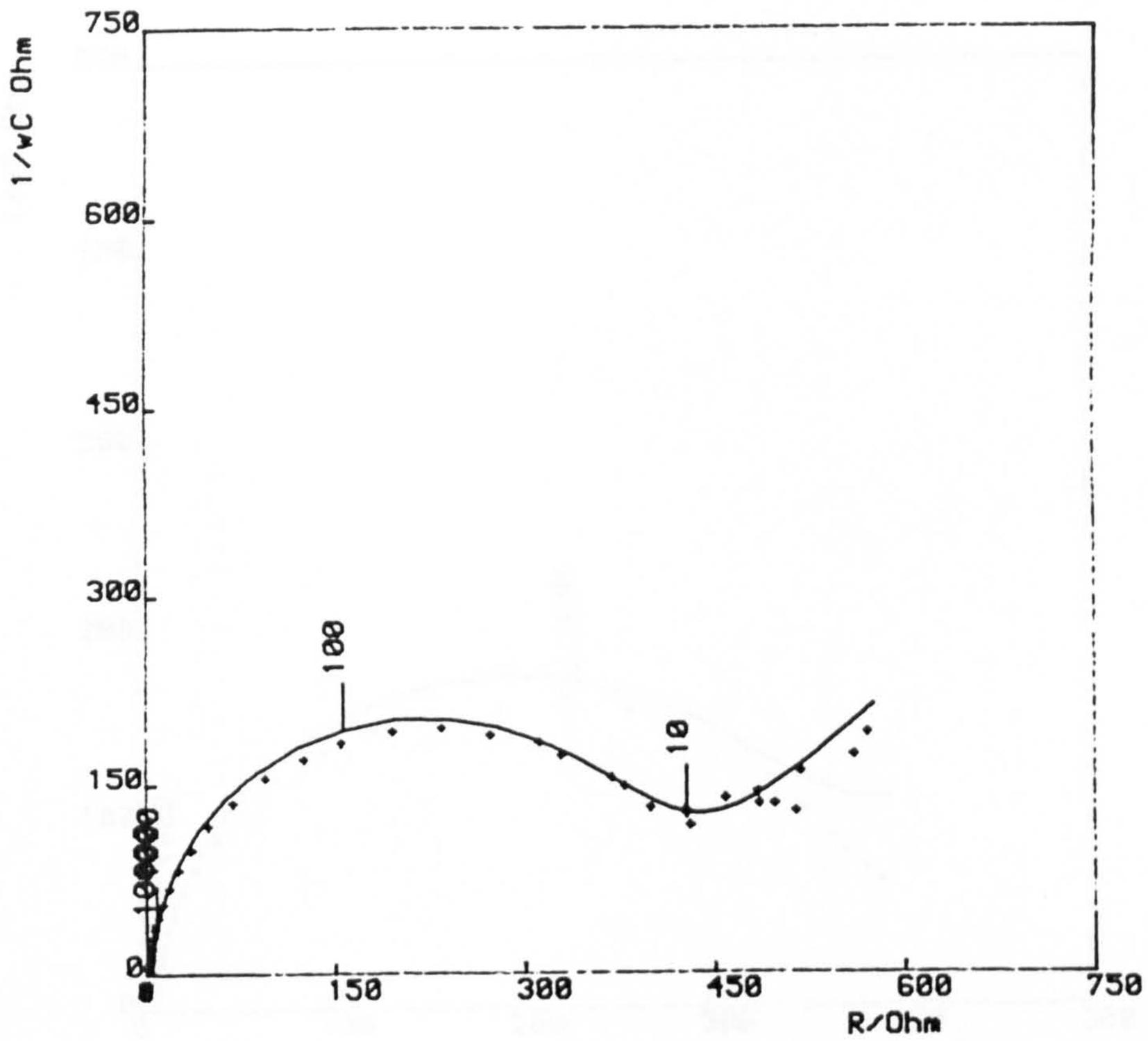

Fig. 7.4.1 Equilibrium impedance spectrum analysed according to the 'R-equation' - 1 mM $Cd(CN)_2$

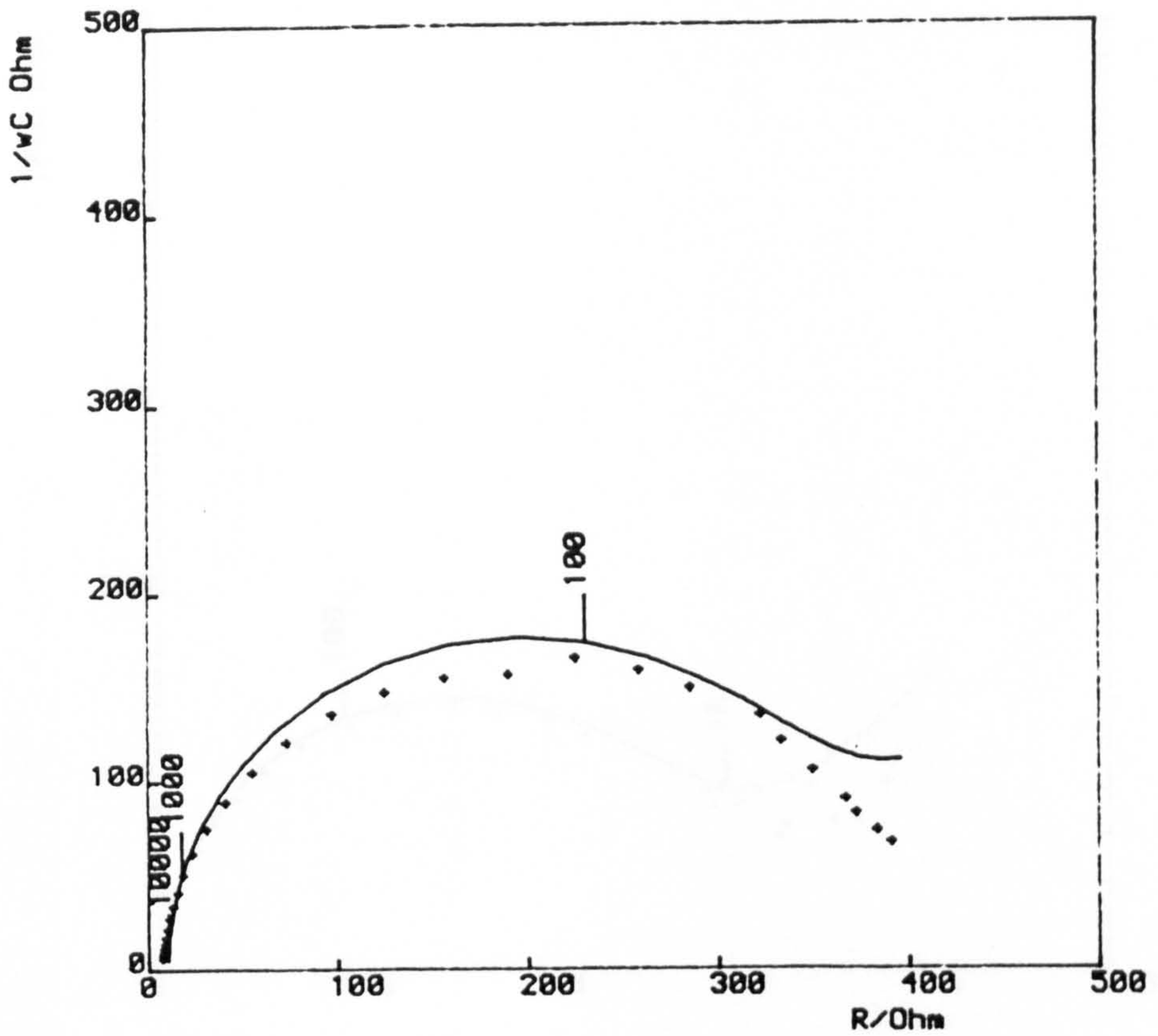

Fig. 7.4.2 Equilibrium impedance spectrum analysed according to the 'R-equation'.- 10 mM $Cd(CN)_2$

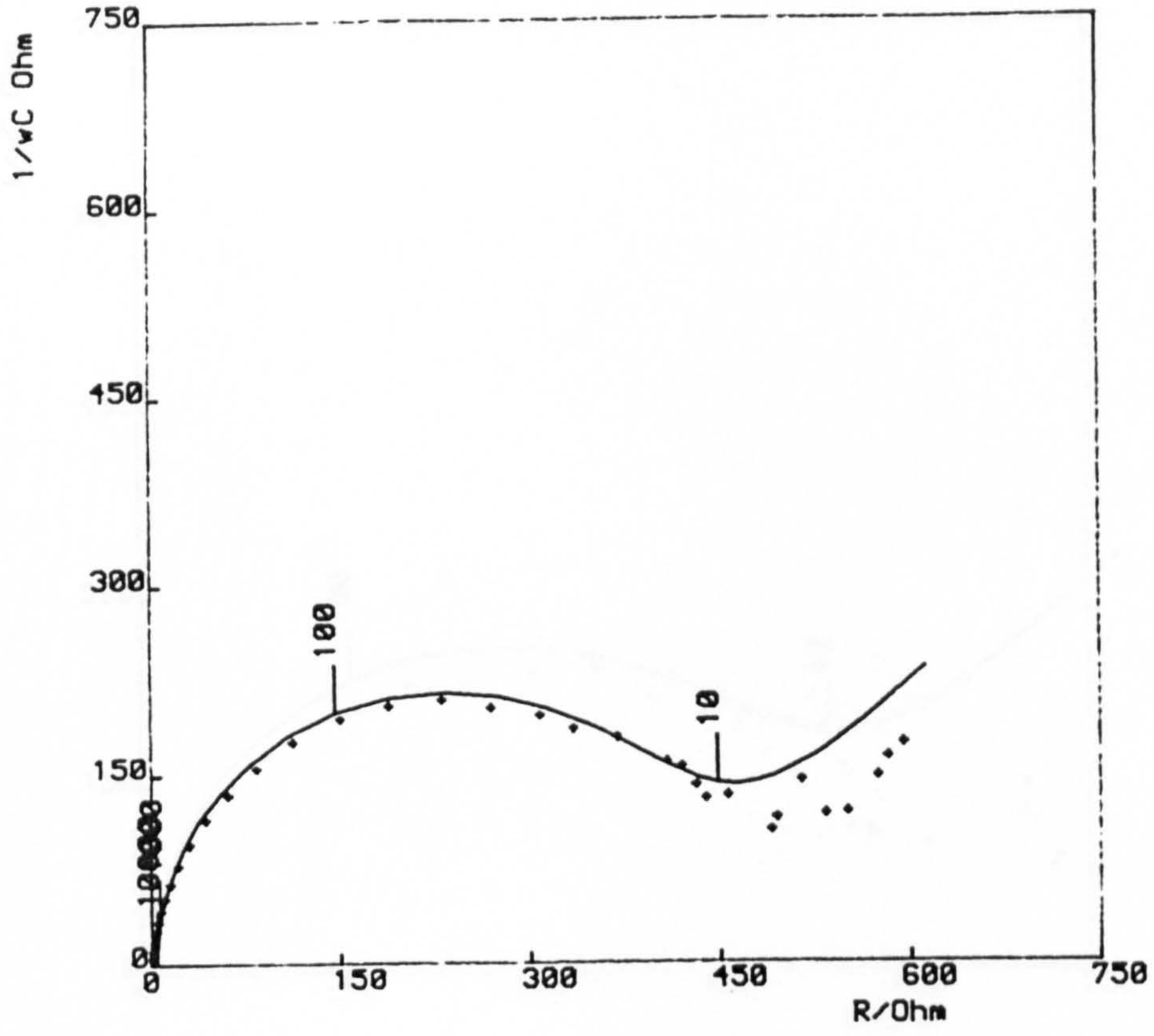

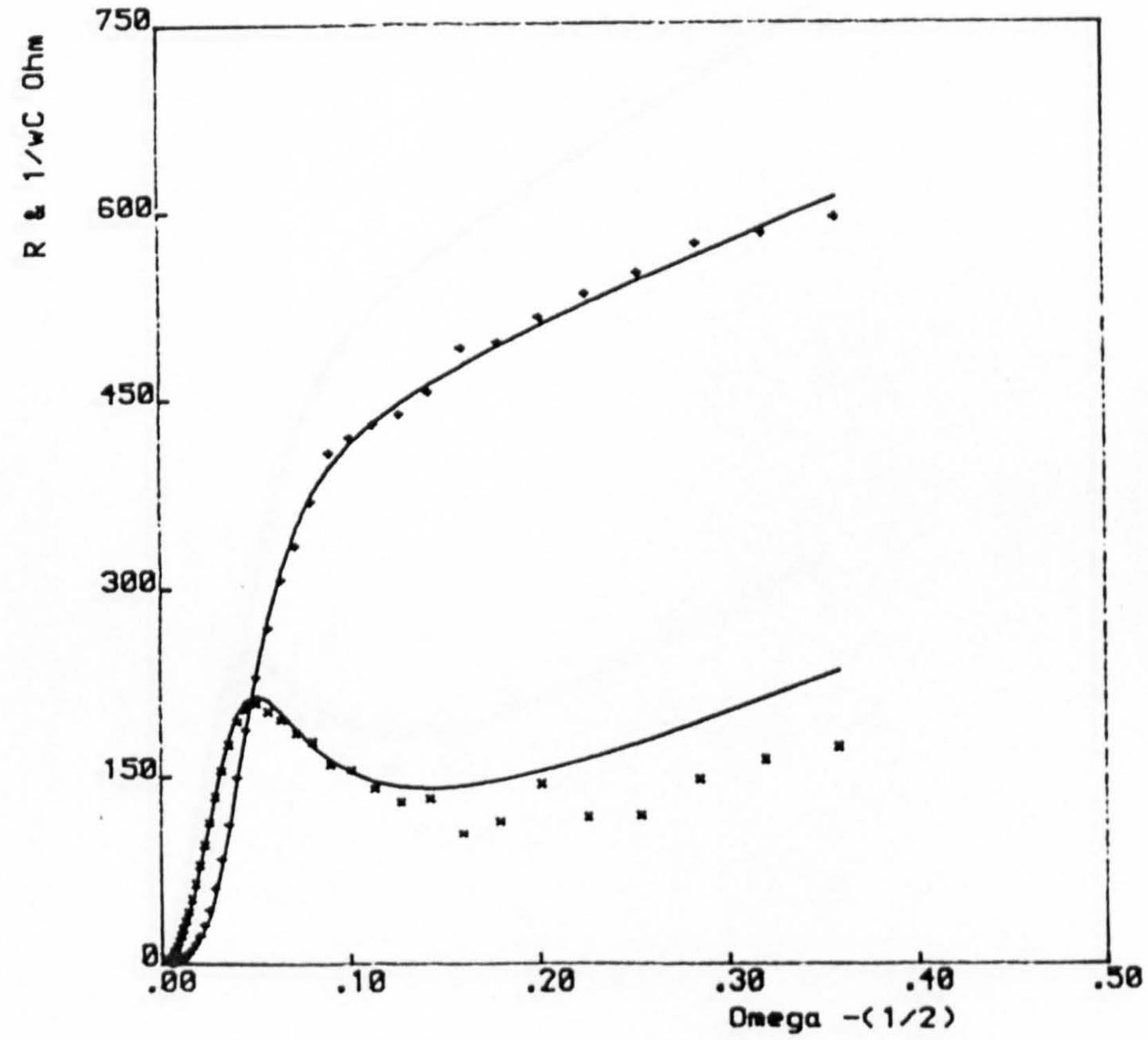

Fig. 7.4.3 Impedance spectrum, at a small cathodic polarisation, analysed according to the 'R-equation' - 1 mM $Cd(CN)_2$

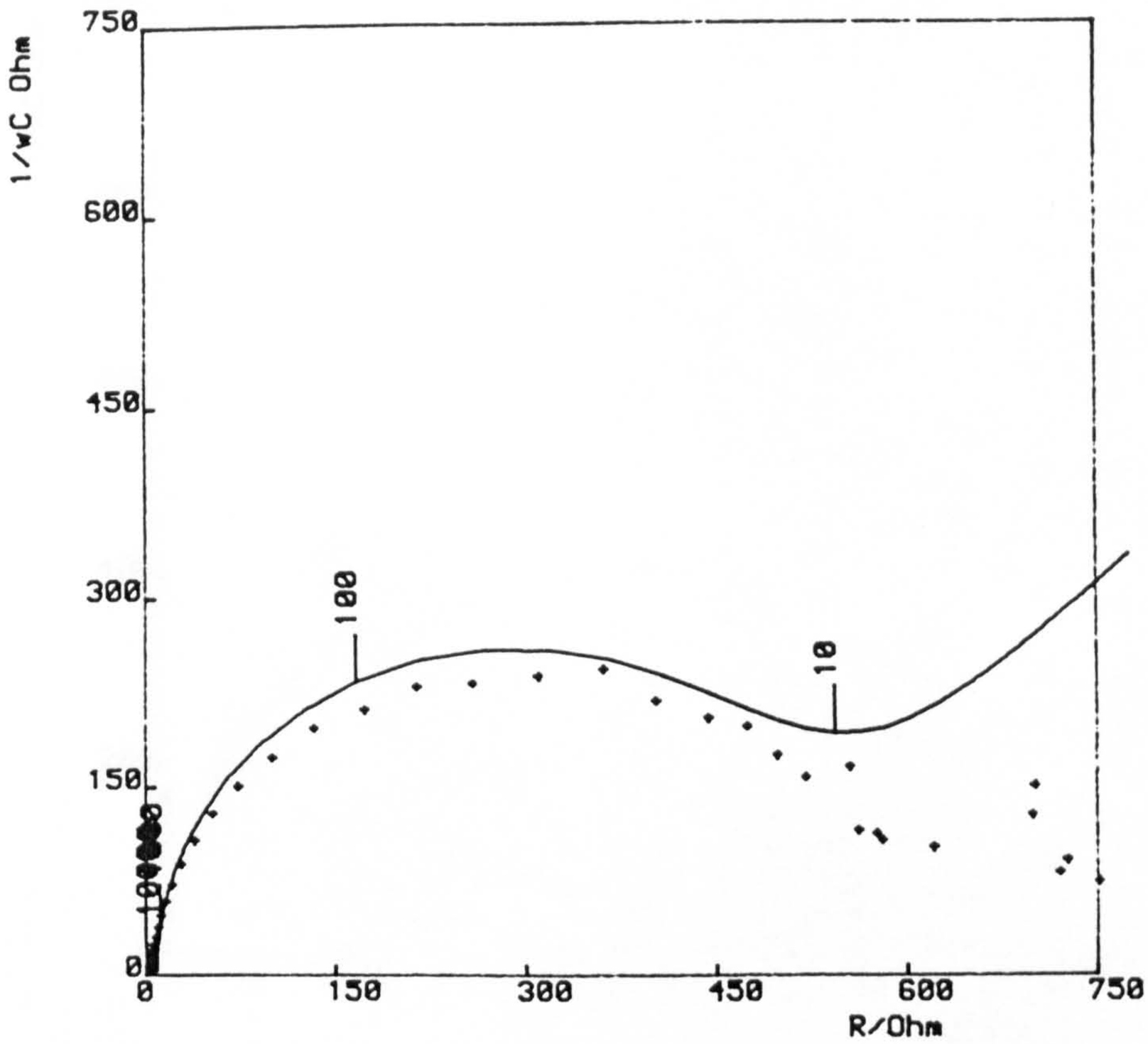

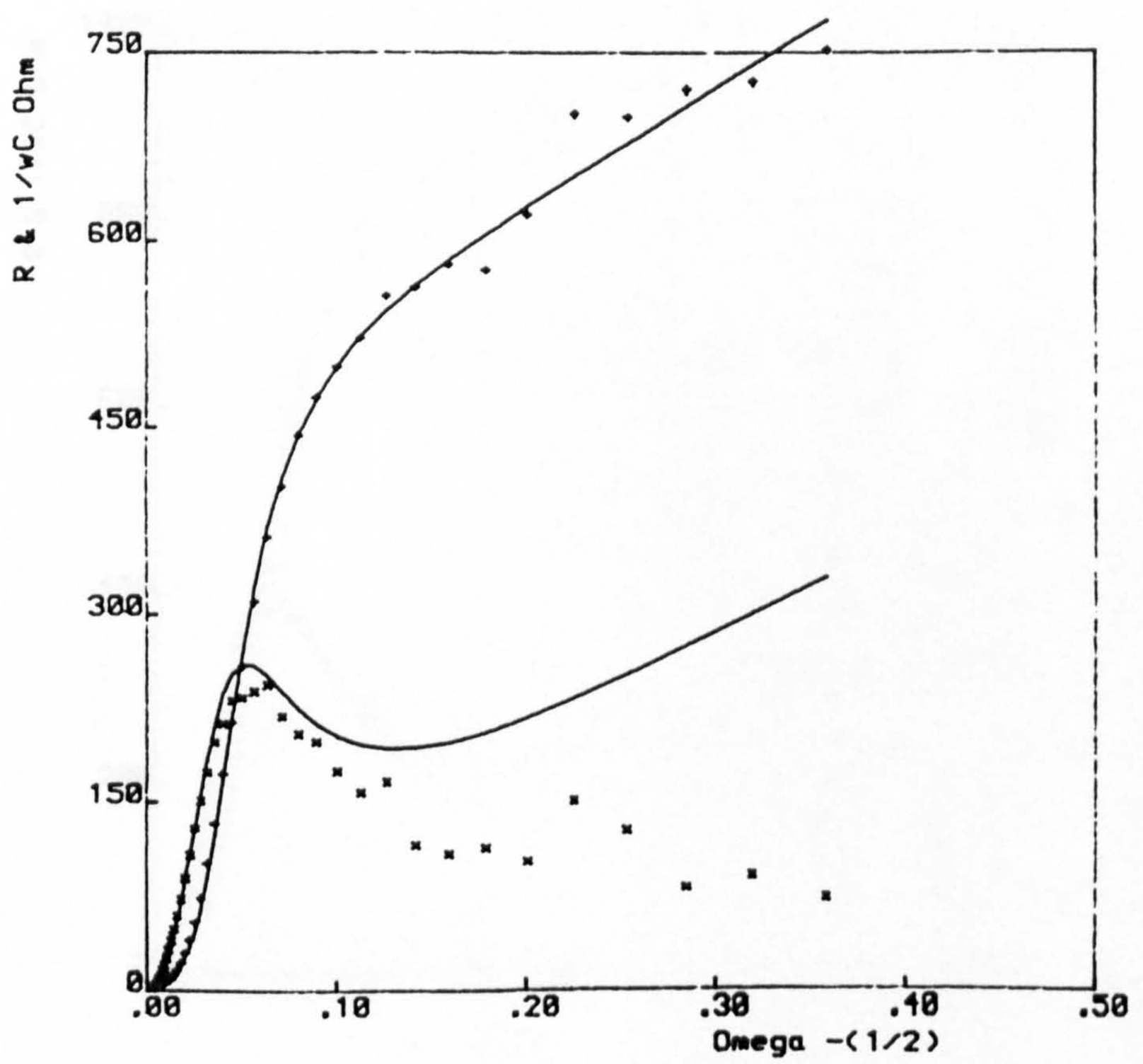

Fig. 7.4.4 Impedance spectrum, at a small anodic polarisation, analysed according to the 'R-equation' - 1 mM $Cd(CN)_2$

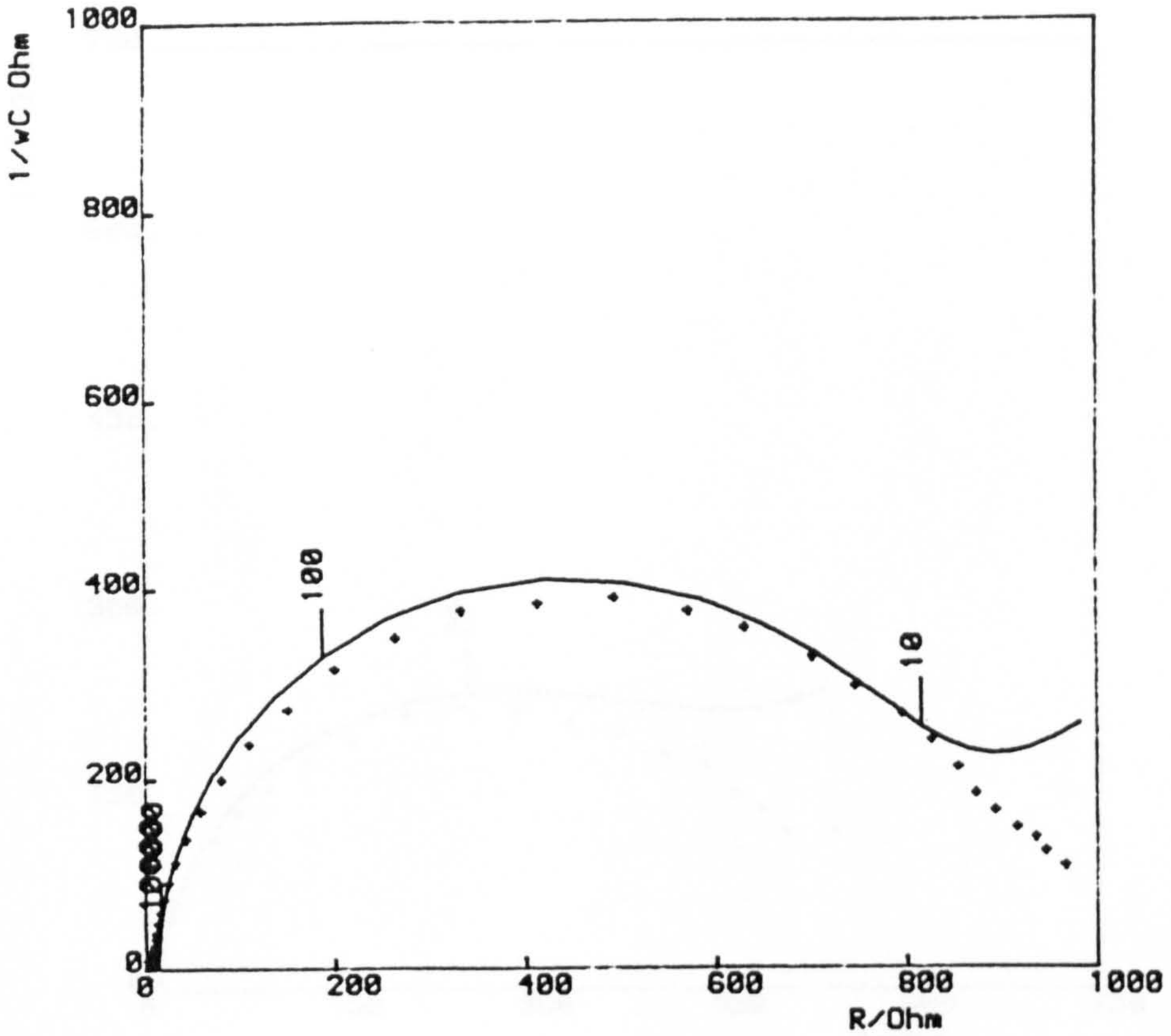

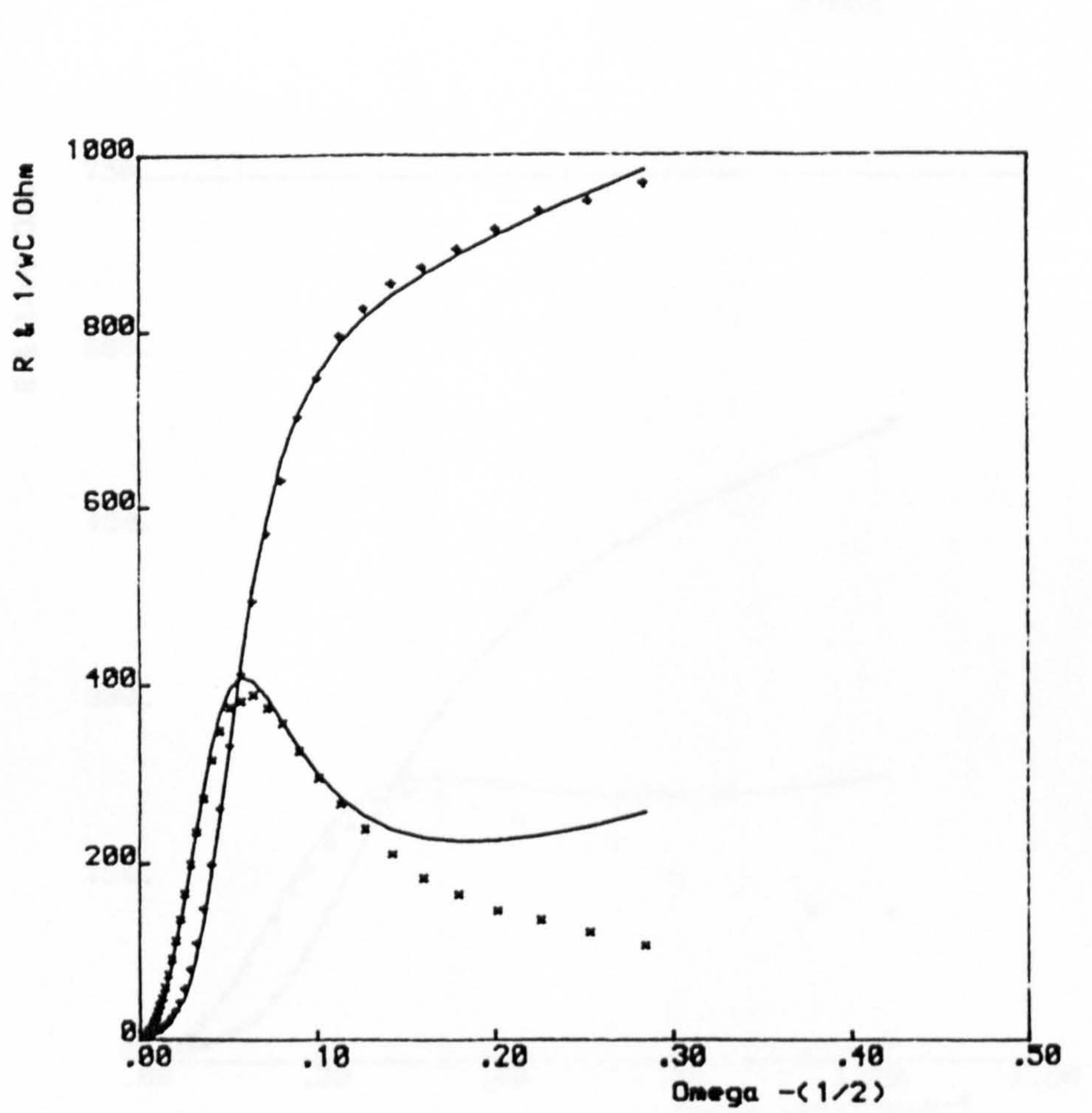

Fig. 7.4.5 Impedance spectrum, at a small cathodic polarisation, analysed according to the 'R-equation' - 10 mM $Cd(CN)_2$

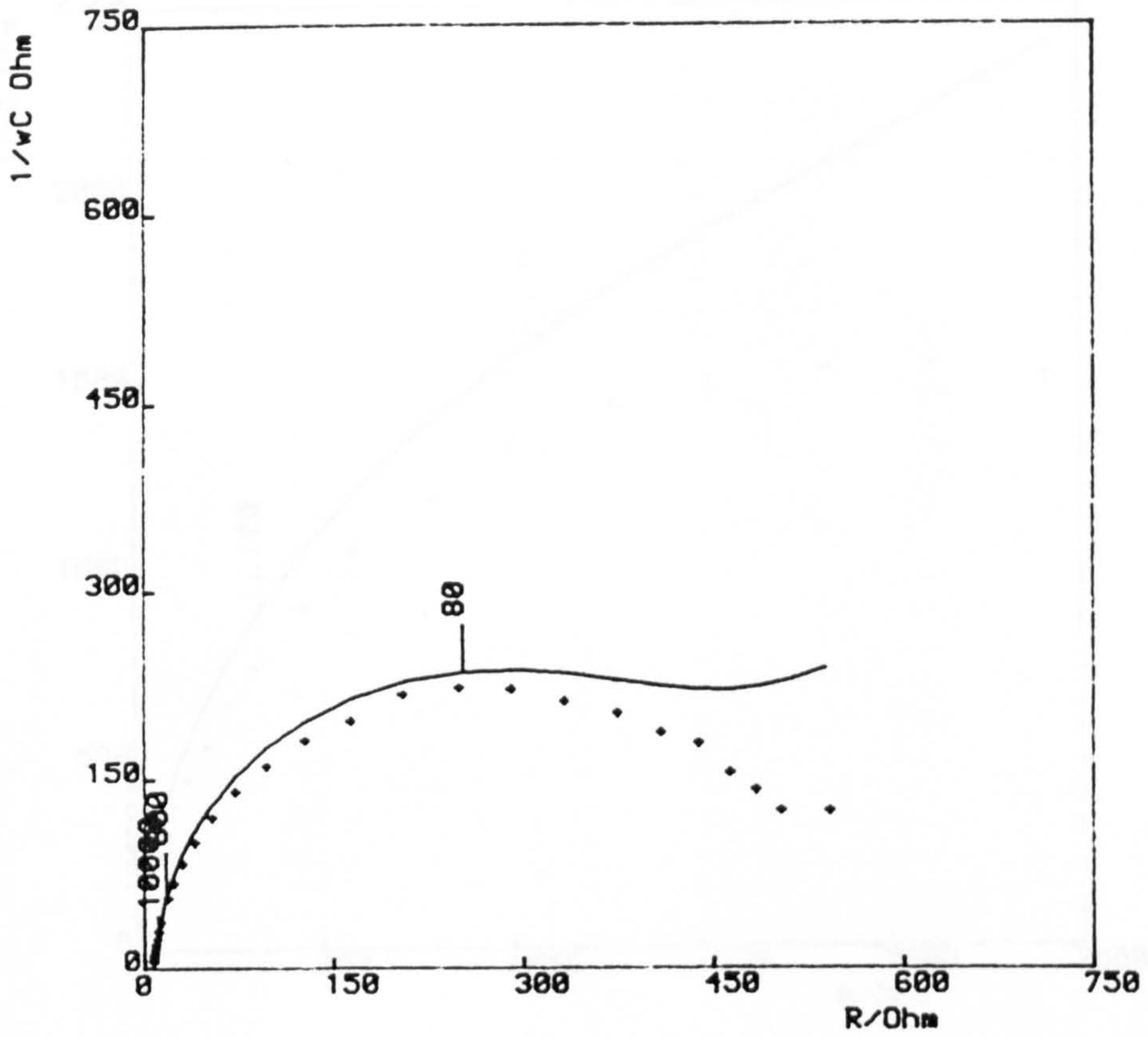

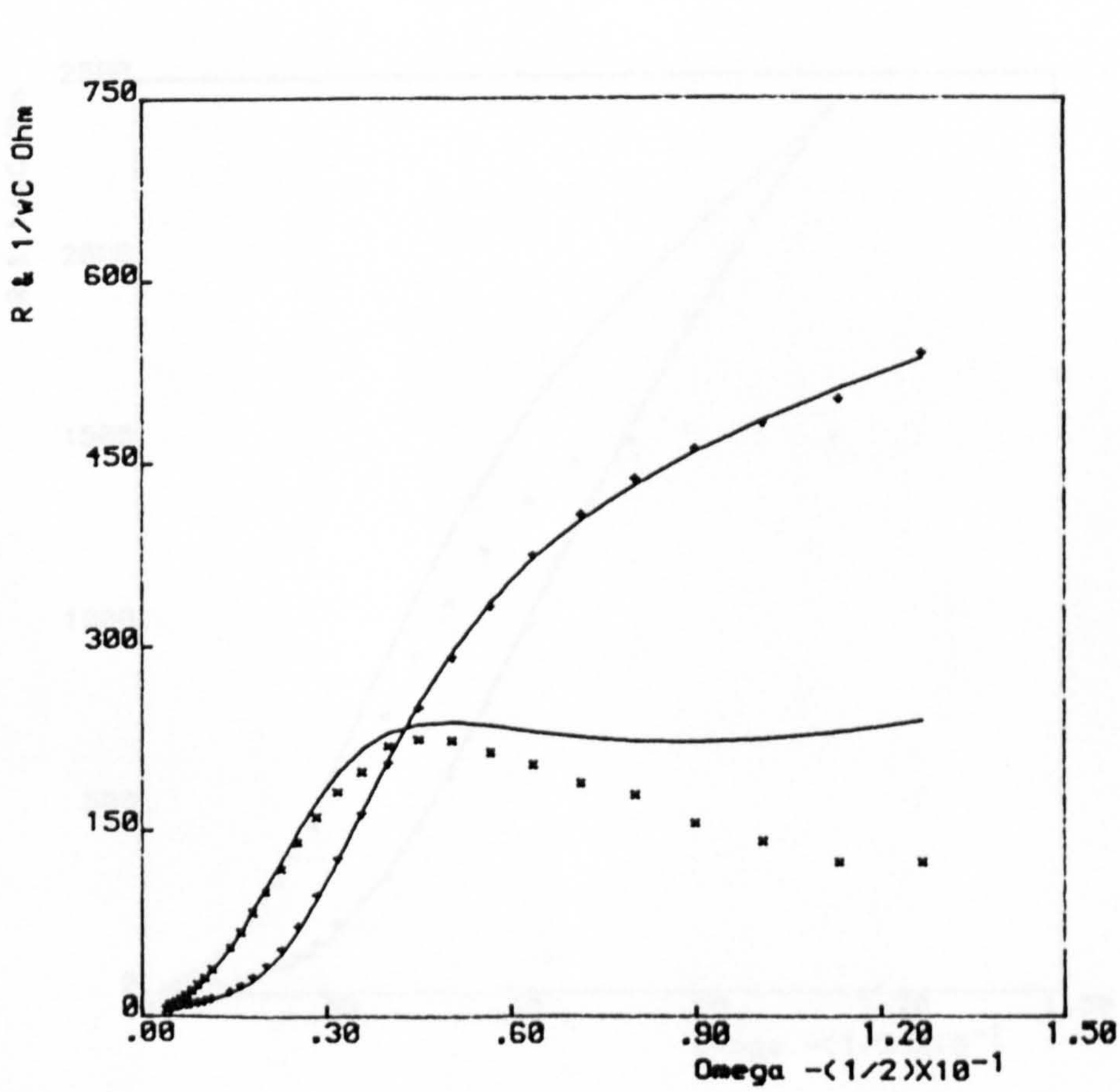

Fig. 7.4.6 Impedance spectrum, at a small anodic polarisation, analysed according to the 'R-equation' - 10 mM $Cd(CN)_2$

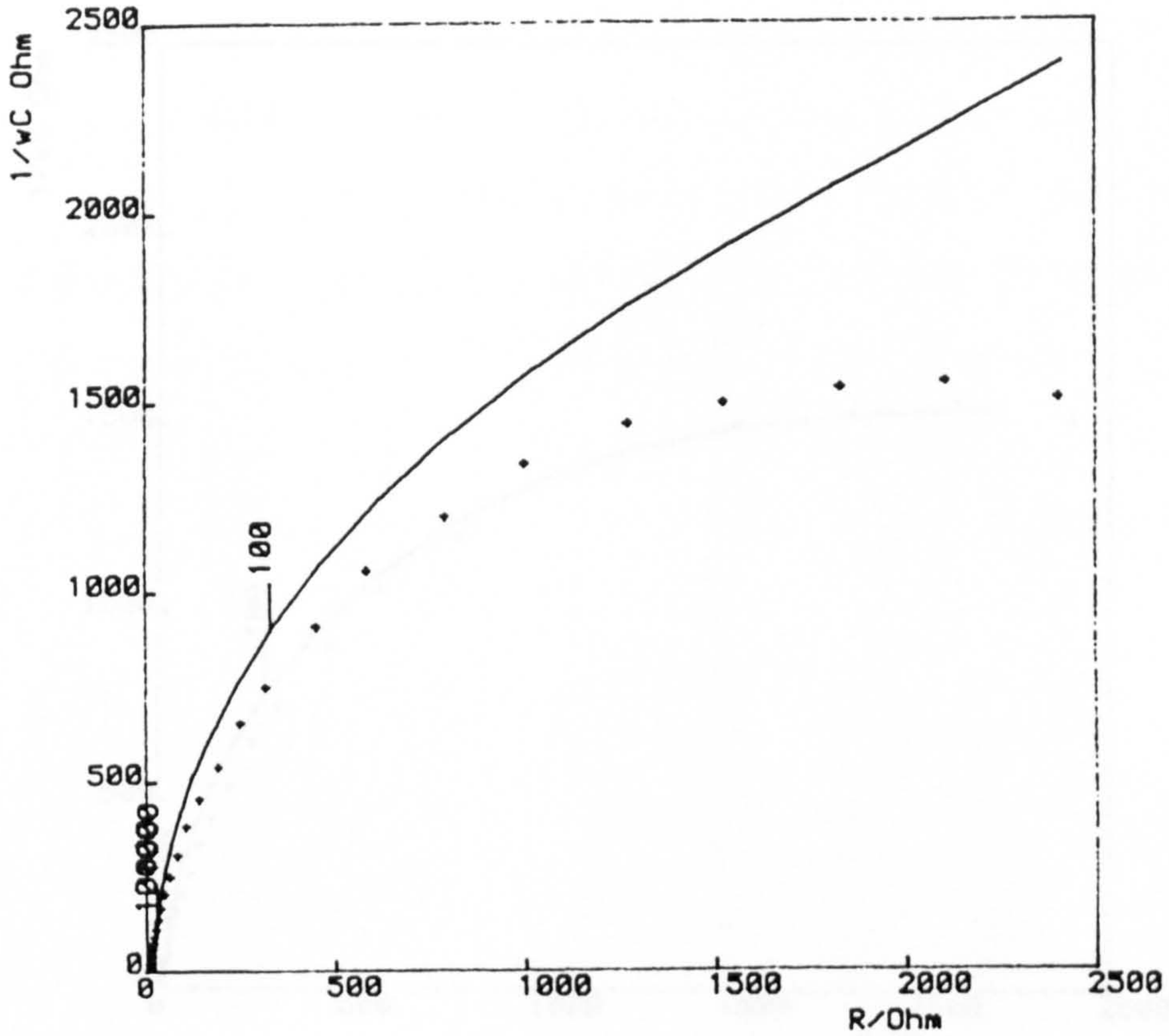

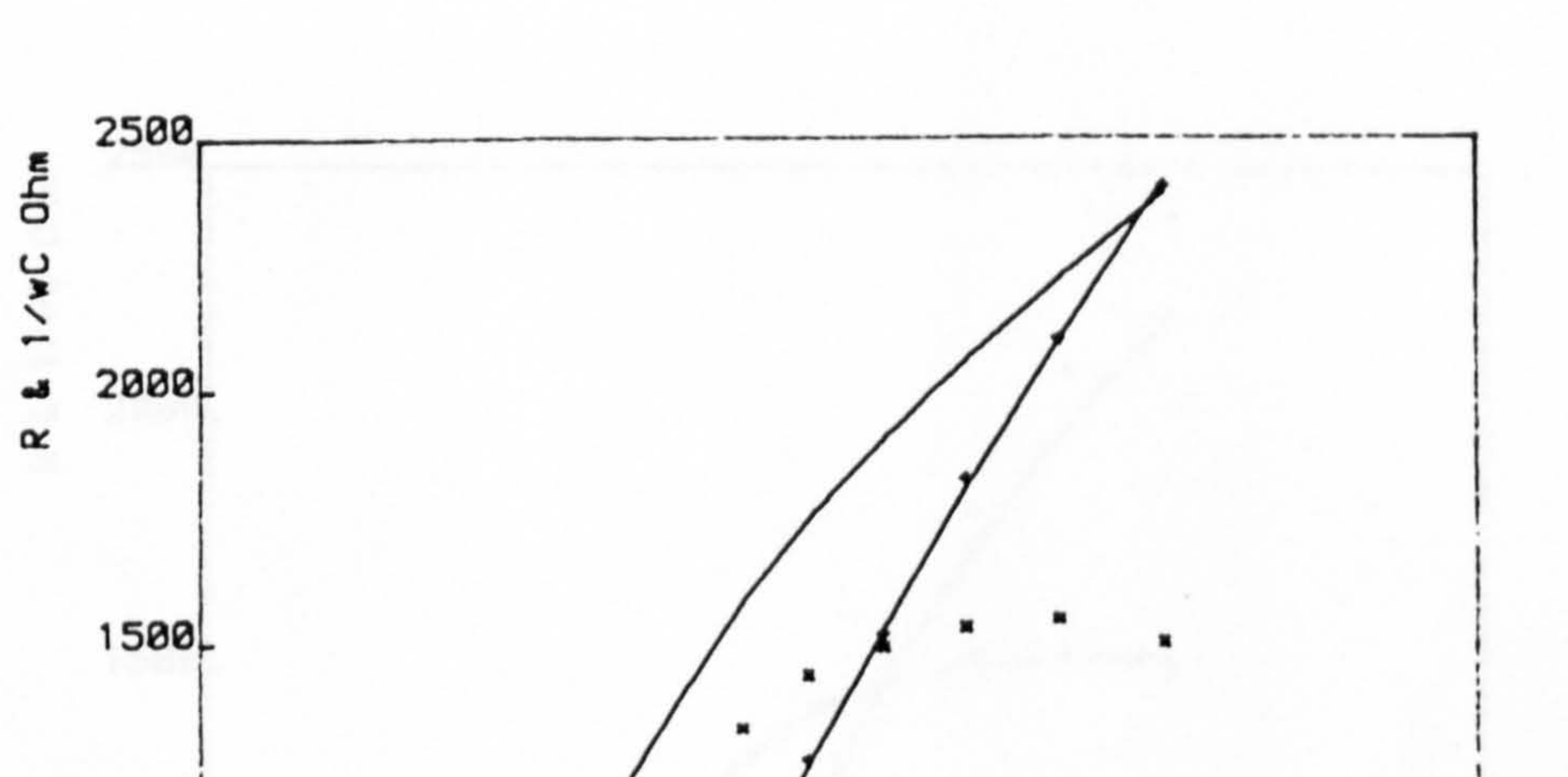

Fig. 7.4.7 Impedance spectrum, at a larger anodic polarisation, analysed according to the 'R-equation' - 10 mM $Cd(CN)_2$

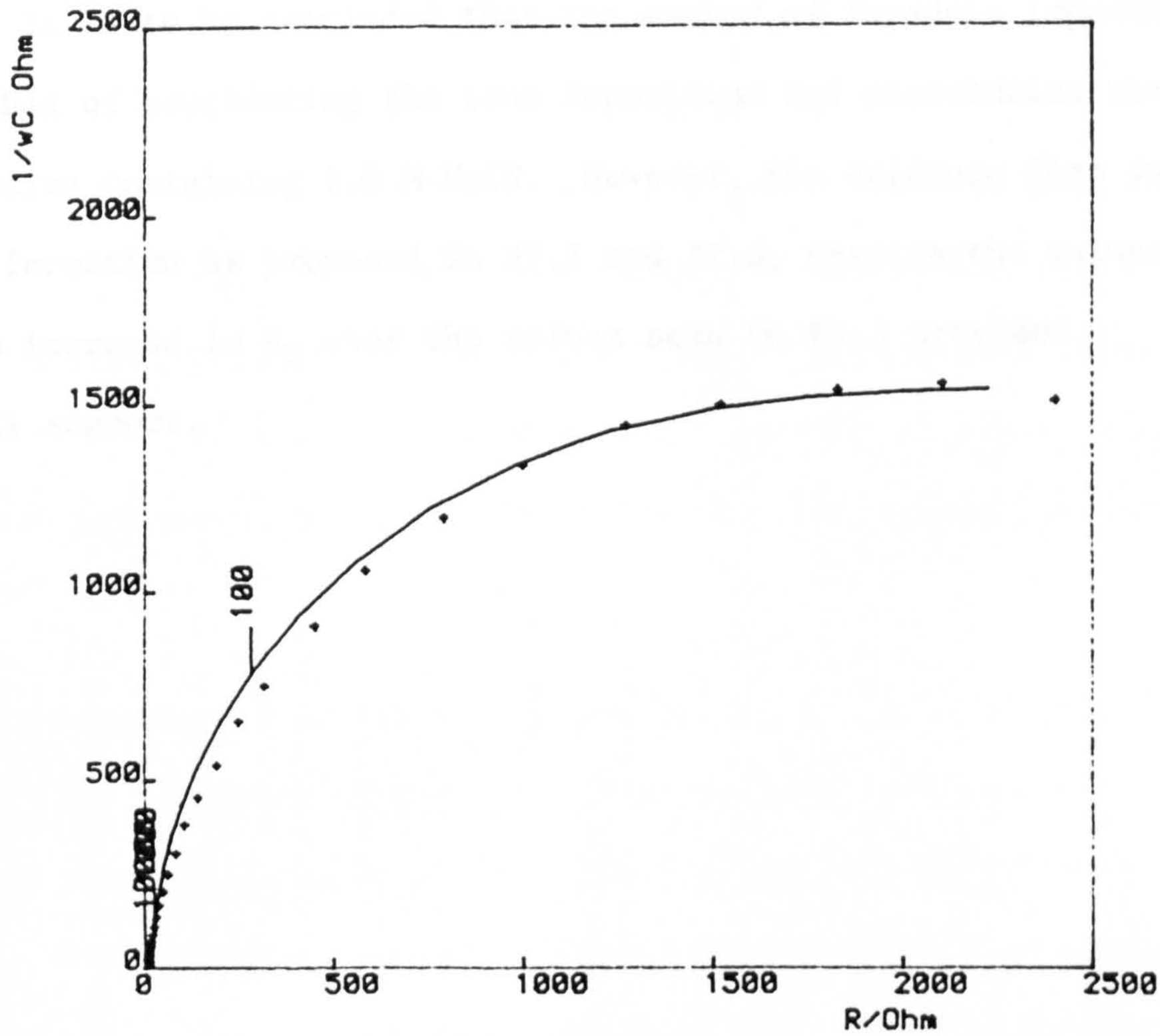

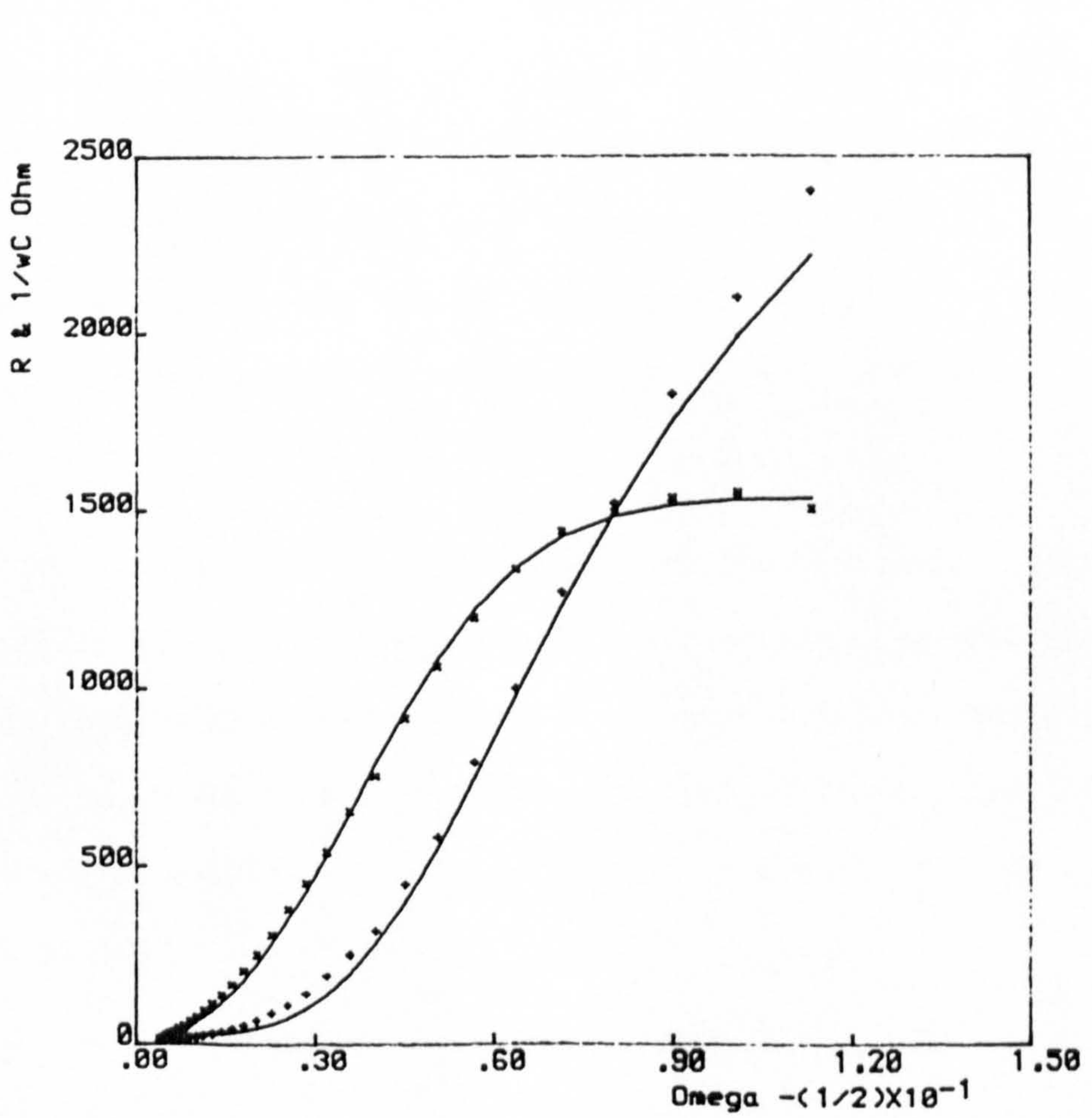

Fig. 7.4.8 Impedance spectrum, at a larger anodic polarisation, analysed according to the 'C-equation' - 10 mM $Cd(CN)_2$

and 7.4.8.

It is to be concluded that the method of faradaic impedance is incapable of elucidating the true deposition and dissolution kinetics in a solution containing 1.0 M NaCN. However, the evidence does support the film formation as proposed in §7.2 and §7.3, despite the values of C_L/A. An increase in R_Ω over the values seen in §5.3 provides additional support.

7.5 Discussion

A combination of the three experimental techniques has led to a working hypothesis for the cadmium electrode in alkaline cyanide solution. It has been difficult throughout to obtain a steady and reproducible equilibrium potential. This was first thought to be a consequence of the method of electrode pre-treatment, but experiments (not discussed) have shown this to be a second order effect. Another possible cause would be the extremely low concentration of the free (potential determining) Cd^{2+} ion.

The preferred explanation, however, is in terms of an ill-defined surface condition caused by film formation. Evidence of passivation has been observed in the linear sweep voltammograms at high cyanide ion concentration, and confirmatory results have been obtained at the rotating disc. The faradaic impedance data is not inconsistent with this interpretation. Results of linear sweep experiments have been interpreted in terms of a one electron transfer, limited by diffusion in solution, for the anodic reaction. The effect of increased cyanide ion concentration is thought to derive from the ability of the ion to shift the pH to values more favourable to the formation of $Cd(OH)_2$.

It has also been possible to examine the electrode kinetics, in solutions of low cyanide concentration, at the rotating disc electrode. The results confirm that the dissolution process involves a one electron transfer, although the degree of irreversibility is small. The cathodic process, however, exhibits a charge transfer valency of two, and is a reversible process.

The suggestion that the cadmium electrode is most likely to be covered by a hydroxide film in the solutions most closely resembling those successfully used for industrial electroplating is disconcerting. Indeed, satisfactory cadmium plating may only be achieved from solutions which contain a minimum of the cyanide ion. As is evident from the results, the film is unlikely to be passivating under the conditions which would be used in practical electroplating and may well be of a more 'dynamic' nature, such that it does not completely cover the electrode. The uncovered areas would then be expected to 'move' over the entire electrode surface by a process of reduction and re-formation. It may well be that a process such as this is partly responsible for the quality of the deposit, at the expense of a little current efficiency. There is no proof of this, however.

CHAPTER EIGHT

EXPERIMENTS IN THE CHEMELEC CELL®

8.1 Introduction

It had been intended, during the course of this project, to pursue four main areas of work. These were to concern the electrode kinetics of both nickel and cadmium electrodeposition, together with corresponding experiments carried out in the Chemelec Cell®

The initial decision was to study the electrode kinetics of cadmium whilst investigating the operation of the Chemelec Cell®for nickel recovery. It was considered that the electrode kinetics of the cadmium system might be easier to determine than those of the nickel system. In view of the toxic nature of the electrolyte, however, and the possible technical difficulties associated with the first time operation of a Chemelec Cell®, it was thought unwise to commence with the study of cadmium recovery in this reactor. The nickel system was, therefore, preferred here.

Unfortunately, difficulties encountered in both of the initially selected areas and also the long time-scale of experiments in the Chemelec Cell®have meant that the scope of the project has been limited to these two areas.

Experiments with the Chemelec Cell®have, therefore, been undertaken only with a Watts-type electrolyte as given in §4.2. Two main studies have been carried out. The effect of cathode potential on the operation of the cell is examined in §8.3 and that of pH in §8.4.

8.2 Cathode current efficiency

The cathode current efficiency is a frequently used measure in electrodeposition. It is defined as the ratio of the current consumed by the process of interest to the total current flowing. The current flowing at any time t' may be obtained as the instantaneous slope of a plot of charge against time, viz.

$$i = \frac{1}{A}(dq/dt)_{t=t'} \cdot \qquad (8.2.1)$$

The partial current consumed by the deposition process may be obtained from a plot of metal ion concentration versus time, given the electrolyte volume V, from:

$$i_{Ni} = -\frac{2FV}{A} \cdot \left(\frac{d[Ni^{2+}]}{dt}\right)_{t=t'} \cdot \qquad (8.2.2)$$

The current efficiency, e_i, is expressed as a percentage by:

$$e_i = -200FV \cdot \frac{\left(\frac{d[Ni^{2+}]}{dt}\right)_{t=t'}}{(dq/dt)_{t=t'}} \cdot \qquad (8.2.3)$$

It is clearly important that, for a commercial process, this quantity be maximised. In the present context, it should also be realised that the current efficiency need not be directly related to either the rate of the deposition process or to the total current, but only to the ratio of the two.

8.3 The effect of cathode potential on the operation of the Chemelec Cell®

8.3.1 Introduction

Whilst commercial operation of the cell has been via galvanostatic control, in view of the nature of the proposed experiments, it was thought that operation in the potentiostatic mode would be more appropriate here. Clearly, the electrode potential is the major control variable and of fundamental importance to the operation of the cell.

The results of the following experiments were presented to the "Fundamentals of Electroplating and Metal Finishing" conference, held at Loughborough University of Technology in September, 1980, and have now been published.[170]

8.3.2 Experimental

Concentration-decay type experiments were conducted at a series of cathode potentials in the range - 1.5 to - 1.71 V (all cathode potentials were measured with respect to the Hg/Hg_2SO_4 electrode; increases in cathode potential should be taken to mean a more negative potential in the absolute sense). The electrolyte in each case was as given in §4.2 and the pH was fixed at 3.4. The geometric area of the cathode was 52.4 cm^2. Several polarisation curves were obtained during each run. Both the charge passed and the nickel ion concentration were followed as functions of time.

8.3.3 Results and Discussion

Fig. 8.3.1 shows the decay in nickel ion concentration as a function of time for experiments at four different cathode potentials in the range specified. It may be seen that in each case the decay in non-linear in time; a smooth curve may be fitted to the data for each potential to show that the deposition rate falls continuously with time (and indeed concentration). There appears to be no particular trend with electrode potential. Indeed, all four sets of concentration-time data are reasonably similar. This suggests that the cell is being operated above the limiting current density for the deposition process. In no case does the concentration cease to fall altogether, although the deposition rate does become exceedingly small.

Fig. 8.3.2 shows the relationship between the charge passed and time for a series of cathode potentials. The data suggests that the charge is a linear function of time; the current density is effectively constant. As expected, the current density does increase with cathode potential. The apparent independence with respect to the nickel ion concentration is, however, contrary to expectation. If we regard the total current density to be composed of the partial current densities for the deposition and hydrogen evolution reactions then, while the current density associated with the evolution reaction is expected to be independent of nickel ion concentration, that for the deposition reaction is not. If, for example, the concentration-time profile were to follow an exponential decay, as for a first order reaction (see Fig. 8.3.3), then we may write:

$$\log\{c\} = m_1 + m_2 t \qquad (8.3.1)$$

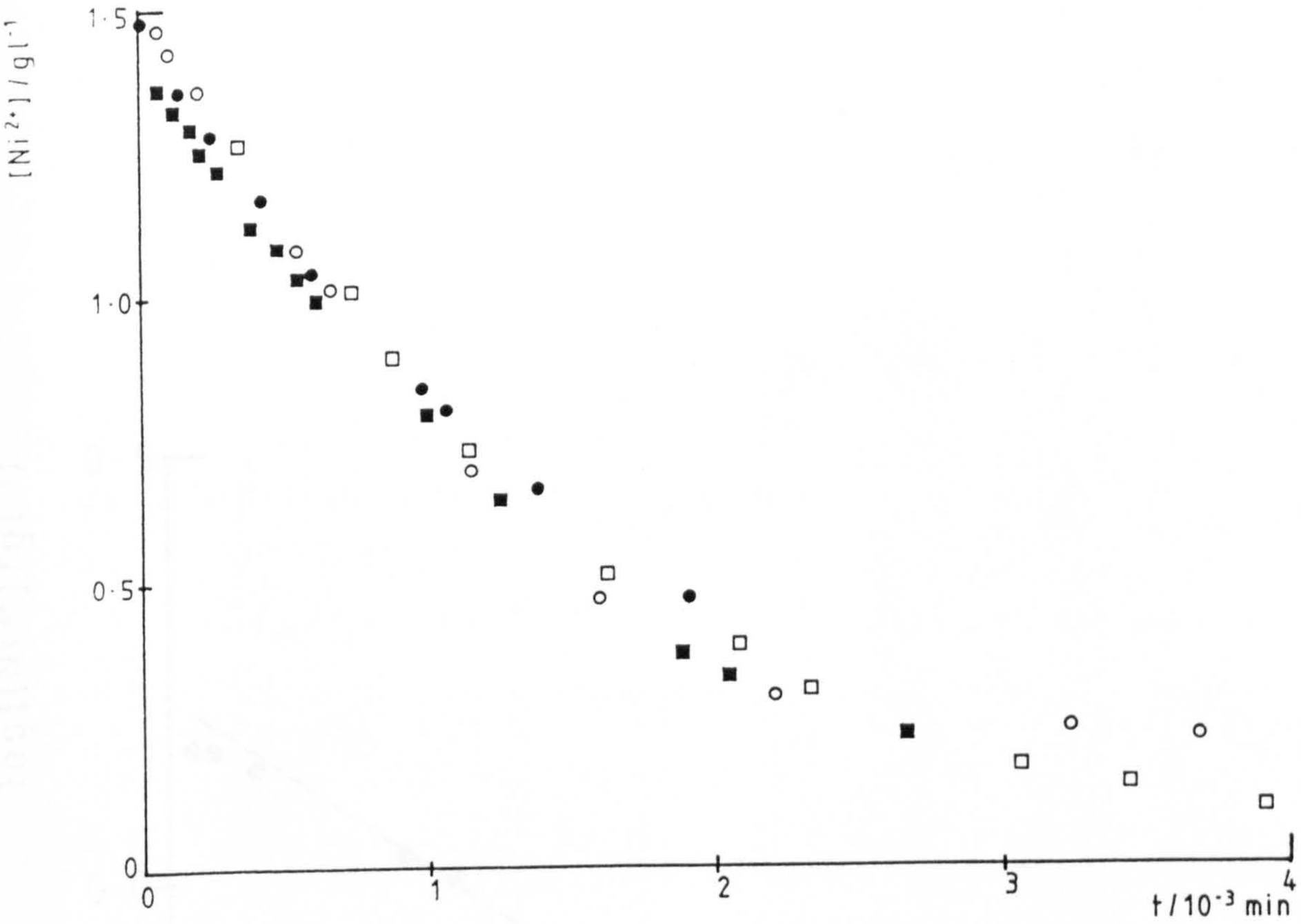

Fig. 8.3.1 $[Ni^{2+}]$ versus t plots at four cathode potentials;
● - 1.71 V, ■ - 1.66 V, ○ - 1.60 V, □ - 1.58 V.

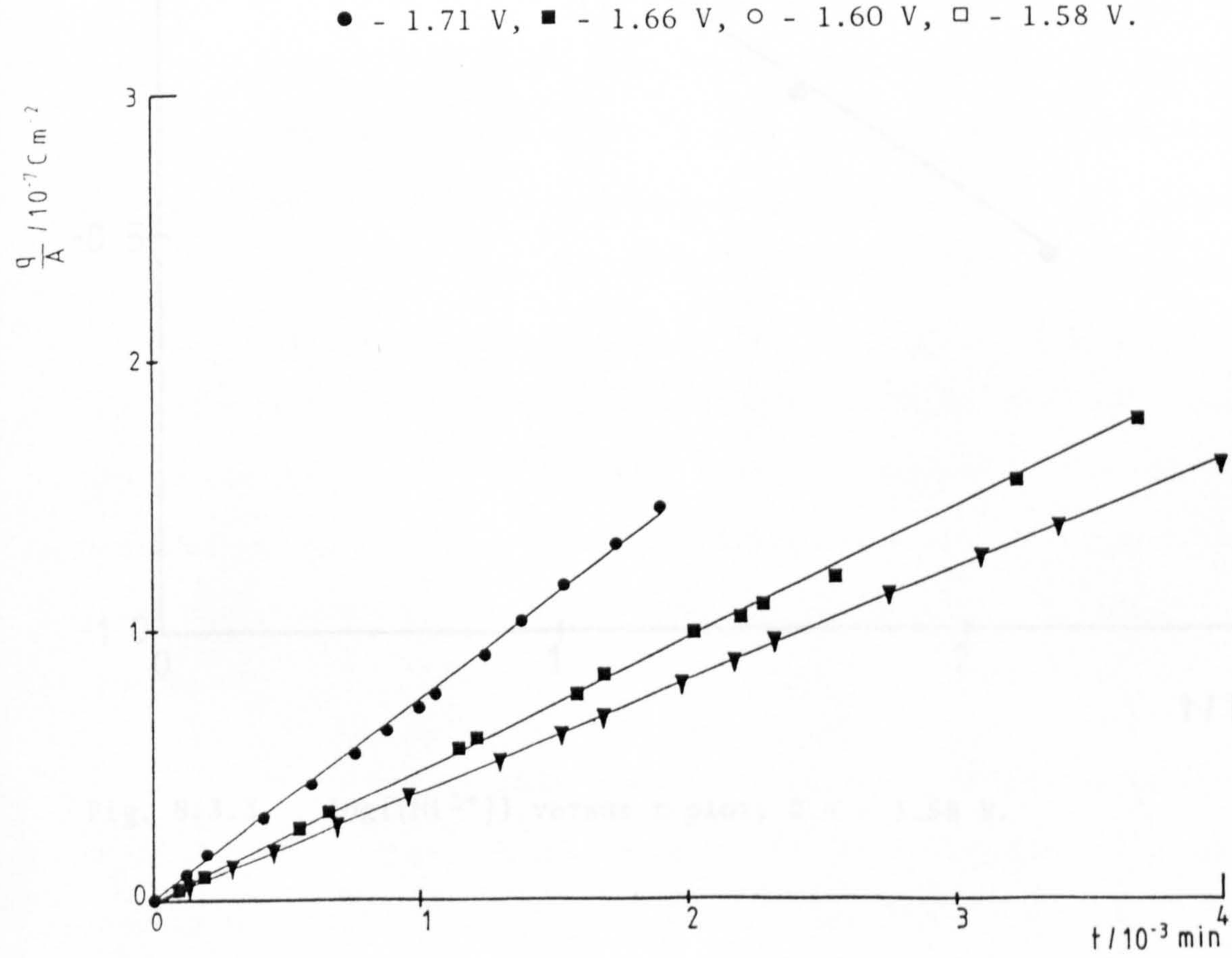

Fig. 8.3.2 Charge density versus time plots for three cathode potentials;
● - 1.71 V, ■ - 1.60 V, ▼ - 1.50 V.

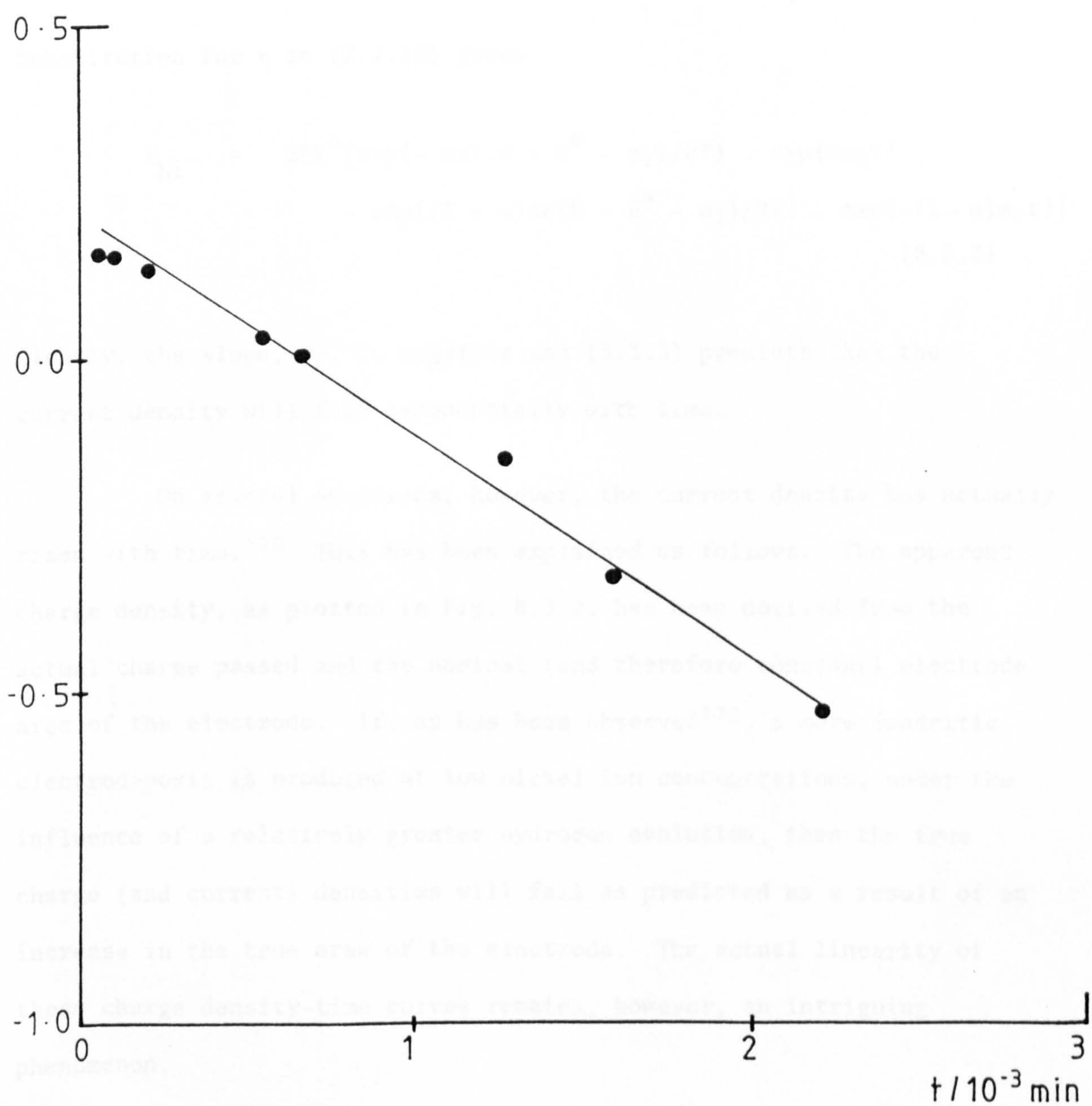

Fig. 8.3.3 $\log\{[Ni^{2+}]\}$ versus t plot; E = - 1.58 V.

where m_2 and m_1 are the slope and intercept of the log{c} versus t plot respectively. Introducing this into the Nernst equation (2.2.6), we obtain via (2.2.19) an expression for the time-dependent overpotential for the deposition process, viz.

$$\eta = E - E^{\ominus} - RT(m_2 t + m_1)/zF \qquad (8.3.2)$$

Substitution for η in (2.2.18) gives:

$$i_{Ni} = zFk^{o}[\exp\{-\alpha zF(E - E^{\ominus} - m_1)/RT\} \cdot \exp\{\alpha m_2 t\} - \exp\{(1-\alpha)zF(E - E^{\ominus} - m_1)/RT\} \cdot \exp\{-(1-\alpha)m_2 t\}] \qquad (8.3.3)$$

Clearly, the slope, m_2, is negative and (8.3.3) predicts that the current density will fall exponentially with time.

On several occasions, however, the current density has actually risen with time.[170] This has been explained as follows. The apparent charge density, as plotted in Fig. 8.3.2, has been derived from the actual charge passed and the nominal (and therefore constant) electrode area of the electrode. If, as has been observed[170], a more dendritic electrodeposit is produced at low nickel ion concentrations, under the influence of a relatively greater hydrogen evolution, then the true charge (and current) densities will fall as predicted as a result of an increase in the true area of the electrode. The actual linearity of these charge density-time curves remains, however, an intriguing phenomenon.

The cathode current efficiency has been calculated (as indicated in §8.2) as a function of concentration for several potentials. The results are shown in Fig. 8.3.4. As expected, the efficiency falls with

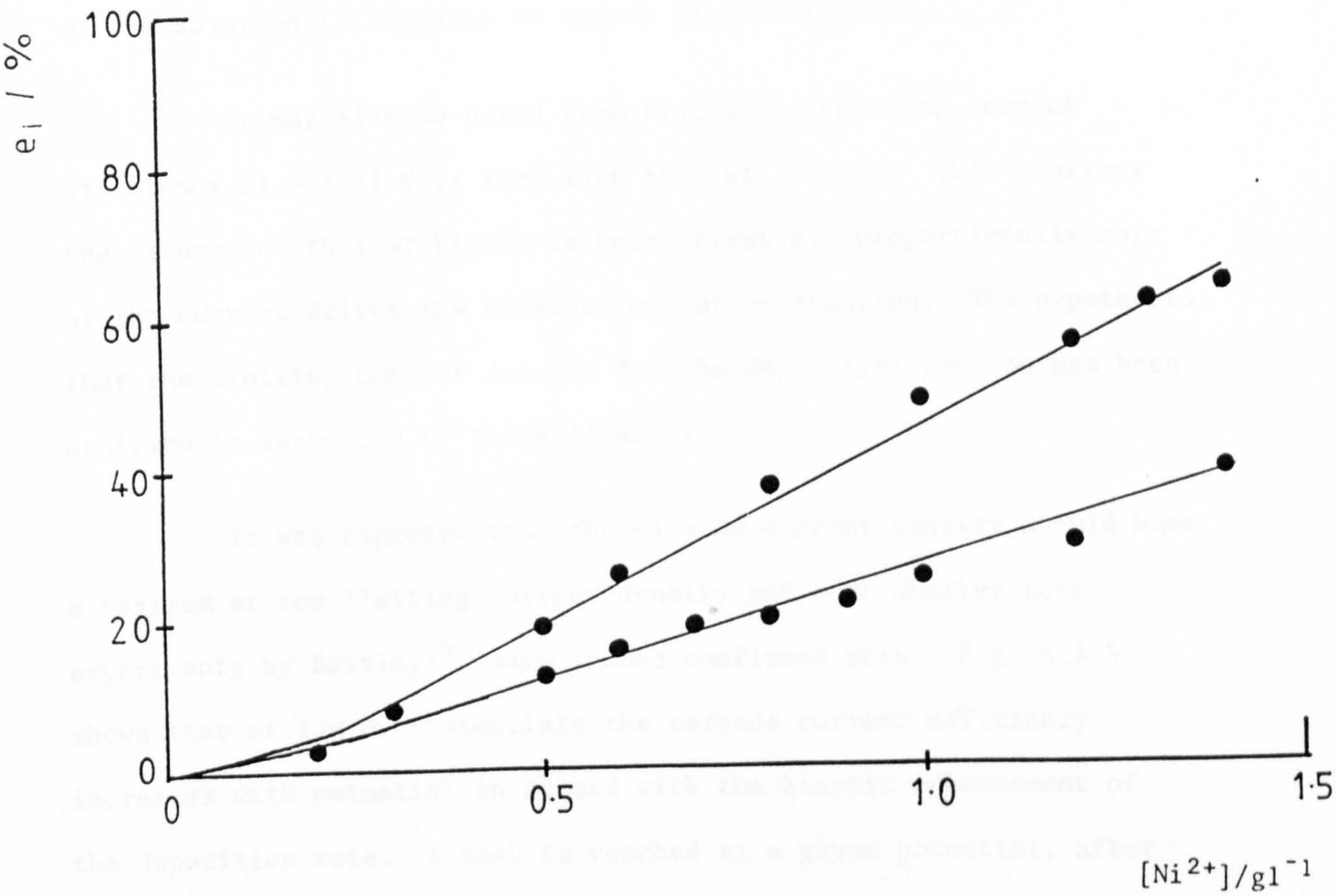

Fig. 8.3.4 e_i versus $[Ni^{2+}]$ plot for two cathode potentials;
upper curve - 1.71 V,, lower curve - 1.60 V.

concentration. The absolute values of the efficiency are somewhat lower than those claimed by the Electricity Council.[30] There may be several explanations for this apparent discrepancy. First, the present experiments were carried out at a more acidic pH, presumably favouring the hydrogen evolution over the electrodeposition reaction. Secondly, equation (8.2.3) makes use of the electrolyte volume, which has been taken to be 51. Since the cell is initially flushed with water prior to adding the 51 of electrolyte, it is likely that the actual volume of the solution is slightly in excess of this figure.

It may also be noted from Fig. 8.3.4 that the current efficiency at - 1.71 V is less than that at - 1.6 V. This confirms the assumption that at higher cathode potentials proportionally more of the current drives the hydrogen evolution reaction. The hypothesis that the limiting current density for the deposition process has been achieved is supported by these findings.

It was expected that the cathode current density should have a maximum at the limiting current density and some shorter term experiments by Bettley[171] have indeed confirmed this. Fig. 8.3.5 shows that at low overpotentials the cathode current efficiency increases with potential in accord with the kinetic enhancement of the deposition rate. A peak is reached at a given potential, after which the efficiency falls with the increased current serving only to promote the hydrogen evolution reaction. The height of the peak varies with the nickel ion concentration, as might be expected on the basis of equation (2.3.9).

Fig. 8.3.6 shows the polarisation data for the experiment at - 1.6 V. Three curves, obtained at different nickel ion concentrations,

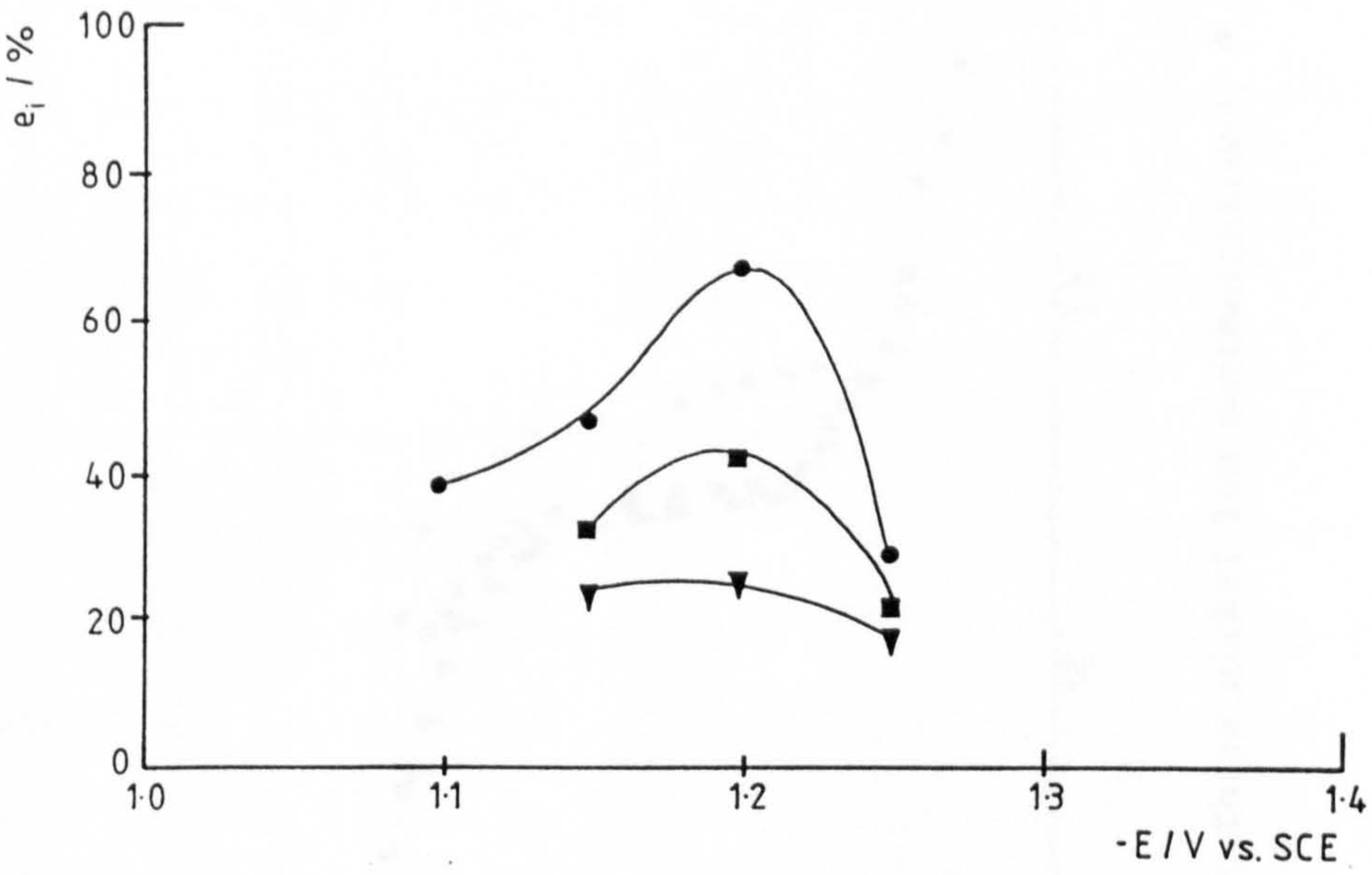

Fig. 8.3.5 e_i versus E plots for three nickel ion concentrations;
● 1.3 gl^{-1}, ■ 1.0 gl^{-1}, ▼ 0.8 gl^{-1}.

$Na_2SO_4 . 10H_2O$	0.57 M
NaCl	0.19 M

20°C (after Bettley[171])

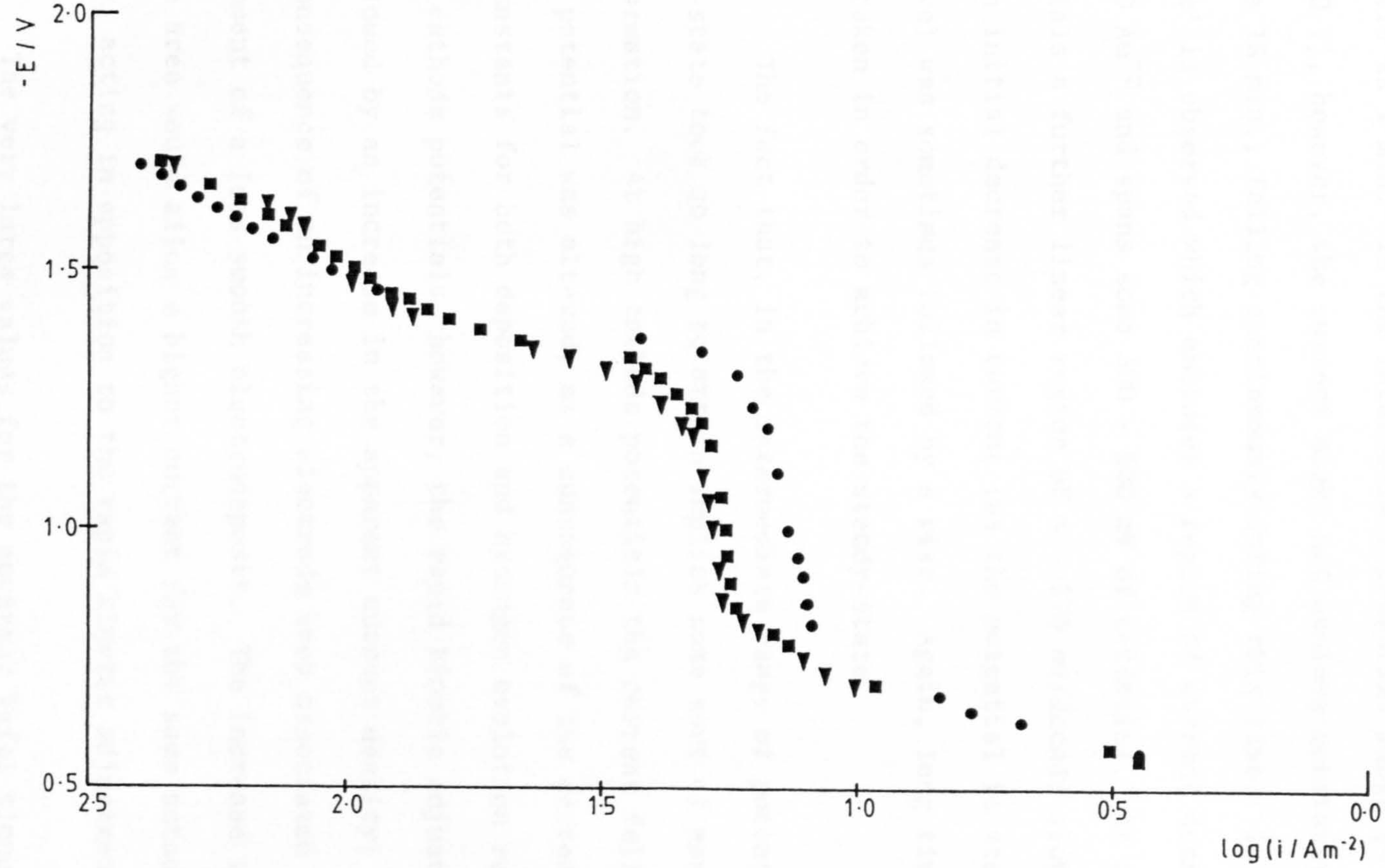

Fig. 8.3.6 Polarisation curves at three nickel ion concentrations; ● 1.255 gl^{-1}, ■ 1.01 gl^{-1}, ▼ 0.3 gl^{-1}

are presented. The curves were retraceable within the limits of the experimental error. The shape of the curves is unusual and quite characteristic. At high cathode potential an almost linear relationship exists between log{i} and E, of approximately - 600 mV/decade slope. The steady-state currents for this region were observed after as little as 1 min. In the intermediate potential range (∿ - 1.5 to ∿ - 1.0 V), however, the current might not achieve constancy for as long as 15 min., falling continuously during this time. In this region, a 'knee' is observed which embraces a region of current density of 10 - 30 Am^{-2} and spans some 300 - 500 mV of potential. At even lower potentials a further linear region of ∿ - 570 mV/decade slope is seen; here an initial decrease in current (as the potential is stepped more positive) was sometimes followed by a rise. Again, long times were often taken in order to achieve the steady-state.

The fact that, in the intermediate range of potential, the steady-state took so long to attain implies some sort of morphological transformation. At high cathode potentials the current fell sharply as the potential was altered, as a consequence of the decrease in rate constants for both deposition and hydrogen evolution reactions. At low cathode potentials, however, the rapid kinetic adjustment may be followed by an increase in the apparent current density; perhaps as a consequence of an increasing electrode area associated with the development of a less smooth electrodeposit. The increase in true cathode area would allow a higher current for the same actual current density, acting in opposition to the rapid kinetic adjustment.

The very large values for the apparent Tafel slopes are inexplicable at present, except in terms of current control by a semi-

conducting phase.

If, as is suggested by the data of Fig. 8.3.5, the potential at which the limiting current density is achieved is ∿ - 1.5 V (versus Hg/Hg_2SO_4), then the plateau-like region of Fig. 8.3.6 cannot be ascribed to the deposition reaction as has been previously suggested.[170] The plateau might represent the limiting current for some other process, probably involving the hydrogen atom. The limiting current density for nickel deposition would then be masked (in Fig. 8.3.6) by the onset of significant hydrogen evolution and the decomposition of water.

The quality of the electrodeposit was excellent in most cases. Its appearance was bright and smooth and was both compact and adherent. Plate VI shows a typical example. The quality of the deposit is especially good considering the fact that it was achieved at lower temperatures than those needed for satisfactory operation of the Watts Bath.

8.3.4 Conclusions

1. The Chemelec Cell® achieves the recovery of nickel as a bright, smooth and adherent electroplate from solutions likely to be encountered in commercial operation, down to 100 mgl^{-1}.
2. The current efficiency is a function of concentration and of potential. The most efficient operation should be achieved at a cathode potential of - 1.5 V.
3. The total current density appears to be independent of concentration in a region of high cathode potential although

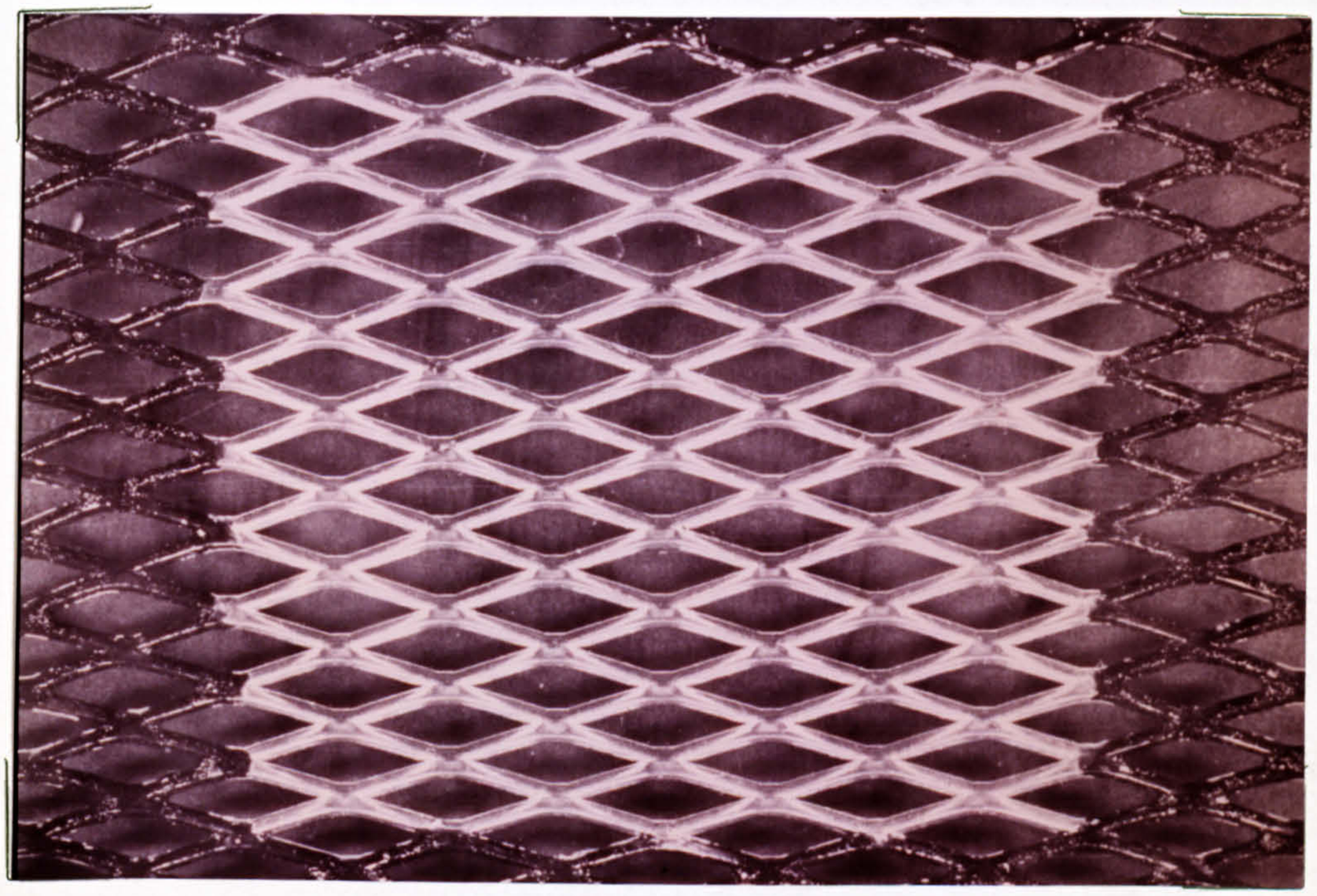

PLATE VI A typical nickel electrodeposit

this is probably due to the fact that the actual surface area of the electrode is not, and is unknown.

4. The polarisation characteristics are complex. Two linear regions of the semi-logarithmic plot of large apparent Tafel slopes are separated by a plateau which may represent the limiting current for some hydrogen atom process.

8.4 The effect of pH on the operation of the Chemelec Cell®

8.4.1 Introduction

Whilst the industrial performance of the Chemelec Cell® for the recovery of nickel is largely satisfactory, there have been some reports of difficulties with poor deposits. Such difficulties were thought to arise from the precipitation of oxy-nickel salts and it was felt that the rôle of pH was of paramount importance here. In addition, it was considered worthwhile to establish criteria for pH in the operation of the cell, in terms of a compromise between the attainment of the maximum cathode current efficiency and the production of satisfactory electrodeposits.

8.4.2 Experimental

Concentration-decay experiments were conducted with the electrolyte of §4.2, at various values of pH in the range pH 3.0 to pH 6.2. The electrode potential was maintained at - 1.5 V in all cases and the geometric area of the cathode was nominally 121.4 cm^2. All other experimental conditions were as in §8.3.2.

8.4.3 Results and Discussion

Perhaps the most important, and indeed surprising result from the point of view of the Chemelec Cell® operator is the apparent insensitivity of the process to changes in the electrolyte pH. Experi-

ments carried out at pH values in the range pH 3.0 to pH 6.2 all produced quite satisfactory deposits. Indeed, no deterioration in the quality of the electroplate was observed as the pH was made more alkaline.

The majority of the apparent problems of deposit quality have been encountered during the early stages of recovery from a fresh drag-out solution. Further to this work Bettley[171] has obtained some evidence to suggest that the presence of boric acid at a concentration in excess of 20 g/l may be beneficial to deposit quality. The mechanism by which boric acid is able to improve deposit quality is not attributable solely to its properties as a buffering agent. Russian workers[172] have shown that succinic acid is less effective in promoting deposit quality than its superior buffer capacity would suggest. Whilst the final deposits obtained in the present work were entirely satisfactory, examination of the cathode after the first few hours of operation has revealed that a more matt deposit is produced at higher nickel ion concentrations than at lower ones. This effect appears to be slightly enhanced at more alkaline pH.

The charge passed is shown, as a function of time, in Fig. 8.4.1 for experiments at different values of the pH. As might be expected, the current densities obtained from these curves decrease as the pH becomes more alkaline with the greatest effects on the current density being observed at the lowest values of pH. Notice also, that especially for the experiment at pH 5.4 a small amount of curvature towards the time axis may be seen. The relationship remains essentially linear as observed in §8.3.

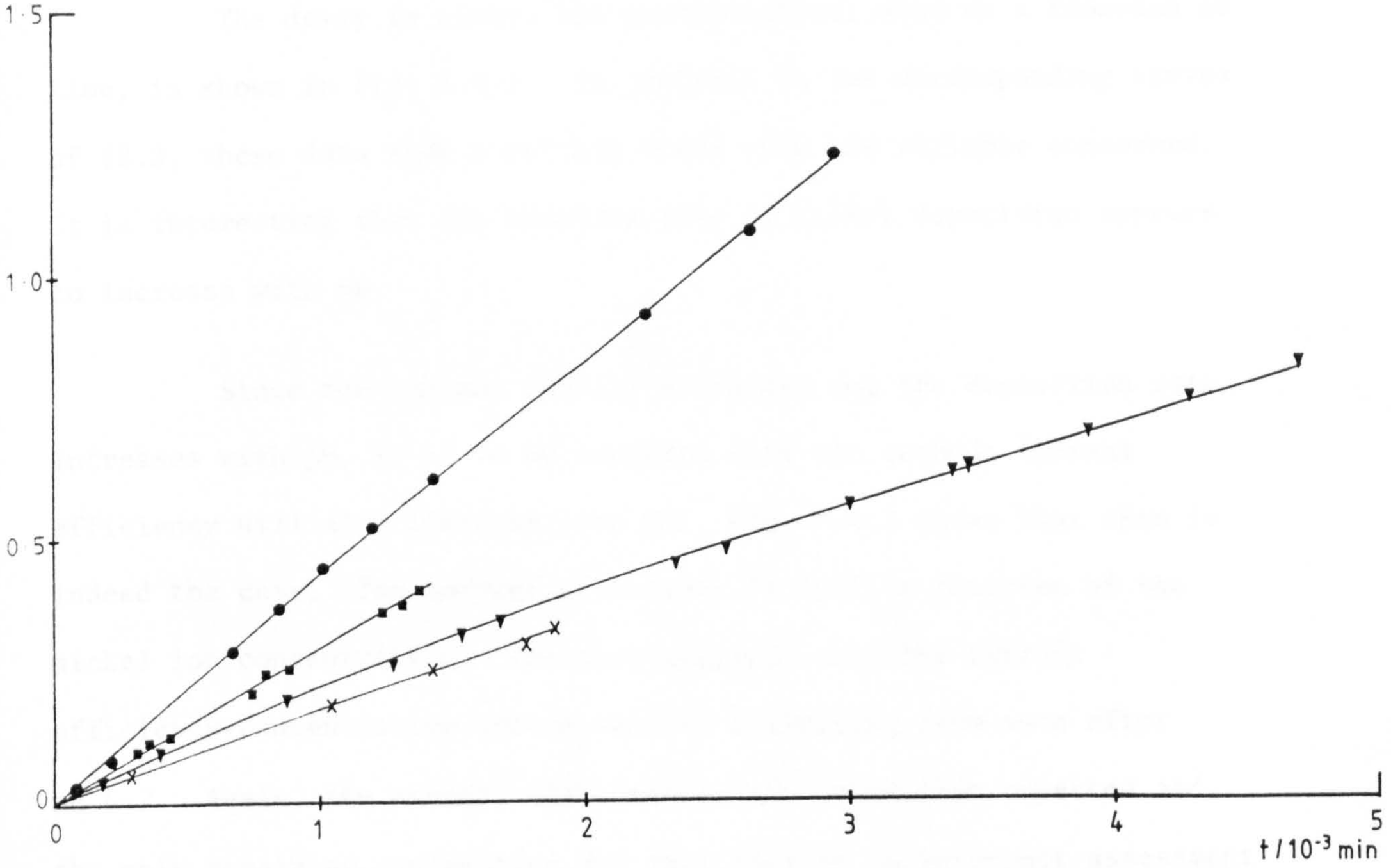

Fig. 8.4.1 Charge density versus time plots at various values of pH;
● pH 3.0, ■ pH 5.0, ▼ pH 5.4, x pH 6.2.

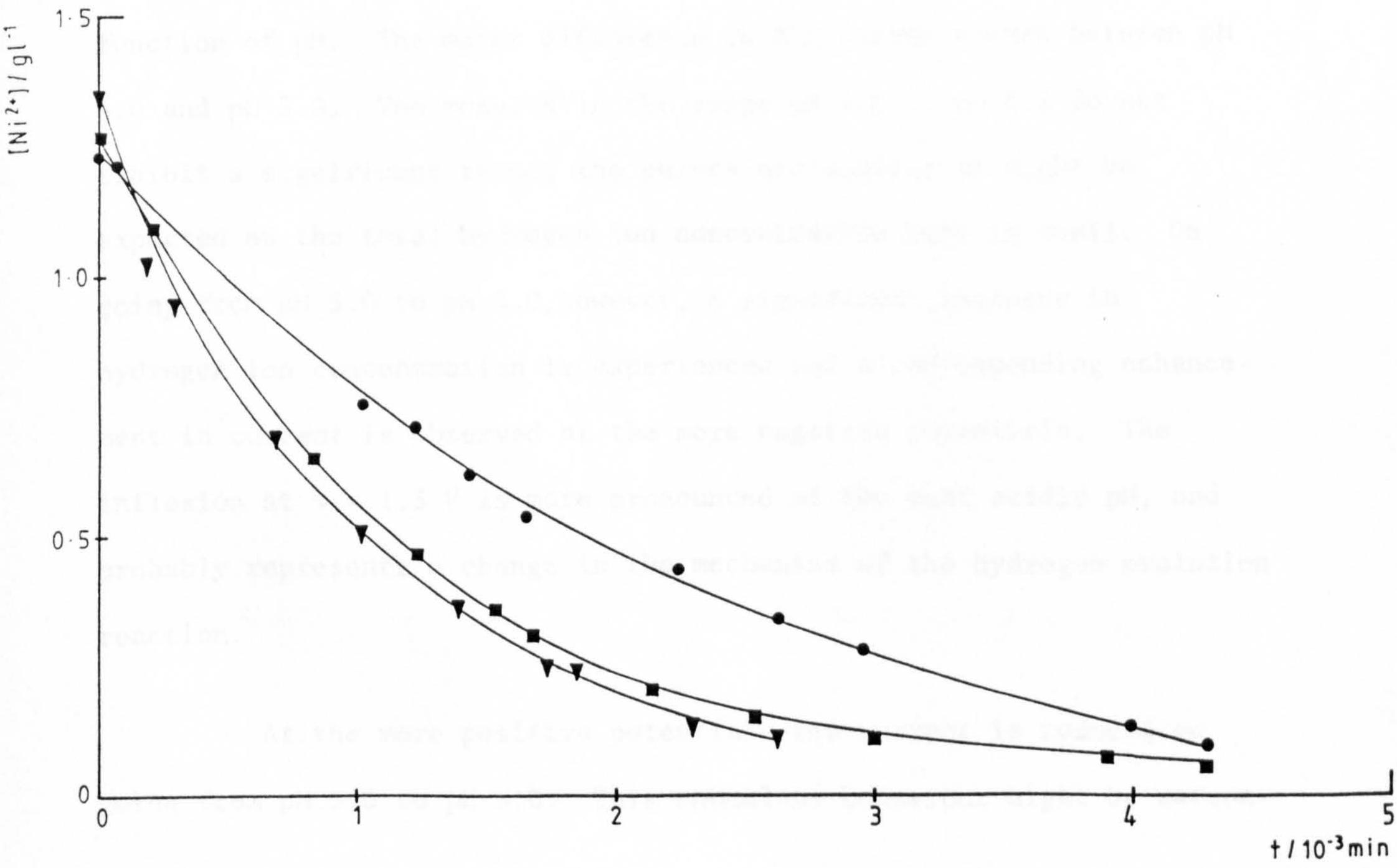

Fig. 8.4.2 [Ni^{2+}] versus t plots at various values of pH;
● pH 3.0, ■ pH 5.4, ▼ pH 6.2.

The decay in nickel ion concentration, also as a function of time, is shown in Fig. 8.4.2. In contrast to the corresponding curves of §8.3, these data show a certain trend with the variable concerned. It is interesting that the absolute rate of nickel deposition appears to increase with pH.

Since the current density decreases and the deposition rate increases with pH, it is to be expected that the cathode current efficiency will also increase with pH. Fig. 8.4.3 shows that this is indeed the case. The current efficiency is still a function of the nickel ion concentration. The data suggests that the current efficiency-concentration curves tend to a limiting form soon after pH 6.2. Again, the overall efficiencies are lower than expected and the only remaining explanation for this lies in an incorrect assessment of the electrolyte volume.

Figs. 8.4.4 to 8.4.8 show the polarisation curves as a function of pH. The major difference in the curves occurs between pH 3.0 and pH 5.0. The results in the range pH 5.0 to pH 6.2 do not exhibit a significant trend; the curves are similar as might be expected as the total hydrogen ion concentration here is small. On going from pH 5.0 to pH 3.0, however, a significant increase in hydrogen ion concentration is experienced and a corresponding enhancement in current is observed at the more negative potentials. The inflexion at $\sim$ - 1.3 V is more pronounced at the most acidic pH, and probably represents a change in the mechanism of the hydrogen evolution reaction.

At the more positive potentials the current is reduced on going from pH 5.0 to pH 3.0. This anomalous behaviour might be ration-

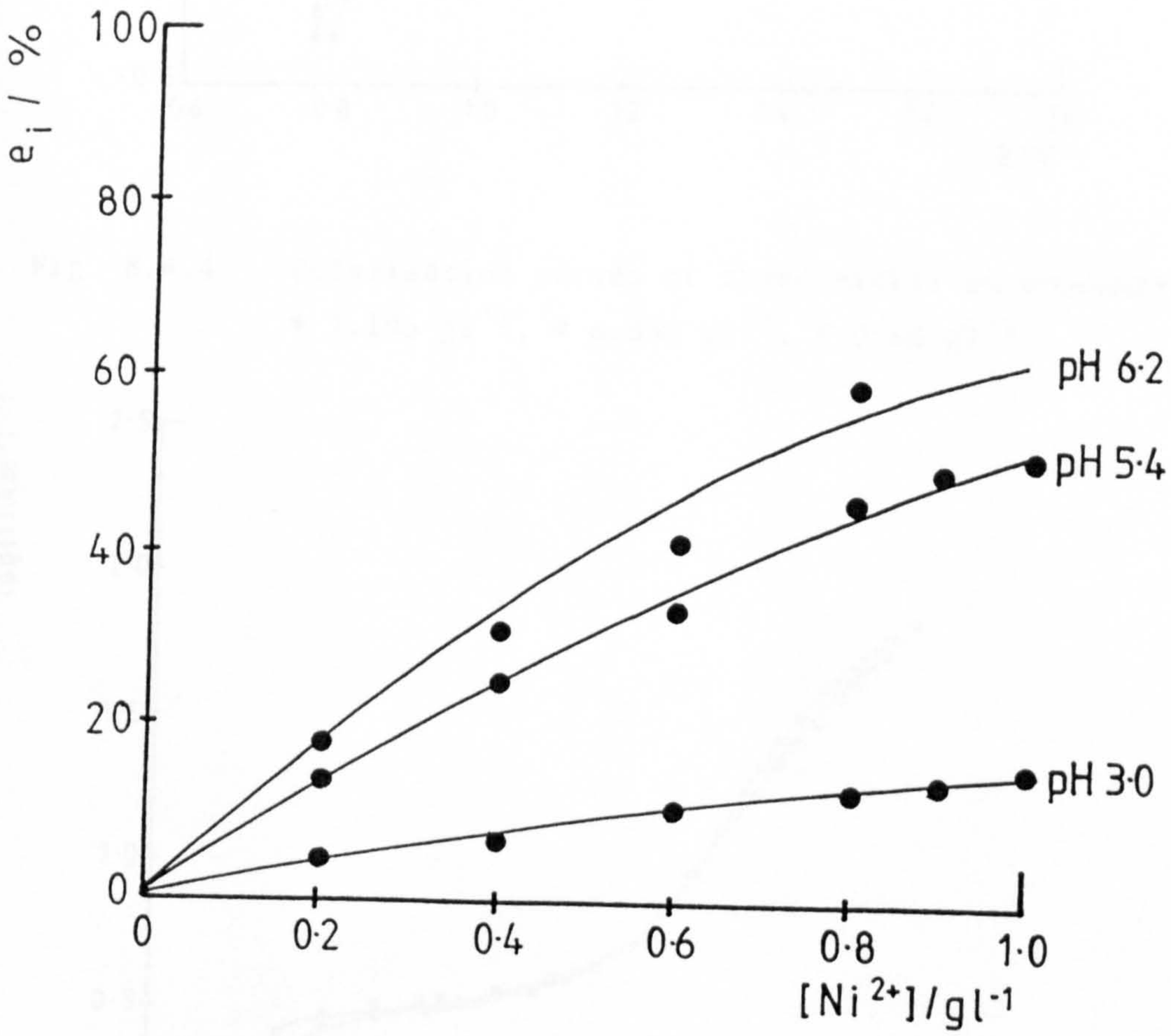

Fig. 8.4.3 e_i versus $[Ni^{2+}]$ plot for three values of pH.

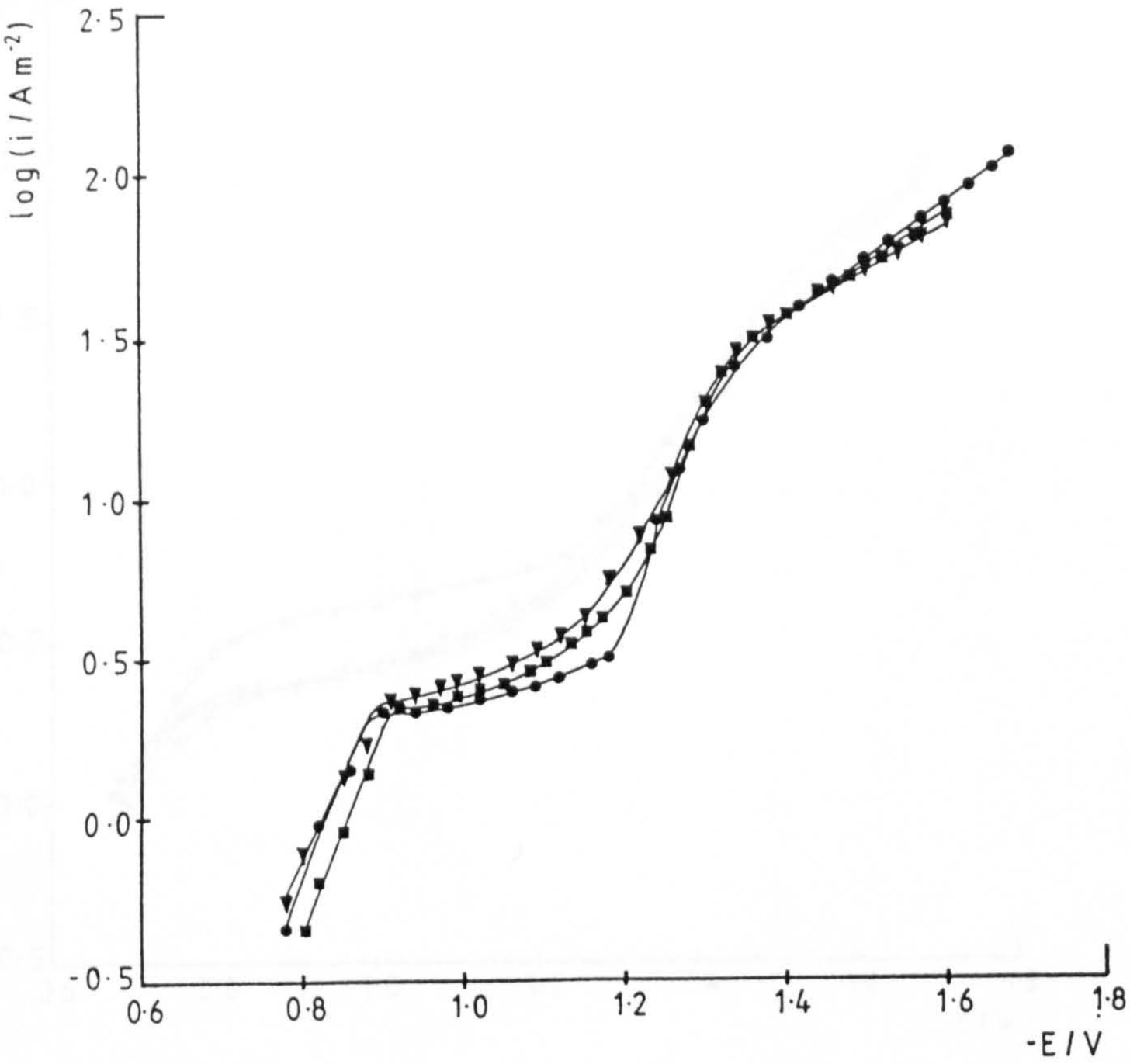

Fig. 8.4.4 Polarisation curves at three nickel in concentrations (pH 3.4); ● 1.195 gl^{-1}, ■ o.835 gl^{-1}, ▼ 0.58 gl^{-1}

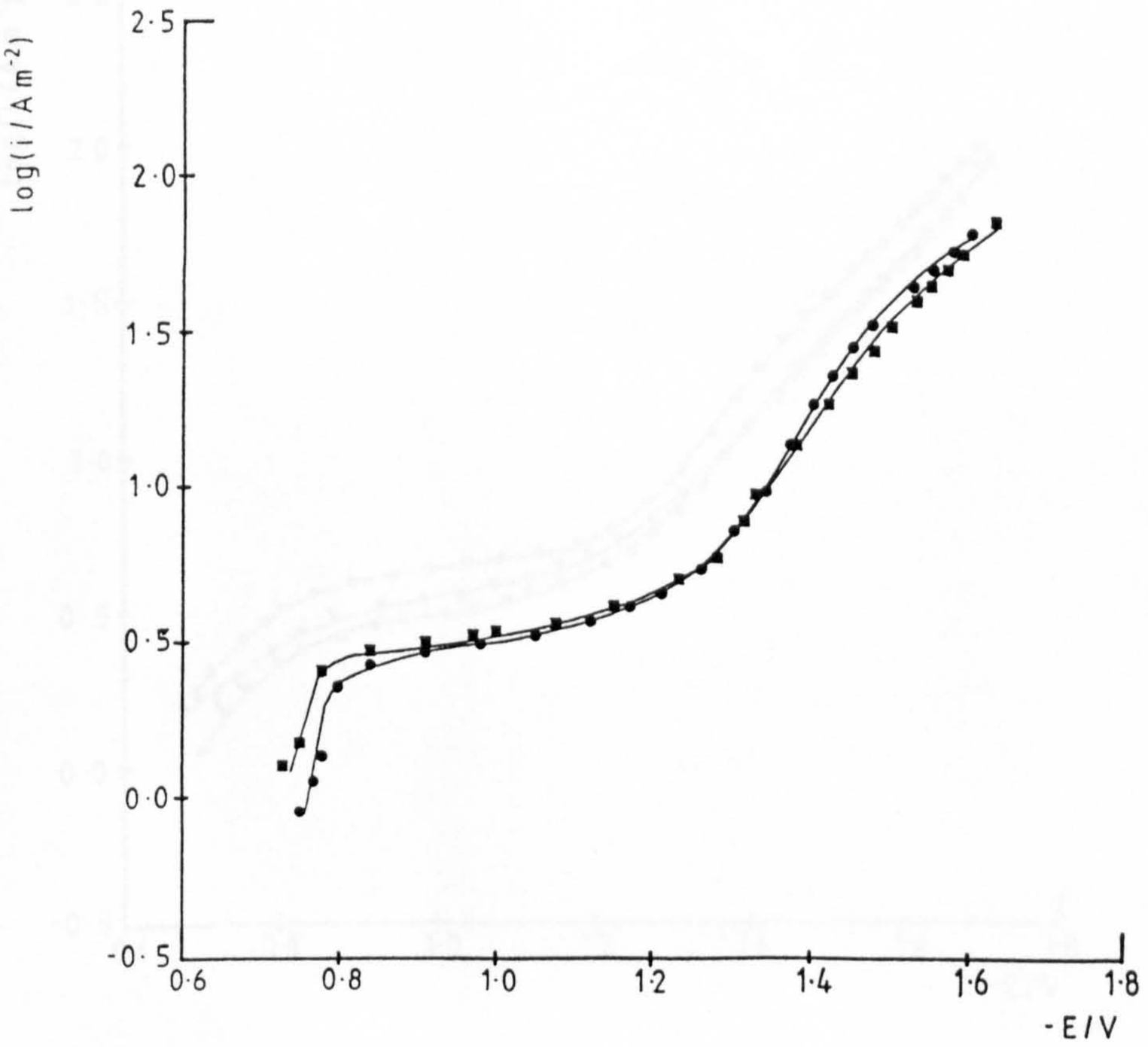

Fig. 8.4.5 Polarisation curves at two nickel ion concentrations (pH 5.0); ● 1.09 gl^{-1}, ■ 0.395 gl^{-1}

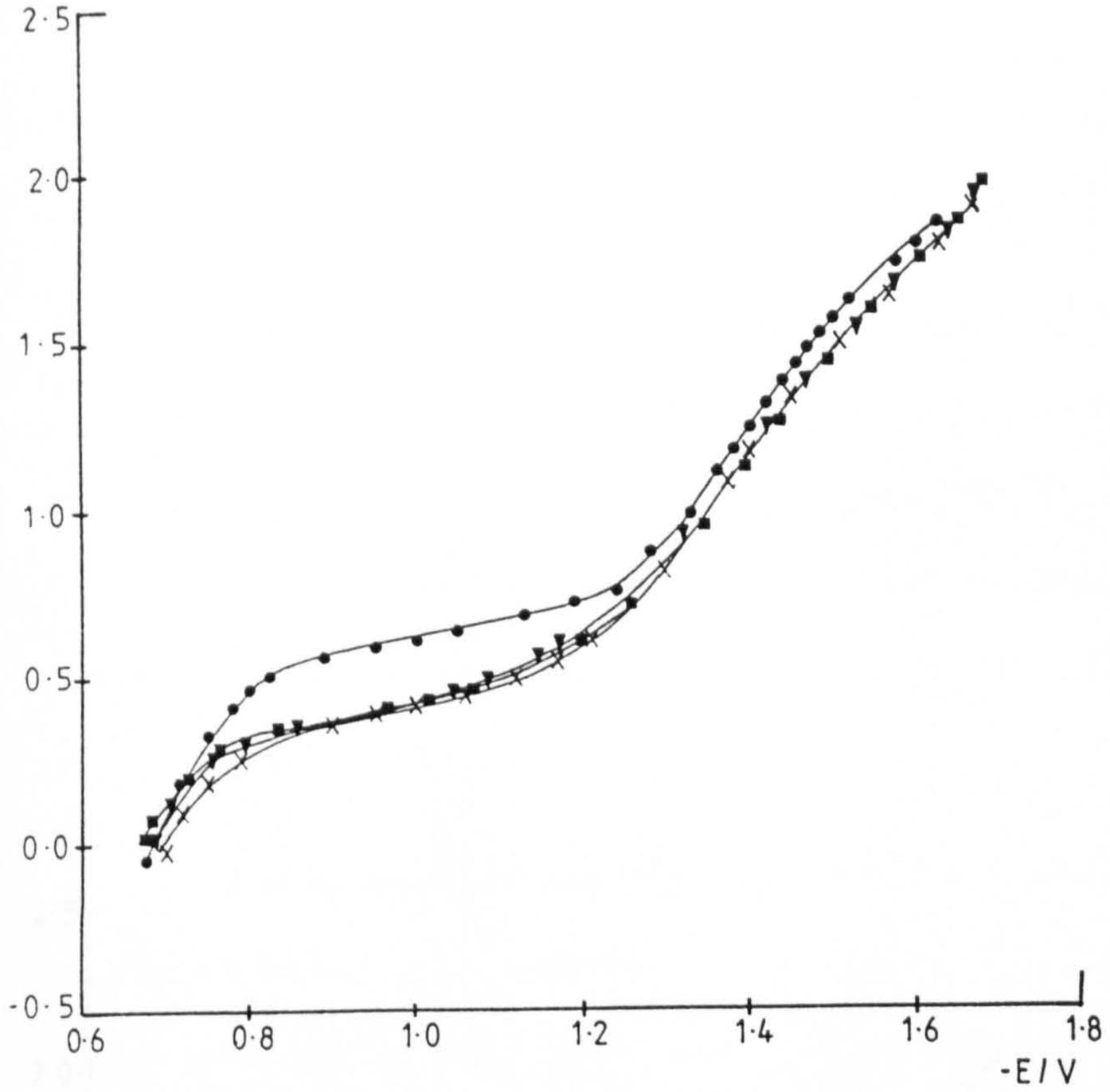

Fig. 8.4.6 Polarisation curves at three nickel ion concentrations (pH 5.4); ● 0.95 gl^{-1}, ■ 0.36 gl^{-1}, ▼ 0.1 gl^{-1}.

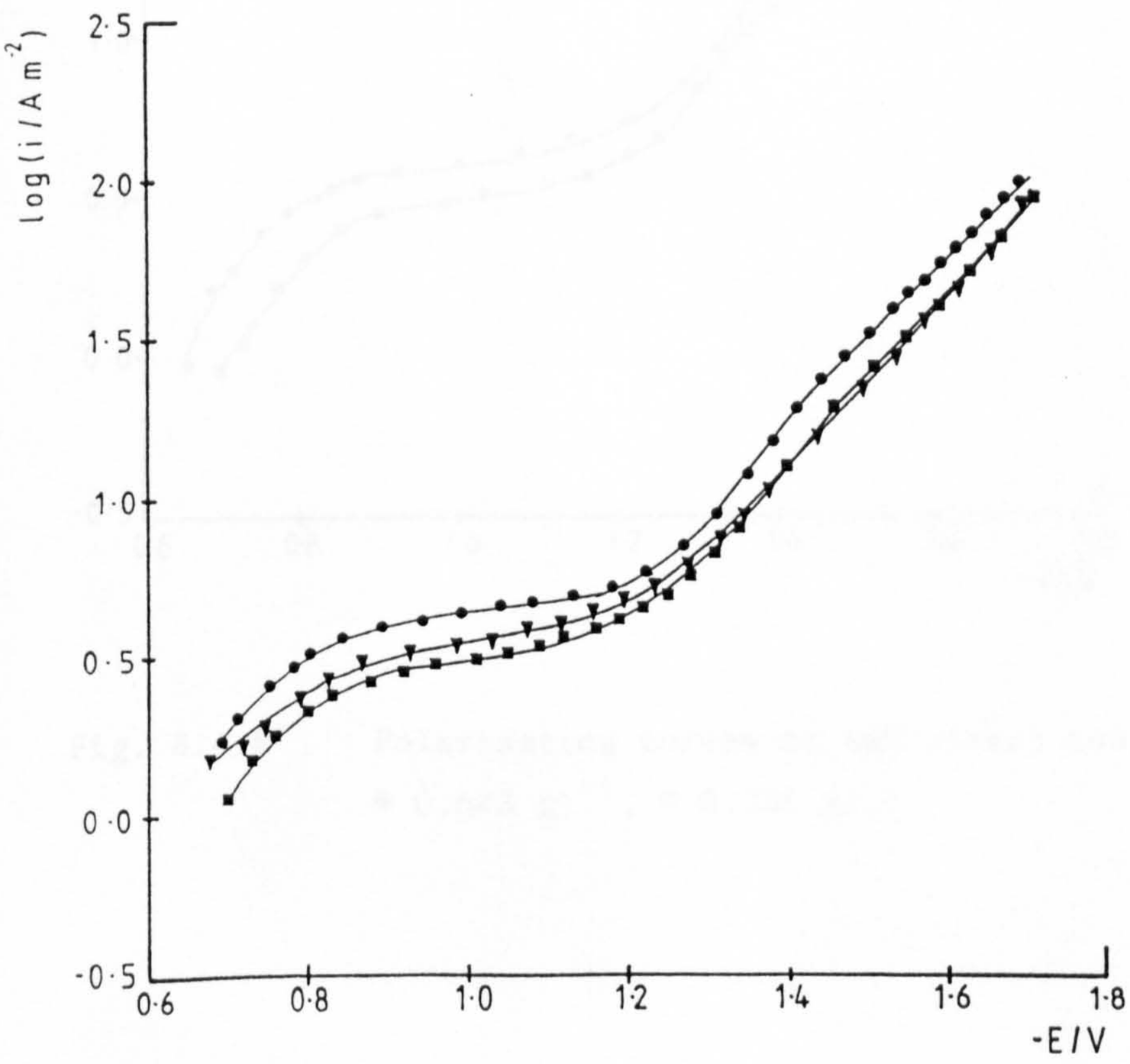

Fig. 8.4.7 Polarisation curves at three nickel ion concentrations (pH 5.8); ● 0.935 gl^{-1}, ■ 0.505 gl^{-1}, ▼ 0.165 gl^{-1}.

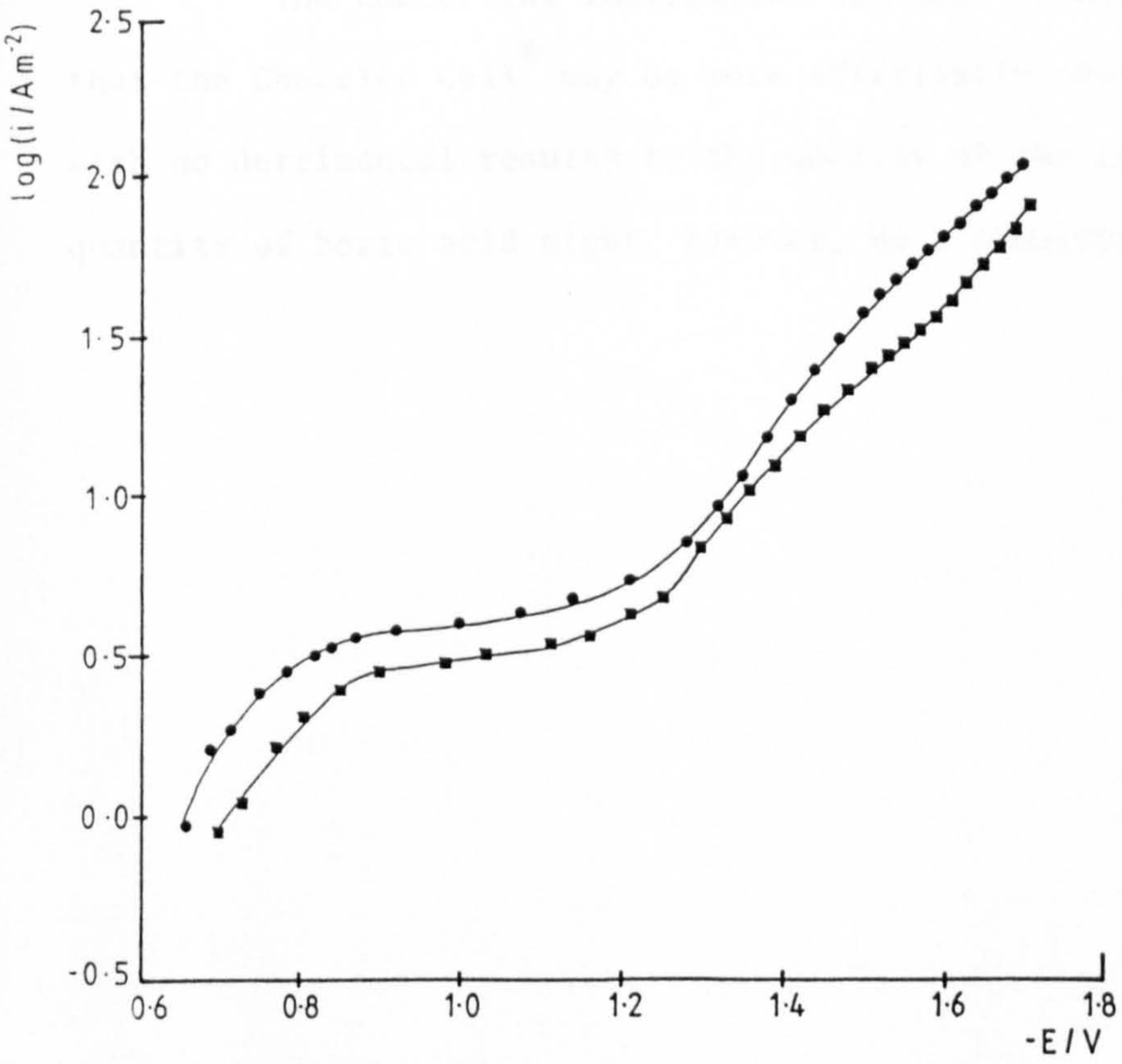

Fig. 8.4.8 Polarisation curves at two nickel ion concentrations (pH 6.2); ● 0.643 gl^{-1}, ■ 0.335 gl^{-1}

alised in terms of the inhibition of the reaction by boric acid, which is likely to be more strongly adsorbed at the more acidic pH.

There is little change in the polarisation curves as the nickel ion concentration falls. Any change is a second order effect compared to the difference observed between the first (highest nickel ion concentration) and subsequent polarisation curves. This difference undoubtedly arises from the presence of a mixed nickel/titanium surface in the former case.

The commercial implication of these results is to suggest that the Chemelec Cell® may be more efficiently operated at higher pH, with no detrimental results to the quality of the deposit. An adequate quantity of boric acid might, however, be a requirement.

CHAPTER NINE

CONCLUDING DISCUSSION

The introductory chapter to this thesis considered the development of commercial electroplating. It was shown that there were both financial and environmental incentives for the efficient use and re-use of water and that conventional effluent treatment methods did little to recover the valuable metal lost to drag-out.

The development of a number of novel processes was mentioned and the Chemelec Cell® viewed against these. The operation of the cell was thought capable of improvement and, to this end, experiments have been performed both with the cell itself and also in an attempt to reveal the electrode kinetics of the relevant systems.

The method of faradaic impedance was applied to the determination of the kinetics of the solid cadmium electrode in perchloric electrolytes. Such electrolytes have little bearing on the operation of the cell, but the cathodic process was shown to occur as a two electron reversible transfer. Measurements at the equilibrium were difficult to achieve and interpret, except in terms of a passivated electrode. Surprisingly, the anodic process was easier to study than the equilibrium, although the true kinetics were obscured by the presence of a monolayer of $Cd(OH)_2$. The anodic process was, however, facile.

The rotating disc electrode was tested on a cyanide/chloride electrolyte. The results showed that, for low concentrations of the cyanide ion, dissolution occurred as a two electron reversible process. At higher cyanide ion concentrations, however, the shift in pH was thought

to account for the development of a filmed surface, obscuring the kinetics. Additions of the cadmium ion to the electrolyte gave rise to results which suggested precipitation of the dissolving cadmium as less cyanide ion became available for complex formation.

Having established the above methods, investigations were carried out in alkaline cyanide solutions. Linear sweeps revealed a tendency towards passivation at high cyanide ion concentrations. Under these conditions, however, evidence was obtained for a one electron reversible anodic process, involving a solution species. At lower cyanide concentration the appearance of several cathodic peaks was ascribed to the reduction of different cadmium complexes. The kinetics were obscured, however. Results at the rotating disc electrode for similar electrolytes showed, at low cyanide concentrations, a one electron reversible dissolution step, but a two electron reversible deposition process. Increasing the cyanide concentration led to film formation. The results of impedance studies largely confirmed these findings. At high cyanide ion concentration, however, the charge transfer process was thought not to be completely inhibited. The Cd/Cd^{2+} exchange was believed to occur through "holes" in an otherwise complete film. The film was considered subject to reduction and re-formation. At large anodic polarisations, however, more complete passivation was occasioned.

The salient features of this section of the work are that the cadmium electrode is frequently covered by a hydroxide film and the development of the film is encouraged by increasing the concentration of the cyanide ion and by the application of more positive potentials. This is surprising inasmuch as the electrolytes most favoured in commercial operation of the cell are those for which film formation is most likely.

At the electrode potentials generally encountered in commercial operation of the cell the film is likely to be incomplete and may serve to improve deposit quality.

As has been stated already, time did not permit these ideas to be tested on the Chemelec Cell®. It would have been interesting, for example, to determine how far the pH could be acidified before the deposit quality suffered.

Experiments in the Chemelec Cell® (with nickel) have shown that the most efficient operation will be at a current density associated with an electrode potential of - 1.5 V (versus Hg/Hg_2SO_4). This is likely to be around 40 Am^{-2}. It would appear that operation at less acidic pH might be desirable but that a minimum amount of boric acid might be required for this. Problems with deposit quality of start-up might be overcome by operation at more acidic pH than otherwise used.

REFERENCES

1. see W.G. McMillan, *A Treatise on Electro-metallurgy*, London: Charles Griffin & Co., 1890.

2. L. Galvani, *De viribus electricitatis in motu musculari commentarius*, Bologna, 1791.

3. A.G.A.A. Volta, *Phil.Trans.R.Soc.*, 90(2) 1800 403.

4. M. Faraday, *Phil.Trans.R.Soc.*, 123(1) 1833 23; 124(1) 1834 77.

5. G. Bird, *Phil.Trans.R.Soc.*, 127(2) 1837 37.

6. J. Shore, *Br.Pat.*, 8 407

7. R. Brugger, *Nickel Plating*, Teddington: Robert Draper Ltd., 1970.

8. A. Smee, *Elements of Electro-metallurgy*, London, 1841.

9. G. Gore, *The Art of Electro-metallurgy, Including All Known Processes of Electrodeposition*, 1855.

10. see J.K. Dennis and T.E. Such, *Nickel and Chromium Plating*, London: Newnes-Butterworth, 1972.

11. I. Adams, *Trans.Am.Electrochem.Soc.*, 9 1906 211.

12. idem, *U.S. Pat.*, 52 271.

13. idem, *ibid.*, 93 157.

14. idem, *ibid.*, 136 634.

15. E. Weston, *U.S. Pat.*, 211 071.

16. J. Powell, *U.S. Pat.*, 229 274.

17. idem, *ibid.*, 228 389.

18. R. Springer, *Z.Elektrochem.*, 7 1900/1 700.

19. W.D. Bancroft, *Trans.Am.Electrochem.Soc.*, 9 1906 217.

20. F. Foerster, *Z.Elektrochem.*, 4 1897/8 160.

21. J. Vandermersch, *Br.Pat.*, 5 300.

22. E.F. Kern, *Trans.Am.Electrochem.Soc.*, 23 1913 145.

23. O.P. Watts, *Trans.Am.Electrochem.Soc.*, 29, 1916 395.

24. L. Cambi and R. Piontelli, *Rend.Inst.Lomb.Sci.*, 72(1) 1939 128.

25, W.A. Wesley and J.W. Carey, *Trans.Electrochem.Soc.*, 75 1939 209.

26. M. Schlötter, *U.S. Pat.*, 1 972 693.

27. L. Weisberg and W.B. Stoddard, *U.S. Pat.*, 2 026 718.

28. T.H. Russell and J.S. Woolrich, *Br.Pat.*, 12 526.

29. W.H. Remington, *U.S. Pat.*, 82 877.

30. C.L. Lopez-Cacicedo, *Report No. ECRC/N999*, Capenhurst: The Electricity Council Research Centre, 1976.

31. A.T. Kuhn, *Chem.Ind.*, July 1978 447.

32. G. Kreysa, *Metalloberfläche*, 35(6) 1981 211.

33. F.C. Walsh and D.R. Gabe, paper presented at the *A.I. Ch. E. Summer Meeting*, Cleveland, Ohio, U.S.A., August/September 1982 (to be published).

34. F. Goodridge, *Proc.24th Int.Cong.Pure and Appl.Electrochem.*, 5 1974 19.

35. P.R. Nadebaum and T.Z. Fahidy, *Nature*, 241(106) 1973 45.

36. idem, *J.Electrochem.Soc.*, 122(8) 1975 1035.

37. idem, *Can.J.Chem.Eng.*, 53(3) 1975 259.

38. idem, *J.Appl.Electrochem.*, 5(3) 1975 249.

39. idem, *ibid.*, 10(1) 1980 13.

40. T. Takahashi, M.I. Ismail and T.Z. Fahidy, *Electrochimica Acta* , 26(12) 1981 1727.

41. T. Takahashi and T.Z. Fahidy, *Electrochimica Acta* , 25(12) 1980 1603.

42. J.A.E. Wilkinson and K.P. Haines, *Trans.Inst.Mining Met.*, 81(Sept.) 1972 157.

43. G.S. James, B.I. Denar and W.R. Moergeli, *U.S. Pat.*, 3 974 049.

44. K. Scott, *J.Appl.Electrochem.*, 11(3) 1981 339.

45. G. Kreysa and R. Brandner, paper presented at the *2nd World Congress of Chemical Engineering*, Montreal, Canada, October 1981.

46. M. Fleischmann, C.J.H. King, J.W. Oldfield, R.E. Plimley and C.L.K. Tenakoon, *Br.Pat.*, 1 419 246.

47. P.M. Robertson, *Ger.Pat.*, 2 415 784; 2 503 819.

48. P.M. Robertson and N. Ibl, *J.Appl.Electrochem.*, 7(4) 1977 323.

49. P.M. Robertson, B. Scholder, G. Theis and N. Ibl, *Chem.Ind.*, July 1978 459.

50. P.M. Robertson, F. Schwager and N. Ibl, *J.Electroanal.Chem.Interfacial Electrochem.*, 65(2) 1975 883.

51. C.L. Lopez-Cacicedo, *Trans.Inst.Met.Finish.*, 53(2) 1975 74.

52. idem, *I.Chem.E.Symposium Ser.*, 42 1975 29.1.

53. idem, *Br.Pat.*, 1 423 369; *U.S. Pat.*, 3 977 951.

54. F.S. Holland, *Br.Pat.*, 1 505 736.

55. idem, *U.S. Pat.*, 4 028 199.

56. idem, *Chem.Ind.*, July 1978 453.

57. F.C. Walsh and D.R. Gabe, *Surf.Tech.*, 12(1) 1981 25.

58. F.C. Walsh, N.A. Gardner and D.R. Gabe, *J.Appl.Electrochem.*, 12(3) 1982 299.

59. D.R. Gabe and F.C. Walsh, *Proc.Interfinish*, Kyoto, Japan, Oct.1980.

60. F.S. Holland and H. Rolskov, *Effluent Water Treatment Convention*, Birmingham, England, Nov.1978.

61. M. Fleischmann, R.E.W. Jansson, G.A. Ashworth and P.J. Ayre, *Br.Pat.*, 1 504 690.

62. M. Fleischmann, R.E.W. Jansson and R.J. Marshall, *Br.Pat.*, 1 522 872.

63. R.E.W. Jansson and R.J. Marshall, *Chem.Eng.*, 315(Nov/Dec.) 1976 769.

64. M. Fleischmann and R.E.W. Jansson, *J.Appl.Electrochem.*, 9(4) 1979 427.

65. M. Fleischmann, J. Ghoroghchian and R.E.W. Jansson, *J.Appl.Electrochem.*, 9(4) 1979 437.

66. M. Fleischmann and R.E.W. Jansson, *Trans.S.A.E.S.T.*, 12(4) 1977 277.

67. B. Fleet and S.D. Gupta, *Nature*, 263(5573) 1976 122.

68. B. Fleet and S.D. Gupta, *Ger.Pat.*, 2 534 357.

69. I.F.T. Kennedy and S.D. Gupta, *Finisher's Management*, July 1978 7.

70. J.M. Williams, *U.S. Pat.*, 3 859 195.

71. G. Kreysa, *Chem.Ing.Techn.*, 50(5) 1978 332.

72. idem, *Metalloberfläche*, 34 1980 494.

73. J.R. Backhurst, J.M. Coulson, F. Goodridge, R.E. Plimley and M. Fleischmann, *J.Electrochem.Soc.*, 116(11) 1969 1600.

74. J.R. Backhurst, M. Fleischmann, F. Goodridge and R.E. Plimley, *Br.Pat.*, 1 194 181.

75. G. Van der Heiden, C.M.S. Raats and H.F. Boon, *Chem.Ind.*, July 1978 465.

76. D.R. Gabe, personal communication.

77. H.L.F. von Helmholtz, *Ann.Phys.(2)*, 89 1853 211; *Ann.Phys.(3)*, 7 1879 337.

78. G. Quincke, *Pogg.Ann.*, 113 1861 513.

79. G. Gouy, *J.Physique (4)*, 9 1910 457; *Compt.rend.*, 149 1910 654.

80. D.L. Chapman, *Phil.Mag. (6)*, 25(148) 1913 475.

81. O. Stern, *Z.Elektrochem.*, 30 1924 508.

82. D.C. Grahame, *Chem.Revs.*, 41 1947 441.

83. J.O'M. Bockris, M.A.V. Devanathan and K. Müller, *Proc.Phys.Soc.*, A274 1963 55.

84. I.L. Cooper and J.A. Harrison, *Electrochimica Acta*, 22(5) 1977 519.

85. idem, *ibid.*, 22(12) 1977 1361; 22(12) 1977 1365.

86. W. Nernst, *Z.Physik.Chem.*, 4 1889 129.

87. T. Erdey-Gruz and M. Volmer, *Z.Physik.Chem.*, 105A 1930 203.

88. J. Tafel, *Z.Physik.Chem.*, 50 1905 641.

89. See 93.

90. A. Fick, *Pogg.Ann.*, 94 1855 59.

91. W. Nernst, *Z.Physik.Chem.*, 47 1904 52.

92. H.R. Valentine, *Applied Hydrodynamics*, London: Butterworths Scientific Publications, 1959.

93. V.G. Levich, *Physicochemical Hydrodynamics*, New Jersey: Prentice-Hall, 1962.

94. idem, *Acta Physicochim.URSS.*, 17 1942 257.

95. V. Yu Filinovsky and Yu V. Pleskov, *Prog.Surf.Membr.Science*, 10(2) 1976 27.

96. P. Delahay, *New Instrumental Methods in Electrochemistry*, New York: Interscience, 1954.

97. B.V. Ershler, *Disc.Faraday Soc.*, 1 1947 269.

98. J.E.B. Randles, *Disc.Faraday Soc.*, 1 1947 11.

99. D.C. Grahame, *J.Electrochem.Soc.*, 99(12) 1952 370C.

100. M. Sluyters-Rehbach and J.H. Sluyters, in *Electroanalytical Chemistry, Vol.4*, ed. A.J. Bard, New York: Marcel Dekker, 1970.

101. R.D. Armstrong, M.F. Bell and A.A. Metcalfe, in *Electrochemistry, Vol.4*, ed. G.J. Hills and H.R. Thirsk, London: The Chemical Society, 1977.

102. E. Warburg, *Wied.Ann.*, 67 1899 493; *Drud.Ann.*, 6 1901 125.

103. R.J. Latham and N.A. Hampson, in *Encyclopædia of Electrochemistry of the Elements, Vol.1*, ed. A.J. Bard, New York: Marcel Dekker, 1973.

104. R.D. Armstrong, K. Edmonson and G.D. West, in *Electrochemistry, Chemical Society Specialist Report, Vol.4*, London: The Chemical Society, 1974.

105. R. Barnard, *J.Appl.Electrochem.*, 11 1981 217.

106. H.S. Harned and M.E. Fitzgerald, *J.Amer.Chem.Soc.*, 58(12) 1936 2624.

107. J.L. Burnett and M.H. Zirin, *J.Inorg.Nucl.CHem.*, 28 1966 902.

108. F.H. Getman, *J.Phys.Chem.*, 35(2) 1931 588.

109. E. Deltcombe, M. Pourbaix and N. De Zoubov, *Atlas of Electrochemical Equilibria in Aqueous Solutions*, ed. M. Pourbaix, London: Pergamon, 1966.

110. T.A. Borisova and B.V. Ershler, *Zhur.Fiz.Khim.*, 24 1950 337.

111. N.V. Nikolavea, N.S. Shapiro and A.N. Frumkin, *Dokl.Akad.Nauk SSSR*, 86 1952 851.

112. V.L. Kheifets and B.S. Krasikov, *Dokl.Akad.Nauk SSSR*, 109 1956 586.

113. N.A. Hampson and D. Larkin, *J.Electrochem.Soc.*, 114(9) 1967 933.

114. V. Ya Bartenev, E.S. Sevast'yanov and D.I. Leikis, *Elektrokhimiya*, 5(12) 1969 1491.

115. idem, *ibid.*, 5(12) 1969 1502.

116. W. Lorenz, *Naturwissenschaften*, 40 1953 578; *Z.Elektrochem.*, 58(10) 1954 912.

117. R.J. Brodd, *J.Res.Nat.Bur.Standards*, 65A(4) 1961 275.

118. K.E. Heusler and L. Gaiser, *J.Electrochem.Soc.*, 117(6) 1970 762.

119. J. Amosse, B. Nguyen and M.J. Barbier, *Electrochimica Acta*, 15(12) 1970 1967.

120. N.A. Hampson, R.J. Latham and D. Larkin, *J.Electroanal.Chem. Interfacial Electrochem.*, 23(2) 1969 211.

121. N.A. Hampson and R.J. Latham, *J.Electroanal.Chem.Interfacial Electrochem.*, 32(2) 1971 175.

122. L.A. L'vova, *Work of Young Scientists*, Vyp. Khim., Izd-vo Sarat, Gos. Un-ta, 1965.

123. L.A. L'vova and A.V. Fortunatov, *Anodic Protection of Metals*, Moscow: Mashinostroenie, 1964.

124. I.L. Weininger and M.W. Breiter, *J.Electrochem.Soc.*, 111(6) 1964 707.

125. P.E. Lake and E.J. Casey, *J.Electrochem.Soc.*, 105(1) 1958 52; 106(11) 1959 913.

126. K. Huber, *J.Electrochem.Soc.*, 100(8) 1953 376.

127. G.T. Croft, *J.Electrochem.Soc.*, 106(4) 1959 278.

128. E. Lange and R.W. Ohse, *Naturwissenschaften*, 45 1958 437.

129. R.W. Ohse, *Z.Elektrochem.*, 64 1960 1171.

130. M.W. Breiter and I.L. Weininger, *J.Electrochem.Soc.*, 113(7) 1966 651.

131. M.A.V. Devanathan and S. Lakshmanan, *Electrochimica Acta*, 13(4) 1968 667.

132. R.D. Armstrong and G.D. West, *J.Electroanal.Chem.Interfacial Electrochem.*, 30(3) 1971 385.

133. L.A. L'vova, D.K. Grachev and V.A. Panin, *Elektrokhimiya*, 5(5) 1969 627.

134. Y. Okinaka, *J.Electrochem.Soc.*, 117(3) 1970 289.

135. J.A. Harrison, D.R. Sandbach and P.J. Stronach, *Electrochimica Acta*, 24(2) 1979 179.

136. J.P.G. Farr and N.A. Hampson, *Electrochem.Technol.*, 6(1/2) 1969 10.

137. N.A. Hampson and R.J. Latham, *J.Electroanal. Chem. Interfacial Electrochem.*, 32 (1971) 337.

138. A.J. Arvia and D. Posadas, in *Encyclopædia of Electrochemistry of the Elements, Vol. 3*, ed. A.J. Bard, New York: Marcel Dekker, 1975.

139. L. Colombier, *C.R. Acad.Sci.*, 199 1934 273.

140. M.M. Haring and E.G. van den Bosche, *J.Phys.Chem.*, 33 1929 161.

141. D.S. Carr and C.F. Bonilla, *J.Electrochem.Soc.*, 99(12) 1952 475.

142. J.W. Larson, P. Cerutti, H.K. Garber and L.G. Hepler, *J.Phys.Chem.*, 72(8) 1968 2902.

143. K. Murata, *Bull.Chem.Soc.Japan*, 3 1928 47.

144. M.A. Lopez-Lopez, *C.R. Acad.Sci.*, 256 1963 2594; 255 1962 3170.

145. W.M. Latimer, *Oxidation Potentials*, New Jersey: Prentice-Hall, 1952.

146. P. Lukovtsev, S. Levina and A.N. Frumkin, *Acta Physicochim.URSS*, 11 1939 21.

147. A. Legran and S. Levina, *Acta Physicochim.URSS*, 12 1940 243.

148. V.L. Kheifets and B.S. Krasikov, *Zh.Fiz.Khim.*, 31 1957 1992.

149. B. Jakuszewski and Z. Koslowski, *Roczniki.Chem.*, 38(1) 1964 93.

150. J.O'M. Bockris, S.D. Argade and E. Gileadi, *Electrochim.Acta*, 14(12) 1969 1259.

151. R. Parsons, *Handbook of Electrochemical Constants*, London: Butterworths, 1959.

152. M. Hollnager and R. Landsberg, *Z.Phys.Chem.*, 212 1959 94.

153. R.C.V. Piatti, A.J. Arvia and J.J. Podestá, *Electrochimica Acta*, 14(7) 1969 541.

154. idem, *An.Asoc.Quím.Argent.*, 57(2) 1969 71.

155. V.V. Batrakov, Gamil'Khanna Avad, E.I. Mikhailova and Z.A. Iofa, *Elektrokhimiya*, 4(5) 1968 601.

156. F. Ovari and A.L. Rotinyan, *Zh.Prikl.Khim.*, 42(1) 1969 227.

157. idem, *Elektrokhimiya*, 6(4) 1970 528.

158. I. Epelboin, *21st Meeting of the International Committee on Thermodynamic and Electrochemical Kinetics*, Prague, 1970.

159. M.J. Nicol and H.I. Philip, *Proc.Int.Symp.Chloride Hydrometal.*, 1977 250; *Nat.Inst.Metal Report no. 1804*, 1976.

160. B. Le Gorrec and J. Guitton, *C.R. Acad.Sci.*, 272C(22) 1971 1784; 272C(25) 1971 2031.

161. F. Ovari, *Proc.2nd Conf.Appl.Phys.Chem.*, 2 1971 337.

162. I. Epelboin and R. Wiart, *J.Electrochem.Soc.*, 118(10) 1971 1577.

163. I. Matsuda, K. Takahashi, S. Tsuda and T. Yoshida, *Denki Kagaku*, 41(9) 1973 692.

164. O.O. Schaus, R.J. Gale and W.H. Gauvin, *Plating*, Aug 1971 801.

165. J.R. Vilche and A.J. Arvia, *Corros.Sci.*, 18(5) 1978 441.

166. R. de Levie, in *Advances in Electrochemistry and Electrochemical Engineering, Vol. 6*, ed. P. Delahay and C.W. Tobias, 1967.

167. S.A.G.R. Karunathilaka, N.A. Hampson, R. Leek and T.J. Sinclair, *J.Appl.Electrochem.*, 10(3) 1980 357; 10(5) 1980 603; 10(6) 1980 799; 11 1981 365.

168. H. Gerischer, *Z.Elektrochem.*, 57 1953 604.

169. Lecture notes for the course *Advanced Instrumental Methods in Electrode Kinetics*, ed. D. Pletcher, Southampton, 1975.

170. A. Bettley, A. Tyson, S.A. Cotgreave and N.A. Hampson, *Surf.Tech.*, 12(1) 1981 15.

171. A. Bettley, personal communication.